DISSERTATION

NON-PERTURBATIVE REGIMES OF LIGHT-MATTER INTERACTIONS

ausgeführt zum Zwecke der Erlangung des akademischen Grades eines Doktors der Naturwissenschaften unter der Leitung von

PROF. PETER RABL

141

ATOMINSTITUT

eingereicht an der Technischen Universität Wien

Fakultät für Physik

von

DANIELE DE BERNARDIS, DOTT. MAG.

Matrikelnummer: 01652053

[redacted]

Wien, am

Diese Dissertation haben begutachtet:

Prof. Dr. J. Keeling

Prof. Dr. J. Feist

Zusammenfassung

Diese Arbeit behandelt die Physik der Resonatorquantenelektrodynamik im sogenannten ultrastarken Kopplungsregime, in dem die Kopplungsstärke zwischen einem einzelnen Photon und einem einzelnen Dipol mit der inneren Energie des Photons vergleichbar wird. In diesem Regime verlieren die meisten der gewöhnlich verwendeten theoretischen Modelle sowie auch unsere physikalische Intuition ihre Gültigkeit und es Bedarf einer neuen Art der Beschreibung.

In dieser Arbeit wird zuerst die Theorie der Resonatorquantenelektrodynamik nochmals von Grund auf neu abgeleitet, um ein minimales Modell zu bekommen, welches auch im ultrastarken Kopplungsregime seine Gültigkeit behält. Dazu wurden viele der gewöhnlichen Näherungen im Detail überprüft und gezeigt, dass zum Beispiel die Gültigkeit der Einzel-Moden Approximation für den Resonator und die Zwei-Niveau Approximation für die Dipole im ultrastarken Kopplungsregime von der Eichung abhängen. Nur durch die Wahl der richtigen Eichung erhält man dann eine gültiges Modell für beliebige Kopplungsstärken.

Basierend auf diesem vereinfachten Model werden in dieser Dissertation dann die Eigenschaften des Grundzustands und der thermischen Zustände eines Multi-Dipol-Resonator-QED-Systems untersucht. Dabei ergeben sich als Funktion der Licht-Materie Kopplungstärke qualitative sehr unterschiedliche Phasen. Für diese Phasen findet man auch sehr unterschiedliche thermodynamische Eigenschaften, welche in einem Experiment durch die Messung der Schwarzkörperstrahlung oder der Suszeptibilität der Dipole bestimmt werden können.

Im letzten Teil der Arbeit diskutieren wir die quantentheoretische Beschreibung der Licht-Materie-Wechselwirkungen in photonischen Strukturen, in denen die Photonen durch ein synthetisches Magnetfeld beeinflusst werden. Es wird gezeigt, dass ein schwach gekoppelter Quantenemitter mit einem einzelnen zirkulierenden Photon einen chiralen gebundenen Zustand bilden kann. Darüber hinaus wird eine effektive Theorie entwickelt, um solche chiralen Atom-Photon Hybridzustände auch für Systeme mit mehreren Atomen und mehreren Photonen zu beschreiben. Diese Analyse zeigt, dass ein solches System eine vielversprechende Plattform darstellt, um die Physik des fraktionalen Quanten-Hall-Effekts zu simulieren.

Abstract

In this thesis we explore the physics of cavity quantum electrodynamics in the so-called ultrastrong coupling regime, where the coupling strength between a single photon and a single dipole is comparable to the internal energy of the photon itself. Under such conditions most of the frequently employed theoretical models ceased to be valid and a lot of our common intuition about light-matter interactions breaks down. In this thesis we reconsider the theory of cavity QED by starting from the quantization of the electromagnetic field and then carefully deriving a simplified minimal model, reevaluating the validity of all the approximations involved. We show that the usual single-mode approximation for the cavity and the two-level truncation for the dipoles become highly non-trivial in the ultra-strong coupling regime and depend, for example, on the chosen gauge of the original full QED Lagrangian. By clarifying these subtleties, we obtain a consistent model for a set of two-level dipoles that are coupled to a single field mode, which is valid for arbitrary coupling strength.

Based on this simplified model, we then calculate the main properties of the ground state of a multi-dipole cavity QED system. Here we highlight the presence of different phases related to different quantum phase transitions as a function of the microscopic parameters. We then evaluate also the thermal equilibrium states of cavity QED. Here we calculate several thermodynamic quantities, highlighting their observability in realistic experiments through quantities like the black body radiation or the dipole's electric susceptibility.

In the last part of the thesis we discuss the quantum theory of light-matter interactions in photonic structures where the photon is subjected to a synthetic magnetic field. Here we show that a weakly coupled quantum emitter can form a chiral bound state with a single circulating photon. We develop an effective theory to describe such chiral atom-photon bound states also for systems with multiple atoms and multiple photons and show that such a system can be a promising platform to simulate the physics of fractional quantum Hall effect.

Contents

Introduction

The interaction between light and matter was a central topic in the understanding of the microscopic world and the advent of quantum mechanics. After more than a century it still constitutes a point of fundamental interest in the development of technologies based on the law of quantum mechanics [1]. Although in conventional systems the physics of light-matter interactions is by now well-understood, still many surprising effects can emerge when such processes are studied in structure electromagnetic environments or under extreme coupling conditions. In this thesis we explore two such unconventional scenarios for light-matter interactions, where our common intuition, but also our usual theoretical descriptions break down. The first and main topic concerns the physics of light-matter interactions in the non-perturbative coupling regime, where the atom-photon coupling exceeds the energy of the photon itself. In the last part of the thesis we will then study the coupling of atoms to "topological" photons, i.e., to photons that are subject to synthetic magnetic field.

Ultra-strong coupling regime of cavity quantum electrodynamics

In a prototype cavity quantum electrodynamics (cavity QED or cQED) setup one or few atoms are located between two parallel mirrors, where a single photon is trapped, bouncing back and forth between the two mirrors [1]. This setup was first used to demonstrate how to create entangled states between a single atom and a single photon and now it is one of the building blocks of the emerging field of *quantum technologies*. Here we study systems which operate at the single photon level, that can be engineered to fulfil a specific tasks, for example implementing a quantum simulator for a specific complex system, or a universal quantum computer [2].

Usually cavity QED systems are studied under the condition that the coupling between the atom a single photon is very small. This is somehow very limiting, because the coupling strength also determines the speed at which a device based on such a technology could operate. So the development of quantum technologies based on light-matter interactions requires also the development of strategies to increase this coupling strength. A major effort has been made to implement the same kind of physics in different systems, such as electronic transitions in solid-state [3] and superconducting circuits [4], in order to explore all the possibilities that we have to make this coupling as

large as we want.

But it was also realized that making the light-matter coupling bigger and bigger could actually change the physics qualitatively and not just quantitatively. To highlight this qualitative difference, in [5] it was first introduced the expression ultrastrong coupling regime for cavity QED systems where the vacuum Rabi splitting becomes comparable to the absolute energy scales of the system. In this reference it was shown that the large coupling strength in solid-state cavities would make clearly visible the so-called dynamical Casimir effect if the system is subjected to a time modulation of the coupling itself.

But the idea of non-perturbative effects due to large coupling in cQED is actually much older, and it can be traced back to Hepp and Lieb and their original proposal of *superradiance phase transition* [6]. Accepting the *Dicke model* [7] as the minimal approximated toy model to describe an ensemble of molecules collectively coupled to a resonant cavity mode, they predicted the existence of a quantum phase transition when the light-matter coupling is large enough. This has opened a long debate about the real existence of this phase transition and its meaning, which has lasted until our recent years. A series of no-go theorems have convinced the community that this phase transition is impossible in atomic/molecular systems, but, with the advent of circuit QED, new fuel was pumped into the debate [8, 9].

While the debate about the superradiant instability was for a long time a purely theoretical discussion, in recent years the USC regime has been reached in solid-state cavity QED [10, 11], in circuit QED [12, 13] and in molecular cavity QED [14]. A big debate is currently going on in the context of molecular cavity QED with particular focus on the possibility of modify chemical bonds by injecting the molecules in cavity where USC is achieved. Experiments have shown that this possibility cannot be excluded [15, 16], but from theoretical perspective the underlying mechanism is not at all clear. Moreover in solid-state cavity QED some data suggested that a Dicke-like instability might occur [17]. Also in this system a clear and simple intuition on what is going on is currently not available.

In this thesis we devote a large part of our discussion to carefully analyse how to model a cavity QED system, starting from the generic non-relativistic QED Lagrangian. Then we will illustrate systematically what are the simplification that we need in order to keep just the relevant degrees of freedom. This passage is of crucial importance to be sure to avoid artefacts related to an oversimplified modelling. We will see that a large part of the debate regarding the superradiant phase transition is actually flawed in principle by assuming a model which does not represent the description of the considered system in that parameters regime. This applies first to the prediction of the superradiant phase transition itself, because it turns out that the Dicke model cannot be considered a good description of the system when the coupling is sufficiently large, but also to the

related no-go theorems that assume that the Dicke model must be corrected at large coupling by the so-called A^2-term, although that derivation is invalid due to the impossibility of performing the *two level truncation* in the Coulomb gauge. Although gauge dependent artefacts in effective light-matter models have been discussed in the literature before [18, 19], they are usually thought of small quantitative corrections. However, as we show in this thesis, it turns out that in the USC regime effective models derived in different gauges give both quantitatively and qualitatively drastically different predictions. This is an important new insight that could already clarify some of the most controversial predictions in this field.

A second important issue that we specifically highlight in this thesis is the correct distinction between electrodynamical and purely electrostatic effects. It has already been pointed out in several earlier works in this field that the superradiant phase transition can be interpreted as a ferro-electric phase transition, when electrostatic effects are included [20, 21, 22]. However, in these models the effect of dipole-dipole interactions was still treated inconsistently and the superradiant instability is still interpreted as a cavity-mediated effect. A very important point about the effective models derived in this thesis is that a clear distinction between electrostatic dipole-dipole interactions and dynamical cavity interactions are made. In particular, this allows us to distinguish between conventional ferro-electric phase transitions, which do not involve the cavity mode, and the actual modification of the dipolar ensemble, which genuinely induced by quantum fluctuations of the dynamical field mode. Having an effective theory that enables us to have this clear distinction is particularly useful to isolate the new physical phenomena that we can relate to the ultra-strong coupling regime. We will explore in particular the consequences on the ground state of an arbitrary cavity QED system and its finite temperature equilibrium states.

Light-matter interactions with topological photons

The simplest way that we have to think about the propagation of electromagnetic radiation is the light ray. In quantum mechanics we may think that an atom emits a photon through light rays directed along all possible directions. Despite its hand-wavy nature, this simple picture is actually not so wrong, because the probability amplitudes in quantum mechanics are, to leading order, given by the path of least action, which, in the case of a photon, is a straight line [23]. But, what would happen if the usual light rays are instead bent into closed loops? How does it look a world in which the path of least action of a photon is a circle?

In the last part of this thesis we will study light-matter interactions in a system where the photons are forced to follow circular trajectories. This idea seems a bit odd and not connected to reality, but it is actually very relevant in the context of *topological photonics systems* [24].

Here the idea is to confine photons in arrays of coupled resonators, implementing a photonic

lattice, in which the photons hop between neighboring lattice sites. The photons thus propagate through this lattice with an engineered dispersion and tunable speed of light [25]. By modulating the coupling between the resonators one can also imprint a nontrivial phase in the hopping amplitudes. This phase chosen in a way that it mimics the presence of a synthetic magnetic field for the photons [24]. In this way such photonic structures can be used to simulate the physics of electrons in strong magnetic fields and all the physics related to the quantum Hall effect [26] and fractional quantum Hall effect [27]. From this analogy with charged particles in a magnetic field, where the Lorentz force bends its trajectory into a loop, we also see the photons in such topological lattices move in circles, rather than light-rays.

One can immediately understand that a photon emitted in such an environment cannot really escape. The emitted photon must be reabsorbed by the atom, once the cyclotron trajectory is completed. The consequence is that the spontaneous emission is broken, and replaced by a bound state, in which the photon "orbits" forever around the atom.

The driving motivation behind this part of the thesis comes from very recent experiments where artificial emitters are placed on the edge of a topological photonic system [28, 29]. In these kind of experiments the light-matter interactions enable one to use the platform for chiral quantum optical purposes [30]. In almost all these recent works the photonic bulk modes are barely considered, and the focus is mostly on the edge physics. In this thesis we show that the coupling of atoms or other emitters to the circulating bulk photons gives rise to a much richer physics dominated by non-Markovian and strong coupling effects. Specifically, we will discuss the properties of a new type of quasi-particles that form under such conditions, which we named Landau-Photon Polaritons (LPP).

Outline of the thesis

This thesis summarises my scientific contributions achieved during the five years of my PhD. The thesis is essentially split in two parts: the first five chapters (Ch. 1-5) are devoted to the study of the ultra-strong coupling regime in cavity QED, while the last chapter (Ch. 6) is about light-matter interactions with topological photons.

Ch. 1 and 2 discuss the main approximations used to derive a minimal toy model to describe cavity QED under non-perturbative light-matter coupling. In particular in Ch. 1 we review the quantisation of the electromagnetic field and its coupling with non-relativistic matter. Starting from Maxwell's equations we try to take the simplest path to arrive at the generic electromagnetic Hamiltonian in Coulomb gauge. Then we perform a series of approximation and we switch to the so-called dipole gauge to finally arrive at the general form of a light-matter Hamiltonian for a single cavity mode, but keeping all the electrostatic contributions.

In Ch. 2 we focus in a next step on how to simplify the matter description in presence of a single electromagnetic mode. In particular we reinvestigate the common *two-level truncation*, where we just keep two levels of every microscopic matter constituents. We show that this approximation is critically sensitive to the gauge choice when the light-matter coupling is strong enough and we proof that this approximation is most accurate in the dipole gauge.

In Ch. 3 we discuss a concrete implementation of our abstract cavity QED models. We consider an LC circuit, where the capacitor is filled by dipolar matter. The matter is described by an ensemble of dipoles fixed on a grid, with dipole moment always perpendicular to the capacitor plates. Such a toy model is very helpful to visualise what is going on in such a system when the coupling is ultra-strong and to provide a simple physical intuition. A particular emphasis is placed on the treatment of electrostatic dipole-dipole interactions in the presence of boundaries, which becomes highly relevant for predicting the properties of dense ensembles of dipoles.

In Ch. 4 we present the main novel predictions of our cavity QED model by analysing in detail its ground state phases. In particular, we point out the distinction between electrostatic effects and "pure quantum corrections", establishing what is the correct parameter regime to have one or the others as the most relevant contribution.

In Ch. 5 we proceed by generalising these considerations for the ground states to equilibrium states at fixed temperature T. We then discuss some of the most interesting thermodynamic features that a cavity QED system exhibits in the ultra-strong coupling regime, again pointing out the distinction between basic electrostatic effects and genuine quantum corrections.

Finally in Ch. 6 we change the subject from ultrastrong coupling to light-matter interactions in topological photonic systems. After having introduced the concept of a synthetic magnetic field for photons, we discuss the coupling between these topological photons and an ensemble of atoms, or other types of quantum emitters. We show how the common spontaneous emission is completely replaced by the formation of chiral atom-photon bound states, giving rise to the concept of Landau-photon polariton. Having multiple atoms and multiple photons in this platform can lead to new interesting physics, becoming a prototype of a tunable quantum simulator for the fractional quantum Hall effect, for instance.

List of publications

The thesis is based on the following peer-reviewed articles:

PHYSICAL REVIEW A 97, 043820 (2018) [31]

Cavity quantum electrodynamics in the non-perturbative regime

Daniele De Bernardis, Tuomas Jaako, and Peter Rabl

We study a generic cavity-QED system where a set of (artificial) two-level dipoles is coupled to the electric field of a single-mode LC resonator. This setup is used to derive a minimal quantum mechanical model for cavity QED, which accounts for both dipole-field and direct dipole-dipole interactions. The model is applicable for arbitrary coupling strengths and allows us to extend the usual Dicke model into the non-perturbative regime of QED, where the dipole-field interaction can be associated with an effective finestructure constant of order unity. In this regime, we identify three distinct classes of normal, superradiant and subradiant vacuum states and discuss their characteristic properties and the transitions between them. Our findings reconcile many of the previous, often contradictory predictions in this field and establish a common theoretical framework to describe ultrastrong coupling phenomena in a diverse range of cavity-QED platforms.

PHYSICAL REVIEW A 98, 053819 (2018) [32]

Breakdown of gauge invariance in ultrastrong-coupling cavity QED

Daniele De Bernardis, Philipp Pilar, Tuomas Jaako, Simone De Liberato, and Peter Rabl

We revisit the derivation of Rabi- and Dicke-type models, which are commonly used for the study of quantum light-matter interactions in cavity and circuit QED. We demonstrate that the validity of the two-level approximation, which is an essential step in this derivation, depends explicitly on the choice of gauge once the system enters the ultrastrong coupling regime. In particular, while in the electric dipole gauge the two-level approximation can be performed as long as the Rabi frequency remains much smaller than the energies of all higher-lying levels, it can dramatically fail in the Coulomb gauge, even for systems with an extremely anharmonic spectrum. We extensively investigate this phenomenon both in the single-dipole (Rabi) and multi-dipole (Dicke) case, and considering the specific examples of dipoles confined by double-well and by square-well potentials, and of circuit QED systems with flux qubits coupled to an LC resonator.

Quantum 4, 335 (2020) [33]

Thermodynamics of ultrastrongly coupled light-matter systems

Philipp Pilar, Daniele De Bernardis, and Peter Rabl

We study the thermodynamic properties of a system of two-level dipoles that are coupled ultrastrongly to a single cavity mode. By using exact numerical and approximate analytical methods, we evaluate the free energy of this system at arbitrary interaction strengths and discuss strong-coupling modifications of derivative quantities such as the specific heat or the electric susceptibility. From this analysis we identify the lowest-order cavity-induced corrections to those quantities in the collective ultrastrong coupling regime and show that for even stronger interactions the presence of a

single cavity mode can strongly modify extensive thermodynamic quantities of a large ensemble of dipoles. In this non-perturbative coupling regime we also observe a significant shift of the ferroelectric phase transition temperature and a characteristic broadening and collapse of the black-body spectrum of the cavity mode. Apart from a purely fundamental interest, these general insights will be important for identifying potential applications of ultrastrong-coupling effects, for example, in the field of quantum chemistry or for realizing quantum thermal machines.

SciPost Phys. 9, 066 (2020) [34]

The Vacua of Dipolar Cavity Quantum Electrodynamics

Michael Schuler, Daniele De Bernardis, Andreas M. Läuchli and Peter Rabl

The structure of solids and their phases is mainly determined by static Coulomb forces while the coupling of charges to the dynamical, i.e., quantized degrees of freedom of the electromagnetic field plays only a secondary role. Recently, it has been speculated that this general rule can be overcome in the context of cavity quantum electrodynamics (QED), where the coupling of dipoles to a single field mode can be dramatically enhanced. Here we present a first exact analysis of the ground states of a dipolar cavity QED system in the non-perturbative coupling regime, where electrostatic and dynamical interactions play an equally important role. Specifically, we show how strong and long-range vacuum fluctuations modify the states of dipolar matter and induce novel phases with unusual properties. Beyond a purely fundamental interest, these general mechanisms can be important for potential applications, ranging from cavity-assisted chemistry to quantum technologies based on ultrastrongly coupled circuit QED systems.

PHYSICAL REVIEW LETTERS 126, 103603 (2021) [35]

Light-Matter Interactions in Synthetic Magnetic Fields: Landau-Photon Polaritons

Daniele De Bernardis, Ze-Pei Cian, Iacopo Carusotto, Mohammad Hafezi, and Peter Rabl

We study light-matter interactions in two-dimensional photonic systems in the presence of a spatially homogeneous synthetic magnetic field for light. Specifically, we consider one or more two-level emitters located in the bulk region of the lattice, where for increasing magnetic field the photonic modes change from extended plane waves to circulating Landau levels. This change has a drastic effect on the resulting emitter-field dynamics, which becomes intrinsically non-Markovian and chiral, leading to the formation of strongly coupled Landau-photon polaritons. The peculiar dynamical and spectral properties of these quasiparticles can be probed with state-of-the-art photonic lattices in the optical and the microwave domain and may find various applications for the quantum simulation of strongly interacting topological models.

Chapter 1

Light-matter interactions in dipolar systems

In this chapter we review the main aspects of non-relativistic light-matter interactions, and introduce the general theoretical framework used throughout this thesis: light-matter interactions with electric dipoles. Dipolar transitions are probably the simplest processes that manifest the interaction between matter and the electromagnetic field at the microscopic level. Indeed the interest in this subject has never stopped since the advent of quantum mechanics. Despite its simplicity, it can still lead to arbitrary complicated problems, making additional approximations necessary. While in the regime of weak interactions of the use the two-level or single-mode approximations is frequently employed, the same approximations become very subtle for larger coupling strength and have led in the past to many inconsistent predictions. For this reason we focus the entire first three chapters of this thesis on the derivation of an effective theory for light-matter interactions, keeping track of every approximation, transformation and change in representation. The idea is to arrive at the end of Ch. 3 with a minimal Hamiltonian which describes an ensemble of dipoles inside a resonant cavity, but remaining "continuously" connected to the original theory, and providing physical intuition.

We start this chapter by briefly reviewing the quantization of the electromagnetic field in the Coulomb gauge. We take a very pragmatic approach, starting from Maxwell's equations and introducing the scalar and vector potentials. The Coulomb gauge condition arises very naturally in order to be able to solve Maxwell's equations in their potential formulation. After imposing the Coulomb gauge, we derive a light-matter Lagrangian and consequently its related Hamiltonian. In doing so we need to take care of the constraint we imposed to fix the gauge, which leads to the definition of longitudinal and transverse delta functions. In our approach we do not pass through the standard relativistic treatment, introducing the anti-symmetric tensor $F_{\mu\nu}$, nor will we discuss the theory of Dirac's constraints when we introduce the canonical formalism. Indeed, in this context, these are

just unnecessary mathematical sophistications. For a general treatment we refer to [36]. To proceed, we switch to the so-called *dipolar gauge*, and we treat the paradigmatic example of a system made of point-like positive and negative charges, localised in regions where the total charge sum up to zero, which in the end is just a general way to introduce the concept of point-like dipoles. In this framework we discuss the role of the direct Coulomb interaction, which, in this gauge, is absorbed into the definition of the dynamical field.

We close this chapter by discussing the electrostatic and radiation limits in the Coulomb and the dipolar gauge and how to finally arrive at an approximated description, which interpolates between these two limiting cases.

1.1 Maxwell's equations and the Coulomb gauge Lagrangian

All classical electromagnetic phenomena known so far are explained by Maxwell's equations:

$$\vec{\nabla}\cdot\vec{E} = \frac{\rho}{\varepsilon_0} \tag{1.1}$$

$$\vec{\nabla}\times\vec{B} = \frac{1}{c^2}\left(\frac{\vec{J}}{\varepsilon_0} + \frac{\partial}{\partial t}\vec{E}\right) \tag{1.2}$$

$$\vec{\nabla}\cdot\vec{B} = 0 \tag{1.3}$$

$$\vec{\nabla}\times\vec{E} = -\frac{\partial}{\partial t}\vec{B} \tag{1.4}$$

where $\vec{E}$ and $\vec{B}$ are the electric and the magnetic field, respectively, and ρ and $\vec{J}$ are the density of charge and its current. Taking the divergence of Eq. (1.2), we see that consistency of Maxwell equations enforces the charge conservation

$$\frac{\partial}{\partial t}\rho + \vec{\nabla}\cdot\vec{J} = 0. \tag{1.5}$$

From now on, we will take Maxwell's equations as a starting axiom, from which we will derive the quantum theory of the electromagnetic field. In order to switch to the canonical formalism and to unambiguously determine the relevant degrees of freedom, we need to introduce the scalar and the vector potential, Φ and $\vec{A}$, which satisfy

$$\vec{E} = -\vec{\nabla}\Phi - \frac{\partial}{\partial t}\vec{A}, \qquad \vec{B} = \vec{\nabla}\times\vec{A}. \tag{1.6}$$

Using this definition we see that the so-called structural equations (1.3), (1.4) are identically satisfied. In a relativistic context this is the so called *Bianchi's identity* [36]. Instead the other two

equations give

$$\begin{aligned} \frac{\partial^2}{\partial t^2}\vec{A} &= -c^2\vec{\nabla}\times\vec{\nabla}\times\vec{A} + \frac{1}{\varepsilon_0}\left(\vec{J} - \varepsilon_0\vec{\nabla}(\partial_t\Phi)\right), \\ -\nabla^2\Phi &= \frac{1}{\varepsilon_0}\left(\rho + \varepsilon_0\frac{\partial}{\partial t}\vec{\nabla}\cdot\vec{A}\right). \end{aligned} \tag{1.7}$$

At this point we must fix the gauge. Indeed the above equations cannot be solved without a further constraint on the potentials. This can be intuitively understood by the fact that the functional map defined by equations (1.6) is not injective in Φ and $\vec{A}$. Indeed all potentials given by $\Phi = -\partial_t f$, and $\vec{A} = \vec{\nabla} f$ (where f is a sufficiently smooth function) generate the zero field solution. While we can in principle invert Maxwell's equations in order to express the fields in terms of their sources, this is no longer possible when we introduce the potentials. To circumvent this problem we just need to make the "potential map" injective. The usual strategy here is to reduce the domain from which we pick our potentials, introducing a new constraint on their choice. One possibility to do so is to impose the standard Coulomb gauge condition,

$$\vec{\nabla}\cdot\vec{A} = 0. \tag{1.8}$$

Considering the vector calculus identity $\vec{\nabla}\times\vec{\nabla}\times\vec{A} = -\nabla^2\vec{A} + \vec{\nabla}(\vec{\nabla}\cdot\vec{A})$, we are finally able to re-write Maxwell's equations as

$$\begin{aligned} -\nabla^2\vec{A} + \frac{1}{c^2}\frac{\partial^2}{\partial t^2}\vec{A} &= \frac{1}{\varepsilon_0 c^2}\left(\vec{J} - \varepsilon_0\vec{\nabla}(\partial_t\Phi)\right), \\ -\nabla^2\Phi &= \frac{\rho}{\varepsilon_0}. \end{aligned} \tag{1.9}$$

Note that the scalar potential Φ is not a dynamical degree of freedom, it doesn't have a second order time derivative involved in the equations of motion. Consequently, given a charge distribution and boundary conditions, we can find the *electrostatic* scalar potential introducing the Green's function of the Laplace operator

$$-\nabla^2 G(\vec{r},\vec{r}\,') = \delta^{(3)}(\vec{r}-\vec{r}\,'). \tag{1.10}$$

The scalar potential follows as

$$\Phi(\vec{r}) = \frac{1}{\varepsilon_0}\int d^3r' G(\vec{r},\vec{r}\,')\rho(\vec{r}\,'). \tag{1.11}$$

Now we can eliminate the electrostatic potential from the equations, making it clear which are the real dynamical degrees of freedom. To do so we make use of the continuity equation (1.5) and the

identity $\Phi\vec{\nabla}\cdot\vec{J} = \vec{\nabla}\cdot(\Phi\vec{J}) - \vec{\nabla}\Phi\cdot\vec{J}$, from which we obtain

$$\frac{\partial}{\partial t}\Phi = \frac{1}{\varepsilon_0}\int d^3r'\vec{\nabla}'G(\vec{r},\vec{r}')\cdot\vec{J}(\vec{r}'), \tag{1.12}$$

where ∇' is the gradient with respect to $\vec{r}'$, and where we considered a vanishing current (and Green's function) on the boundary. At the end we find that the dynamical degrees of freedom of the electromagnetic field are fully determined by the equation

$$-\nabla^2\vec{A} + \frac{1}{c^2}\frac{\partial^2}{\partial t^2}\vec{A} = \frac{1}{\varepsilon_0 c^2}\left(\vec{J} - \int d^3r'\vec{\nabla}\vec{\nabla}'G(\vec{r},\vec{r}')\cdot\vec{J}(\vec{r}')\right), \tag{1.13}$$

together with the Coulomb gauge condition. We can immediately see that in the right-hand-side (RHS) of the equation there appears a modified current, the *transverse current*. It can be written in coordinates as $J^i_\perp = \sum_j \int d^3r'\delta^\perp_{ij}(\vec{r},\vec{r}')J^j(\vec{r}')$, where we introduced the *generalised transverse delta function* [37, 22]

$$\delta^\perp_{ij}(\vec{r},\vec{r}') = \delta_{ij}\delta^{(3)}(\vec{r}-\vec{r}') - \frac{\partial^2}{\partial r^i \partial r'^j}G(\vec{r},\vec{r}'). \tag{1.14}$$

The generalised transverse delta function is a projector, that projects any vector field in the subspace of divergenceless vector fields. It ensures that the Coulomb gauge condition is always respected. We will see in the next section that the generalised transverse delta is a crucial concept to derive the canonical formalism and finally to quantize electromagnetism.

After this long tour of formal manipulation of the Maxwell's equations, we arrive to the goal of this first section: the general Lagrangian density of electromagnetism in Coulomb gauge

$$\mathcal{L}_{\text{Coulomb}} = \frac{\varepsilon_0}{2}\left(|\dot{\vec{A}}|^2 + c^2\vec{A}\cdot\nabla^2\vec{A}\right) + \vec{J}_\perp\cdot\vec{A} - \frac{1}{\varepsilon_0}\rho\, G\star\rho + \mathcal{L}_{\text{Matter}}, \tag{1.15}$$

where we keep implicit the dependence on $\vec{r}$. The Lagrangian is then given by $L = \int d^3r\mathcal{L}(\vec{r})$. We also introduce the short-hand notation $\rho\, G\star\rho = \rho(\vec{r})\int d^3r'G(\vec{r},\vec{r}')\rho(\vec{r}')$, which is nothing else than the usual Coulomb interaction, just written in a general form.

1.2 The Coulomb gauge Hamiltonian

Given the Lagrangian density above we can use the Legendre transform to derive the corresponding Hamiltonian. The procedure is rather standard and we don't report it here. The resulting Hamiltonian density is

$$\mathcal{H}_{\text{Coulomb}} = \frac{|\vec{\Pi}|^2}{2\varepsilon_0} - \frac{\varepsilon_0 c^2}{2}\vec{A}\cdot\nabla^2\vec{A} - \vec{J}_\perp\cdot\vec{A} + \frac{1}{\varepsilon_0}\rho\, G\star\rho + \mathcal{H}_{\text{Matter}}, \tag{1.16}$$

where the canonical momentum of the vector potential is just the transverse component of the electric field

$$\vec{\Pi} = \varepsilon_0 \dot{\vec{A}}. \tag{1.17}$$

Naturally, also the transverse current and the matter Hamiltonian must be expressed using the appropriate canonical momenta of the matter's degrees of freedom. We will come back to this point later below. What is really important is that we finally have the Hamiltonian of the electromagnetic field, coupled with a certain non-relativistic system of charges (continuous or discrete), from which we can derive its quantized theory. In order to do so we need to impose the *canonical commutation relations*. A naive approach would suggest us to just impose

$$[A_i(\vec{r}), \Pi_j(\vec{r}\,')] = i\hbar\delta_{ij}\delta^{(3)}(\vec{r} - \vec{r}\,'), \tag{1.18}$$

but this isn't quite right. Indeed it is inconsistent with the Coulomb gauge condition $\vec{\nabla} \cdot \vec{A} = 0$, as one can directly verify from the equation above. This inconsistency comes from the fact that we are quantising the theory in a constrained domain. A full mathematical explanation would require, as already mentioned, the theory of Dirac's brakets in presence of constraints, but for our purposes it is sufficient to fix it "by hand". Indeed we see that the left-hand-side (LHS) of equation (1.18) contains operators (fields, in case of Poisson brakets) that are defined in the "transverse space". The RHS instead is defined everywhere. If we multiply both sides by the transverse delta function the RHS remains the same, while the LHS becomes the transverse delta function itself. So we found the correct commutation relations

$$[A_i(\vec{r}), \Pi_j(\vec{r}\,')] = i\hbar\delta^{\perp}_{ij}(\vec{r}, \vec{r}\,'). \tag{1.19}$$

We can now consider the following normal mode expansion, which holds in bounded domains

$$\begin{aligned} \vec{A}(t, \vec{r}) &= \frac{1}{\sqrt{\varepsilon_0 V}} \sum_{k,\lambda} q_{k,\lambda}(t) \vec{f}^{k,\lambda}(\vec{r}), \\ \vec{\Pi}(t, \vec{r}) &= \sqrt{\frac{\varepsilon_0}{V}} \sum_{k,\lambda} P_{k,\lambda}(t) \vec{f}^{k,\lambda}(\vec{r}), \end{aligned} \tag{1.20}$$

where we make explicit the sum over the eigenvalues index k and the sum over the different polarizations $\lambda = 1, 2$, V is the total quantization volume. The normal modes are eigenfunctions of the Laplace operator $-\nabla^2 \vec{f}^{k,\lambda} = \omega_k^2/c^2 \vec{f}^{k,\lambda}$, together with the Coulomb gauge constraint $\vec{\nabla} \cdot \vec{f}^{k,\lambda} = 0$, which reduces the independent polarizations from three to two. These normal modes are orthogonal,

but they don't sum up to a delta function, as usual, but rather to the transverse delta function

$$\begin{aligned} \frac{1}{V}\int d^3r \vec{f}^{k,\lambda}(\vec{r})\cdot\vec{f}^{k',\lambda'}(\vec{r}) &= \delta_{kk'}\delta_{\lambda\lambda'}, \\ \frac{1}{V}\sum_{n,\lambda} f_i^{k,\lambda}(\vec{r}) f_j^{k,\lambda}(\vec{r}\,') &= \delta_{ij}^{\perp}(\vec{r},\vec{r}\,'). \end{aligned} \tag{1.21}$$

To respect the commutation relations (1.19), we impose $[q_{k,\lambda}, P_{k',\lambda'}] = i\hbar\delta_{k,k'}\delta_{\lambda,\lambda'}$. Using this expansion we can see that the purely electromagnetic part of our Coulomb Hamiltonian is nothing more than a set of harmonic oscillators

$$H_{\text{E.m.}} = \sum_{k,\lambda}\frac{P_{k,\lambda}^2}{2} + \frac{\omega_k^2}{2}q_{k,\lambda}^2 = \sum_{k,\lambda}\omega_k a_{k,\lambda}^\dagger a_{k,\lambda}, \tag{1.22}$$

where $a_{k,\lambda} = q_{k,\lambda}\sqrt{\omega_k/2} - iP_{k,\lambda}/\sqrt{2\omega_k}$. From here on, we use a short notation, where we absorb the polarization index λ in the mode index k. We also use $\hbar = 1$ in all main equations and in the expression of Hamiltonians, while we keep regular units for other quantities where the scaling with $\hbar$ is non obvious. In general we use "frequency" as a synonym of "energy".

1.3 Localised neutral system of charges: the dipole Hamiltonian

After having developed the correct formalism to describe light-matter interactions in a generic non-relativistic system (bounded or unbounded), we introduce here a few new assumptions, which lead to the final approximated form of the light-matter Hamiltonian that we will use for the rest of this thesis. We restrict ourself here to the case of neutral systems, such as molecules or electron-hole pairs in semiconductors. Then we focus on the cases in which the short wavelengths of the electrodynamic field can be neglected. This leads us to the *long wavelength approximation*. Finally we introduce the dipole Hamiltonian.

Let us consider a system of localised regions containing an equal amount of negative and positive charges, where the distance between different regions R_{AB} is much larger than their own size ξ, as schematically depicted in Fig. 1.1. As in the main textbooks [18, 38], we consider for simplicity a system in which we have just two separated subsets of charges A/B, but the generalisation to other sets of charges is straightforward. In the generic Coulomb Hamiltonian density (1.16) we consider $\rho(\vec{r}) = \sum_i q_i\delta^{(3)}(\vec{r}-\vec{r}_i)$, and $\vec{J}(\vec{r}) = \sum_i q_i\dot{\vec{r}}_i\delta^{(3)}(\vec{r}-\vec{r}_i)$, where q_i is the charge of the i-th particle.

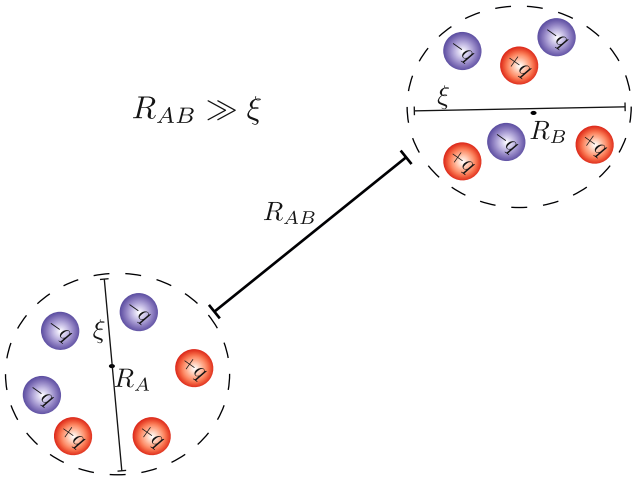

Figure 1.1: A sketch of a system in which charges are well localised in two well separated regions in space.

The total Coulomb Hamiltonian becomes

$$\begin{aligned} H_C = &\sum_{\alpha\in A} \frac{1}{2m_\alpha}\left[\vec{p}_\alpha - q_\alpha \vec{A}(\vec{R}_A)\right]^2 + \sum_{\beta\in B} \frac{1}{2m_\beta}\left[\vec{p}_\beta - q_\beta \vec{A}(\vec{R}_B)\right]^2 \\ &+ V^{AA}_{Coul.} + V^{BB}_{Coul.} + V^{AB}_{Coul.} \\ &+ \sum_k \omega_k \left(a_k^\dagger a_k + \frac{1}{2}\right), \end{aligned} \tag{1.23}$$

where we make the fundamental assumption that the vector potential does not change on a length scale on the order of the localised region's size or smaller. This allows us to replace the particle's position inside the vector potential with the center of mass position of the whole neutral spot, $\vec{A}(\vec{r}_\alpha) \approx \vec{A}(\vec{R}_A)$. The canonical momentum of each particle is then given by

$$\vec{p}_\alpha = m_\alpha \dot{\vec{r}}_\alpha + q_\alpha \vec{A}(\vec{R}_A), \tag{1.24}$$

which is different from its kinetic momentum. We also introduce the standard notation for the Coulomb electrostatic potential $\frac{1}{\varepsilon_0}\rho G \star \rho = V^{AA}_{Coul.} + V^{BB}_{Coul.} + V^{AB}_{Coul.}$, where $V^{AA\,(BB)}_{Coul.}$ contains all the terms that represent the Coulomb interactions between charges of the same region and $V^{AB}_{Coul.}$ the cross terms between the different regions. To stay consistent with the long-wavelength approximation introduced in the vector potential, we need to introduce it also in this Coulomb cross term. Because of the assumption of having distant localised regions, centred on $\vec{R}_X$ (where $X = A, B...$ labels the possible spots), the position of each charge can be rewritten as $\vec{r}_\alpha = \delta\vec{r}_\alpha + \vec{R}_A$. The displacement from the center of mass position $\vec{R}_A$ is intended to be small, so we can expand $V^{AB}_{Coul.}$

to lowest order, and obtain

$$\begin{aligned} V^{AB}_{Coul.} &= \sum_{\alpha\in A,\beta\in B} q_\alpha q_\beta \frac{G(\vec{r}_\alpha,\vec{r}_\beta)}{\varepsilon_0} + \alpha \leftrightarrow \beta \\ &\approx \frac{1}{2\varepsilon_0}\sum_{i,j}\mu^i_A\mu^j_B \left.\frac{\partial^2 G}{\partial r_i \partial r'_j}\right|_{\vec{R}_A,\vec{R}_B} + \alpha \leftrightarrow \beta + O(\delta r^3), \end{aligned} \tag{1.25}$$

where all the terms of lower order gives exactly zero contribution because of the charge neutrality condition. We introduced the dipole's moment of each localised region,

$$\vec{\mu}_{A(B)} = \sum_{\alpha\in A(B)} q_\alpha \delta\vec{r}_\alpha. \tag{1.26}$$

Note that the kernel of the AB-Coulomb interaction, under the long-wavelength approximation, is proportional to the complement of the transverse delta function defined in (1.14). This term can be called *longitudinal delta function*

$$\delta^{\parallel}_{ij}(\vec{r},\vec{r}') = \left.\frac{\partial^2 G}{\partial r_i \partial r'_j}\right|_{\vec{r},\vec{r}'} = \delta_{ij}\delta^{(3)}(\vec{r}-\vec{r}') - \delta^{\perp}_{ij}(\vec{r},\vec{r}'). \tag{1.27}$$

Comments on H_C:

- A and B denotes the two subsets of charges, always well separated. In each subset we have M_A (M_B) charges, each of them with arbitrary charge $q_\alpha \in \mathbb{R}$ and arbitrary mass $m_\alpha > 0$. The two subsets are electrically neutral $\sum_{\alpha\in A,B} q_\alpha = 0$.

- Under the long wave-length approximation we assume that the electromagnetic vector potential $\vec{A}$ is constant across each subset. In each subset its value is approximated by the value that it takes in the center of mass $\vec{R}_A$, $\vec{R}_B$. This means that we are actually following the modes of the electromagnetic field in which the wave-length is much larger than the typical size of each subset.

- We neglect the motional degrees of freedom of the center of mass of A and B. Including motional degrees of freedom for centres of mass makes everything more complicated, but, in the (reasonable) regime in which we have a decoupling of energy scales, it doesn't change the general picture that we are going to develop in the next sections.

- The interaction between the charges inside each subset is just the instantaneous Coulomb force, given by $V^{AA}_{Coul.}$, $V^{BB}_{Coul.}$. This follows again from the long wave-length approximation. We are looking for events that take place at larger distances, everything that happens inside each subset's spot can be considered instantaneous.

- As usual in the Coulomb gauge, we have a *residual* instantaneous interaction between A and B, $V^{AB}_{Coul.}$, on top of the photon-mediated one. In free space, this term has the shape of dipole-dipole interaction between A and B,

$$V^{AB}_{Coul.} = \frac{1}{4\pi\varepsilon_0}\left(\frac{\vec{\mu}_A\cdot\vec{\mu}_B}{R^3_{AB}} - \frac{3(\vec{\mu}_A\cdot\vec{R}_{AB})(\vec{\mu}_B\cdot\vec{R}_{AB})}{R^5_{AB}}\right), \tag{1.28}$$

  where $\vec{R}_{AB}$ is the distance between the two centres of mass. More generally this term is proportional to the longitudinal delta function, which is defined by the Laplace Green's function. In App. A one can find all the details about the Laplace Green's function in bounded domains, with the full calculation of the case in which the system is confined between two parallel mirrors.

As it will become clear later in the next chapters, the Coulomb gauge is not the best gauge to perform calculations of light-matter interactions (actually in the early days of electrodynamics it was introduced to describe radiation from a far-away source, that is why it is also called *radiation-gauge* [39]) and it can cause some problems in the quantum mechanical framework [32]. So it is preferable to pick a more convenient and intuitive gauge: the dipole gauge. Starting from (1.23), we implement the gauge-change by a canonical transformation given by the generating function

$$F(\vec{r}_\alpha,\vec{A}) = \vec{\mu}_A\cdot\vec{A}(\vec{R}_A) + \vec{\mu}_B\cdot\vec{A}(\vec{R}_B). \tag{1.29}$$

In the Hilbert space, it would correspond to making a unitary transformation

$$U = \exp\left[-\frac{i}{\hbar}F\right]. \tag{1.30}$$

The effect of this transformation is just to displace the canonical momenta of both the particles and the electromagnetic field:

$$\begin{aligned} U\vec{\Pi}(\vec{r})U^\dagger &= \vec{\Pi}(\vec{r}) - \frac{i}{\hbar}\left[\int d^3r'\vec{P}(\vec{r}')\cdot\vec{A}(\vec{r}'),\vec{\Pi}(\vec{r})\right] = \vec{\Pi}(\vec{r}) + \vec{P}^{\perp}(\vec{r}) \\ U\vec{p}_{\alpha(\beta)}U^\dagger &= \vec{p}_{\alpha(\beta)} - \frac{i}{\hbar}\left[\int d^3r'\vec{P}(\vec{r}')\cdot\vec{A}(\vec{r}'),\vec{p}_{\alpha(\beta)}\right] = \vec{p}_{\alpha(\beta)} + q_{\alpha(\beta)}\vec{A}(\vec{R}_{A(B)}), \end{aligned} \tag{1.31}$$

where we have introduced the polarization density $\vec{P}(\vec{r}) = \vec{P}(\vec{r})_A + \vec{P}(\vec{r})_B = \sum_\alpha \vec{\mu}_\alpha\delta^{(3)}(\vec{r}-\vec{R}_\alpha) + \sum_\beta \vec{\mu}_\beta\delta^{(3)}(\vec{r}-\vec{R}_\beta)$. It is worth noticing that the new canonical momentum of the electromagnetic field is displaced by the transverse part of the polarization density. This is due to the constrained commutation relations (1.19) described in the previous section. After the transformation the new canonical momentum of the particles coincide with their kinetic momentum, $\vec{p}\,'_{\alpha(\beta)} = m_{\alpha(\beta)}\dot{\vec{r}}_{\alpha(\beta)}$,

while the momentum of the electromagnetic field no longer describes the transverse part of the electric field $\vec{E}$, but rather the *displacement field*, $\vec{D}$ [39]. Using the polarization density we can rewrite the direct Coulomb interaction between A and B as

$$V^{AB}_{Coul.} = \frac{1}{\varepsilon_0}\int d^3r' \vec{P}^{\parallel}_A(\vec{r}') \cdot \vec{P}^{\parallel}_B(\vec{r}'). \tag{1.32}$$

This term is non-local, and makes distant dipoles to interact. However, we see that when we expand the square of the new canonical momentum of the electromagnetic field, another similar term pops up in the new Hamiltonian, which is given by $\sim 1/\varepsilon_0 \int d^3r' \vec{P}^{\perp}_A(\vec{r}') \cdot \vec{P}^{\perp}_B(\vec{r}')$. When we sum up the two terms we get a new, completely local, term $\sim 1/\varepsilon_0 \int d^3r' \vec{P}_A(\vec{r}') \cdot \vec{P}_B(\vec{r}') \approx 0$. This term is zero because of the assumption of having localised regions. The resulting Hamiltonian is [18, 38]

$$\begin{aligned} H_D \approx & \left[\sum_\alpha \frac{\vec{p}_\alpha^{\,2}}{2m_\alpha} + V^{AA}_{Col.} + \epsilon^{A}_{dip.}\right] + \left[\sum_\beta \frac{\vec{p}_\beta^{\,2}}{2m_\beta} + V^{BB}_{Col.} + \epsilon^{B}_{dip.}\right] + \sum_k \omega_k a_k^\dagger a_k \\ & - \vec{\mu}_A \cdot \frac{\vec{D}(\vec{R}_A)}{\varepsilon_0} - \vec{\mu}_B \cdot \frac{\vec{D}(\vec{R}_B)}{\varepsilon_0}, \end{aligned} \tag{1.33}$$

where the dipolar self energies are $\epsilon^{A(B)}_{dip.} = 1/(2\varepsilon_0)\int d^3r' |\vec{P}^{\perp}_{A(B)}(\vec{r}')|^2$. The electromagnetic part takes again the shape of a set of harmonic oscillators:

$$H_{EM} = \int d^3r \frac{|\vec{D}(\vec{r})|^2}{2\varepsilon_0} + \frac{\varepsilon_0 c^2}{2}|\vec{B}(\vec{r})|^2 = \sum_k \omega_k a_k^\dagger a_k, \tag{1.34}$$

where

$$\vec{D}(\vec{r}) = -\sqrt{\frac{\varepsilon_0}{2V}}\sum_k \sqrt{\omega_k} i (a_k - a_k^\dagger)\vec{f}^{\,k}(\vec{r}), \tag{1.35}$$

and

$$\vec{A}(\vec{r}) = \sqrt{\frac{1}{2\varepsilon_0 V}}\sum_k \sqrt{\frac{1}{\omega_k}}(a_k + a_k^\dagger)\vec{f}^{\,k}(\vec{r}). \tag{1.36}$$

We can immediately generalise the result to the N-dipoles case from which we get the very general structure

$$\boxed{H = \sum_{i=1}^{N} H^i_m + H_{EM} - \sum_{i=1}^{N} \vec{\mu}_i \cdot \frac{\vec{D}(\vec{R}_i)}{\varepsilon_0}}. \tag{1.37}$$

(See App. B for an equivalent derivation valid also in the polarization continuum limit).

Comments on H_D:

- The light-matter interaction is now completely local. No residual dipole-dipole interactions between A and B are present [18, 38]. The interaction between A and B is now fully mediated by the electromagnetic field, which is represented by the vector potential and its canonical

momentum, the electric displacement.

- A photon is not always a photon. The annihilation (creation) operator a_k has a different physical meaning than in the Coulomb gauge, because of the transformation of the canonical momentum of the electromagnetic field.

- The new dipole Hamiltonian gives infinite energies. The two dipole *self-energies* $\epsilon^A_{dip.}$ and $\epsilon^B_{dip.}$ require an explicit cut-off in the electromagnetic wavelengths, otherwise these quantities diverge. This is not surprising, since we are working in the long-wavelength limit, and a natural cut-off is given by the typical size of A and B. In this way it is possible to regularise these self-energies, which give a correction to the energy levels of each region, as one can see in [40]. Otherwise these terms are often simply dropped. In our treatment we keep these terms. We will see that they are automatically cancelled when the higher modes are adiabatically eliminated.

1.4 The electrostatic limit in different gauges

In this section we discuss the limit in which the dynamics of the electromagnetic field is much faster than the motion of the charges and what is left is just the usual electrostatic Coulomb interaction. The argument proposed here is mainly classical, but because it relies only on the structure of the Hamilton equations it can be generalised to the quantum case by using second order perturbation theory (see for instance Ch. 6 of [38]). Mathematically this can be quite cumbersome, so the aim of this section is primarily to develop a basic intuition about the meaning of the electrostatic limit in the Hamiltonian formalism.

In the Coulomb gauge it is clear that completely neglecting the dynamics of the electromagnetic field would only leave the electrostatic Coulomb interaction, which is the correct expected limit, when radiation effects are negligible. In order to explicitly see this, it would be sufficient to set $\vec{A} = 0$ and $\vec{\Pi} = 0$, and the Coulomb Hamiltonian would be reduced just to the matter Hamiltonian, together with the electrostatic Coulomb interaction.

On the other side, in the dipolar gauge, there is no obvious way to extract the electrostatic limit, since all the interactions are mediated by the dynamical field. Indeed taking $\vec{A} = 0$ and $\vec{\Pi}' = -\vec{D} = 0$ does not really work in this case, since it would give back just the non interacting matter Hamiltonian. The presence of the electrostatic Coulomb term even in the absence of radiation implies that in the dipolar gauge we need to relax the assumptions of zero field. The new assumption is that just the time derivative of the fields is zero, $\dot{\vec{A}} = 0$ and $\dot{\vec{D}} = 0$. Taking the Hamilton equations

for the electromagnetic field

$$\begin{aligned}\dot{\vec{A}} &= \frac{1}{\varepsilon_0}\left(\vec{\Pi}' + \vec{P}^{\perp}\right),\\ \dot{\vec{\Pi}}' &= \varepsilon_0 c^2 \nabla^2 \vec{A},\end{aligned} \tag{1.38}$$

and using the assumption of vanishing time derivative we have

$$\vec{\Pi}' = -\vec{P}^{\perp}, \tag{1.39}$$

where the transverse polarization shows up here as a consequence of the Poisson brakets (commutation relation) (1.19). We see now that reinserting this expression in the Hamiltonian (1.37), we obtain

$$H_D \xrightarrow{\text{electrostatic}} H_{\text{Matter}} - \frac{1}{2\varepsilon_0}\int d^3r |\vec{P}^{\perp}(\vec{r})|^2. \tag{1.40}$$

This correspond exactly to the correct Hamiltonian in the electrostatic limit. It is particularly insightful to explicitly work out the example of the two charge spots A and B:

$$\begin{aligned}H_D \approx &\left[\sum_\alpha \frac{\vec{p}_\alpha^{\,2}}{2m_\alpha} + V_{Col.}^{AA}\right] + \left[\sum_\beta \frac{\vec{p}_\beta^{\,2}}{2m_\beta} + V_{Col.}^{BB}\right]\\ &- \frac{1}{\varepsilon_0}\int d^3r \vec{P}_A^{\perp}(\vec{r})\cdot\vec{P}_B^{\perp}(\vec{r})\\ &+ \left(\epsilon_{dip.}^A + \epsilon_{dip.}^B - \frac{1}{2\varepsilon_0}\int d^3r |\vec{P}_A^{\perp}(\vec{r})|^2 - \frac{1}{2\varepsilon_0}\int d^3r |\vec{P}_B^{\perp}(\vec{r})|^2\right).\end{aligned} \tag{1.41}$$

The dipolar self energies in the third line identically vanish, while the second line gives

$$-1/\varepsilon_0 \int d^3r \vec{P}_A^{\perp}(\vec{r})\vec{P}_B^{\perp}(\vec{r}) = 1/\varepsilon_0 \int d^3r \vec{P}_A^{\parallel}(\vec{r})\vec{P}_B^{\parallel}(\vec{r}) = V_{Coul.}^{AB}. \tag{1.42}$$

This means that

$$H_D \approx \left[\sum_\alpha \frac{\vec{p}_\alpha^{\,2}}{2m_\alpha} + V_{Col.}^{AA}\right] + \left[\sum_\beta \frac{\vec{p}_\beta^{\,2}}{2m_\beta} + V_{Col.}^{BB}\right] + V_{Coul.}^{AB}, \tag{1.43}$$

as it has to be.

What can we say more about it? Electrodynamics is mainly characterised by radiation and electrostatic forces. Those two phenomena typically live in completely separated time scales, where electrostatics mainly reveals itself at very slow velocities, while radiation is typically relevant for fast degrees of freedom. This is also closely linked to a fundamental aspect of QED: the small value of the *fine structure constant* $\alpha_{\text{fs}} \simeq 1/137$, and the consequential perturbative character of QED. The

fine structure constant is indeed the fundamental adimensional constant that regulates light-matter interactions. It is worth noticing that this fundamental constant can be re-interpreted as the ratio between the Coulomb energy of two electrons at distance d between each other, and the energy to create a confined photon with wavelength $\sim 1/d$, (in SI units)

$$\alpha_{\rm fs} = \frac{e^2}{4\pi\varepsilon_0 c\hbar} = \frac{E_c}{E_{ph}} \simeq \frac{1}{137}, \tag{1.44}$$

where $E_c = e^2/(4\pi\varepsilon_0 d)$ and $E_{ph} = c\hbar/d$.

In the Coulomb gauge neglecting the radiation means to neglect the transverse part of the field, which is the dynamical degree of freedom of the electromagnetic field. So we can say that this gauge choice makes more explicit this two sides of electromagnetism, radiation and electrostatics. In the dipolar gauge on contrary the dynamical transverse field carries both radiation and electrostatic forces. Here the correct way to neglect radiation is evidently to take the limit in which the field is static, and then to adiabatically eliminate it.

1.5 Resonant processes in the electrostatic limit

The process of adiabatic elimination works properly provided that there are no resonances between the matter frequencies and the electromagnetic modes. If this is the case adiabatic elimination loses its meaning. However, it is still possible to have an intermediate situation, in which the matter system is resonant with the lowest mode of the electric field, but, because there are large energy gaps between the modes, we can either just neglect or adiabatically eliminate the higher modes, depending by the gauge we decide to use.

Again it is particularly insightful to see the outcome on our bipartite system. In the Coulomb gauge we have Hamiltonian (1.23). The vector potential is given by Eq. (1.36). It is now particularly important to notice that the vector potential scales with the inverse square root of the mode frequencies. If the matter system is mainly resonant with the lowest mode $k = c$ (labelled as *the cavity mode*), the other modes are off-resonant and also more weakly coupled. Here it depends a bit on the details of the problem, but in an ideal situation we can imagine that the other frequencies $\omega_{k\neq c}$ are so far detuned that their influence on the matter system is completely negligible (In Ch. 3 we discuss an explicit setup, where this is indeed the case). If so, we are left with the single mode Coulomb Hamiltonian

$$\begin{aligned} H_C \approx & \sum_{\alpha\in A}\left[\frac{1}{2m_\alpha}\left(\vec{p}_\alpha - q_\alpha \vec{A}_c(\vec{R}_A)\right)^2 + V^{AA}_{Coul.}\right] + \sum_{\beta\in B}\left[\frac{1}{2m_\beta}\left(\vec{p}_\beta - q_\beta \vec{A}_c(\vec{R}_B)\right)^2 + V^{BB}_{Coul.}\right] \\ & + V^{AB}_{Coul.} + \omega_c\left(a_c^\dagger a_c + \frac{1}{2}\right) \end{aligned} \tag{1.45}$$

where

$$\vec{A}_c(\vec{R}) = \sqrt{\frac{1}{2V\varepsilon_0\omega_c}}\vec{f}^c(\vec{R})(a_c + a_c^\dagger), \tag{1.46}$$

is the cavity mode vector potential. Now we can switch to the dipolar gauge just by adopting the gauge transformation given by

$$U = \exp\left[-\frac{i}{\hbar}F\right], \tag{1.47}$$

where

$$F = \sqrt{\frac{1}{2V\varepsilon_0\omega_c}}\left(\vec{\mu}_A \cdot \vec{f}^c(\vec{R}_A) + \vec{\mu}_B \cdot \vec{f}^c(\vec{R}_B)\right)(a_c + a_c^\dagger), \tag{1.48}$$

and $\vec{\mu}$ are the dipole moments, as defined in Eq. (1.26). The effect of this transformation is exactly the same as for the full dipolar gauge unitary, as in Eq. (1.31), and the resulting Hamiltonian is what we will call *the cavity QED Hamiltonian*

$$\begin{aligned} H^{AB}_{\text{cQED}} = {} & \omega_c\left(a_c^\dagger a_c + \frac{1}{2}\right) + \sum_{\alpha\in A}\left(\frac{\vec{p}_\alpha^{\,2}}{2m_\alpha} + V^{AA}_{Coul.}\right) + \sum_{\beta\in B}\left(\frac{\vec{p}_\beta^{\,2}}{2m_\beta} + V^{BB}_{Coul.}\right) \\ & + i\sqrt{\frac{\omega_c}{2V\varepsilon_0}}(a^\dagger - a)\sum_{i=A,B}\mu_i^c + \frac{1}{2V\varepsilon_0}\left(\sum_{i=A,B}\mu_i^c\right)^2 \\ & + V^{AB}_{Coul.}. \end{aligned} \tag{1.49}$$

Here to shorten the notation, we introduced the cavity-projected dipole moment

$$\mu_i^c = \vec{\mu}_i \cdot \vec{f}^c(\vec{R}_i). \tag{1.50}$$

Comments on H_{cQED}:

- The cavity QED Hamiltonian interpolates between a fully electrostatic Hamiltonian and the usual single mode Hamiltonians that are typically used to model dilute atoms in a cavity [1]. In the standard scenario, relevant for atomic physics, the matter system is so dilute that the direct Coulomb interaction is always negligible with respect to the typical energy scales in the game, which are on the order of the optical frequencies. In this way we would be allowed to set $V_{AB} \sim 0$.

- A more refined derivation would treat the higher k modes in perturbation theory, instead of just neglecting them. This would provide corrections to the direct Coulomb potential $V^{AB}_{Coul.}$, as well as in molecular physics the transitions rate are different from the one given by just standard dipole-dipole interaction, and that result is recovered just in the limit where the transition energy is very small with respect to the optical scales [38]. Anyway this does not affect the general form of the cavity QED Hamiltonian. Another approach can be instead

to keep a few modes other than the cavity mode, like it is done in [41]. This treatment is necessary when the coupling strength is as large as the energy of the higher modes.

- In this cavity QED setting the direct Coulomb interaction V_{AB} is always affected by the boundary of the confined system. In Ch. 3 we will show a simple realistic setting where the presence of the boundaries is clearly visible.

- If the dipole moments are small (or their matrix elements in a quantum framework), such as all interaction energies can be regarded as small compared to the bare Hamiltonian, we are in the dilute regime, and weakly interacting with the single cavity mode. We notice that all the interaction terms scale with the dipole square $\sim (\mu)^2$, except for the light-matter interaction cross-term $\sim (a + a^\dagger)\mu$, which is linear, and thus is the dominant contribution.

- The term
$$H_{P^2} = \frac{1}{2V\varepsilon_0}\left(\sum_{i=A,B}\mu_i^c\right)^2 \tag{1.51}$$
is called P^2-term, because it is proportional to the dipole's polarization square. Apparently it looks like an interaction between the two dipoles, which does not depend on the distance. This sounds of course a bit strange. However, the presence of this term is fundamental in order to recover the correct electrostatic limit. Indeed we can see that, repeating the adiabatic elimination for the cavity mode too, the contribution from the cavity is exactly cancelled by this term in the electrostatic limit. So in the end we are left just with the Coulomb interaction, as it has to be. This term can be interpreted as the single mode version of the dipole's self energies that we encountered in the dipolar gauge. Also there those contributions are exactly cancelled in the electrostatic limit.

With the help of the polarization density this result is readily generalised to many dipoles, as we will see in Ch. 3.

Chapter 2

Two-level approximation in light-matter interactions

In the previous chapter we developed a general theory that treats arbitrary dipoles interacting among each other via the electrostatic force and at the same time collectively interacting with a single radiative mode of the electromagnetic field. By restricting the discussion to electric dipole transitions and excluding all but one dynamical mode of the electric field, the Hamiltonian already simplified considerably. But in order to perform numerical or analytical calculations we need further approximations on the internal degrees of freedom of the dipoles.

Indeed, in the last chapter we assigned to each i-th localised spot of charges (e.g. a dipole) its own matter Hamiltonian H_m^i, without making any further comments on it. Naturally, having H_m^i as complicated as we want will make the whole problem of light-matter interactions at least as complex, and in general intractable when systems with multiple dipoles are considered.

Fortunately, atoms, molecules, quantum dots and other types of dipoles that are of interest in cavity QED have a very nonlinear spectrum. For weakly coupled systems this usually allows us to restrict the internal dynamics of the dipoles to only two internal states that are in resonance with the cavity mode. This *two-level approximation* (TLA) is obviously a great simplification, which allows us to treat problems that are otherwise impossible to solve. However, in the ultrastrong coupling regime the validity of this approximation is not at all obvious. More importantly, It turns out that depending on the chosen gauge, implementing the TLA can lead to drastically different prediction, a fact that has been ignored in this field for a long time. In this chapter we will systematically investigate the TLA and we will show that even in extremely simple and idealised scenarios it can lead to inconsistencies and erroneous predictions when the light-matter coupling is considered. But, at the same time this analysis also answers the question which gauge is most suitable for describing cavity QED systems in the USC regime.

The history of gauge issues in non-relativistic light-matter interactions in the quantum regime is very long, including important contributions from Lamb, Cohen-Tannoudji, Scully, Power, Zoller, but also many others [42, 19, 43, 44, 45, 46, 47]. It was often referred to as the "$p \cdot A$" versus "$\mu \cdot E$" debate. Despite the large amount of work which has already been done on this subject a clean view with details and examples was still missing. Moreover all the previously mentioned works just consider the case of a dipole in an external field and they never consider the fundamental case in which the electric field is itself another quantised degree of freedom. In our work we provide a general framework, discussing the TLA from weak to ultra-strong coupling. We show that when the system is in a weak coupling regime the truncation can be done efficiently in all gauges, while fundamental discrepancies arise in the USC regime.

The results contained in this chapter have been obtained in collaboration with Philipp Pilar, Tuomas Jaako, Simone De Liberato and Peter Rabl and were published in Physical Review A 98, 053819 (2018). In this work I contributed as the leading author doing most of the analytical and numerical calculations. Philipp Pilar had a very large contribution in producing the finally published figures. Sec. 2.10 is mainly based on the analysis by Philipp Pilar and Tuomas Jaako. The whole work was done under the supervision of Peter Rabl.

2.1 A single particle with a single cavity mode

A common way to describe the dynamics of the dipole transition of our matter system is to model all its degrees of freedom as a single effective particle in a potential well

$$H_m^i = \frac{\vec{p}_\xi^{\,2}}{2m_i} + V_i(\vec{\xi}_i). \tag{2.1}$$

Here the dynamical variable is the dipole displacement, $\vec{\xi}$ (we remind that it is related to the dipole moment by $\vec{\mu} = q\vec{\xi}$, where q is the charge, it is in principle a vector, but from now on we will always consider just its z component), the effective mass m_i and the effective potential V_i must be determined from the full microscopic model. In cases where we deal with true dipoles composed out of two point particles with charges $+q$ and $-q$ this description is exact, but it is usually also a good model to describe dipole transitions in more complex systems. From now on we just simply assume that this model is valid, focusing on its consequences rather than its justifications.

Once the description of our dipole in terms of a particle in a potential well is established, we need to pick a choice for a specific system. Despite the fact that at the the end of the day every particular problem will have its own particular treatment, it is possible to make a few general remarks, and then restrict our discussion to just a few paradigmatic cases.

We start from noticing that no matter how complicated the potential looks like, if it has a

minimum, it can always be approximated by an harmonic potential

$$V(\xi) \sim \frac{\omega_0^2}{2}(\xi - \xi_{\min})^2 + O(\xi^4), \tag{2.2}$$

provided that the dynamics will remain in the energy range in which the expansion is reasonable. This approximation makes always sense classically [48], if we know that our dipole is stuck around the minimum $\xi_{\min}$, and we impose that the maximal energy that our dipole can reach is always small enough, for which the dipole can only make small oscillations around $\xi_{\min}$. Quantum mechanically the situation is a bit more subtle, and the quadratic expansion of the potential around a certain minima can only make sense if that is the only one absolute minimum. Indeed, if we consider a *double well potential* with two minima that are very close in energy (the absolute minimum could be unique here, but it does not matter if the second minimum is very close!) then, because of tunnelling, any low energy process cannot be described by just considering one minimum or the other. So, it is clear that the double well potential in quantum mechanics should be regarded as another paradigm next to the harmonic oscillator. In between these two cases there is another potential that is worth to be included, in which the center is flat, or almost flat. The simplest realisation of this situation is certainly *square well potential*, another standard textbook example. We can say that these three cases represent the simplest paradigmatic cases, and so we will restrict our treatment just to these ones. To simplify the number of parameter that we need to specify for each potential, we introduce a characteristic length scale ξ_0 and a characteristic energy scale E_d. These two scales are determined by the original parameters of each potential. Rescaling lengths as $\tilde{\xi} = \xi/\xi_0$ and energies as $\tilde{H}_m = H_m/E_d$ allows us to pick just the minimal number of parameters required to describe the system. So finally we can list our three potentials:

- Harmonic potential: $V_{\text{harm}}(\xi) = \frac{m\omega_0^2}{2}\xi^2$.

  The scales are given by $\xi_0 = (\hbar/(m\omega_0))^{1/2}$, $E_d = \hbar\omega_0$ and the total Hamiltonian becomes

$$\tilde{H}_m = \frac{\tilde{p}_\xi^2}{2} + \frac{\tilde{\xi}^2}{2} \tag{2.3}$$

- Double well potential: $V_{\text{dw}}(\xi) = -\frac{b}{2}\xi^2 + \frac{\lambda}{4}\xi^4$.

  The scales are given by $\xi_0 = \left(\hbar^2/(m\lambda)\right)^{1/6}$, $E_d = \hbar^2/(m\xi_0^2)$,and the total Hamiltonian becomes:

$$\tilde{H}_m = \frac{\tilde{p}_\xi^2}{2} - \frac{\beta}{2}\tilde{\xi}^2 + \frac{\tilde{\xi}^4}{4}, \tag{2.4}$$

  where a single rescaled parameter $\beta = bm\xi_0^4/\hbar^2$ remains.

- Square well potential: $V_{\text{sw}}(\xi) = 0$ if $|\xi| < L/2$, $V_{\text{sw}}(\xi) = +\infty$ if $|\xi| \geq L/2$

The scales are given by $\xi_0 = L$, $E_d = \hbar^2/(mL^2)$:

$$\tilde{H}_m = \frac{\tilde{p}_\xi^2}{2}, \tag{2.5}$$

with the dynamical variable defined in $\tilde{\xi} \in [-1/2, 1/2]$, and assuming Dirichtlet boundary conditions.

The shape of these three potentials are shown in Fig. 2.1, together with their first four energy levels with relative wavefunctions.

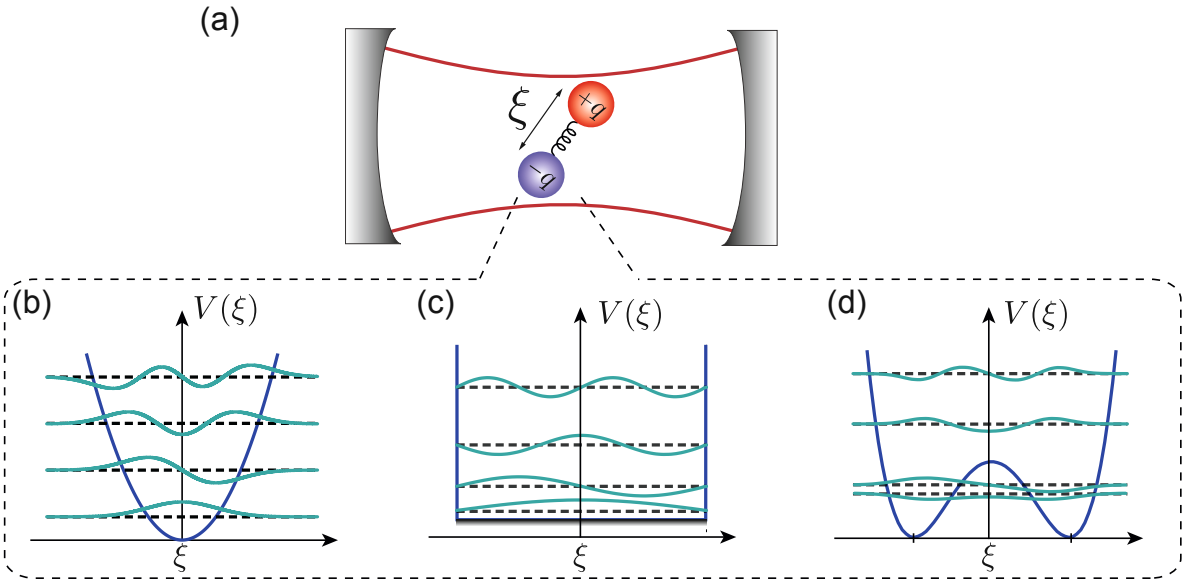

Figure 2.1: (a) Sketch of a dipole in a resonant cavity. (b) Harmonic potential (c) Square well potential, (d) Double well potential. The dashed lines indicate the first for eigenenergies and the solid lines indicate the corresponding wavefunctions.

Once we have clarified the details of our dipole, we need to include the photon's degree of freedom. To do so we adopt a simplified description, in which the electromagnetic field is just described by one harmonic mode with frequency ω_c. The vector potential (projected on the z-axis) is then given by $A = \mathcal{A}_0(a + a^\dagger)$, where $\mathcal{A}_0$ is kept as a generic parameter for the moment. In the Coulomb gauge, the resulting minimal coupling Hamiltonian for the combined systems is

$$H_C = \frac{(p - qA)^2}{2m} + V(\xi) + \omega_c a^\dagger a. \tag{2.6}$$

As we did in Ch. 1, we can change the representation for the canonical variables, and switch to another gauge. Among all this possibilities, there is one of them, which is particularly relevant: the dipole gauge. Using the unitary transformation $U = \exp[-iqA\xi/\hbar]$, we simultaneously shift the

particle's canonical momentum and the photon's annihilation operator

$$\begin{aligned} p &\longmapsto p + qA, \\ a &\longmapsto a + iq\mathcal{A}_0\xi, \end{aligned} \tag{2.7}$$

giving the Hamiltonian for our system in the dipole gauge

$$H_D = UH_CU^\dagger = \frac{p^2}{2m} + V(\xi) + \frac{mD^2}{2}\xi^2 + \omega_c a^\dagger a - i\omega_c q\mathcal{A}_0(a - a^\dagger)\xi, \tag{2.8}$$

where for later convenience we introduced the frequency

$$D^2 = 2q^2\mathcal{A}_0^2\omega_c/(\hbar m), \tag{2.9}$$

and the "bare coupling"

$$\frac{g_0}{\omega_c} = \sqrt{\frac{2\hbar D^2}{E_d\omega_c}}\frac{|\langle\varphi_0|\xi|\varphi_1\rangle|}{\xi_0}. \tag{2.10}$$

2.2 The quantum Rabi model

Having established the details regarding the "quasi-microscopic" description of our cavity-dipole system, we will now introduce what is considered the most paradigmatic model to represent light-matter interaction at the quantum level: the quantum Rabi model. We will present it by deriving it.

Consider the dipole linearly coupled to the single-mode electric field

$$H_{\text{linear}} = \omega_p a^\dagger a + H_d + \sigma(a + a^\dagger)X, \tag{2.11}$$

where H_d is the dipole's Hamiltonian, X is a generic dipole's operator, linear in p and ξ, and ω_p and the coupling parameter σ are free parameters. We expand the dipole's Hamiltonian in its own eigenstates, and we re-express the X operator in this diagonal basis:

$$H_d = \sum_{n=0}^{\infty}\omega_n|\varphi_n\rangle\langle\varphi_n|, \qquad X = \sum_{m,n}X_{mn}|\varphi_m\rangle\langle\varphi_n|, \tag{2.12}$$

where $X_{mn} = \langle\varphi_m|X|\varphi_n\rangle$. The last step is to truncate $m, n = 0, 1$, so we introduce the pseudo-spin notation

$$s_z = \frac{1}{2}\left(|\varphi_1\rangle\langle\varphi_1| - |\varphi_0\rangle\langle\varphi_0|\right) \qquad s_x = \frac{1}{2}\left(|\varphi_1\rangle\langle\varphi_0| + |\varphi_0\rangle\langle\varphi_1|\right), \tag{2.13}$$

having the same spin-1/2 algebra. Our linear Hamiltonian now becomes

$$H_{\text{linear}} \simeq \omega_X a^\dagger a + \omega_{10} s_z + \sigma X_{01}(a + a^\dagger)s_x + \frac{\omega_0}{2}\mathbf{1}. \tag{2.14}$$

We drop the identity contribution, and to shorten the notation we set $\omega_{10} = \omega_d$, and we introduce the generalised coupling constant $g_X = \sigma X_{01}$, where X_{01} can be considered a real number without loss of generality. In this way we obtain the quantum Rabi model

$$H_{\text{Rabi}} = \omega_p a^\dagger a + \omega_d s_z + g_X(a + a^\dagger)s_x. \tag{2.15}$$

This model has been the subject of extensive investigations [49] and nowadays is considered as the most basics build-block of light-matter interactions at the quantum level. Instead of focusing directly on its predictions, we rather address here the question about its validity in the USC regime. The first thing we want to understand here is the relation between the microscopic parameters and the parameters in the Rabi model. Even though it seems to be simple to answer, it brings up a non-trivial problem that is often ignored in the literature: as a starting point for our derivation we can use one of the two unitarily equivalent Hamiltonians in Eq. (2.6) and Eq. (2.8), which both can be written in the form given in Eq. (2.11). Since the original parameters may combine together differently in the two different representations, we may end up with two Rabi models but with different parameters. So the relevant question is, are the two Rabi models derived in different gauges identical and if not, which one is the correct one? Let's go through it, and calculate the Rabi parameters in both gauges to make this discussion concrete:

Coulomb gauge

- $\omega_p = \sqrt{\omega_c^2 + D^2} =: \tilde{\omega}_c$

  The A^2-contribution deriving from the minimal substitution has been included in the photon's Hamiltonian, shifting the cavity frequency and rescaling the photon'c annihilation operator according to $(a + a^\dagger) \mapsto \sqrt{\omega_c/\tilde{\omega}_c}(a + a^\dagger)$.

- $\omega_d = \omega_{10} =: \omega_0$

  The dipole's frequency is just given by the ground state - first excited state energy difference of the bare dipole's Hamiltonian $H_d = H_m$.

- $g_X = 2q\mathcal{A}_0|p_{10}|/(\hbar m)\sqrt{\omega_c/\tilde{\omega}_c} =: g_C$

  The Coulomb Rabi coupling has a non-linear dependence on the charge q, through the shifted cavity frequency $\tilde{\omega}_c$, and depends on the dipole's canonical momentum matrix element.

Dipole gauge

- $\omega_p = \omega_c$

  The photon's frequency is just the bare cavity frequency.

- $\omega_d = \tilde{\omega}_{10} =: \tilde{\omega}_0$

  The dipole's frequency is given by the first energy difference of the modified dipole's Hamiltonian

$$H_d = H_m + mD^2/2\xi^2. \tag{2.16}$$

  If H_m is non-harmonic $\tilde{\omega}_0(D)$ has a different dependence from D than the cavity case.

- $g_X = 2q\mathcal{A}_0\omega_c|\tilde{\xi}_{10}|/(\hbar m) =: g_D$

  The dipole Rabi coupling is non-linear in the dipole's charge q, because the dipole's displacement matrix element $\langle\tilde{\varphi}_m|\xi|\tilde{\varphi}_n\rangle$ is calculated with respect the eigenstate of the modified dipole's Hamiltonian H_d.

2.3 No-go and counter no-go theorems

Although in the previous section we have seen that in the two gauges we end up with two Rabi model with different sets of parameters, $\mathcal{S}_C = \{\tilde{\omega}_c, \omega_0, g_C\}$, $\mathcal{S}_D = \{\omega_c, \tilde{\omega}_0, g_D\}$, it could still happens that their combination in the Rabi model would give invariant predictions. However, it turns out that this is not the case and the predictions of the two models are even drastically different in the USC regime. As a relevant quantity we consider the *coupling parameter* of the Rabi model

$$\zeta_X = \frac{g_X^2}{\omega_p\omega_d}, \tag{2.17}$$

which tells us how much the dipole and the cavity are coupled together. If this parameter comes out different in the two gauges it means that the two models, for the same microscopic parameters, have a very different spectrum, so there must be something wrong.

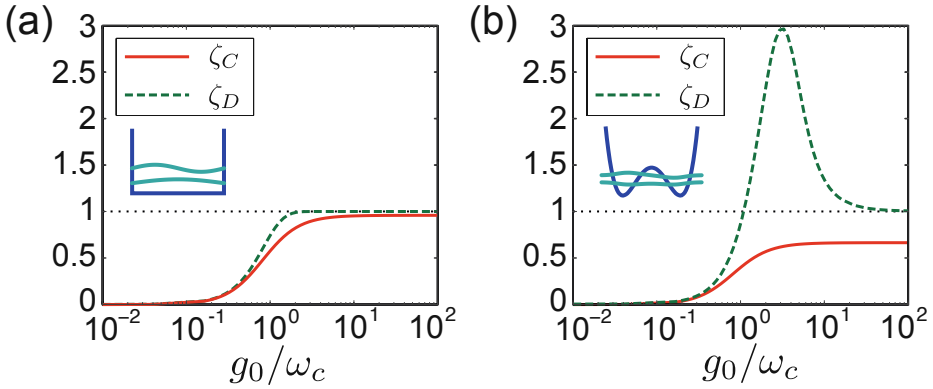

Figure 2.2: The dimensionless coupling parameters ζ_C and ζ_D as defined in Eq. (2.18) and (2.23) are plotted as a function of the bare coupling strength $g_0 \sim q$ for (a) a square-well potential and (b) a double-well potential with $\beta \approx 2.4$. For both plots $\omega_c = \omega_{10}$ and the charge q is used as a tunable parameter to vary the coupling strength.

Using what we have explained just above in the last section, we compute the Coulomb gauge coupling parameter

$$\zeta_C = \frac{D^2}{\omega_c^2 + D^2} f, \tag{2.18}$$

where we used that

$$p_{nk} = im(\omega_n - \omega_k)\xi_{nk}, \tag{2.19}$$

and where we introduced the oscillator strength

$$f = \frac{2m\omega_{10}}{\hbar}|\xi_{10}|^2. \tag{2.20}$$

The oscillator strength plays an important role in the so called Thomas-Reiche-Kuhn (TRK) sum rule,

$$\sum_n (\omega_n - \omega_k)|\xi_{nk}|^2 = \frac{\hbar}{2m}, \tag{2.21}$$

which follows directly from $[\xi, [\xi, H_d]] = -\hbar^2/m$ and is valid for arbitrary potentials and arbitrary level k. Using the TRK sum rule we have $f \leq 1$, which implies

$$\zeta_C \leq 1. \tag{2.22}$$

This inequality is actually a sort of no-go theorem for USC. Following this inequality we are lead to say there exists no system that can reach the USC regime of the Rabi model.

The situation looks completely different in the dipole gauge. Indeed, the dipole coupling parameter is

$$\zeta_D = \frac{D^2}{\tilde{\omega}_{10}^2} \tilde{f} \leq \frac{D^2}{\tilde{\omega}_{10}^2}, \tag{2.23}$$

where, again, in the last inequality we have used the TRK sum rule for the oscillator strength $\tilde{f} = 2m\tilde{\omega}_{10}|\tilde{\xi}_{10}|^2/\hbar \leq 1$. If the dipole is in a harmonic potential, $V(\xi) = m\omega_{10}^2\xi^2/2$, we have $\tilde{\omega}_{10}^2 = \omega_{10}^2 + D^2 > D^2$ and Eq. (2.23) reproduce the same bound as in the Coulomb gauge. The situation is drastically different if the dipole follows a strongly anharmonic potential, where $\tilde{\omega}_{10}^2 < D^2$. In this case $\zeta_D > 1$ is possible and the two gauges disagree. This can be seen in Fig. 2.2, where we calculate ζ_C and ζ_D for the square well case and the double well case as a function of the bare coupling g_0. It is clear that in the Coulomb gauge we will never reach the USC regime, accordingly to our bound (2.22), for both the square well and the double well. In contrast, in the dipole gauge we can reach the USC regime in the case of the double well potential.

It is worth noticing that the bound in Eq. (2.22) was used in the proof for the no-go theorem of the so called *superradiant phase transition* [50]. Our analysis above shows that this no-go-theorem only holds in the Coulomb gauge and not in the dipole gauge. At this stage it is still not clear why we have this ambiguity nor which is the correct description. But we already see that clarifying this issue goes far beyond the validity of the quantum Rabl model and is of essence of the whole field of USC.

2.4 Role of the potential shape in the dipole gauge

From the example above we can see that the dipole's potential plays a crucial role in defining the properties of the dipole Rabi model. In particular, the potential's shape tells us immediately whether the system can or cannot reach the USC regime in the dipole gauge. To understand better this point we consider the limit where $q \to \infty$. In this limit the quadratic shift due to the light-matter interaction $\sim q^2\xi^2$ dominates and the dipole's potential $V(\xi)$ becomes a perturbation to it. In principle we should calculate $\tilde{\omega}_{10}$ by using second order perturbation theory, and then plug the result in the definition of ζ_D. But we can take an easier way and arrive to the same result. In this limit the confining potential is mostly harmonic, and so the eigenstates will be mainly localised around $\xi = 0$. Therefore, we only need to compute the corrections that arise when expanding $V(\xi)$ around $\xi = 0$ to lowest order. For a symmetric potential the lowest order is quadratic and so we find

$$\lim_{q\to\infty}\left[\frac{mD^2}{2}\xi^2 + V(\xi)\right] \simeq \frac{m}{2}\tilde{\omega}_{10}^2\xi^2, \qquad \tilde{\omega}_{10}^2 = (D^2 + \Omega^2), \tag{2.24}$$

where

$$\Omega^2 = \frac{1}{m}\left.\frac{\partial^2 V}{\partial\xi^2}\right|_{\xi=0}, \tag{2.25}$$

is given by the curvature of the potential at the origin. Considering that the oscillator strength $\lim_{q\to\infty} \tilde{f} = 1$, because the system is harmonic in this limit, we then obtain

$$\lim_{q\to\infty} \zeta_D = \frac{D^2}{(D^2+\Omega^2)}. \tag{2.26}$$

When $\Omega^2 < 0$ this value is larger than one, which means that it has a maximum in the USC regime for a finite value of the charge q (or, equivalently, the bare coupling g_0).

2.5 Two level truncation: the validity depends on the gauge

To understand what is going on we take a step back and return to our general linear coupling Hamiltonian (2.11). The general assumption we make in order to justify our TLA is that the coupling between the dipole and the electromagnetic mode does not drive the system outside of the two-level subspace of the dipole. In this sense the discrepancy that we found above must be related to the different matrix element between the ξ and p operators that are involved in the different gauges. In particular, for a standard bounded, quadratic in p Hamiltonian we have the fundamental relation Eq. (2.19) which says that p matrix elements grow with the energy difference, effectively connecting all distant levels. Therefore, we expect that this explains the failure of the TLA in the Coulomb gauge.

Let us elaborate this argument in more detail. Assuming a resonance condition between the photon and the two level subspace, $\omega_c \simeq \omega_0$ we thus need a condition on the matrix element of the coupling Hamiltonian. In particular we want to have large transition elements inside the TL subspace and small ones for anything outside. In the whole thesis we only consider the ground state and the first excited state as TL-subspace, but the argument can be generalised to TL-subspaces in the excited spectrum. Of course in such a situation all the conclusions we draw here might be completely different and in general one should re-do the whole analysis with care every time a different system is considered.

In order to understand whether the TL-subspace is preserved by the coupling to the cavity we need a comparison between the coupling energy scale within the TL-subspace and the coupling energy scale to bring the system outside the TL-subspace. The most relevant energy scale that represents the coupling inside the TL-subspace is $E_{in} \sim \sigma|X_{10}|$ (where we use the general notation as in Eq. (2.11)). The relevant energy scale that brings the system outside of the TL-subspace can be given in perturbation theory as $E^{nm}_{out} \sim \sigma^2|X_{nm}|^2/(\omega_{nm}-\omega_c)$, where $m = 0, 1$ and $n > 1$. Evidently we have multiple energy scales that bring us outside the TL-subspace. If the energy that keep the system in the TL-subspace is greater than all these outside transitions summed together the TLA is valid. So we have $E_{out} \sim \sigma^2 \sum_{n>1} |X_{nm}|^2/(\omega_{nm})$. The energy difference in this denominator

is minimized by $\omega_{nm} - \omega_c \leq \omega_{21} - \omega_{10}$ (where we used the resonance condition $\omega_c \simeq \omega_{10}$). So the condition we look for is

$$\frac{1}{2}\frac{\sigma}{|\omega_{21}-\omega_{10}|}\left(\sum_{n>1}|X_{n0}|^2+\sum_{n>1}|X_{n1}|^2\right) < |X_{10}|, \tag{2.27}$$

where we put a factor $1/2$ to take an average between transitions from the "0" level and the "1" level. By summing and subtracting $|X_{10}|^2$ we have

$$\frac{1}{2}\frac{\langle 1|X^2|1\rangle + \langle 0|X^2|0\rangle}{|X_{10}|} - |X_{10}| < \frac{|\omega_{21}-\omega_{10}|}{\sigma}. \tag{2.28}$$

Accordingly with the definitions given in Sec. 2.2 we have

$$\sigma = \frac{g_X}{|X_{10}|}. \tag{2.29}$$

Then the quantity

$$\Delta_X = \frac{1}{2}\left(\frac{\langle 1|X^2|1\rangle + \langle 0|X^2|0\rangle}{|\langle 0|X|1\rangle|^2}\right) - 1, \tag{2.30}$$

becomes a good estimator of the strength of the transitions that would eventually breakdown the TLA. By definition we have $\Delta_X \geq 0$. If $\Delta_X < 1$ the matrix element are larger for transitions inside the TS-subspace than outside, and it is the opposite for $\Delta_X > 1$. For $\Delta_X = 1$ all in/out transitions have the same weight, which is the case, for instance for the ξ and p operators in the harmonic case. This has to be compared to the out-coupling scale of the dipole

$$\alpha_g = \frac{|\omega_{21}-\omega_{10}|}{g_X}. \tag{2.31}$$

$\alpha_g \simeq 0$ indicates a quite harmonic system, for which the TLA is hardly applicable, while $\alpha_g \gg 1$ is a system where the coupling is small enough with respect to the anharmonicity of the system. Following usual perturbative arguments it is quite natural to combine Δ_X and α_g in an estimate condition on the applicability of the TLA in our linearly coupled system

$$\Delta_X < \alpha_g. \tag{2.32}$$

It is worth to relate this condition to the recipe we gave to obtain the TLA in the dipole gauge. In particular we notice that in the dipole gauge we need to modify the bare dipole's Hamiltonian to include the ξ^2-term, as shown in Eq. (2.16). When the condition (2.32) is fulfilled this term is negligible. Indeed in this regime if we truncate the ξ^2 operator in the TL-subspace we obtain

$$\hat{\xi}^2_{TLA} \approx |\xi_{10}|^2\hat{\mathbf{1}}. \tag{2.33}$$

Since it is approximated by the identity operator it doesn't give any contribution and one may just drop it. Notice that the condition in Eq. (2.33) was identified as the validity condition for the TLA in [51]. Despite of what is claimed in this reference, what is derived in [51] is no more and no less of what is written here, only using a different language.

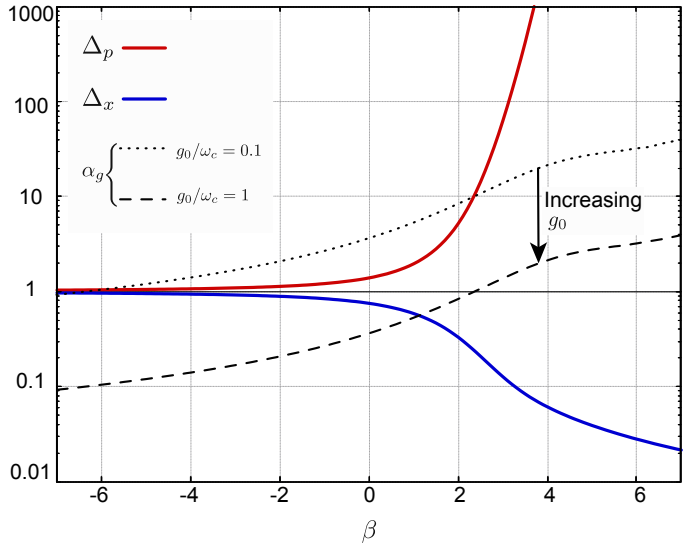

Figure 2.3: The matrix element estimator Δ_X for the ξ and p operators (solid blue/red lines) and the parameter α_g defined in Eq. (2.31) in the case of the double well potential given by Eq. (2.4), as a function of β.

In Fig. 2.3 we show a simple example for the double well potential, where we sweep the parameter from $\beta < 0$ (almost harmonic system, single well) to $\beta > 0$ (strongly anharmonic system, double well regime). Here we fix the gauge dependent coupling to be just the bare coupling, $g_X \sim g_0$. We can see that Δ_ξ and Δ_p have completely opposite behaviour, and in particular we notice that in this specific example

$$\Delta_\xi \lesssim 1, \tag{2.34}$$

and

$$\Delta_p \geq 1. \tag{2.35}$$

Despite that the first inequality is not true in general and only valid for the double well potential case (without proof, but just through numerical observation), this second inequality can be proved in general using the TRK sum rule (see App. C). This means that in any gauge in which the coupling is proportional to the momentum operator p the TLA would not work except for very small coupling. Any interpolation between the Coulomb and the dipole gauge would not give good results, except if the system is fully in the dipole gauge. Note this conclusion contradicts the recent

claim in [52], where an intermediate gauge was found to be optimal. However, a closer inspection shows that this is only the case in situations were the TLA as a whole is no longer valid. Quite surprisingly we further notice from Fig. 2.3 that the condition (2.32) is not satisfied for the p coupling even at small coupling if β is large enough. This is somehow very counter intuitive if we think just in terms of energy scales, where $\alpha_g \gg 1$. To have a better understanding of this point we consider the Rabi model (2.15) in the dipole and Coulomb gauge $H^D_{\rm Rabi}$, $H^C_{\rm Rabi}$ and we expand their eigenvalues for low coupling $g_0/\omega_c < 1$. Always keeping the resonance condition $\omega_c = \omega_{10}$ we obtain

$$\Delta E^C_{1,2} = E^C_{1,2} - E^C_0 \simeq \hbar\omega_c \mp \frac{\hbar g_0}{2} + \frac{\hbar g_0^2}{4\omega_c}\frac{1}{f}, \tag{2.36}$$

for the first two excitation energies in the Coulomb gauge and

$$\Delta E^D_{1,2} = E^D_{1,2} - E^D_0 \simeq \frac{\hbar\omega_c + \hbar\tilde{\omega}_{10}}{2} \mp \frac{\hbar g_0}{2}, \tag{2.37}$$

in the electric dipole gauge. At first order in g_0/ω_c both gauges gives the correct expected Rabi splitting, but the second order there is a clear disagreement. While in the dipole gauge the second order vanishes it is present in the Coulomb gauge with a peculiar scaling in $1/f$. The oscillator strength can be seen as another measure of the anharmonicity of the dipole and it is $f = 1$ for an harmonic oscillator, while $f \ll 1$ for a strongly anharmonic dipole (such as a double well potential). This discrepancy

$$\Delta E^C_1 - \Delta E^D_1 \simeq \frac{\hbar g_0^2}{4\omega_c}\frac{1}{f}, \tag{2.38}$$

is thus more evident when $f \ll 1$, which exactly matches our expectation from the analysis above on Δ_ξ and Δ_p. Here we can have another hint about the invalidity of TLA in the Coulomb gauge. This artificial shift proportional to $1/f$ represent a quadratic Bloch-Siegert shift, which has never been observed, in contrast to the third order shift that one obtains in the dipole gauge [53].

Putting together these general considerations already suggests that the Coulomb gauge is heavily non optimal to perform the dipole's two level truncation, while the dipole gauge seems to be much more favourable in this sense. In particular from the analysis of the matrix elements, given in general by the quantity Δ_ξ, it emerges that the dipole gauge has a clear monotonic link between the dipole's anharmonicity and the increasing quality of the TLA. For these reasons, under our general assumptions, the dipole gauge represent the correct basis in which to operate with the dipole's truncated Hilbert space.

2.6 Examples: double well and square well dipole

In this section we focus on two practical examples: the dipole in a double well potential with large anharmonicity, described by the Hamiltonian in Eq. (2.4), and the dipole in a square well potential which is described by Eq. (2.5).

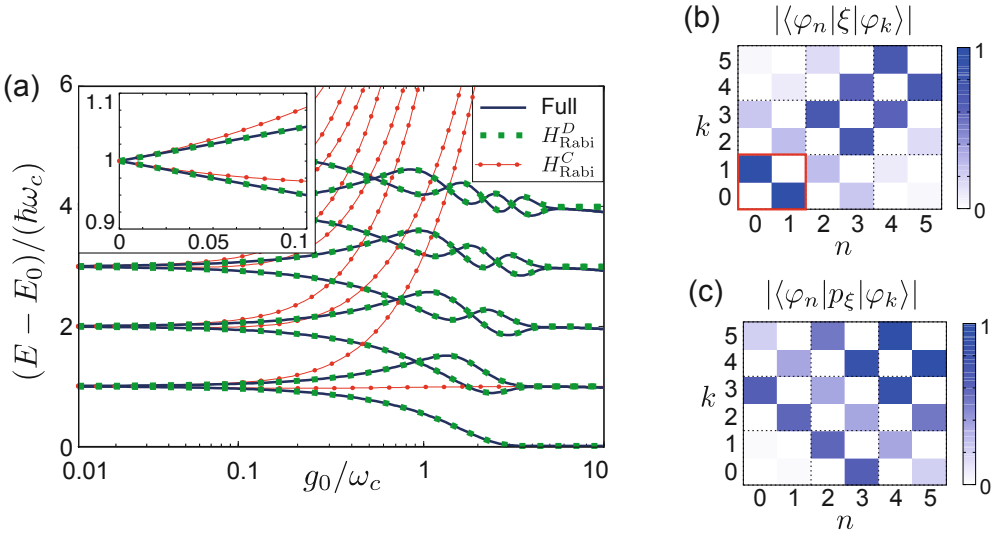

Figure 2.4: Double-well potential. (a) Comparison of the energy spectra obtained from the full model H_C (solid blue line), the quantum Rabi model $H^D_{\rm Rabi}$ derived in the dipole gauge (green dashed line) and the quantum Rabi model $H^C_{\rm Rabi}$ derived in the Coulomb gauge (red dotted line). For these plots a double-well potential with parameters $\beta \approx 3.7$ and $\omega_{10} = \omega_c$ (which fixes the value of E_d) have been assumed. The inset shows a zoom of the predicted Rabi splitting between the first two excited energy levels. (b) Matrix elements of the dimensionless position operator ξ and (c) matrix elements of the dimensionless momentum operator p_ξ evaluated for the lowest eigenstates $|\varphi_n\rangle$ of the same double-well potential. For the sake of clarity, the values of the matrix elements have been normalized by the largest matrix element in each plot.

Starting with the double well dipole, we solve numerically the coupled linear Hamiltonian, in the Coulomb and dipole gauge, with and without the TLA. We consider $\beta \approx 3.7$, which gives a quite large anharmonicity $|\omega_{21} - \omega_{10}|/\omega_{10} \approx 100$. In Fig. 2.4(a) we plot the lowest part of the spectrum as a function of the coupling strength g_0/ω_c, keeping fixed all the other parameters, and always considering resonance $\omega_{10} = \omega_c$. The full numerics is obtained by including a large number of dipole's states. In this case the Coulomb gauge and the dipole gauge correctly give the same result (the numerics is constructed just following what discussed in Sec. 2.2. The dipole's Hamiltonian and coupling operator is represented in its energy eigenbasis and then truncated up to a certain level. If the truncation is high enough the lowest levels are correctly reproduced). The situation is drastically different when just two dipole's levels are included in the whole Hamiltonian. The dipole gauge TLA correctly reproduces the spectrum up to very large couplings $g_0/\omega_c \approx 10$. This is in line with what one can expect from our estimate criterion (2.32). The Coulomb gauge instead already visibly fails at rather weak coupling $g_0/\omega_c \approx 0.1$. Moreover, one clearly sees the artificial "$1/f$-shift"

in the Coulomb gauge at weak coupling, given by Eq. (2.38). In Fig. 2.4(b-c) we represent the matrix elements of the ξ and p operators. The ξ operator has a well defined TL-subspace, for which all the matrix elements that connect it with the rest of the spectrum are strongly suppressed. This is exactly opposite in the p operator, confirming our simple argument from the previous section.

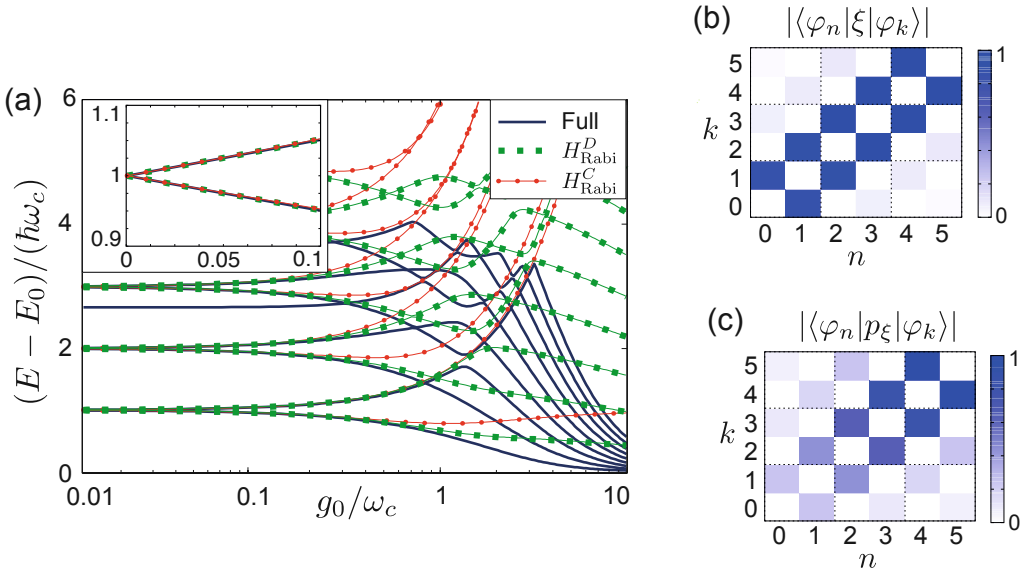

Figure 2.5: Square-well potential. (a) Comparison of the energy spectra obtained from the full model H_C (solid blue line), the quantum Rabi model $H^D_{\rm Rabi}$ derived in the dipole gauge (green dashed line) and the quantum Rabi model $H^C_{\rm Rabi}$ derived in the Coulomb gauge (red dotted line). For these plots a square-well potential and $\omega_{10} = \omega_c$ (which fixes the value of E_d) has been assumed. The inset shows a zoom of the predicted Rabi splitting between the first two excited energy levels. (b) Matrix elements of the dimensionless position operator ξ and (c) matrix elements of the dimensionless momentum operator p_ξ evaluated for the lowest eigenstates $|\varphi_n\rangle$ of the same square-well potential. For the sake of clarity, the values of the matrix elements have been normalized by the largest matrix element in each plot.

In Fig. 2.5(a) we show the same plot for the square well case. The anharmonicity is $|\omega_{21} - \omega_{10}|/\omega_{10} = 8/3$, so it is not so large with respect to the previous case. For small coupling strength the spectrum is correctly reproduced by both gauges, and, in particular, we see that the artificial $1/f$ shift introduced by the Coulomb gauge is much less relevant here. This is a consequence of the oscillator strength, which is very close to unity $f \approx 0.96$. But when the coupling starts to be close to the USC regime, $g_0/\omega_c \approx 0.1$ we see that the TLA is not giving good results any more. For large couplings the TLA fails in both gauges. In Fig. 2.5(b-c) we see the ξ and p matrix elements of the square well. There is no TL-subspace which is possible to isolate and in general all neighbouring levels are similarly coupled. This is in line to what we expect from Fig. 2.3 when $\beta = 0$, which represents a case very similar to the square well potential.

2.7 Multiple dipoles, Dicke and extended Dicke model

A crucial point in the research about USC regime concerns the collective coupling of a dipole ensemble to a single resonant mode. We already introduce the formalism to treat this system in Ch. 1, and we will discuss it further in all the remainder of the thesis. Light-matter ultra-strong interactions through collective matter excitation is actually the first example of a successful experiment where the USC regime has been reached [54]. Since also in this context the TLA is widely used, it becomes very important to see whether the discrepancies between different gauges encountered before survive even in the collective case.

As already anticipated in Ch. 1 the Coulomb gauge Hamiltonian for an ensemble of dipoles collectively coupled to a single resonant mode is

$$H_C = \sum_{i=1}^{N} \left[\frac{(p_i - qA)^2}{2m} + V(\xi_i) \right] + \hbar\omega_c a^\dagger a + H_{\rm dd}. \tag{2.39}$$

The last term $H_{\rm dd}$ is the direct dipole-dipole interaction. This term is gauge independent so it plays no role in the following discussion. For this reason we simply neglect it, focusing only on the dynamical part of the light-matter interaction, where, instead, the TLA plays a subtle role.

The collective Coulomb Hamiltonian is unitary equivalent to the collective dipole Hamiltonian $H_D = UH_CU^\dagger$, where $U = \exp(-iqA\sum_i \xi_i/\hbar)$. After this transformation we obtain

$$H_D = \sum_i \left[\frac{p_i^2}{2m} + \tilde{V}(\xi_i) \right] + \hbar\omega_c a^\dagger a + i\omega_c q\mathcal{A}_0(a^\dagger - a)\sum_i \xi_i + \frac{mD^2}{2}\sum_{i\neq j} \xi_i\xi_j. \tag{2.40}$$

Notice that the last term is the collective version of the ξ^2-term that we encountered before. It looks like an infinite range interaction but it is not, as explained in Ch. 1. Moreover the last term generates also a "local" ξ^2-term (by taking the $i = j$ contribution), which is already included in the dipole's potential $\tilde{V}(\xi_i) = V(\xi_i) + mD^2\xi_i^2/2$ as usual.

In contrast to what we discussed so far, the relevant regime for this type of collective cavity QED is weak coupling for each single dipole $g_0/\omega_c \ll 1$, but strong or ultra-strong collective coupling coupling $G_0/\omega_c = \sqrt{N}g_0/\omega_c \gg 1$. The concept of collective USC will be discussed in more details later in the thesis, but now we just need to grasp its basic idea: each dipole is weakly coupled to the cavity, but the whole ensemble is instead strongly coupled because it is composed out of many dipoles. In order to have a finite collective coupling G_0 the single dipole coupling must scale at most as $g_0 \sim 1/\sqrt{N}$. Under this condition it seems straightforward to apply the TLA in every gauge and for every potential and always to obtain reasonable answers.

Performing the TLA on H_C we arrive at the well known *Dicke model*

$$H_{\mathrm{DM}} = \hbar\tilde{\omega}_c a^\dagger a + \hbar\omega_{10} S_z + \hbar g_C (a + a^\dagger) S_x, \tag{2.41}$$

where $S_k = 1/2 \sum_i \sigma_k^i$ are collective spin operators and $\tilde{\omega}_c = \sqrt{\omega_c^2 + ND^2}$. In the thermodynamic limit $N \to \infty$ one can apply the Holstein-Primakoff approximation to the collective spin operators (see App. D for more detail) and obtain an Hamiltonian of two coupled harmonic oscillators

$$H_{\mathrm{DM}} \approx \tilde{\omega}_c a^\dagger a + \omega_{10} b^\dagger b + \frac{\sqrt{N} g_C}{2} (a + a^\dagger)(b + b^\dagger). \tag{2.42}$$

This Hamiltonian can be diagonalised by two polariton modes, having frequencies

$$\omega_{C\pm}^2 = \frac{1}{2}\left[\omega_{10}^2 + \tilde{\omega}_c^2 \pm \sqrt{(\tilde{\omega}_c^2 - \omega_{10}^2)^2 + 4N g_C^2 \tilde{\omega}_c \omega_{10}}\right]. \tag{2.43}$$

The stability of the system requires that $\omega_{C\pm}^2 > 0$, which is satisfied as long as the collective coupling parameter

$$N\zeta_C^{(N)} = \frac{N g_C^2}{\tilde{\omega}_c \omega_{10}} < 1. \tag{2.44}$$

This inequality is very similar to the one proved in the no-go theorem for USC (2.22) (except for the factor of N). In the same way as we did in that case, one can use the TRK sum rule to show that this inequality is always true

$$\frac{N g_C^2}{\tilde{\omega}_c \omega_{10}} \leq \frac{ND^2}{\omega_c^2 + ND^2} < 1. \tag{2.45}$$

So the Coulomb gauge Dicke model is always stable. This is a very important point that we will re-discussed in Ch. 4 in the context of the debate around the *superradiant phase transition*.

Now we repeat the same reasoning for the dipole gauge. In the single dipole case we found an inconsistency due to the TLA by just looking at the coupling parameter in the different gauges, so that is the first thing to check here. In the collective case in particular the collective coupling parameter is related to the stability of the polariton modes, so if there is a discrepancy it would be really striking. Applying the TLA to (2.40) we obtain the extended Dicke model [55]

$$H_{\mathrm{EDM}} = \hbar\omega_c c^\dagger c + \hbar\tilde{\omega}_{10} S_z + \hbar g_D (c + c^\dagger) S_x + \frac{\hbar g_D^2}{\omega_c} S_x^2. \tag{2.46}$$

Again using the Holstein-Primakoff approximation we arrive to a two coupled oscillators Hamilto-

nian, from which we extract the eigenfrequencies

$$\omega_{D\pm}^2 = \frac{1}{2}\left[\Omega_{10}^2 + \omega_c^2 \pm \sqrt{\left(\Omega_{10}^2 - \omega_c^2\right)^2 + 4Ng_D^2\tilde{\omega}_{10}\omega_c}\right], \tag{2.47}$$

where $\Omega_{10} = \sqrt{\tilde{\omega}_{10}(\tilde{\omega}_{10} + Ng_D^2/\omega_c)}$. If $Ng_D^2 > \Omega_{10}^2(\omega_c/\tilde{\omega}_{10})$ the lower polariton frequency becomes imaginary and the system is unstable. By repeating the same calculation using the TRK sum rule one can show that

$$\frac{Ng_D^2}{\Omega_{10}^2(\omega_c/\tilde{\omega}_{10})} \leq \frac{ND^2}{\tilde{\omega}_{10}^2 + ND^2} < 1, \tag{2.48}$$

ensuring the stability also in the dipole gauge.

On contrary to the single dipole case it seems that, in the collective regime, the TLA approximation does not introduce any dramatic discrepancies.

2.8 The fake depolarization shift in the Coulomb gauge

We have shown so far that the TLA preserves the stability of the two gauges in the collective regime. But it is still unclear whether the truncation in the two gauges produces equivalent results. The answer is no, and it emerges clearly when the dipole potential is strongly anharmonic (for instance in the double well potential), with a striking effect in the collective USC $G_0/\omega_c \gg 1$.

To show how the discrepancy emerges we consider again the polariton frequencies in the two gauges, but rearranging the terms differently from above

$$\omega_{C\pm}^2 = \frac{1}{2}\left[\omega_{10}^2 + \omega_c^2 + ND^2 \pm \sqrt{\left(\omega_{10}^2 + \omega_c^2 + ND^2\right)^2 - 4\omega_c^2\omega_{10}^2 - 4N(1-f)D^2\omega_{10}^2}\right], \tag{2.49}$$

$$\omega_{D\pm}^2 = \frac{1}{2}\left[\omega_{10}^2 + \omega_c^2 + fND^2 \pm \sqrt{\left(\omega_{10}^2 + \omega_c^2 + fND^2\right)^2 - 4\omega_c^2\omega_{10}^2}\right], \tag{2.50}$$

where we introduced the oscillator strength $f = 2m\omega_{10}|\xi_{10}|^2$, which is a measure of the single dipole's anharmonicity. Expanding the two frequencies at lowest order in $G_0/\omega_c \ll 1$ (and assuming $\omega_c = \omega_{10}$ as usual) we find

$$\omega_{C\pm} - \omega_{D\pm} \simeq \frac{G_0^2}{4\omega_c}\left(\frac{1}{f} - 1\right). \tag{2.51}$$

This discrepancy resembles quite a lot the artificial $1/f$-shift found in Sec. 2.6.

But there is more. Indeed if we take the collective USC limit we found that the lower polariton in the Coulomb gauge approaches a finite value

$$\lim_{G_0\to\infty} \omega_{C-} = \omega_{10}\sqrt{1-f} > 0. \tag{2.52}$$

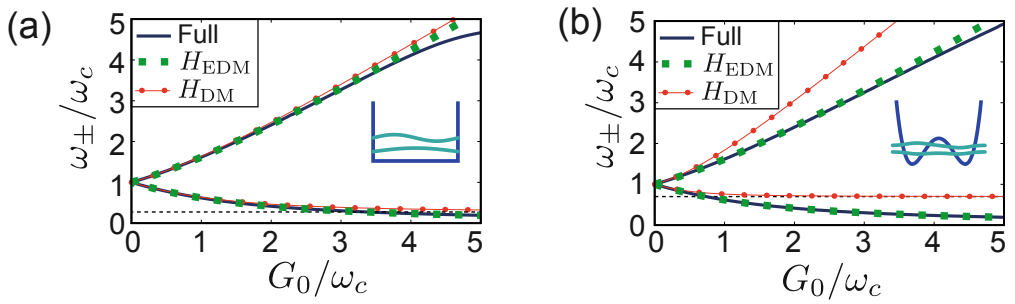

Figure 2.6: The frequencies $\omega_\pm$ of the two lowest polariton modes are plotted in the limit $N \gg 1$ as a function of the collective coupling strength $G_0 = g_0\sqrt{N}$ and for $\omega_{10} = \omega_c$. In (a) the case of a square-well potential ($f_{\rm sq} \approx 0.96$) and in (b) the case of a double-well potential with $\beta \approx 2.3$, and $f_{\rm dw} \approx 0.71$ is considered. The different lines represent the results obtained from the Dicke model $H_{\rm DM}$ derived in the Coulomb gauge ($\omega_{C\pm}$, red solid-dotted), the extended Dicke model $H_{\rm EDM}$ derived in the electric dipole gauge ($\omega_{D\pm}$, green squares) and the two lowest branches of the full spectrum (blue solid line). In both plots, the horizontal dashed line represents the fake depolarization shift in the Coulomb gauge, as given in Eq. (2.52).

In Fig. 2.6 we can see the Coulomb gauge always approaches this asymptotic frequency, while the dipole gauge seems to go always to zero (at very large collective couplings). The effect is more evident for dipole's potentials with larger anharmonicity, as we can see comparing Fig. 2.6 (a) and (b). In the language of electrodynamics such a shift in the lower Coulomb gauge polariton frequency is often called *depolarization shift*. The depolarization shift in photonic system is a physical observable [56] which is related to the direct interaction between the dipoles (we will see this in detail in the next chapter). In the current analysis we dropped any direct interaction between the dipoles, so we do not expect any depolarization shift. We can actually prove this in the next section, proving also in a fully analytical way that the TLA goes wrong in the Coulomb gauge even in the collective case.

2.9 The TRK sum rule forbids the depolarization shift

In this section we want to prove that the depolarization shift (2.52) found in the Coulomb gauge after the TLA is an artefact of the TLA. To do so we would need to solve the full many body Hamiltonian, which is of course very difficult, to not say impossible. Fortunately, for a very large number of dipoles the description can be simplified again.

We start noticing that the collective coupling operators in both gauges involve a sum over the whole ensemble

$$\Pi = \sum_i p_i, \qquad \Xi = \sum_i \xi_i. \tag{2.53}$$

We can then re-think these operators represented on a many-body basis, made of symmetric or anti-symmetric states [57]. The most relevant transitions due to our collective coupling operators

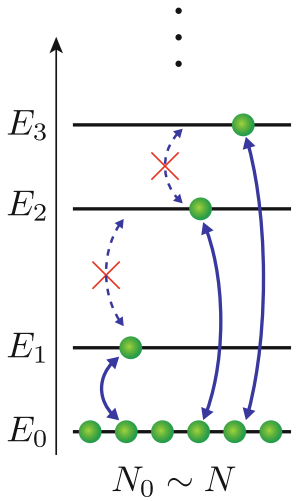

Figure 2.7: Sketch of the relevant energy levels of the full multi-dipole Hamiltonian H_C in the weak-excitation regime. In this limit, most dipoles occupy the lowest potential state with energy E_0 and cavity-induced transitions between pairs of higher states can be neglected.

are between dipole states of this form

$$|\text{Coll. ex.}\rangle \sim \frac{1}{\sqrt{\mathcal{N}}}(|n_1, n_2 \dots n_N\rangle + \text{ all possible permutations}), \tag{2.54}$$

where $\mathcal{N}$ is a suitable normalization factor, and where each j-th dipole is in its n_j level. Notice that if all the dipoles are in the same state $\mathcal{N} = 1$, while in any other case the normalization must scale at least as $\mathcal{N} \sim N$. This immediately implies that matrix elements of collective operators such as (2.53) scale as $\sim \sqrt{N}$ if taken between a collective state where all the dipoles are in the same state and a state where at least one dipole is different, while they scale at most as ~ 1 between states where the dipoles are in different states. To ensure having a finite collective coupling the single dipole coupling must scale as $g_0 \sim 1/\sqrt{N}$, meaning that light-matter induced transitions between collective excited states go as $\sim 1/\sqrt{N}$. If we are just interested in low energy processes (as we are!) then this means that only transitions from the ground state to excited states are relevant when the thermodynamics limit is considered $N \to \infty$. To this end we define quasi-bosonic operators

$$b_n^\dagger = \frac{1}{\sqrt{N}} \sum_{i=1}^{N} |n_i\rangle\langle 0_i|, \tag{2.55}$$

which creates a collective excitation in the n-th energy level of the bare dipole Hamiltonian. In the thermodynamic limit they obey bosonic commutation relation [58]

$$[b_n, b_m^\dagger] \simeq \delta_{nm}. \tag{2.56}$$

Expressing the collective light-matter Hamiltonian in this collective basis and then discarding transitions between excited states we are left with the low energy effective Coulomb Hamiltonian

$$H_C \simeq \tilde{\omega}_c a^\dagger a + \sum_n \omega_n b_n^\dagger b_n - \frac{G_C}{2}\left(a + a^\dagger\right)\sum_n \nu_n \left(b_n + b_n^\dagger\right), \tag{2.57}$$

where $\tilde{\omega}_c = \sqrt{\omega_c^2 + ND^2}$, $G_C = \sqrt{N} g_C = G_0\omega_{10}/\sqrt{\omega_c \tilde{\omega}_c}$ and $\nu_n = (\xi_{n0}/\xi_{10})(\omega_{n0}/\omega_{10})$. This low energy approximation is basically exact in the thermodynamic limit and since we didn't perform a TLA, it is still gauge invariant. One can still apply the unitary transformation to switch to the dipole gauge in this low energy manifold and find exactly the low energy version of H_D as it would appear repeating the same approximation starting from H_D itself.

We can now compute the spectrum of Eq. (2.57). Following standard procedure for bosonic quadratic Hamiltonians, we find that the eigenfrequencies ω are solutions of the equation

$$\omega^2 + G_0^2 \sum_n \frac{\nu_n^2 \omega_{10}^2/(\omega_{n0}\omega_c)}{1 - \omega^2/\omega_{n0}^2} = \omega_c^2 + ND^2, \tag{2.58}$$

where we recall that $D = g_0^2\omega_{10}/(\omega_c f)$. This equation looks generally different for each different gauge, but its eigenfrequencies are gauge invariant, as one can directly verify. We focus now on the lower polariton solutions. To this end we consider that $\omega_- \ll \omega_c, \omega_{n0}$, so we can expand the equation for $\omega \sim 0$. We then get the approximate result

$$\omega_-^2 \simeq \frac{\omega_c^2 + ND^2\left(1 - \frac{2m}{\hbar}\sum_n \xi_{n0}^2 \omega_{n0}\right)}{1 + G_0^2 \sum_n \frac{\nu_n^2 \omega_{10}^2}{\omega_{n0}^3 \omega_c}}, \tag{2.59}$$

which holds only in the USC regime, for $G_0/\omega_c \gg 1$. If all the levels are included the only coupling dependent term in the numerator is zero

$$ND^2\left(1 - \frac{2m}{\hbar}\sum_n \xi_{n0}^2 \omega_{n0}\right) = 0, \tag{2.60}$$

as a consequence of the TRK sum rule. We thus conclude that

$$\lim_{G_0 \to \infty} \omega_- = 0. \tag{2.61}$$

The lowest solutions of Eq. (2.58) are represented as solid blue lines in Fig. 2.6, and they perfectly match the polariton frequencies predicted by the dipole gauge under the TLA.

2.10 A simple circuit implementation and the few-dipoles case

The theory that we have developed so far have a broad range of applicability in various fields of physics. In order to give a taste of concreteness to this otherwise quite abstract chapter we present an example from one of the most lively branches of QED: circuit QED.

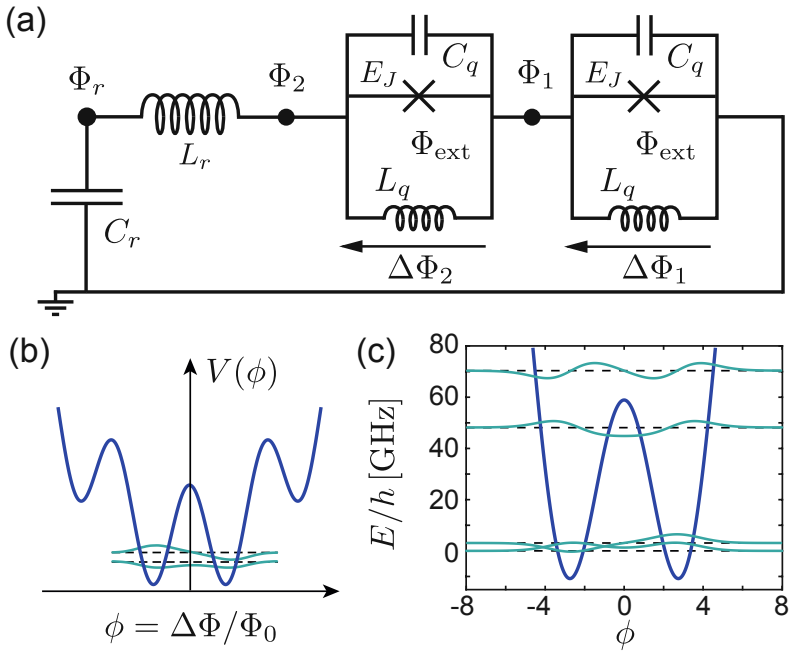

Figure 2.8: Circuit QED with flux qubits. (a) Sketch of a multi-qubit circuit QED system, where two flux qubits are coupled to a lumped-element LC resonator with inductance L_r and capacitance C_r. In the simplest case, each flux qubit is realized by an rf-SQUID circuit and can be modeled as an effective particle with a dimensionless coordinate $\phi = \Delta\Phi/\Phi_0$ moving in an effective potential $V(\phi)$. (b) Typical shape of the potential $V(\phi)$ for a generic flux-qubit where the two lowest tunnel-coupled states form an isolated two-level subspace. (c) Shape of the potential $V(\phi)$ and the lowest eigenstates $|\varphi_n\rangle$ for a specific flux qubit with parameters $E_{L_q}/h = 7$ GHz, $E_{C_q}/h = 12$ GHz and $E_J/h = 50$ GHz.

We focus on a prototype circuit setup where $N = 2$ flux qubits are coupled in series to an LC circuit with inductance L_r and capacitance C_r. In this example the LC circuit plays the role of the cavity mode, while the qubits play the role of the dipoles. The system is represented in Fig. 2.8(a). We introduce the generalised flux variables

$$\Phi_\eta(t) = \int_{-\infty}^{t} ds\, V_\eta(s), \qquad \eta \in \{r, 1, 2\}, \tag{2.62}$$

where V_η is the voltage at the respective node (see the nodes in Fig. 2.8(a)). The equations of motion for the variables Φ_η are derived by considering the Lagrangian $\mathcal{L} = T - V_{\rm tot}$, where

$$T = \frac{C_r \dot{\Phi}_r^2}{2} + \sum_{i=1}^{N} \frac{C_q (\Delta\dot{\Phi}_i)^2}{2}, \tag{2.63}$$

is the capacitive energy, which plays the role of the kinetic energy, while the energy stored in the inductance, equivalent to potential energy, is

$$V_{\text{tot}} = \frac{(\Phi_r - \Phi_2)^2}{2L_r} + \sum_{i=1}^{N}\left[\frac{(\Delta\Phi_i)^2}{2L_q} - E_J\cos\left(\frac{\Delta\Phi_i + \Phi_{\text{ext}}}{\Phi_0}\right)\right]. \tag{2.64}$$

Here we introduce the relative variables $\Delta\Phi_1 \equiv \Phi_1$ and $\Delta\Phi_2 = \Phi_2 - \Phi_1$, which represent the phase jumps across each of the qubits. Then $\Phi_0 = \hbar/(2e)$ is the reduced flux quantum and Φ_{ext} is the external flux through each of the qubit. Here we consider $\Phi_{\text{ext}}/\Phi_0 = \pi$, such that for a Josephson energy $E_J > \Phi_0^2/L_q$ we obtain a double-well potential for the fluxes $\Delta\Phi_i$. To finally have the Hamiltonian of the system we calculate the canonical momenta $Q_r = \partial\mathcal{L}/\partial\dot{\Phi}_r = C_r\dot{\Phi}_r$, and $Q_i = \partial\mathcal{L}/\partial\Delta\dot{\Phi}_i = C_q\Delta\dot{\Phi}_i$, which represent the charges on each capacitor. As a standard procedure we introduce the rescaled variables $\phi_r = \Phi_r/\Phi_0$, $\phi_i = \Delta\Phi_i/\Phi_0$ and $\mathcal{Q}_\eta = Q_\eta/(2e)$, and we then impose the canonical commutation relations $[\phi_\eta, \mathcal{Q}_{\eta'}] = i\delta_{\eta,\eta'}$. The Hamiltonian for the two qubits-LC system is then given by

$$H_\Phi = 4E_{C_r}\mathcal{Q}_r^2 + \frac{E_{L_r}}{2}\left(\phi_r - \sum_{i=1}^{N}\phi_i\right)^2 + \sum_{i=1}^{N}\left[4E_{C_q}\mathcal{Q}_i^2 + E_J\cos(\phi_i) + \frac{E_{L_q}}{2}\phi_i^2\right], \tag{2.65}$$

where $E_{L_{r,q}} = \Phi_0^2/L_{r,q}$ and, $E_{C_{r,q}} = e^2/(2C_{r,q})$. We show now that this Hamiltonian is completely equivalent to H_D as it is defined in Eq. (2.40). In order to do so we introduce the creation/annihilation operators for the LC circuit such that

$$\begin{aligned}\phi_r &= \sqrt[4]{2\frac{E_{C_r}}{E_{L_r}}}(a^\dagger + a),\\ \mathcal{Q}_r &= i\sqrt[4]{\frac{E_{L_r}}{32E_{C_r}}}(a^\dagger - a),\end{aligned} \tag{2.66}$$

which diagonalise the LC Hamiltonian with frequency $\omega_c = \sqrt{8E_{C_r}E_{L_r}}/\hbar$. The qubit variables ϕ_i and $\mathcal{Q}_i$ represent the coordinate and momentum of an effective particle moving in a potential

$$V(\phi_i) = E_J\cos(\phi_i) + E_{L_q}\phi_i^2/2. \tag{2.67}$$

The light-matter coupling in the dipole gauge is then given by

$$g_D = \omega_c\left(\frac{E_{L_r}}{2E_{C_r}}\right)^{\frac{1}{4}}|\langle\tilde{\varphi}_0|\phi|\tilde{\varphi}_1\rangle|, \tag{2.68}$$

where $\tilde{\omega}_{10}$ and the eigenstates $|\tilde{\varphi}_n\rangle$ are obtained diagonalising the modified qubit Hamiltonian

$$\tilde{H}_q = 4E_{C_q}\mathcal{Q}^2 + V(\phi) + E_{L_r}\phi^2/2, \tag{2.69}$$

with the inclusion of the ϕ^2-term, which is the circuit equivalent of the previously discussed ξ^2-term for the dipole.

We can now represent the flux Hamiltonian (2.65) in the so-called charge gauge, which is equivalent to the Coulomb gauge. We then introduce the unitary transformation $U = e^{-i\mathcal{Q}_r \sum_i \phi_i}$, and the charge Hamiltonian $H_Q = U H_\Phi U^\dagger$, given by

$$H_Q = 4E_{C_r}\mathcal{Q}_r^2 + \frac{E_{L_r}}{2}\phi_r^2 + \sum_i \left[4E_{C_q}\left(\mathcal{Q}_i - \mathcal{Q}_r\right)^2 + V(\phi_i)\right]. \tag{2.70}$$

Introducing $\tilde{\omega}_c = \sqrt{8(E_{C_r} + NE_{C_q})E_{L_r}}/\hbar$ and the light-matter coupling in the Coulomb gauge

$$g_C = \frac{8E_{C_q}}{\hbar}\sqrt{\frac{\omega_c}{\tilde{\omega}_c}}\left(\frac{E_{L_r}}{2E_{C_r}}\right)^{\frac{1}{4}} |\langle\varphi_0|\mathcal{Q}|\varphi_1\rangle|, \tag{2.71}$$

we can directly map this Hamiltonian on H_C, given by Eq. (2.39).

We can then consider the TLA for H_Φ and H_Q in the relevant case with two qubits. We use rather realistic parameters E_J, E_{L_q} and E_{C_q} in order to have the frequency $\omega_{10} \approx 3$ GHz and anharmonicity $|\omega_{10} - \omega_{21}|/\omega_{10} \approx 15$ in line with current experiments [59]. In Fig. 2.9(a) we show the spectrum as a function of $g_0 \sim \sqrt[4]{1/L_r}$, always keeping fixed the resonance condition $\omega_c = \omega_{10}$. The TLA in the charge gauge fails already for quite small coupling, while it remains quite accurate in the flux gauge. Nevertheless we see that also in the flux gauge the TLA gives quite incorrect energies at large coupling. This is the effect of having included in the bare dipole's Hamiltonian the ϕ^2-correction (in the dipoles language ξ^2-term), accordingly to (2.69). However if we completely neglect this term we still find a quite acceptable prediction, as we can see in Fig. 2.9(b). The reason is that the ξ^2-term gives a positive contributions to the energies that should be exactly compensated by the light-matter coupling term. This compensation involves higher levels transitions. If we keep this term in the single particle Hamiltonian, but we truncate it in the light-matter coupling term, we make an inconsistent approximation. The right way to go would be to include it in perturbation theory together with the perturbative terms originating from higher levels transitions. But this would end up in quite complicated low energy Hamiltonian, so, unless it is necessary we wish to avoid such complications. In Fig. 2.9(c) we show that characteristic ground state quantities such as mean photon number $\langle a^\dagger a\rangle$ or single qubits entropy $\mathcal{S}_1 = \mathrm{Tr}[\rho_1 \log_2[\rho_1]]$ are still nicely represented up to very large coupling strength.

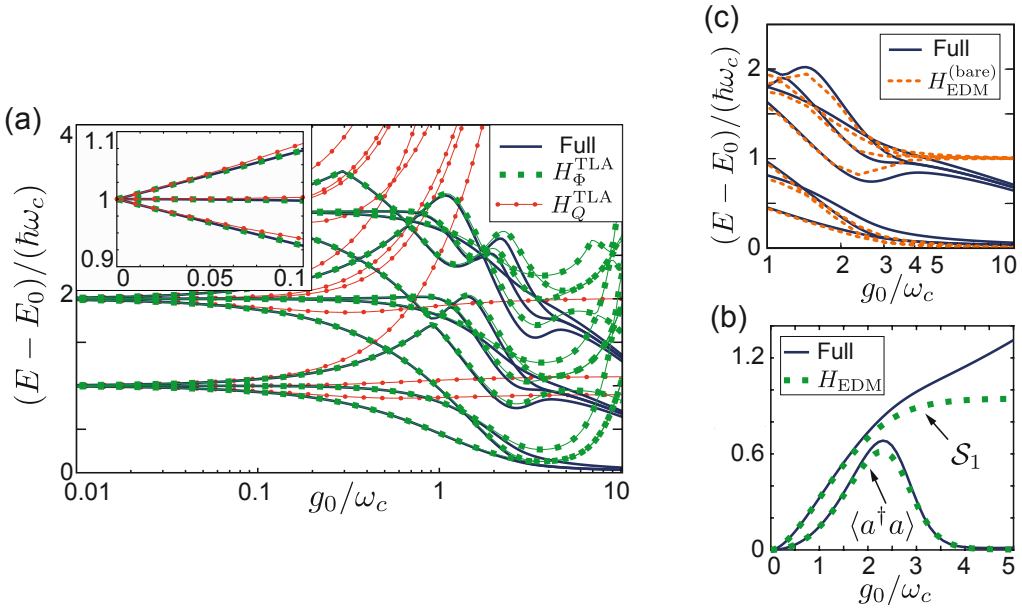

Figure 2.9: Two-qubit circuit QED. (a) Comparison of the energy spectra obtained from the full model H_Φ (solid blue line), the extended Dicke model $H_{\rm EDM}$ derived from H_Φ (green dashed line) and the Dicke model $H_{\rm DM}$ derived from Hamiltonian H_Q (red dotted line) for $N = 2$ flux qubits. The inset shows a zoom of the first three excitation energies for small couplings. (b) Dependence of the ground-state photon number $\langle a^\dagger a\rangle$ and the single qubit entanglement entropy $\mathcal{S}_1 = -{\rm Tr}\{\rho_1 \log_2(\rho_1)\}$ on the coupling strength g_0. Here ρ_1 is the reduced density matrix for a single qubit obtained from the density matrix of the ground state $\rho = |{\rm GS}\rangle\langle{\rm GS}|$ evaluated for the full model H_Φ and for the corresponding effective model $H_{\rm EDM}$. (c) The lowest eigenenergies (dashed orange lines) of the extended Dicke model without the x^2-correction, $H_{\rm EDM}^{\rm (bare)}$, are compared with the corresponding energies of the full model (solid lines). For all the plots the value of L_r has been used as a tuning parameter and C_r has been adjusted to keep the resonance condition $\omega_{10} = \omega_c = \sqrt{8E_{C_r}E_{L_r}}/\hbar$ fixed. The parameters for the flux qubits are the same as in Fig. 2.8(c).

Chapter 3

A minimal model of cavity QED

In this chapter we review the main regimes of cavity QED that can be found in the current research and we explain how to formulate a theory able to capture (at least qualitatively) them all. This is done by putting together the notions of the last two chapters to finally arrive at the *minimal model* of cavity QED. The idea behind the minimal model is to find the simplest model which holds up to arbitrary large coupling strength and which treats consistently electrostatic and dynamics effects.

The results of this chapter are mostly contained in Physical Review A 97, 043820 (2018). In this project I was the leading author, in collaboration with Tuomas Jaako and Peter Rabl. All the results here reported are obtained by me, under the supervision of Peter Rabl.

3.1 Dipoles coupled to a single electromagnetic mode

From the general considerations about the quantization of the electromagnetic field, we have already argued that when restricted to a single near-resonant mode the Hamiltonian for light-matter interactions is of the form

$$\begin{aligned} H \approx{}& \omega_c a^\dagger a + H_{\text{matter}} \\ &+ \sqrt{\frac{\omega_c}{2\varepsilon_0 V}}(a + a^\dagger) \int d^3r \vec{f}_c(\vec{r}) \cdot \vec{P}(\vec{r}) + \frac{1}{2\varepsilon_0 V}\left(\int d^3r \vec{f}_c(\vec{r}) \cdot \vec{P}(\vec{r}) \right)^2 \\ &+ \frac{1}{2\varepsilon_0} \int d^3r \vec{P}_\parallel(\vec{r}) \cdot \vec{P}_\parallel(\vec{r}). \end{aligned} \tag{3.1}$$

Here $\vec{f}_c(\vec{r})$ is the cavity mode function, $\vec{P}(\vec{r})$ is the matter polarization density, and $\vec{P}_\parallel(\vec{r})$ is its longitudinal part. The first line of this Hamiltonian represent the free cavity and the free matter. The second line describes the cavity-matter interaction and the third line represents the matter-matter interaction due to the electrostatic force. What is left to do now is to specify the parameters of the cavity, its mode functions, and specify a model for the free matter and its polarization.

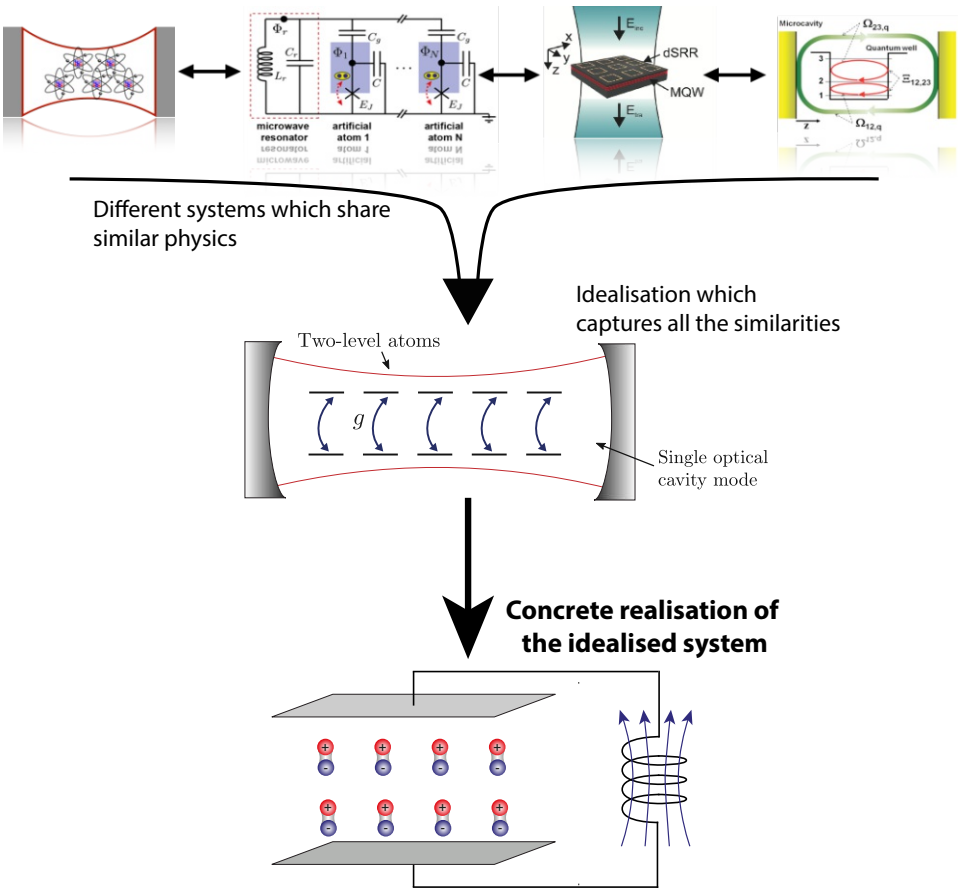

Figure 3.1: A simple toy model for cavity QED. Many different systems, ranging from atomic gases to more complex structures in solid state can be classified as cavity QED systems. Collecting all their basics common properties we arrive at an abstract idealised mathematical description, presented by an Hamiltonian which couples together two-level systems and harmonic modes. A faithful physical realization of such an abstract Hamiltonian is given by an ensemble of dipoles inside the capacitor of a single-mode LC resonator.

As one of the simplest examples for a material system, we will consider in the following discussion an ensemble of point-like dipoles, located at fixed positions on a lattice. In the case of a simple square lattice we can rewrite the total number of dipoles in terms of their number along each direction

$$N = N_x N_y N_z. \tag{3.2}$$

For the dynamics of each dipole we consider the two extreme cases of two-level dipoles or fully harmonic dipoles. Concerning the cavity, the simplest situation is when the cavity mode function is approximately homogeneous across the ensemble in space, in this case dipoles are resonant with a spatially homogeneous electric field, and we assume that the frequency of that mode is much lower than all the other electromagnetic modes. This last requirement seems a bit tricky in a standard Fabry-Perot resonator, where the cavity frequencies are typically equispaced. To overcome this limitation one needs to "slow-down" the resonant mode in a controlled way. The simplest physical

realization of such a system is an LC circuit. When the capacitor is large enough, the electric field due to the charge oscillating through the circuit is to a good approximation homogeneous, while the frequency can be tuned, in principle without constraints, by changing the values of the inductance or the capacitance. The dipolar matter can be placed inside the capacitor, realising a genuine collective coupling with the current flowing in the circuit. As sketched in Fig. 3.1 this system is an exact representation of many approximated descriptions used for a large variety of cavity QED systems. To arrive at the final cQED Hamiltonian is worth to proceed in a more pedagogical way, constructing it step by step from the equations of motions of our toy model, and at the end verifying that it matches the general shape (3.1).

The LC-resonator frequency is given by $\omega_c = 1/\sqrt{LC}$, where L is its inductance and C its capacitance. The dipoles are fixed on a lattice, with positions $\vec{r}_i = (x_i, y_i, z_i)$. We assume that each dipole is formed by two charges q and $-q$, and we label the displacement between them as ξ. Therefore, the dipole moment of each i-th dipole is

$$\mu_i = q\xi_i, \tag{3.3}$$

where we assume for simplicity that they are all directed just along the z-axis (perpendicular to the capacitor plates). The schematic view on the system is shown in Fig. 3.2(a).

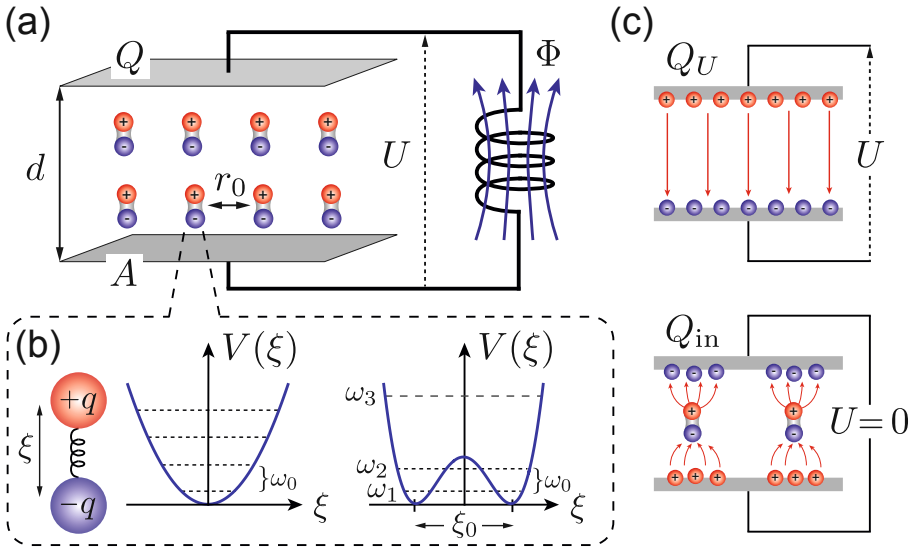

Figure 3.2: (a) Sketch of the cavity QED setup considered in this work. (b) Different effective potentials $V(\xi)$ for the dipole variable ξ are used to model either harmonic or two-level dipoles of frequency ω_0. (c) Illustration of the two different contribution to the total charge $Q = Q_U + Q_{\rm in}$ on the upper capacitor plate. See text for more details.

The dynamics of the dipole moment can be thought as the dynamics of a particle in one dimension, with coordinate ξ, mass m, and subjected to the given potential $V(\xi)$, as shown in Fig. 3.2(b). We will mainly focus on the two most paradigmatic examples: the harmonic potential, and the

double-well potential. In particular, we will use the harmonic dipoles to discuss all the features that can be classified as "classical", in the sense that the same properties would be encountered as well in the classical theory of dielectrics (see Drude-Lorentz theory for instance [39]). The double well potential instead represents a "fully quantum scenario", in the sense that, since tunneling dynamics has no classical counter-part, in this case we will find strong deviations from the classical predictions once we enter the ultrastrong coupling regime. To handle this case in a reasonably simple way we will make use of the two-level approximation developed in the previous chapter.

The LC circuit dynamics instead is determined by its Kirchhoff equations. The voltage between the capacitor plates is related to the flux through the inductor by $U = \dot{\Phi}$, where Φ is the magnetic flux (which is the dynamical coordinate of the circuit). The flux is related to the current flowing out from the capacitor by $\dot{Q} = -\Phi/L$. When the dipoles (or, more generally, the dielectric material) are located between the capacitor plates the total charge Q can be written as $Q = Q_U + Q_{\rm in}$. Here Q_U is the charge that accumulates on the capacitor giving rise to a voltage drop. The second contribution $Q_{\rm in}$ is the charge induced by the dipoles, which still accumulates on the capacitor, but does not give rise to any voltage drop, because it exactly compensate the electric field produced by the dipoles themselves (it is actually a consequence of having metallic plates as boundary of the dipole system). We have a sketch of this idea in Fig. 3.2(c). Using all these relations we obtain the equation of motion for the LC circuit

$$C\ddot{\Phi} + \frac{\Phi}{L} = -\dot{Q}_{\rm in} \simeq \frac{q}{d}\sum_i \dot{\xi}_i, \tag{3.4}$$

where in the last step we used the fact that, for large enough system, the total charge induced by a single dipole is given by $\sim -q\xi/d$, where d is the distance between the plates.

The motion of the dipoles instead is just given by equating the dipole's acceleration to the sum of the forces acting on it. The forces on the dipole are given by the "internal" dipole potential, and the total electric field at the dipole's position. For the i-th dipole we have the equation $m\ddot{\xi}_i = -\partial_\xi V(\xi_i) + qE(\vec{r}_i)$. The electric field can be further decomposed into the electric field due to a voltage drop between the capacitor plates and the electric field generated by the surrounding dipoles

$$qE(\vec{r}_i) = -\frac{q}{d}\dot{\Phi} - m\omega_{\rm P}^2 \sum_j \mathcal{D}_{ij}\xi_j, \tag{3.5}$$

where we introduce the *plasma frequency*

$$\omega_{\rm P} = \sqrt{\frac{q^2}{\varepsilon_0 m r_0^3}}, \tag{3.6}$$

and the matrix $\mathcal{D}_{ij}$ gives the adimensional amplitude of the electric field at the position $\vec{r}_i$ generated

by a dipole in the position $\vec{r}_j$. In free space it takes the shape

$$\mathcal{D}_{ij} = \frac{r_0^3}{4\pi} \frac{r_{ij}^2 - 3(\vec{r}_{ij} \cdot \vec{e}_z)^2}{r_{ij}^5}, \tag{3.7}$$

where $\vec{r}_{ij} = \vec{r}_i - \vec{r}_j$. Following the discussion in the first chapter, we will show that this quantity is strongly influenced by the boundaries, due to the presence of image charges. It is important to notice that, when $i = j$, $\mathcal{D}_{ii}$ has a divergent part, which is reminiscent of the divergent self energy ϵ_A that we found in the first Ch. 1, and a finite part. The divergent part is independent of the boundaries and it should be removed by mass-renormalization [60]. In our case, we just drop it. The finite part instead depends on the boundaries and it is a physical effect which should be considered. However, since it is just a quadratic energy shift, it can be safely absorbed in the definition of the dipole potential, $V(\xi_i) + m\omega_{\mathrm{P}}^2 \mathcal{D}_{ii}\xi_i^2/2 \mapsto \tilde{V}(\xi_i)$. In conclusion, we obtain the equations for the dipoles inside the capacitor of the LC circuit

$$m\ddot{\xi}_i + \partial_\xi V(\xi_i) + m\omega_{\mathrm{P}}^2 \sum_j \mathcal{D}_{ij}\xi_j = -\frac{q}{d}\dot{\Phi}. \tag{3.8}$$

3.2 The LC-dipole system and the generic cavity QED Hamiltonian

From general physical considerations we have derived the main equations describing the system in Fig. 3.2(a). So we are in the position to derive the corresponding Lagrangian, then the Hamiltonian, and finally to quantize the system. The Lagrangian of the system is given by

$$\mathcal{L} = C\frac{\dot{\Phi}^2}{2} - \frac{\Phi^2}{2L} + \dot{\Phi}Q_{\mathrm{in}} + \sum_i \left[\frac{m}{2}\dot{\xi}_i^2 - V(\xi_i)\right] - \frac{m\omega_{\mathrm{P}}^2}{2}\sum_{i\neq j} \mathcal{D}_{ij}\xi_i\xi_j. \tag{3.9}$$

The canonical momenta are given as usual by

$$\Pi = \frac{\partial \mathcal{L}}{\partial \dot{\Phi}} = c\dot{\Phi} + Q_{\mathrm{in}}, \qquad p_i = \frac{\partial \mathcal{L}}{\partial \dot{\xi}_i} = m\dot{\xi}_i. \tag{3.10}$$

We note that Π represents the total physical charge accumulated on the capacitor, thus $\Pi = Q = Q_U + Q_{\mathrm{in}}$, while p_i just represents the kinetic momentum of the dipole's displacement. The Hamiltonian follows as

$$H = \frac{(\Pi - Q_{\mathrm{in}})^2}{2C} + \frac{\Phi^2}{2L} + \sum_i H_i^d + \frac{m\omega_{\mathrm{P}}^2}{2}\sum_{i\neq j} \mathcal{D}_{ij}\xi_i\xi_j, \tag{3.11}$$

where $H_i^d = p_i^2/(2m) + V(\xi_i)$. Using $Q_{\rm in} \simeq -q\sum_i \xi_i/d$ we can rewrite this Hamiltonian as the expected general cQED Hamiltonian (3.1) derived in the first Ch. 1

$$\begin{aligned} H \simeq\ & \omega_c a^\dagger a + \sum_i \left[\frac{p_i^2}{2m} + V(\xi_i)\right] \\ & + \frac{q}{d}\sqrt{\frac{\omega_c}{2C}}(a + a^\dagger)\sum_i \xi_i + \frac{1}{2C}\left(\frac{q}{d}\sum_i \xi_i\right)^2 \\ & + \frac{m\omega_{\rm P}^2}{2}\sum_{i\neq j}\mathcal{D}_{ij}\xi_i\xi_j. \end{aligned} \tag{3.12}$$

To match the general expression given by (3.1), we need to consider that the matter polarization vector is given by $\vec{P}(\vec{r}) \mapsto q\sum_i \xi_i \vec{e}_z \delta^{(3)}(\vec{r} - \vec{r}_i)$, where $\vec{e}_z$ is a unit vector directed along the z-axis (normal to the capacitor plates). Since the electric field inside the capacitor is to good approximation homogeneous, and normal to the plates, the cavity mode function is approximately $\vec{f}_c(\vec{r}) \approx \vec{e}_z$. The parameters are matched considering $\varepsilon_0 V \mapsto Cd^2$, which is actually consistent with having $V = A\cdot d$, and with the usual capacitance of a parallel plate capacitor, $C = \varepsilon_0 A/d$ (where A is the area of the plates).

3.3 Polaritons and dynamical instabilities in LC cavity

In this section we take a closer look at equations (3.4)-(3.8). In particular, we focus on the case of harmonic dipoles, for which

$$V(\xi) \simeq \frac{m\omega_0^2}{2}\xi^2. \tag{3.13}$$

In this case the equations of motion can be solved by introducing their own normal modes, as it is common practice in all coupled harmonic systems [48]. Then the "quantum problem" and the classical one coincide, i.e. finding the normal modes is equivalent to finding the eigenstates of the quantized system. The normal modes will be given in terms of *polaritons*, because the coupling between the dipoles and the cavity will hybridize light and matter. But there is another important feature here which is given by the dipole-dipole interactions. The dipole-dipole interactions, expressed in terms of the matrix $\mathcal{D}_{ij}$ will also give rise to *dipolar modes*, in which the oscillation can be shifted in a non trivial way. In the end the system exhibits something that we could name *dipolar-polaritons*, meaning that the normal modes will be a complicated mixture of dipolar modes and the LC resonance. To proceed further we first consider the dipolar modes, which are solutions of the eigenvalues equation

$$\sum_j \mathcal{D}_{ij}c_n(j) = \eta_n c_n(i). \tag{3.14}$$

Since $\mathcal{D}_{ij}$ is real and symmetric, the modefunctions $c_n(i)$ are an orthonormal basis, from which we can reconstruct the dipole ensemble

$$\xi_i = \sum_n X_n c_n(i). \tag{3.15}$$

The equations of motion become

$$\begin{aligned} \ddot{X}_n &= -(\omega_0^2 + \eta_n \omega_{\mathrm{P}}^2) X_n - \omega_{\mathrm{P}} \sqrt{\frac{\omega_0}{\omega_c}} \sqrt{\nu_n} \dot{\Phi}, \\ \ddot{\Phi} &= -\omega_c^2 \Phi + \omega_{\mathrm{P}} \sqrt{\frac{\omega_c}{\omega_0}} \sum_n \sqrt{\nu_n} \dot{X}_n, \end{aligned} \tag{3.16}$$

where we introduce the *mode-dependent filling factor*

$$\nu_n = \frac{r_0^3 |\sum_i c_n(i)|^2|}{V}, \tag{3.17}$$

which measures the overlap between the n-th dipole mode and the cavity. It is important to notice that the filling factor is sensitive to the phase of the given dipole modes, and, for instance, it is zero if the dipoles oscillate completely out of phase (anti-ferroelectric dipolar mode), while it is maximum when the dipoles oscillate in-phase (ferroelectric dipolar mode). Moreover, the filling factor tells us about the importance of the cavity-dipole coupling compared to the dipole-dipole interaction. This can be seen by considering a ferroelectric mode (fe), in which all dipoles are in phase. For such a mode $c_n(i) = 1/\sqrt{N}\ \forall\ i$, so the filling factor is $\nu_{\mathrm{fe}} = r_0^3 N/V = V_{\mathrm{d}}/V$, which the ratio between the volume occupied by the dipoles and the total cavity volume. For a dense dipole ensemble it could be the case where the dipole volume is very small with respect to the cavity, the plasma frequency is very large, but the overall cavity-dipole coupling is very small. Note that the strength of light-matter coupling in this context is given by the plasma frequency ω_{P}, which regulates both the dipole-dipole and the cavity-dipole interaction.

Moving on, we can transform Eq. (3.16) in Fourier space and derive the polynomial eigenvalue equation for the polariton frequencies ω

$$(\omega^2 - \omega_c^2) \prod_n (\omega^2 - \omega_n^2) \left[1 - \sum_n \frac{\nu_n \omega_{\mathrm{P}}^2 \omega^2}{(\omega^2 - \omega_c^2)(\omega^2 - \omega_n^2)} \right] = 0, \tag{3.18}$$

where we used the compact notation $\omega_n^2 = \omega_0^2 + \eta_n \omega_{\mathrm{P}}^2$. When the system is large and regular enough, the dipolar modes become sines and cosines, and only the zero-th mode has a relevantly large filling factor. This zero-th mode, which is often called *the collective mode*, is completely ferroelectric, so

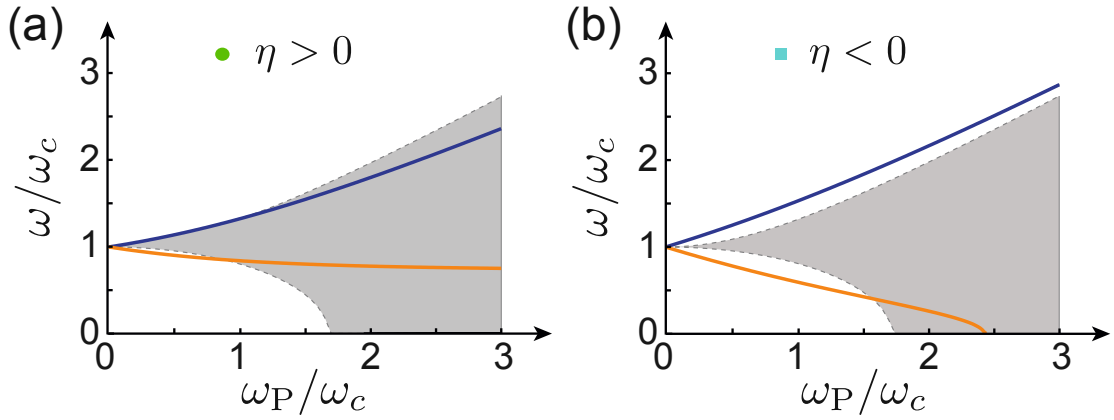

Figure 3.3: The spectrum of the two bright polariton branches is plotted as a function of ω_p and for $\omega_c = \omega_0$. In (a) a positive value of $\eta \approx 0.3$ and in (b) a negative value of $\eta \approx -0.2$ has been assumed. In both plots the orange (lower) and the dark blue (upper) lines represent the spectrum obtained from Eq. (3.20), while the shaded area indicates the range of frequencies of all other dark polariton modes obtained from the numerical solution of the full eigenvalue problem given by Eq. (3.18). The values of η and the full coupling matrix $\mathcal{D}_{ij}$ used in the calculations of the polariton spectra in (a) and (b) have been obtained for the case $N_x = 10$, $N_y = N_x$, with three layers on z, $N_z = 3$, and a total number of dipoles $N = N_x N_y N_z$. The values of $h/d = \nu \approx 0.2$ and $h/d = \nu \approx 0.9$, respectively. See section 3.5 for the definition and explanation of h/d and for further details.

all the dipoles are in phase, therefore $c_0(i) \simeq 1/\sqrt{N}\ \forall\ i$, which gives $\nu_0 \simeq r_0^3 N/V$ and

$$X_0 = \frac{\sum_i \xi_i}{\sqrt{N}}, \qquad \eta_0 = \frac{1}{N}\sum_{i\neq j} \mathcal{D}_{ij}, \tag{3.19}$$

(for simplicity of notation we will drop the index "0" in the following). In this limit the other dipolar modes are basically decoupled from the cavity, and, because the dipoles are harmonic, also uncoupled among each other. Therefore we have $N-1$ *dark modes*, while the collective mode gets strongly hybridized with the EM field and splits into two polariton modes, as depicted in Fig. 3.3. Restricting ourselves to this collective mode, we can solve Eq. (3.18), which gives the two polariton frequencies

$$\omega_\pm^2 = \frac{\omega_d^2 + \omega_c^2 + \nu\omega_P^2 \pm \sqrt{(\omega_d^2 + \omega_c^2 + \nu\omega_P^2)^2 - 4\omega_d^2\omega_c^2}}{2}, \tag{3.20}$$

where $\omega_d^2 = \omega_0^2 + \eta\omega_P^2$ is the frequency of the collective dipolar mode. In Fig. 3.3(a-b) we see two examples of the polariton spectrum, indicated by the blue and red lines. In the first case (a) $\eta > 0$ and we see that the polariton frequencies are always positive, meaning that the system is dynamically stable. In the second case (b) instead $\eta < 0$, and we can see from Fig. 3.3(b) that the lower polariton branch goes to zero at sufficiently large coupling. Despite the fact that from this perspective it might seem to be related to the light-matter coupling, this instability is actually just due to an instability occurring in the collective dipolar mode itself. Indeed setting the condition

$\omega_-^2 = 0$, we find that

$$\sqrt{-\eta}\omega_P = \omega_0, \tag{3.21}$$

which just means that $\omega_d^2 = 0$. This is not surprising because the light-matter coupling is proportional to ω_P, which also regulates the strength of the dipole-dipole interaction. Looking at Fig. 3.3 we see that eventually most of the dipolar modes (the grey shaded region) go unstable when the plasma frequency is large enough.

A vanishing oscillation frequency means that dipolar system becomes unstable and the assumed harmonic approximation is no longer valid. In particular what has to be reconsidered here is the harmonic approximation for the dipoles. If we reintroduce a finite non-linearity, which is the case in every real physical system, the instability can be cured and eventually replaced by a phase transition. This phase transition will be one of the subjects of the next chapters, and for now we limit ourself to acknowledging that something happens when the dipolar energy becomes negative and comparable to the bare dipole frequency, in general for any given dipole mode $\eta_n\omega_P^2 = -\omega_0^2$.

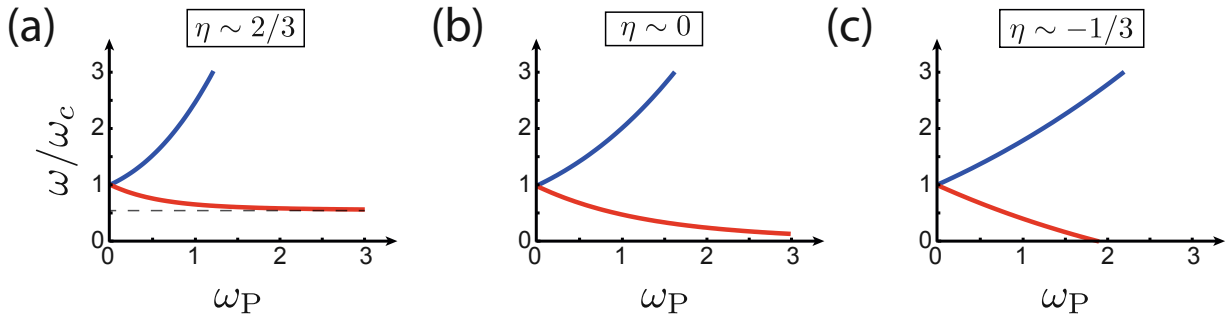

Figure 3.4: Plot of the frequencies $\omega_\pm$ of the two bright polariton modes as a function of the plasma frequency ω_P^2. See Eq. (3.20). The three plots show the cases of (a) $\eta > 0$, (b) $\eta = 0$ and (c) $\eta < 0$.

Focusing just on the two polariton modes, we see that depending on the value of η, there are three different limiting cases for the behaviour of the lower polariton mode at very large couplings:

$$\begin{aligned} \eta = 0 \;&\Rightarrow\; \lim_{\omega_P\to\infty} \omega_- = 0, \\ \eta > 0 \;&\Rightarrow\; \lim_{\omega_P\to\infty} \omega_- = \omega_c\sqrt{1 - \frac{\nu}{\nu+\eta}}, \\ \eta < 0 \;&\Rightarrow\; \lim_{\omega_P\to\omega_P^c} \omega_- = 0 \quad \text{Instability}. \end{aligned} \tag{3.22}$$

These three different cases are illustrated in Fig. 3.4. In the next section we will go a bit more in the details of the η-parameter, focusing on the physical realisation of these three cases.

3.4 The η-parameter and the macroscopic field inside a dielectric

Since the filling factor is bounded by $\nu_n \leq 1 \; \forall \; n$, when $\omega_{\rm P} \sim \omega_c, \omega_0$ the dipole-dipole interaction gives a dominant contribution to the physics of cavity QED, giving a central role to the parameter $\eta = 1/N \sum_{i \neq j} \mathcal{D}_{ij}$. This bring us from the field of dilute emitters (e.g. atoms) to the field of strongly interacting dielectrics. We want here to establish a connection between our theory and the usual theory of macroscopic dielectrics. To do so, we need to understand the static case, where all dipoles are polarised and where there is no dynamics. This analysis will give us the correct intuition that we will apply to the dynamical case where the external electric field is given by the cavity and it is also a dynamical degree of freedom itself.

Let's consider the case in which the dipolar ensemble is subjected to an external electric field. The total electric field in space is given by (considering all fields just directed along z)

$$E = E_{ext} - E_{\rm dip}(\vec{r}), \tag{3.23}$$

where $E_{\rm dip}(\vec{r})$ is the field generated by all the dipoles and it is in general non homogeneous. The dipolar field can be expressed in terms of the longitudinal delta function and the polarization density $P(\vec{r})$

$$E_{\rm dip}(\vec{r}) = \frac{1}{\varepsilon_0} \int d^3r' \delta^{\parallel}_{zz}(\vec{r}, \vec{r}\,')P(\vec{r}\,') = \frac{1}{4\pi\varepsilon_0} \int d^3r' \frac{|\vec{r} - \vec{r}\,'|^2 - 3\left[(\vec{r} - \vec{r}\,') \cdot \vec{e}_z\right]^2}{|\vec{r} - \vec{r}\,'|^5} P(\vec{r}\,'), \tag{3.24}$$

where the last equality holds only in free space, while it should be corrected by additional terms in cavities, to take account of the image charges. A crucial question in the physics of macroscopic dielectric is how to relate the macroscopic polarization, which is measured, to the electric field inside the dielectric and finally to the microscopic polarization. To this end we introduce the average dipole electric field,

$$E_{\rm D} = \frac{1}{N} \sum_{i=1}^{N} E_{\rm dip}(\vec{r}_i), \tag{3.25}$$

which is the average field that each dipole sees, due to the other dipoles. Note that in this average we remove by hand the contribution of the self-field which is generated by the dipole itself (which is actually infinite). The total average field inside of the dielectric is given by

$$E_{\rm avg} = E_{ext} - E_{\rm D}. \tag{3.26}$$

Assuming a meanfield approach we describe the dynamics of each dipole as if it feels the average

electric field rather than the true local one

$$m\ddot{\xi}_i \approx F(\xi_i) + qE_{\text{avg}}, \tag{3.27}$$

where $F(\xi_i)$ is the generic internal force of each dipole.

If we consider a strong enough external field, we can assume that all the dipoles are polarized in the same way, having all the same dipole moment $\mu_i \simeq \mu_0 = q\xi_0 \ \forall i$. So we are considering an homogeneously polarized medium. Its induced total electric field is then given by

$$qE_{\text{D}} = m\omega_{\text{P}}^2 \left(\frac{1}{N} \sum_{i \neq j} \mathcal{D}_{ij} \right) \xi_0 = \eta m \omega_{\text{P}}^2 \xi_0. \tag{3.28}$$

Here we see the central result of this section, the η-parameter just represents the average electric field amplitude felt by each dipole, due to the others. If we want now to calculate the equilibrium value of ξ_0 subjected to the external electric field we have

$$\xi_0 = \frac{q}{m\omega_0^2} E_{\text{avg}} \tag{3.29}$$

where we consider that each dipole has an harmonic dynamics with frequency ω_0 (as usual). Using the definitions (3.23), (3.28) and the definition of η (3.19) we find the final closed expression for each single dipole displacement

$$\xi_0 = \frac{N\sigma}{1 + \eta N\sigma} \frac{\varepsilon_0 r_0^3}{q} E_{ext}, \tag{3.30}$$

where $N\sigma = \omega_{\text{P}}^2/\omega_0^2$. Defining the collective static polarization density as $P = q\xi_0/r_0^3$, we have

$$P = \frac{N\sigma}{1 + \eta N\sigma} \varepsilon_0 E_{ext}. \tag{3.31}$$

For a non-interacting system we would have $P = N\sigma\varepsilon_0 E_{ext}$, which corresponds to have $\eta = 0$.

For any $\eta > 0$ the consequent static polarization is smaller than the non-interacting one, so we say that the dipole-dipole interaction has a *de-polarizing* effect. As shown in the last section, this de-polarization can be observed in the polariton spectrum too, through the relative *depolarization shift*, see Fig. 3.4(a).

For $\eta < 0$, instead, the static polarization becomes larger than the non-interacting one. At the critical density, expressed by the relation $N\sigma = -1/\eta$ the static polarization diverge. As anticipated in the previous section, this signals the onset of a ferroelectric phase transition. At this density the harmonic approximation for the dipoles ceases to be valid, and a more detailed description must be assumed. We will see in the next chapters that it will be still possible to keep a reasonably simple description of our dipoles to grasp the physics at this high densities, thanks to the two-level

approximation. But this requires to restrict ourself to a more special class of systems.

3.5 Dipole-dipole interactions and geometry

So far we have never really commented on how to obtain different values for η. Since η does not depend on any of the other parameters, it can only be influenced by the geometry of the dipolar lattice and the boundaries. Indeed from the classical theory of dielectrics [61] we know that the geometrical shape of the dielectric plays an important role for its response to an electric field. This translates in our language in a variety of values for η, which in the end determines most of the important properties of the system (above all its dynamical stability).

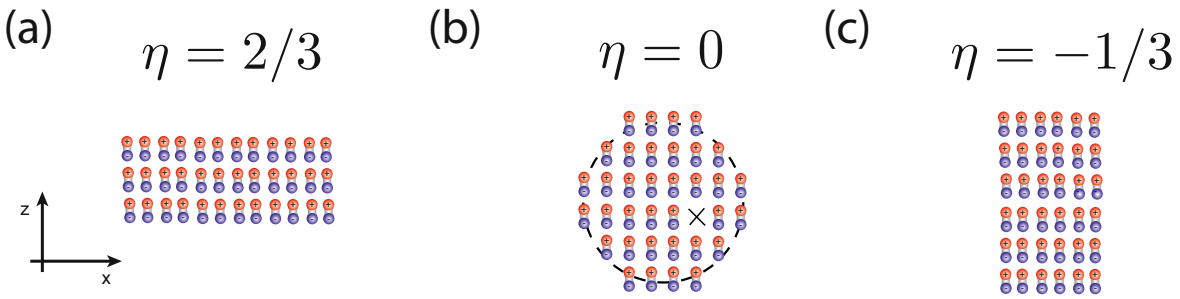

Figure 3.5: Schematic view of the three different most relevant dipoles configurations. The three figures are three dimensional, but just their projection on the (x, z) plane is represented.

The three situations above, $\eta > 0$, $\eta = 0$, and $\eta < 0$ corresponds to different geometrical realisations of the dipole's lattice, due to the anisotropy of the dipole-dipole interaction:

- $\eta > 0$, this is the case of a pancake-like arrangement, where the dipoles are placed on a simple square lattice on (x, y) plane, and directed along z (as usual). If we take a single infinite layer in the (x, y) plane, we have

$$\eta = \frac{1}{4\pi} \sum_{(n,m)\in\mathbb{Z}^2/0} \frac{1}{(n^2+m^2)^{3/2}} = \frac{\zeta(3/2)L(3/2,\chi_4)}{\pi} \approx 0.72, \tag{3.32}$$

  where the last equality is calculated in Ref. [62, 63]. This value is the largest value that one achieves on a regular square lattice. It still holds in a thin slab, where many layers are packed on top of each other, provided that the number of dipoles along z is smaller than the in-plane dipole's number, as it is schematically represented in Fig. 3.5(a). In App. E.4 one can find a few numerical example while in App. E the same calculation is performed in the continuum polarization limit, including the famous Lorentz correction term [39].

- $\eta = 0$ does not necessarily mean that the system is non-interacting or so dilute that electrostatic forces are negligible. Indeed in a simple cubic lattice, assuming that the dipole is located

in the center of the cell, the electric field at the center, generated by the six nearest neighbour dipoles, is exactly zero for any density. Actually in a infinite cubic lattice all positive contributions coming from in-plane dipoles are exactly compensated by the negative contributions from all the dipoles along z. In a finite system this cancellation still holds provided that the system has the shape of a sphere, as indicated in Fig. 3.5(b). In a cube there will be still a very small contribution from the surface boundary.

- $\eta < 0$, this is the case of a dipolar ensemble elongated along the z-axis. In the limiting case where all the dipoles are aligned on top of each other one obtains

$$\eta = -\frac{1}{2\pi} \sum_{n \in \mathbb{Z}/0} \frac{1}{|n|^3} = -\frac{\zeta(3)}{\pi} \approx -0.38. \tag{3.33}$$

This value is the minimum value achievable. It still holds for a quasi one-dimensional, cigar shaped system, as in Fig. 3.5(c).

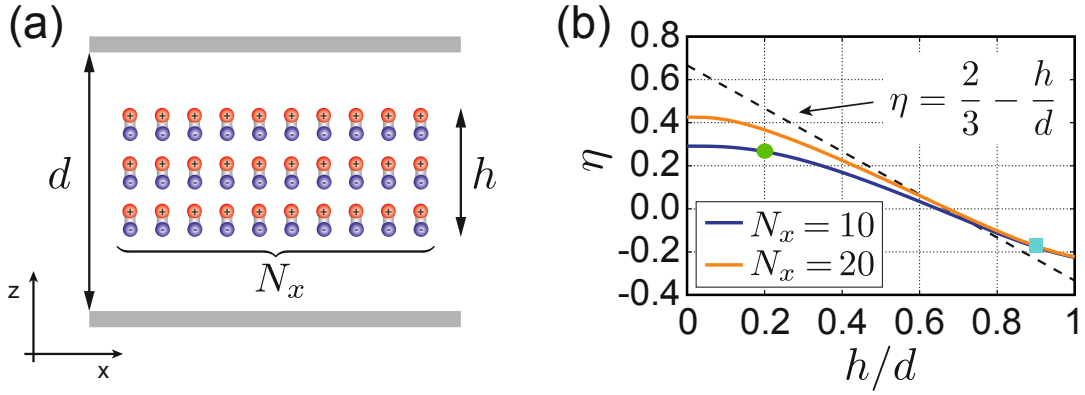

Figure 3.6: (a) Sketch of an ensemble of $N = 3 \times N_x^2$ dipoles, which are arranged in three layers on a square lattice with spacing r_0 and placed between two capacitor plates. For this configuration the resulting value of η is plotted in (b) for varying $d \geq h$ and different N_x.

The value of η actually strongly depends on the boundary condition of our electrostatic problem. In particular all the discussion reported above is valid in free space. When the system is enclosed in a finite region, with metallic boundaries (such as our capacitor of the LC cavity), the dipole-dipole interaction is modified by the presence of the image charges (see Ch. 1), and so is η. For a thin slab, consisting of a few layers with very large area, we obtain

$$\eta \approx \frac{2}{3} - \frac{h}{d}, \tag{3.34}$$

where h is the thickness of the dipolar slab. This effect is reported in Fig. 3.6 and it is discussed in more detail in App. E.5. This linear dependence on h is necessary in order to keep the zero potential

drop across the plates. It can be easily understood considering the relation between the induced charge (the charge needed on the capacitor plates to satisfy the metallic boundary conditions) and the surface charge on the flat dielectric slab $Q_{\text{surf}} = AP$, where A is the surface's area of the dielectric. Following the result in Ch. 1 we have

$$Q_{\text{im}} = \frac{\sum_i q\xi_i}{d} = \frac{q\xi_0}{d} N \frac{n_d}{n_d} = q\xi_0 n_d \frac{V_d}{d} = PA\frac{h}{d} = Q_{\text{surf}}\frac{h}{d}, \tag{3.35}$$

where n_d is the density of dipoles, $V_d = h \times A$ is the volume occupied by the dipolar lattice, and we use the fact that for an homogeneously polarised medium the polarisation density is $P = q\xi_0 n_d$. The electric field generated by this image charge is in opposition to the field generated from the dipoles and contributes to the average local field as

$$E_D \longmapsto E_D - \frac{h}{d}\frac{Q_{\text{surf}}}{\varepsilon_0 A} \approx \left(\frac{2}{3} - \frac{h}{d}\right)\frac{P}{\epsilon_0}. \tag{3.36}$$

This means that in the case of a slab inserted in between two grounded metallic plates, with $h \approx d$, we expect

$$\eta \simeq -\frac{1}{3}. \tag{3.37}$$

As we have verified numerically, this means that the presence of the plates can change the sign of the macroscopic field inside of the dielectric, potentially inducing a ferroelectric phase transition in the dipole's ground state.

3.6 Coupling parameters and effective fine structure constant

In this section we take a closer look at the coupling parameter in our cavity QED system. We start from the generic Hamiltonian (3.12) describing a dipolar ensemble inside the capacitor of an LC circuit, and assign an intrinsic length scale to the dipoles, ξ_0. This can be, for instance, the matrix element between two levels. The single particle coupling is then given by

$$g = \frac{q\xi_0}{d}\sqrt{2\frac{\omega_c}{\hbar C}} = \omega_c\sqrt{8\pi\alpha}. \tag{3.38}$$

Here we introduced the *effective fine structure constant*

$$\alpha = \alpha_{\text{fs}}\left(\frac{q}{e}\right)^2\left(\frac{\xi_0}{d}\right)^2\frac{Z}{Z_0}, \tag{3.39}$$

where $\alpha_{\text{fs}} = e^2/(4\pi\varepsilon_0\hbar c)$, e and c are the elementary electron's charge, and the speed of light, $Z = \sqrt{L/C}$ is the LC impedance, and $Z_0 = \sqrt{1/(\varepsilon_0 c)}$ is the vacuum impedance. The effective fine

structure constant is a useful concept which highlights the connection between cavity QED and the underlying general theory of quantum electrodynamics. In particular it is important to notice that we have just two ways to boost it above unity (we recall that $\alpha_{\rm fs} \sim 1/137$): either increasing the charge of the dipole or increasing the impedance of the cavity (the LC circuit). It is also important to stress that just increasing the effective size of the dipole will not be enough, since, in order to fit into the cavity, it must be that $\xi_0 < d$. This last point was crucial in setting the bound for USC with Rydberg atoms in optical cavities [64]. Instead in an "artificial" cavity, where its impedance is different from the vacuum one, it is possible in principle to achieve arbitrary coupling strength.

It is important to emphasize that the coupling "g" defined in Eq. (3.38) is the coupling between a single dipole and the cavity field. This must not be confused with having a large coupling between the cavity and the ensemble as a whole. Indeed, as a consequence of the long-wavelength approximation, which leads to the collective coupling, we could define a *collective coupling*, for the collective polarization $P \sim \sum_i \xi_i$. The matrix element of such operator between the dipoles ground state and their first excited state scales like $P_{01} \sim \sqrt{N}\xi_0$, assuming the dipoles are not correlated. Then the collective coupling can be defined as

$$G = \sqrt{N} g. \tag{3.40}$$

This quantity can be very large even for weakly interacting dipoles. The collective coupling is directly related to the plasma frequency, defined in (3.6), by

$$G = \sqrt{\nu}\omega_{\rm P}\sqrt{\frac{2m\xi_0^2}{\hbar}\omega_c} \simeq \sqrt{\nu}\omega_{\rm P}\sqrt{\frac{\omega_c}{\omega_0}} \tag{3.41}$$

Here the last equality follows when the dipoles can be approximated as harmonic oscillators. This relation clearly shows that the collective coupling essentially depends only on the dipole density and is thus directly proportional to the typical scale of the dipole-dipole interactions, i.e., the plasma frequency.

3.7 Coupling regimes of cavity QED

In this last section we partially review the usual classification of light-matter regimes [65, 66]. They can be characterised by comparing the energy stored in the dipole-field coupling to the other energy scales in the system. We restrict this discussion to the case of a single dipole. In general the dipole-field coupling can be characterised by the quantity

$$\bar{g} = \frac{\mu_0 E_0}{\hbar}, \tag{3.42}$$

where $\mu_0 = \sqrt{\langle \hat{\mu}^2 \rangle}$ is the ground state expectation value of the dipole operator of our dipole, while $E_0 = \sqrt{\langle \hat{E}^2 \rangle}$ is the vacuum expectation value of the electric field operator. In general matter and cavity have multiple energy scales, but in the simplest scenario we can say that they are characterised by at least two energy scales

$$\omega_c \ , \ \omega_0, \tag{3.43}$$

i.e., the cavity frequency and the dipole frequency. There are actually other two scales that we need to consider even in the simplest situation which are the cavity losses and the dipole friction

$$\gamma \ , \ \kappa. \tag{3.44}$$

In the standard quantum optical literature three regimes are mainly reported, based on the relations between these three energy scales

- *Weak coupling* (WC) is characterized by the hierarchy $g \ll \gamma, \kappa \ll \omega_c, \omega_0$. The losses are weak enough to resolve the individual transitions of the cavity and the dipole, but larger than the coupling between them. So it is impossible to resolve the Rabi oscillations between dipole and cavity. A photon has to bounce back and forth in the cavity too many times before being absorbed, so it is more likely it leaves the cavity before starting to "talk" with the atom.

- *Strong coupling* (SC) is characterized by the hierarchy $\gamma, \kappa \ll g \ll \omega_c, \omega_0$. In this regime it is possible to observe the coherent coupled dynamics. The eigenstates of the system are polariton states, where light and matter degrees of freedom hybridize. One of the main achievement in recent technology was to have access to this regime on various platforms of cavity QED, from optical cavities [1], to solid state devices [67], or superconducting circuits [68]. When the harmonic or the two-level approximation holds for the dipoles, this regime supports an approximate conservation law, *the conservation of the total excitation number*. For example, considering just two-level dipoles, the total excitation number is defined as $N = a^\dagger a + \sum_i s_z^i$. Promoting this quantity to a conserved one, means that we need $[N, H] \sim 0$. This is possible just neglecting some terms in the light-matter interaction, which is often presented in the literature as *rotating-wave approximation* (RWA). In particular the ground state of the approximated system coincide with the ground state of the uncoupled system. Because this ground state is characterised by having $\langle \mathrm{GS}_{\mathrm{RWA}} | N | \mathrm{GS}_{\mathrm{RWA}} \rangle = 0$, it is often call *the vacuum state*.

- *Ultra-strong coupling* (USC) is characterised by the hierarchy $\gamma, \kappa \ll \omega_c, \omega_0 \ll g$. The dominant energy scale is the light-matter coupling. This regime can be also considered "non-perturbative", in the sense that the coupling cannot be addressed perturbatively with respect

to the matter and cavity bare energies (as opposed to the previous two regimes). The RWA is no longer applicable. As a consequence the ground state is no longer empty. It is often said that the vacuum state in USC is populated by virtual excitations. The role of these virtual excitations has caused many debates in the literature [69]. Note that in parts of the literature another distinction between ultra-strong coupling, where $g \sim \omega_c, \omega_0$, and *deep-strong coupling* where $g > \omega_c, \omega_0$ is made [66, 65]. This distinction is physically not well motivated, so we will not adopt it in this thesis.

Although this is the standard nomenclature in cQED, it is not the optimal one. The reason is that "weak coupling" (WC) and "strong coupling" (SC) were introduced historically having in mind a comparison between losses and coupling, taking for granted that the bare energies where anyway fixed on a complete different scale, which is the case in atomic physics. With the rise of artificial atoms in solid state or circuit QED all the energy scales have a broad variability, making this nomenclature obsolete. In the specific case of "ultra-strong coupling" (USC) it is clear that we must consider all three energy scales. In order to have all the possibilities without too much confusion one should use a more complete nomenclature, based on the importance of losses, and the importance of the coupling. We have three regimes for the damping (for simplicity we denote all possible damping rates by γ and the other internal energy scales of the dipoles or the cavity by generically $\omega_1, \omega_2, \dots$)

- *Ideal*, where the damping is smaller than all the internal energy scales of the system $\gamma \ll \omega_1, \omega_2 \dots$.
- *Damped*, where some internal energy scales are smaller than the damping and some other are larger $\omega_1 \ll \gamma \ll \omega_2 \dots$.
- *Over-damped*, where all internal energy scales of the system are smaller than the damping rate $\omega_1, \omega_2 \cdots \ll \gamma$.

We have then two coupling regimes (here we explicitly consider only the cavity frequency ω_c and the dipole frequency ω_0 as the internal energy scales of the system to compare to the coupling strength g)

- *Weak coupling*, $g \ll \omega_c, \omega_0$.
- *Strong coupling* $\omega_c, \omega_0 \ll g$.

This discussion assumes in any case a general resonance condition, for which $g > |\omega_c - \omega_0|$. Without this condition a further classification concerning the detuning is needed.

Anyway, we will not really adopt any strict classifications on coupling regimes and we will typically refer to USC or WC, with the meaning "coupling large" or "coupling small" with respect to the bare energies. Except if specified, we will always assume ideal systems with negligible losses.

Chapter 4

The vacua of cQED

In this chapter we start to investigate the physics implied by our minimal model for cavity QED, developed in the previous chapters. We mainly focus here on the predicted ground state (or vacuum state) as a function of the model's parameters, giving particular attention to the transition from weak coupling to ultra-strong coupling. The study of the ground state of cavity QED is of a fundamental importance and it still remain the center of an 40-years old debate about the existence of the so-called *superradiant phase transition*.

The concept of a superradiant phase arose from analysing the ground state of the Dicke model [7], which was used to model the collective decay of an ensemble of molecules collectively coupled to a single resonant mode [70] (in the original paper by Dicke the electric mode was not treated as a degree of freedom, and the main focus was on calculating the spontaneous emission rate by using Fermi's golden rule. The quantized electric field as an independent degree of freedom was later introduced by Tavis and Cummings [71], following the notorious approach which led to the Jaynes-Cummings model [72], for just a single dipole). The idea of Dicke was mainly to show that when an ensemble of emitters decay in resonance with a single mode, there are collective effects, even in the absence of direct interaction, which significantly enhance the spontaneous emission rate. In particular the emission rate of the system, taken as a coherent ensemble, is largely increased, from which Dicke coined the term *superradiant* emission.

Roughly 20-years later Hepp and Lieb [6] took a closer inspection of the Dicke model (or, better to say, the Tavis-Cummings model), and they noticed that, as a function of the light-matter coupling strength, a phase transition arises in the thermodynamic limit. This phase transition is a second order transition with the emergence of an order parameter that spontaneously breaks a symmetry. This order parameter is the ground state expectation value of the photon's annihilation operator $\varphi = \langle 0|a|0\rangle$ and the broken symmetry is the discrete $\mathbb{Z}_2$ symmetry of flipping the sign of the electric field and simultaneously flipping the sign of the dipole moments. The peculiarity of this transition is that it is controlled by the light-matter coupling suggesting a crucial role played by

the vacuum fluctuations of the electromagnetic field. This also opened a quite interesting link to other vacuum properties in quantum electrodynamics, like the Casimir effects or Unruh radiation, topics which always remain among the most popular leitmotivs in modern physics [69]. Moreover the macroscopic presence of photons in the ground state makes this prediction quite intriguing and also a little mysterious, as it represents a Bose-Einstein condensate of photons, which is also another recurrent topic in modern debate [67, 73]. All these implications generated a lot of interest in this seemingly new type of phase transitions. However, there was also a lot of scepticism about the applicability of the Dicke model to describe real light-matter systems. It all ended up in a 40 years long debate, with a series of *no-go theorems* and *counter no-go theorems*, examples and counter examples [6, 21, 74, 8, 75, 76, 22, 77, 78, 79, 50, 20, 80, 81]. Here we try to clarify this issue, and to understand what is really behind the Dicke model and its phase transition. To do so we will not just rely on mathematical statements derived from our heavily approximated models, but we will always try to link every prediction with some generic physical intuition, which we believe is, in the end, the most solid proof.

The results reported in this chapter are mainly based on the two publications Physical Review A 97, 043820 (2018) and SciPost Phys. 9, 066 (2020). In the first article I am the first author, but for the results reported in Sec. 4.3, 4.4, 4.5, 4.6, 4.8 Tuomas Jaako made essential contributions to the numerical and analytical results. The result reported in Sec.4.9 have been primarily obtained by Michael Schuler, but are included in this thesis for the completeness of the physical discussion.

4.1 A quick review of the Dicke model and its phase transition

We consider an ensemble of two-level dipoles (atoms, quantum dots...emitters), which are all identical. Their Hamiltonian is just the sum of each individual Hamiltonian $H_d = \omega_0 \sum_i^N s_z^i = \omega_0 S_z$, where it is convenient to use collective spin operators. We assume that all the molecules are coupled to a single cavity mode with Hamiltonian $H_{\rm ph} = \omega_c a^\dagger a$. The molecules couple to the electric field via the usual dipole coupling $\sim \sum_i^N \vec{\xi}_i \cdot \vec{E}$, which gives $H_{\rm I} = g(a+a^\dagger)S_x$, where the coupling constant $g \sim \vec{\xi}_{01} \cdot \vec{E}_0$ is just the product of the matrix element between the two levels of the individual dipole and the vacuum field amplitude. Altogether we end up with the Dicke model

$$H_{\rm Dicke} = \omega_c a^\dagger a + \omega_0 S_z + g(a + a^\dagger)S_x. \tag{4.1}$$

Since this model was intended to be used for this specific situation not too much care has been given to its derivation and its range of validity. This completely made sense at that time, because the model was compatible with the simplest physical intuition and its basic core idea of collective coupling was subsequently proved experimentally by the discovery of superradiance [82].

As already mentioned above the ground state of the Dicke model can undergo a so-called superradiant phase transition. The presence of this phase transition can be easily spotted by considering the Holstein-Primakoff approximation (see App. D) for the dipoles, which reduces the collective spin operators to operators of a single harmonic oscillator, by identifying $S_z \simeq b^\dagger b - N/2$, $S_x \simeq \sqrt{N}/2(b + b^\dagger)$. This approximation can be justified when we are only interested in the dynamics of small fluctuations around the state for which $\langle S_z \rangle = -N/2$. In our particular case this condition is motivated by the fact that the intuitive ground state of such a system should be the so-called *normal ground state* $|\mathrm{GS}\rangle \simeq |0_{\mathrm{ph}}, \mathrm{S_z} = -\mathrm{N}/2\rangle$, where zero photons are present and the dipoles are all in their individual ground state. The Dicke Hamiltonian is thus reduced to the *Dicke-Holstein-Primakoff* Hamiltonian

$$H_{\mathrm{Dicke}} \simeq H_{\mathrm{D-HP}} = \omega_c a^\dagger a + \omega_0 b^\dagger b + \frac{g\sqrt{N}}{2}(a + a^\dagger)(b + b^\dagger). \tag{4.2}$$

Summing and subtracting the quantity $g^2 N/(4\omega_c)(b + b^\dagger)^2$ we can complete the square, leading to

$$H_{\mathrm{D-HP}} = \omega_c \tilde{a}^\dagger \tilde{a} + \tilde{\omega}_0 b^\dagger b, \tag{4.3}$$

where $\tilde{a} = a + g\sqrt{N}/(2\omega_c)(b + b^\dagger)$ is a hybrid light-matter operator (which, however, is not an independent degree of freedom) while the dipoles are still described by the same harmonic degree of freedom with renormalised energy

$$\tilde{\omega}_0 = \omega_0 \sqrt{1 - \frac{g^2 N}{\omega_c \omega_0}}. \tag{4.4}$$

Although the Dicke-Holstein-Primakoff Hamiltonian appears to be diagonal, it is not, because the $\tilde{a}$ and b operators do not commute. But we can still learn something about its range of stability. The stability of this Hamiltonian requires that all the frequencies involved are real and larger than zero. But at the critical coupling $g_c = \sqrt{\omega_0 \omega_c / N}$ the dipoles frequency vanishes $\tilde{\omega}_0 = 0$, while for larger coupling it becomes imaginary and the Hamiltonian is no longer hermitian. This means that we are crossing the range of validity of the Holstein-Primakoff approximation and the ground state in such a regime is no longer given by the normal ground state $|\mathrm{GS}\rangle \simeq |0_{\mathrm{ph}}, \mathrm{S_z} = -\mathrm{N}/2\rangle$.

4.2 General considerations about the vacuum of dipolar QED

Here we want to introduce some very basics thoughts that shine light on the Dicke model and the Dicke transition, contextualised in equilibrium electrodynamics.

In particular we want to clarify the apparent prediction of a ground state BEC of photons

and how the existence of this phase transition can be understood from a very general ground. To fully see the relation with BEC, we explicitly write the Dicke superradiant ground state in the thermodynamics limit [7]

$$\lim_{g\to\infty} |\mathrm{GS}_{\mathrm{Dicke}}\rangle = |\alpha\rangle| \to\to \dots\rangle, \tag{4.5}$$

where $\alpha = -g\sqrt{N}/\omega_c$ indicates the amplitude of a coherent state of photons [83], and $|\to\rangle$ is an eigenstate of s_x. This state has the property that $\langle a\rangle = \alpha$, thus it spontaneously breaks the symmetry of the original Hamiltonian, in complete analogy with the BEC transition, characterised by a non-vanishing ground state expectation value of the field operator $\langle\hat{\varphi}\rangle = \varphi$ [84]. However, this interpretation is rather misleading, or at least ambiguous. Indeed, as we have seen in the previous chapters, the photon's annihilation operator appearing in the Dicke model involves a combination of the canonical momentum and the transverse vector potential of the electromagnetic field, projected on a certain mode. We can schematically say that

$$a \sim P_k - iq_k. \tag{4.6}$$

This means that an eventual finite expectation value of this operator implies a non-vanishing expectation value of the momentum or the vector potential. Because the canonical momentum is not gauge invariant, we need to specify which gauge we intend to use. Here we focus only on the Coulomb gauge and the dipole gauge.

In the Coulomb gauge the canonical momentum expectation value (for the ground state, and more general for an eigenstate) is always zero. This can easily be verified by considering that

$$\langle \mathrm{GS}|\vec{\Pi}_{\mathrm{C}}|\mathrm{GS}\rangle = \varepsilon_0\langle \mathrm{GS}|\dot{\vec{A}}|\mathrm{GS}\rangle = -i\varepsilon_0\langle \mathrm{GS}|[\vec{A}, H]|\mathrm{GS}\rangle = \vec{0}, \tag{4.7}$$

where we used the fact that any time derivative operator expectation value vanishes over an eigenstate of the full Hamiltonian. On the other side the vector potential does not have to vanish, but instead it follows the relation

$$-\varepsilon_0 c^2\langle \mathrm{GS}|\nabla^2\vec{A}|\mathrm{GS}\rangle = \langle \mathrm{GS}|\vec{J}_\perp|\mathrm{GS}\rangle, \tag{4.8}$$

which, again, follows from the fact that $\varepsilon_0 c^2\nabla^2\vec{A} + \vec{J}_\perp = \dot{\vec{\Pi}}$. This implies that we can write the expectation of the vector potential convoluting the transverse current with the Laplace Green's function

$$\langle \mathrm{GS}|\vec{A}|\mathrm{GS}\rangle = \frac{1}{\varepsilon_0 c^2} G \star \langle \mathrm{GS}|\vec{J}_\perp|\mathrm{GS}\rangle. \tag{4.9}$$

Therefore, in the Coulomb gauge the only way to have a photon's annihilation operator with non-

vanishing expectation in the ground state is to have a non-vanishing transverse current. But this means that we are just observing the average magnetostatic field generated by a permanent magnet. In this case our "photon BEC" would just be the magnetic field outside a polarized magnet. The electromagnetic field without matter cannot fulfil the requirements of a BEC. However, since we didn't include the spin degree of freedom in our theory, also the expectation value of the transverse current will always be zero in the ground state. This follows again from taking the expectation value over an eigenstate of a time derivative of an operator (for instance, when we take the dipole approximation we have explicitly $\dot{\vec{P}}^{\perp} = \vec{J}^{\perp}$, as detailed in App.B.).

It's worth to repeat the same calculation in the dipole gauge. Following the same reasoning as above, we find that the canonical momentum expectation does not vanish in this case, while it is the vector potential to be always vanishing here.

$$\langle \mathrm{GS}|\vec{\Pi}_{\mathrm{D}}|\mathrm{GS}\rangle = \langle \mathrm{GS}|\vec{P}^{\perp}|\mathrm{GS}\rangle, \tag{4.10}$$

$$\langle \mathrm{GS}|\vec{A}|\mathrm{GS}\rangle = \vec{0}. \tag{4.11}$$

We notice that, in a quite complementer way, in the dipolar gauge the expectation value over the ground state of the canonical momentum is equal to the transverse polarization. This means that in this gauge a "photon BEC" would appear as the electrostatic field generated by a ferroelectric material (a material which spontaneously polarizes even at zero temperature). Despite the fact it seems that the two gauges give different predictions, this is not the case. Indeed the only difference is that they deal with different variables. In particular in the Coulomb gauge it seems that there is no electrostatic field linked to the matter polarization. This is obviously wrong, cause we are forgetting the direct Coulomb interaction, which is not present in the definition of the canonical momentum, since we take it as just the transverse component of the electric field. So in Coulomb gauge we have that the electrostatic field in the ground state is just given by the direct Coulomb term, which gives the transverse polarization (i.e. the expectation of the canonical momentum in dipolar gauge) under the dipole approximation

$$\langle \mathrm{GS}|\vec{E}|\mathrm{GS}\rangle = -\langle \mathrm{GS}|\vec{\nabla}\phi|\mathrm{GS}\rangle \xrightarrow{\text{Dip.approx.}} -\langle \mathrm{GS}|\vec{\Pi}_{\mathrm{D}}|\mathrm{GS}\rangle. \tag{4.12}$$

Even though it is clear that a ground state BEC of photons is a misleading concept it is still often presented like this in the current literature [85, 86, 87].

From the previous analysis it is clear that any phase transition in the photon's field is just a mirror of a phase transition in the matter part. But the way in which this mirroring is implemented depends on the representation we choose for the electromagnetic field in terms of its potential. Thus it is crucial to specify how we derived the Dicke model. This ambiguity was actually central in the

debate around the Dicke model, but somehow there was never a clear statement about it. A lot of words were spent to discuss whether or not the "A^2-term" should or shouldn't be included in the Dicke Hamiltonian, as a direct proof of the existence of this phase transition. However a quick look to the constrained relations between the degrees of freedom involved already says that yes, it exists, it is a transition between having or not having a static field generated by spontaneously polarized matter [20, 21, 76].

4.3 The extended Dicke model and a the phase diagram of cQED

As discussed in the last section, the proof of the existence of a phase transition in the quantized electromagnetic field does not require any specific approximated model (as the Dicke model, for instance). But it can be argued already based on from basics considerations. In contrast, to have more information about the role of the quantized field in the phase transition and to start to have quantitative prediction, we do need a specific model. In particular, we want to understand the possible ground state phases in cavity QED and the role of quantum fluctuations in their realisation. In our case we take the model we developed in the previous chapters, which is given by the Hamiltonian

$$H_{\text{cQED}} = \omega_c a^\dagger a + \omega_0 S_z + g(a + a^\dagger)S_x + \frac{g^2}{\omega_c} S_x^2 + \frac{g^2}{\omega_c}\frac{N}{\nu}\sum_{ij} s_x^i \mathcal{D}_{ij} s_x^j. \tag{4.13}$$

This model strongly depends on the arrangement of the dipoles, through the dipole-dipole interaction described by $\mathcal{D}_{ij}$. In general this term introduces a large complexity, making the problem very hard to solve, or even unsolvable. In order to have at least a first grasp on what is going on, we introduce a very important simplification: we replace the finite range dipole-dipole interaction with an infinite range interaction, weighted by the average value of the dipole force over the given geometry

$$N\sum_{ij} s_x^i \mathcal{D}_{ij} s_x^j \longmapsto \eta S_x^2. \tag{4.14}$$

With this approximation the cavity QED Hamiltonian becomes the so-called *extended Dicke model* (EDM)

$$H_{\text{cQED}} \approx H_{\text{EDM}} = \omega_c a^\dagger a + \omega_0 S_z + g(a + a^\dagger)S_x + \frac{g^2}{\omega_c}(1+\varepsilon) S_x^2, \tag{4.15}$$

where $\varepsilon = \eta/\nu$, and all the geometrical information is now contained in the average dipole-dipole energy

$$\eta = \frac{1}{N}\sum_{ij} \mathcal{D}_{ij}. \tag{4.16}$$

The great simplification of this model is that it commutes with the total collective-spin operator,

$$[H_{\rm EDM}, S^2] = 0, \tag{4.17}$$

where $S^2 = S_x^2 + S_y^2 + S_z^2$. This symmetry makes the Hamiltonian block diagonal, with each block given by a spin sector, labelled by the quantum number $s = 0 \ldots N/2-2, N/2-1, N/2$. The Hilbert space related to each sector (assuming a cutoff in the photon's number $N_{\rm ph}$) has dimension $\dim\mathcal{H} = N_{\rm ph} \times (2s+1)$, which scales linearly with the number of dipoles. Now the problem can be efficiently tackled with both analytical and numerical methods.

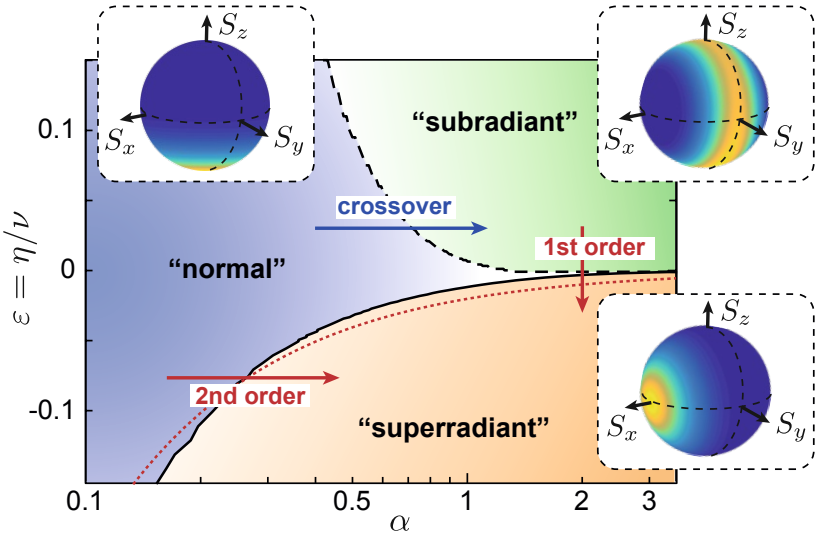

Figure 4.1: Ground-state phase diagram of the extend Dicke model $H_{\rm EDM}$ as a function of the effective finestructure constant $\alpha = g^2/(2\pi\omega_c^2)$ (horizontal axis) and the average dipole-dipole interaction strength $\varepsilon = \eta/\nu$ (vertical axis). For this plot $\omega_0/\omega_c = 1$ and $N = 8$. The red dotted line indicates the value of the critical coupling strength given in Eq. (4.24) and the other phase boundaries are defined in the text. For each phase, the insets illustrate the reduced state of the dipoles, ρ_d, in terms of a Bloch-sphere representation. The color shows the value of the Q-function $Q(\vec{n}) = \langle\vec{n}|\rho_d|\vec{n}\rangle \in [0,1]$, where $\vec{n}$ is a unit vector and $|\vec{n}\rangle$ the corresponding coherent spin state. Note that for a better visibility, the three insets have been plotted with different colorscales.

To proceed we restrict ourself to the resonant case, where $\omega_0 = \omega_c$ and we move between the different regimes varying (g, ε), the light-matter coupling and the dipole-dipole energy. The sign of the dipole energy indicates attraction, $\varepsilon < 0$, or repulsion, $\varepsilon > 0$, between the dipoles. As a consequence ferroelectric states, where all the dipoles align, are favoured when $\varepsilon < 0$, while anti-ferroelectric states are favoured when $\varepsilon > 0$. The case of non-interacting dipoles, $\varepsilon = 0$, is also very relevant, because in this limit the influence of the quantized photon's field is most prominent. It is worth noticing that the extended Dicke model is not just an approximated model for dipoles in a cavity, but it also shows up in circuit QED [55] and in more complicated solid state light-matter systems, for instance in the field of intersubbands transitions [88]. Therefore, it represents a model

which is fundamental in our understanding of light-matter interaction, where the standard Dicke model is contained as the special case $\varepsilon = -1$. This corresponds to a system where dipoles are arranged in a geometry which favours ferroelectric order.

In Fig. 4.1 we show the phase diagram of the ground state of the EDM parametrised by the adimensional *effective fine structure constant* $\alpha = g^2/(2\pi\omega_c^2)$ and the adimensional dipole-dipole energy ε. The system is mainly divided into three phases:

- *Normal* phase. Virtual photons are mostly absent, $\langle a^\dagger a\rangle \approx 0$, and the dipoles are approximately in their individual ground state, giving $\langle S_z\rangle \approx -N/2$. This phase is characteristic of the weak coupling regime, where $\alpha \ll 1$. In this regime, for a small numbers of dipoles, one can still obtain accurate predictions by neglecting the dipole-dipole interaction and implementing the RWA (even though counter-rotating terms could still provide important perturbative corrections). When the number of dipoles becomes large dipole-dipole interaction and counter-rotating terms are non-negligible, the ground state is still well represented by the normal ground state, but one has to add the corrections that comes from the Holstein-Primakoff approximation on top of it. So the normal ground state picks up some harmonic polaritonic contributions. The majority of cavity QED experiments operate in this regime.

- *Superradiant* phase (or also ferroelectric phase). The $\mathbb{Z}_2$ symmetry of the EDM is spontaneously broken and $\langle a\rangle \neq 0$. This implies the presence of an electrostatic field, generated by the polarized dipoles, which also give $\langle S_x\rangle \neq 0$. The ground state in this phase is qualitatively identical to the superradiant Dicke ground state. This phase requires $\varepsilon < 0$ and large-enough α. While this phase exists for arbitrary small coupling, its boundary to the normal phase is strongly modified by the coupling to the cavity mode in the USC regime.

- *Subradiant* phase (or also anti-ferroelectric phase). As in the normal phase the symmetry is preserved and this phase is characterised by anti-aligned dipoles, which gives $\langle S_x\rangle \approx 0$, $\langle S_z\rangle \approx 0$. Virtual photons are mostly gone, giving $\langle a^\dagger a\rangle \approx 0$. It is possible to show that no entanglement is present between the dipoles and the cavity, so we can say that light and matter are effectively decoupled. As we discuss in more detail below this phase is separated only by a smooth crossover from the normal phase. In contrast to the superradiant phase, it only appears for $\alpha > 1$ and is thus a genuine feature of the USC regime.

In the phase diagram in Fig. 4.1 the border between the normal and the superradiant phase is derived by considering the maximum in the dipoles fluctuations $\Delta S_x^2 = \langle S_x^2\rangle - \langle S_x\rangle^2$, while the crossover to the subradiant phase is defined by the maximum in the photon number expectation value. Specifically, the subradiant phase is defined through the condition $\partial\langle a^\dagger a\rangle/\partial g < 0$. In every numerical simulation we have added a small bias perturbation $H_{\text{perturb}} \sim \lambda S_x$, which explicitly

breaks the $\mathbb{Z}_2$ symmetry. This is needed in order to observe the superradiant phase even for finite N.

4.4 Normal phase

The normal phase is characterised by small light-matter coupling, $\alpha \ll 1$, and moderate values of ε (which could be both positive and negative). For a single dipole, $N = 1$, the EDM reduces to the standard Jaynes-Cummings model, where the ground state is simply $|\mathrm{GS}\rangle = |0_{\mathrm{ph}}, \downarrow\rangle$. When $N > 1$ the solution is more complicated, and, in particular for $N \gg 1$, counter-rotating terms and dipole-dipole interaction are non-negligible. However, in the limit $N \gg 1$ the model is still approximatively solvable. Indeed it can be verified that in this regime the true ground state has just minor corrections on top of the normal ground state,

$$|\mathrm{GS}\rangle = |0_{\mathrm{ph}}, \downarrow, \downarrow \ldots \downarrow\rangle + |\delta(\mathrm{GS})\rangle. \tag{4.18}$$

Therefore, we can proceed by expanding the collective spin operators according to the Holstein-Primakoff approximation, meaning that we consider just small perturbations on top of the normal ground state

$$\begin{aligned} S_z &\approx -\frac{N}{2} + b^\dagger b, \\ S_x &\approx \frac{\sqrt{N}}{2}(b + b^\dagger). \end{aligned} \tag{4.19}$$

The EDM becomes

$$H_{\mathrm{EDM}} \approx H_{\mathrm{HP}} = \omega_c a^\dagger a + \omega_0 b^\dagger b + \frac{G}{2}(a + a^\dagger)(b + b^\dagger) + \frac{G^2}{4\omega_c}(1 + \varepsilon)(b + b^\dagger)^2, \tag{4.20}$$

and the *collective coupling* is given by $G = g\sqrt{N}$. This Hamiltonian can be diagonalised introducing the two polaritons modes

$$H_{\mathrm{HP}} = \Omega_+ d_+^\dagger d_+ + \Omega_- d_-^\dagger d_-, \tag{4.21}$$

with polaritons frequencies

$$\Omega_\pm^2 = \frac{\omega_0^2\left(1 + (1+\varepsilon)\frac{G^2}{\omega_c\omega_0}\right) + \omega_c^2 \pm \sqrt{\left[\omega_0^2\left(1 + (1+\varepsilon)\frac{G^2}{\omega_c\omega_0}\right) + \omega_c^2\right]^2 - 4\omega_c^2\omega_0^2\left(1 + \varepsilon\frac{G^2}{\omega_c\omega_0}\right)}}{2}. \tag{4.22}$$

Using these Holstein-Primakoff polaritons modes, it is possible to calculate various quantities,

for instance the ground state photon's number, which, for moderate collective coupling scales as

$$\langle a^\dagger a\rangle \simeq \frac{G^2}{4(\omega_0+\omega_c)^2}\left(1-\varepsilon\frac{G^2}{\omega_c\omega_0}\right). \tag{4.23}$$

These kind of results, regarding the normal phase and its linearised excitations, can be found, treated in more detail, in many previous works such as [89, 90].

4.5 Superradiant (ferroelectric) phase

The superradiant phase can only emerge when the dipole-dipole interaction is attractive, i.e. $\varepsilon < 0$. Under these conditions the Holstein-Primakoff Hamiltonian has an unstable point when

$$g = g_c = \sqrt{\frac{\omega_c\omega_0}{-\varepsilon N}}. \tag{4.24}$$

At this value of the coupling strength (fixed ε) the HF Hamiltonian becomes unstable and the whole approximation breaks down. This instability is the key signature of a phase transition, which sharply changes the ground state. This instability is exactly the Dicke phase transition, which leads to a superradiant state, generalised for various values of ε. For $g \geq g_c$ it is possible to calculate the order parameter $\langle a\rangle$, which breaks the symmetry, and the collective spin polarization [91]

$$\begin{aligned}\langle a\rangle &= \pm\frac{g}{\omega_c}\frac{N}{2}\sqrt{1-\left(\frac{g_c}{g}\right)^4},\\ \langle S_x\rangle &= \mp\frac{N}{2}\sqrt{1-\left(\frac{g_c}{g}\right)^4}.\end{aligned} \tag{4.25}$$

It is important to point out that the two quantities are not just coincidentally related. Indeed, as explained in Sec. 4.2, the expectation value of the matter polarization is always linked to the expectation of the electromagnetic canonical momentum in the dipole gauge. In the context of the EDM this can be easily verified by considering the following equation of motion

$$i\partial_t a = \omega_c a + gS_x, \tag{4.26}$$

from which we get (remember that any time derivative operator expectation value over an eigenstate gives zero)

$$\langle a\rangle = -\frac{g}{\omega_c}\langle S_x\rangle. \tag{4.27}$$

In Fig. 4.2(a) we show the behaviour of the order parameter $|\langle a\rangle|$ from a numerical simulation, and its fluctuations $\Delta a^2 = \langle a^\dagger a\rangle - |\langle a\rangle|^2$, together with the fluctuations of the polarization $\Delta S_x^2 =$

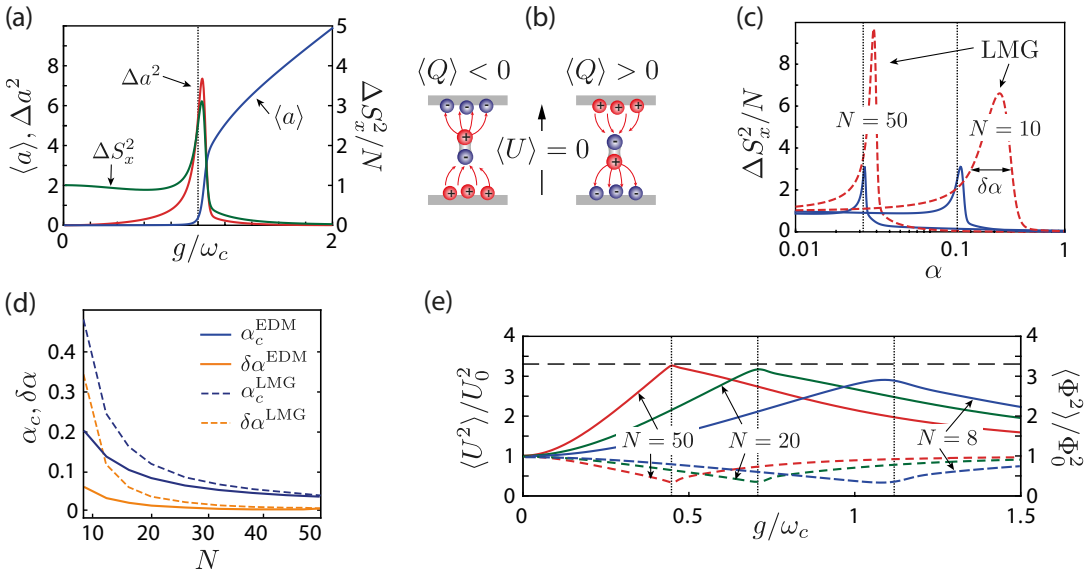

Figure 4.2: Superradiant phase transition. (a) Dependence of the mean value $\langle a\rangle$ and the spin- and field fluctuations across the superradiant phase transition point. (b) Illustration of the two possible superradiant ground states in terms of polarized dipoles and the corresponding induced charges. (c) Comparison of the spin fluctuations ΔS_x evaluated with the extended Dicke model and the Lipkin-Meshkov-Glick (LMG) Hamiltonian for two different numbers of dipoles. The value of α_c, where the fluctuations reach there maximum, as well as the width of the fluctuations at half of the maximum, $\delta\alpha$ are plotted in (d) for varying N. (e) Plot of the fluctuations of the voltage operator U (solid lines) and flux operator Φ (dashed lines) for different numbers of dipoles. The horizontal dashed line marks the approximate analytic result given in Eq. (4.33). In all plots $\omega_0 = \omega_c$ and a value of $\varepsilon = -0.1$ have been assumed and the vertical dotted lines indicate the analytic phase transition point given in Eq. (4.24). In all numerical simulations a symmetry-breaking bias field, $H_{\rm bias} = \lambda S_x$, where $\lambda/\omega_c = 10^{-3}$, has been added to the bare Hamiltonians $H_{\rm EDM}$ and $H_{\rm LMG}$.

$\langle S_x^2\rangle - \langle S_x\rangle^2$. As expected from a second order phase transition near the critical point we experience a narrow peak in fluctuations, which eventually diverges in the $N \to \infty$ limit.

It is worth to spend again a few words on the phase transition condition (4.24). We can express this condition invoking again the coupling parameter, generalised to contain the dipole-dipole parameter

$$\zeta_\varepsilon = -\varepsilon \frac{g^2 N}{\omega_c \omega_0}, \tag{4.28}$$

where the superradiant phase appears when

$$\zeta_\varepsilon > 1. \tag{4.29}$$

We recall that we can write $g/\omega_c = \sqrt{2\pi\alpha}$, where $\alpha = \alpha_{\rm fs}(q\xi_0)^2/(ed)^2 Z/Z_0$ is the effective fine structure constant, associated with the artificial dipole coupled to the cavity, where Z is the generalised impedance of the cavity. Apparently the coupling parameter depends both on the dipoles and the cavity. But, after rearranging the terms, we can see that this is not the case. The coupling

parameter depends only on dipole parameters (and the real fine structure constant and the vacuum impedance)

$$\zeta_\varepsilon = -2\pi\alpha_{\rm fs}\eta\left(\frac{q}{e}\right)^2\frac{Z_{\rm d}}{Z_0}, \tag{4.30}$$

where we introduced the *dipole's impedance*

$$Z_{\rm d} = \frac{\xi_0^2}{\varepsilon_0 r_0^3\omega_0}. \tag{4.31}$$

(to avoid confusion in the notation, ε_0 here is the vacuum electric permeability!). The message here is again very clear, modifications of the cavity degree of freedom have no influence on the superradiant phase transition, which is only a property of the dipoles. The only modifications we can introduce are related to the electrostatic environment and they enter through a change in the value of the dipole-dipole parameter η.

We can take profit of our toy model, discussed in Ch. 3, to fully visualise the physical meaning of the SR phase. Fig. 4.2(b) illustrates what happens when the dipoles spontaneously polarize. This leads to an accumulation of charge on the boundaries of the system, in order to compensate the electric field generated by the dipoles. This is the physical meaning of Eq. (4.26). In this system, the charge on the capacitor Q represents the canonical momentum of our photon, conjugated to the dynamical variable Φ, the magnetic flux through the inductor. The charge is a proper and legit observable, however it is not the most convenient one in any realistic experiments. Instead what is really important for observations is its *kinetic momentum*, which in our setup corresponds to the voltage across the capacitor

$$U = \dot{\Phi} = U_0\left[a + a^\dagger + \frac{2g}{\omega_c}S_x\right]. \tag{4.32}$$

Here $U_0 = Q_0/C = \omega_c\Phi_0 = \omega_c\sqrt{\frac{\hbar Z}{2}}$ is the vacuum voltage amplitude, which plays the role of the vacuum electric field amplitude in the more general framework of QED. Again, as for the electric field, since the voltage is the time derivative of the flux, its expectation value over the ground state is always zero. This makes a direct observation of this transition just by looking at cavity-observables quite difficult. But, even if one cannot directly observe the order parameter of this transition, it is still possible to detect clear signatures of the change of phase. This is given for instance by the fluctuations in the voltage, $\langle U^2\rangle$, which are shown in Fig. 4.2(e). We can see a characteristic kink, precisely at the transition point for $N \gg 1$, which is reminiscent of the famous *Lambda-transition* in super-fluids. The kink's maximum scales approximately as

$$\frac{\langle U^2\rangle}{U_0^2} \approx \sqrt{1 + \frac{1}{|\varepsilon|}\left(\frac{\omega_0}{\omega_c}\right)}. \tag{4.33}$$

This maximum does not scale with α, nor with N (even if some information regarding the dipole's number is still contained in the parameter ε). It is also accompanied by a minimum in the flux-fluctuations $\Phi^2_{g=g_c} \simeq \hbar^2/(4C^2\langle U^2\rangle)$, which suggests that the cavity is in a squeezed state.

Until this point we have found that the cavity does not play any role in the origin of the superradiant phase transition, which is only a property of the interacting dipoles. The cavity seems just "to passively watch" the transition through the fluctuations in voltage and flux. But this is not entirely true. Actually we found that the cavity has instead an important feedback on the dipoles, but this, again, is just manifested by the fluctuations of the dipoles. In Fig. 4.2(c) and 4.2(d) we compare the predictions from the Lipking-Meshkov-Glick (LMG) Hamiltonian to the EDM, where

$$H_{\rm LMG} = \omega_0 S_z + \varepsilon \frac{g^2}{\omega_c} S_x^2. \tag{4.34}$$

The LMG model basically represents the EDM in absence of the cavity field. When $|\varepsilon|N \ll 1$ the transition appears at rather large values of g/ω_c and the two model give significantly different predictions regarding the transition point and the range of polarization fluctuations, ΔS_x^2. Therefore, although the cavity mode cannot by itself induce a superradiant phase transition, it can still change its properties once the system enters the USC regime.

4.6 Subradiant (anti-ferroelectric) phase

When the dipole-dipole interaction is repulsive and $\varepsilon > 0$, we expect that the ground state is very close to the normal state, presenting eventually a certain amount of squeezing in its virtual population. This can be seen by considering our Holstein-Primakoff approximation expressed by Eq. (4.20). Following this approach we can compute the ground state photon's number, finding that it saturates at a finite value when the light-matter coupling is sufficiently high

$$\lim_{\alpha\to\infty} \langle a^\dagger a\rangle|_{\rm HP} = \frac{1+2\varepsilon-2\sqrt{\varepsilon(\varepsilon+1)}}{4\sqrt{\varepsilon(\varepsilon+1)}} > 0. \tag{4.35}$$

In this sense it looks like the USC limit of a repulsive dipolar ensemble has a ground state very similar to what we call the normal ground state. However this is true only under the approximation that each dipole behaves as an harmonic oscillator. In the extreme case, as considered in this chapter, where the dipoles are represented by two level systems, the USC ground state in the presence of repulsive dipole-dipole interactions is surprisingly very different from the normal one. Already looking at the photon's number in the ground state, we see that it goes to zero for an even number of dipoles, while it keeps growing for an odd number, and it never saturates as we can see in Fig. 4.3(a). This observation is motivates us to define a new subradiant phase. This phase can

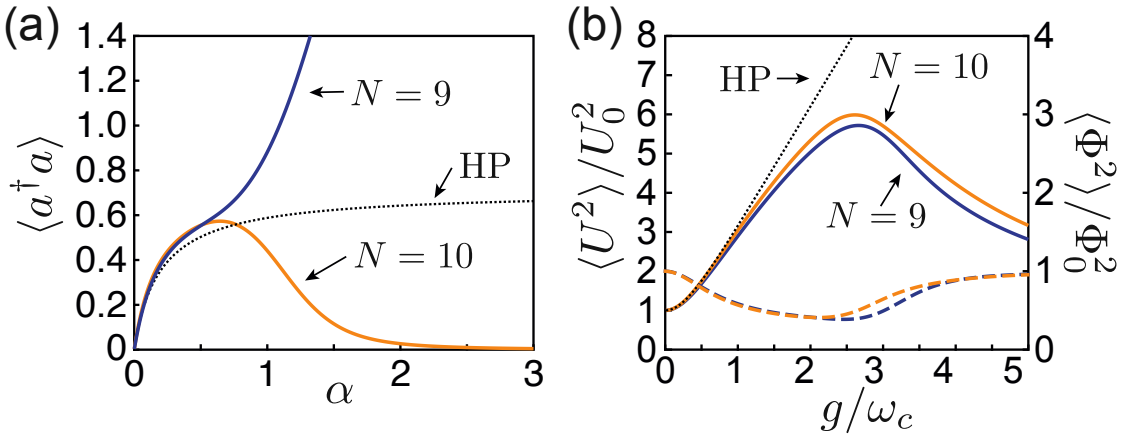

Figure 4.3: Subradiant phase. (a) Plot of the ground state photon number as a function of the coupling parameter α for an even and an odd number of dipoles. (b) Dependence of the voltage (solid lines) and flux (dashed lines) fluctuations on the coupling strength g. In both plots the parameters $\varepsilon = 0.05$ and $\omega_c = \omega_0 = 1$ have been assumed and the dotted lines shows the corresponding results for $\langle a^\dagger a\rangle$ and $\langle U^2\rangle$ obtained from the ground state of the Holstein-Primakoff (HP) Hamiltonian $H_{\rm HP}$ for $N = 10$. In all numerical simulations a symmetry-breaking bias field, $H_{\rm bias} = \lambda S_x$, where $\lambda/\omega_c = 10^{-4}$, has been added to the bare Hamiltonians $H_{\rm EDM}$.

be defined by the abstract condition

$$\frac{\partial}{\partial g}\langle a^\dagger a\rangle \leq 0, \tag{4.36}$$

which is exactly what we have used to mark the phase boundary in Fig. 4.1. Also looking at more realistic observables, such as voltage/flux fluctuations, we see a strong disagreement between the full predictions and the approximated HP approach, Fig. 4.3(b). In particular, it shows that the voltage (flux) fluctuations grow (decrease) to a maximum (minimum), and then both approach their uncoupled values when the coupling reach larger values. In this case there is no difference between even/odd dipole numbers.

These last two observations somehow suggest that the subradiant ground state is composed out of the cavity in its uncoupled vacuum state and the dipoles in another state, completely disentangled from the cavity. In order to test this intuition we quantify the degree of entanglement between the dipoles and the cavity by considering the von Neumann entropy of the dipolar ensemble

$$\mathcal{S}_d = -\mathrm{Tr}[\rho_d \log_2(\rho_d)], \tag{4.37}$$

where $\rho_d = \mathrm{Tr}_c[\rho]$ is the reduced density matrix of the dipolar ensemble. From Fig. 4.4(a) we immediately see the disentangling crossover in the case of N even, while for N odd the cavity-dipoles entanglement seems to saturate at a maximally entangled state. This maximally entangled state for the N odd case is very similar to the USC state of just $N = 1$ dipole. This state is a "cat"

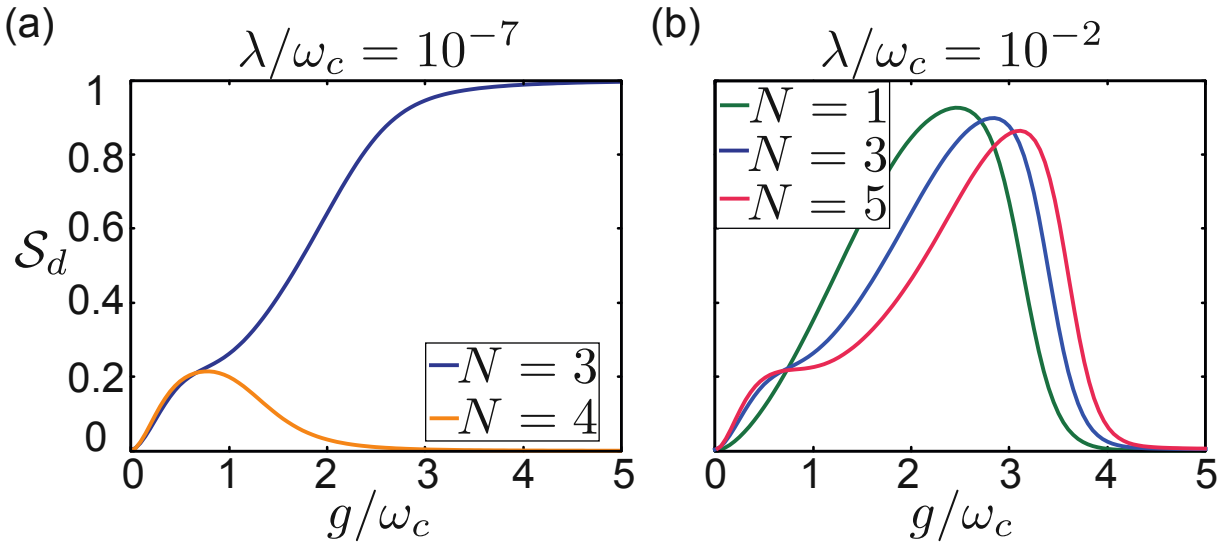

Figure 4.4: Entanglement entropy of the dipole's ensemble for $\varepsilon = 1$ in various cases. (a) Low bias field $H_{\text{bias}} = \lambda S_x$ added to the bare Hamiltonians H_{EDM}, where $\lambda/\omega_c = 10^{-7}$. This value is smaller than the usual one, in order to maintain the system fairly symmetric. Doing so it is clear that the decay of entanglement in the $N = 4$ case is really due to a different physical mechanism, while the case $N = 3$ converges to an highly entangled state. (b) High bias field $\lambda/\omega_c = 10^{-2}$. This has negligible impact on the N even case, so it is not reported here. Instead we compare $N = 1, 3, 5$. The effect of the bias field manifests itself at large coupling in both cases.

state which can be written as

$$|\text{GS}_{N=1}\rangle \approx \frac{1}{\sqrt{2}} \left(|\alpha\rangle |\downarrow\rangle \pm |-\alpha\rangle |\uparrow\rangle \right), \tag{4.38}$$

which is very similar to the superradiant case, with the only difference that it needs a fixed finite value of λ/ω_c to break the symmetry through the perturbation of the bare Hamiltonian $H_{\text{bias}} = \lambda S_x$ (while for the large N superradiant phase one only needs an infinitesimal amount). The very similar behaviour between $N = 1$ and $N > 1$ odd is shown in Fig. 4.4(b), where we compare $\mathcal{S}_d(g/\omega_c)$ for $N = 1, 3, 5$. For moderate coupling the two cases have different behaviours, which is expected to increase in difference for larger dipole's number. In particular it seems that there is the formation of a plateau with increasing N. For larger coupling all cases collapse to $\mathcal{S}_d \approx 0$. This sudden change happens for all cases at very similar coupling, suggesting that the basic mechanism can be already grasped from the $N = 1$ case, even though is clear that there is a certain dependence from N. Here the effect of the bias field is simply to collapse the "cat" ground state, giving back a factorised state without any entanglement between cavity and dipole

$$|\text{GS}_{N=1}\rangle \approx |\alpha\rangle |\downarrow\rangle. \tag{4.39}$$

A less hand-wavy explanation for this curious difference in even/odd dipole's number entanglement

behaviour is non trivial and it requires some care. We will postpone it for the next section, where we will develop an effective theory that will provide a generic picture of the USC phases.

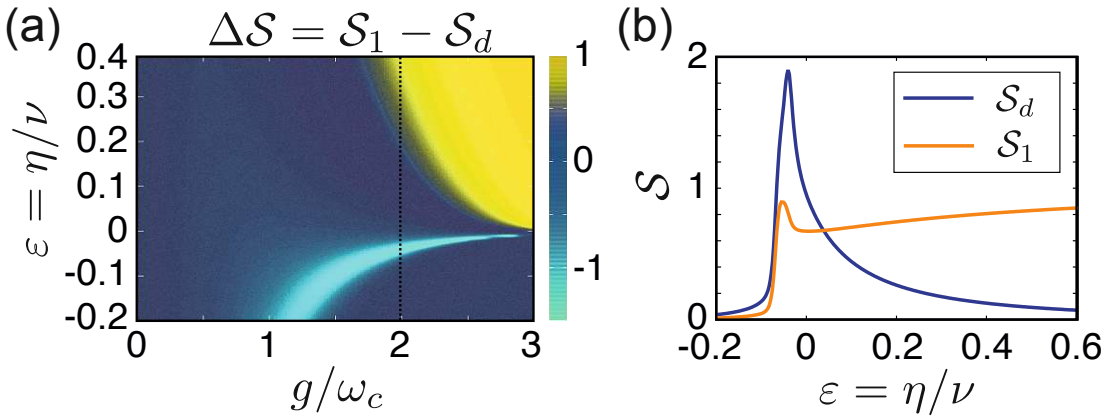

Figure 4.5: Subradiant phase. (a) Plot of the residual single-spin entropy $\Delta\mathcal{S}$ of the ground state of $H_{\rm EDM}$ for $\omega_0 = \omega_c$ and $N = 4$. (b) The entanglement entropies for a single dipole and for all dipoles are plotted for a fixed $g/\omega_c = 2$ and otherwise the same parameters as in (a). In all numerical simulations a symmetry-breaking bias field, $H_{\rm bias} = \lambda S_x$, where $\lambda/\omega_c = 10^{-4}$, has been added to the bare Hamiltonians $H_{\rm EDM}$.

Another interesting consequence of the subradiant phase is the order picked by the dipoles themselves. Indeed, focusing on the case N even, we can see that the dipoles enter in a state which exhibits a high degree of entanglement between the dipoles. So the dipoles disentangle from the cavity, but at the same time they get highly entangled among each other. This can be quantified by considering the entropy of a single dipole

$$\mathcal{S}_1 = -\mathrm{Tr}[\rho_1 \log_2(\rho_1)], \tag{4.40}$$

where $\rho_1 = \mathrm{Tr}_{N-1}[\rho_d]$ is the reduced density matrix of a single dipole. It is worth to notice that in the EDM this quantity does not depend on the particular dipole, since, within this approximated model, they are all equivalent. To avoid any effect of the cavity we consider the difference between those two entropies

$$\Delta\mathcal{S} = S_1 - S_d. \tag{4.41}$$

In Fig. 4.5(a) we can see a complete phase diagram of $\Delta\mathcal{S}(g/\omega_c, \varepsilon)$, which can be thought as another way to derive our generic phase diagram in Fig. 4.1. In this phase diagram we have $\Delta\mathcal{S} = 0$ when the dipoles are not entangled between them, but there could be still entanglement between the dipoles and the cavity. In this way the normal and the superradiant phase cannot really be distinguished. However it is possible to see the boundary between these two phases, given by a negative spike in the entropy difference. This marks the region where the phase transition happens, which is characterised by strong fluctuations both in the dipoles and in the cavity. The

subradiant phase, instead, is well separated and well recognisable from all the other phases. As we did for the superradiant phase, also the subradiant phase can be compared to the antiferroelectric phase of the LMG model (4.34). For small g/ω_c the two models give similar predictions concerning the subradiant phase, but for large coupling there are significant deviations. This will be clarified in the next section.

4.7 The polaron frame EDM

Before continuing our exploration of the various phases of cavity QED we take a short technical detour.

A large boost in the understanding of a physical system is often given by a clever choice of coordinates. In our case it turns out that the EDM, as it is expressed in Eq. (4.15), is not the best representation for that Hamiltonian, at least to derive approximated predictions regarding the USC. Indeed we have to keep in mind that the form of the EDM expressed in Eq. (4.15) is a consequence of the chosen dipolar gauge in the original QED Hamiltonian and it is dictated by the the two-level and the single-mode approximations. On the other hand, once the EDM is derived, we still have the freedom to re-express it through another unitary equivalent Hamiltonian $\tilde{H}_{\rm EDM} = U H_{\rm EDM} U^\dagger$. For various spin-bosons models it is known that is possible to build a *disentangling unitary* U in such a way to minimize the ground state entanglement between light and matter [92, 93]. Using this approach the feedbacks between light and matter are minimized for particular states (typically the lowest part of the spectrum, as these are basically low energy approaches), giving rise the possibility of generating low energy effective descriptions of the system which are very easy to handle numerically. Because of the unwritten rule of the "conservation of complexity" this simplifications are always related to the fact that U is always inversely complicated. The variables transformed according to our disentangling unitary will be complicated combinations of our original variables. Since in our case we can solve almost all the relevant cases using simple numerics, an involved and complicated construction of U, to just simplify the numerics, has basically no benefit. Luckily, in this case, there exists a transformation that partially simplifies the system, without messing up the physical meaning of our variables. This is the so called *polaron transformation*

$$U = \exp\left[\frac{g}{\omega_c}(a^\dagger - a)S_x\right]. \tag{4.42}$$

The polaron transformation can be seen as photon-dependent spin-rotation around x-axis or as a spin-dependent photon displacement

$$U = \exp\left[-i\hat{\theta}S_x\right] = \exp\left[\hat{\alpha}(a^\dagger - a)\right], \tag{4.43}$$

where $\hat{\theta} = ig/\omega_c(a^\dagger - a)$, and $\hat{\alpha} = g/\omega_c S_x$. Following this last consideration, it is straightforward to see how the EDM Hamiltonian transforms. One just needs to consider that

$$\begin{aligned} UaU^\dagger &= a - \hat{\alpha} = a - \frac{g}{\omega_c} S_x, \\ US_zU^\dagger &= \cos(\hat{\theta}) S_z - \sin(\hat{\theta}) S_y \\ &= \cosh\left[g/\omega_c(a^\dagger - a)\right] S_z - i \sinh\left[g/\omega_c(a^\dagger - a)\right] S_y, \end{aligned} \tag{4.44}$$

where the hyperbolic operators can be written in terms of standard displacement operators

$$\begin{aligned} \cosh\left[\alpha(a^\dagger - a)\right] &= \frac{e^{\alpha(a^\dagger - a)} + e^{-\alpha(a^\dagger - a)}}{2}, \\ \sinh\left[\alpha(a^\dagger - a)\right] &= \frac{e^{\alpha(a^\dagger - a)} - e^{-\alpha(a^\dagger - a)}}{2}. \end{aligned} \tag{4.45}$$

Then the extended Dicke model in the polaron frame becomes

$$\tilde{H}_{\text{EDM}} = \omega_c a^\dagger a + \varepsilon \frac{g^2}{\omega_c} S_x^2 + \frac{\omega_0}{2}\left[e^{\frac{g}{\omega_c}(a^\dagger - a)} \tilde{S}_- + e^{-\frac{g}{\omega_c}(a^\dagger - a)} \tilde{S}_+\right], \tag{4.46}$$

where the collective $\pm$ operators along x-axis are given by $\tilde{S}_\pm = S_z \pm i S_y$. These operators are the same as the usual spin up/down operators, just with respect to the eigenstates of S_x. We conclude this derivation by noticing that the polaron transformation used above represent the Coulomb gauge transformation Eq. (1.30) restricted to the two-level subspace (this can be checked directly recalling the correspondence between photon/spin operators and the original electric-field/dipole operators).

At first sight, the polaron EDM doesn't seem to give any advantage. It looks actually more complicated than the original frame, since we transformed a linear coupling to a very non-linear one, mediated by the displacement operators, which contains all powers of photon's creation operator. But it is precisely because of this displacing coupling that this frame is suitable for interesting approximations. The reason is due to the fact that the displacement operator is unitary, which implies that all its matrix elements are smaller than one

$$|\langle n| e^{-\frac{g}{\omega_c}(a^\dagger - a)} |m\rangle| \leq 1. \tag{4.47}$$

When $\omega_0 \leq \omega_c$ this calls for perturbation theory, where we take

$$\begin{aligned} H_0 &= \omega_c a^\dagger a + \varepsilon \frac{g^2}{\omega_c} S_x^2, \\ H_I &= \frac{\omega_0}{2}\left[e^{\frac{g}{\omega_c}(a^\dagger - a)} \tilde{S}_- + e^{-\frac{g}{\omega_c}(a^\dagger - a)} \tilde{S}_+\right], \end{aligned} \tag{4.48}$$

as the bare Hamiltonian and the perturbative interaction, respectively.

4.8 Ultrastrong-coupling effective theory

What we want to do here is to derive an effective Hamiltonian, simpler than the original one, that we can use to deepen our understanding about the phases of cavity QED. In particular we want to understand what is the effect of the cavity on the dipole ensemble. This last point emerges quite naturally from the fact that most of the basics properties of the cQED ground state are a direct consequence of direct dipole-dipole interactions, meaning that the internal properties of the dipole ensemble are of primary importance in the characterization of the system. On the other hand we have seen that in the USC regime certainly something different happens, which is just given by the presence of the cavity.

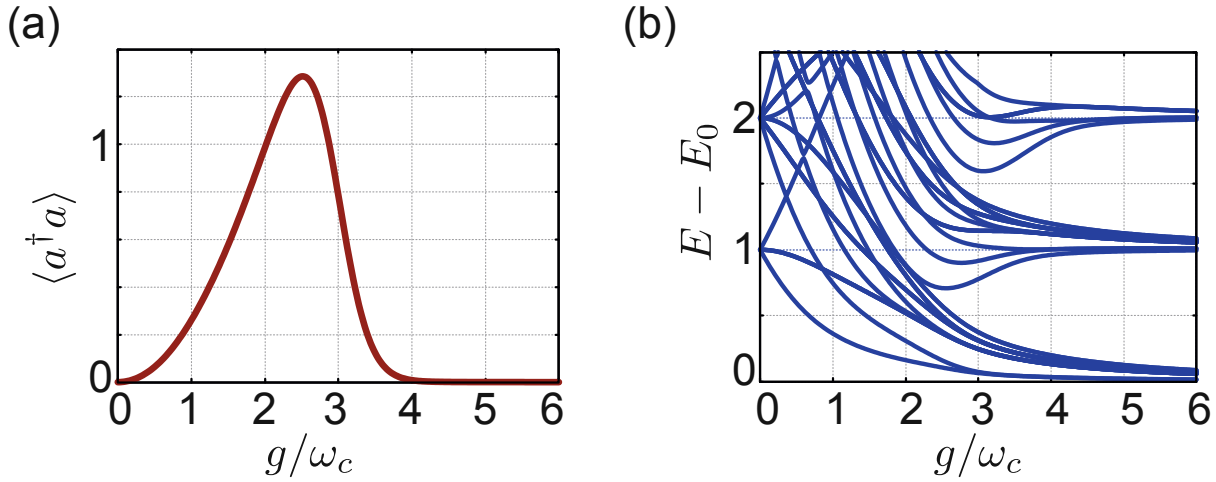

Figure 4.6: (a) Ground state photon's number $\langle a^\dagger a\rangle$ of the EDM in the standard frame. (b) Spectrum $E_n - E_0$ of the EDM. This simulation has been done with $N = 4$, $\omega_c = \omega_0 = 1$, $\eta = 0$.

When $\omega_0 \leq \omega_c$ the polaron Hamiltonian can be split into a bare part, H_0, plus an interacting part, H_I, accordingly to Eq. (4.48). From Fig. 4.6(a) we can see that even for $\omega_0 = \omega_c$ the ground state photon number remains always small $\langle a^\dagger a\rangle \approx 0$, meaning that the photon part of the ground state must be something close to the photon's vacuum $|\mathrm{GS}\rangle \approx |0_{\mathrm{ph}}\rangle|\psi_{\mathrm{spins}}\rangle$. When $\varepsilon \approx 0$ it can also be seen that for large g/ω_c the spectrum is organized in quasi-degenerate manifolds, see Fig. 4.6(b). Each of these manifold is separated by an energy $E \sim \omega_c$ from the other nearest one. This seems to suggest that the spectrum in the polaron frame (when dipole-dipole interactions are small!) is given by states like

$$|E\rangle \sim |n, m\rangle = |n_{\mathrm{ph}}\rangle|\psi^{(n,m)}_{\mathrm{spins}}\rangle. \tag{4.49}$$

With this in mind we can build an effective Hamiltonian as described in the App. F using Eq. (F.2) where the low energy manifold $\mathcal{H}_{\mathrm{low}}$ is given by all the states with zero photons, $\sim |n = 0_{\mathrm{ph}}\rangle|\psi^{(n=0,m)}_{\mathrm{spins}}\rangle$, and the high energy ones are all the other states in which there is at least one photon. The full expression is derived in App. F and, in principle, it is valid for any value of the

light-matter coupling. Unfortunately, in this way it is not possible to write it in a close form, which makes this expression not very useful for intuitive understanding. A further simplification comes when the coupling is larger than unity $g/\omega_c > 1$. In this regime the effective Hamiltonian can be written as [55]

$$H_{\text{eff}} \approx \omega_0 e^{-\frac{g^2}{2\omega_c^2}} S_z + \frac{\omega_0^2 \omega_c}{2g^2}\left(S_x^2 - \vec{S}^2\right) + \varepsilon \frac{g^2}{\omega_c} S_x^2. \tag{4.50}$$

We compare now this effective Hamiltonian with the LMG model, defined in Eq. (4.34), which represents the dipole ensemble without the cavity photons. Defining

$$\tilde{\omega}_0 = \omega_0 e^{-g^2/(2\omega_c^2)}, \qquad \tilde{\varepsilon} = \varepsilon + (\omega_0^2 \omega_c^2)/(2g^4), \tag{4.51}$$

we can rewrite the effective dipole model as an effective LMG model

$$H_{\text{eff}} = \tilde{\omega}_0 S_z + \tilde{\varepsilon} \frac{g^2}{\omega_c} S_x^2 - \frac{\omega_0^2 \omega_c}{2g^2} \vec{S}^2, \tag{4.52}$$

with the additional "total spin" contribution proportional to $\vec{S}^2$. From this effective Hamiltonian we can already say quite a lot about the origin of the ground state. First we notice that the most convenient basis to express the dipoles state is the spin-x basis, given by all states $|S, m_x\rangle$, where

$$\vec{S}^2 |S, m_x\rangle = S(S+1)|S, m_x\rangle, \qquad S_x |S, m_x\rangle = m_x |S, m_x\rangle. \tag{4.53}$$

Indeed, when the coupling is large, the S_z component is exponentially suppressed, such that the ground state is mainly determined by the terms S_x^2 and $\vec{S}^2$. In particular, because of the high symmetry of the EDM expressed in Eq. (4.17), we can immediately say that the ground state lies in the sub-space with highest total spin, i.e., with quantum number $S = N/2$. Of course, as assumed from the very beginning, the cavity remains approximately in its vacuum state $|0_{\text{ph}}\rangle$. For this reason we speak about *light-matter decoupling* when the system reaches this regime. When transformed back to the original frame we can say that the ground state is a superposition of spin-dependent displaced photon's states

$$|\text{GS}\rangle \approx \sum_{m_x=-N/2}^{N/2} c_{m_x} e^{-m_x \frac{g}{\omega_c}(a^\dagger - a)} |0_{\text{ph}}\rangle |S = N/2, m_x\rangle. \tag{4.54}$$

In the USC regime, when $\tilde{\omega}_0/\omega_c \approx 0$, the ground state is then completely determined by the S_x^2-term, and it is characterised by a single m_x quantum number. If $\tilde{\varepsilon} < 0$ the dipoles are in the state with maximum spin-x projection, which is $m_x = \pm N/2$. If $\tilde{\varepsilon} > 0$ the ground state depends on the parity of the number of dipoles, and it gives $m_x = 0$ if N is even, or $m_x = \pm 1/2$

if N is odd. It is remarkable that the vacuum effect from the cavity is to suppress an eventual ferroelectric instability of the dipolar ensemble by shifting the dipole-dipole energy accordingly to Eq. (4.51)(right). Combined with the exponential suppression of the internal dipole's energy, given in Eq. (4.51)(left), we can derive the critical dipole-dipole strength to have a ferroelectric transition in the USC

$$\varepsilon_c \approx -\frac{\omega_0^2\omega_c^2}{2g^4}. \tag{4.55}$$

We notice that this expression is independent from the number of dipoles. If we look back to the "standard" condition for the superradiant phase in Eq. (4.29), we find

$$\varepsilon_c^{\mathrm{HP}} = -\frac{\omega_0\omega_c}{Ng^2}, \tag{4.56}$$

where we used the label HP to highlight that this equation is valid just in the Holstein-Primakoff approximation, where ultra-strong coupling effects from the cavity are considered negligible. This type of approach can be used to study a transition from the normal state to the superradiant one, but when $g/\omega_c > 1$ one has to take into account that the normal ground state cannot be used, not even when the dipole-dipole interaction is exactly zero, as it is clearly visible from Fig. 4.7(a).

Finally, in order to have a major understanding of the transition between ferroelectric and anti-ferroelectric, we make use of the so-called *adiabatic potential* (in the standard representation of the EDM)

$$V_{\mathrm{ad}}(X) = \frac{X^2}{2} + E_0(X), \tag{4.57}$$

where $X = (a + a^\dagger)/\sqrt{2}$ is interpreted as a simple c-number. $E_0(X)$ is the ground state energy of the bare spin Hamiltonian, parametrised by X,

$$H_{\mathrm{EDM}}(X) = \omega_0 S_z + \sqrt{2}gXS_x + \frac{g^2}{\omega_c}(1+\varepsilon)\,S_x^2. \tag{4.58}$$

In Fig. 4.7(b) we plot this adiabatic potential for the three cases, $\varepsilon > \varepsilon_c$, $\varepsilon \approx \varepsilon_c$, and $\varepsilon < \varepsilon_c$, in the case of N even. From a full numerical calculation, shown in Fig. 4.7(c), we can see that the transition from ferroelectric to anti-ferroelectric as a function of ε is characterised by a sharp jump in $\langle a \rangle$, as well as in a pronounced peak in the voltage fluctuation $\langle U^2 \rangle$. This is somehow reminiscent of a first order phase transition with the peculiarity that at the phase transition point all possible states become degenerate.

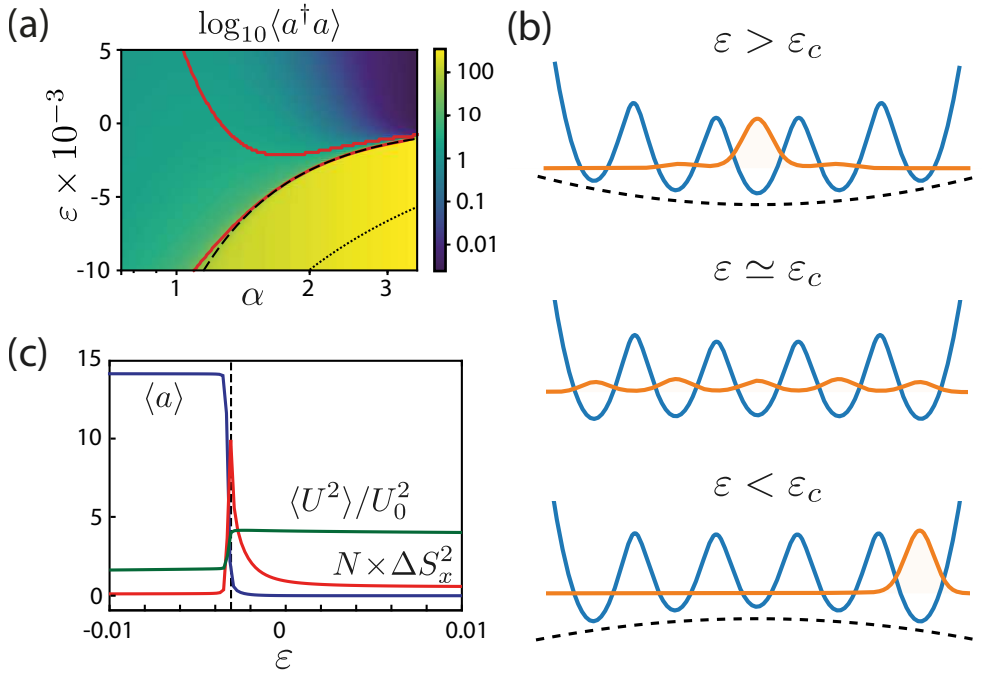

Figure 4.7: Subradiant-to-superradiant phase transition. (a) Zoom of the ground state phase diagram in the region $|\varepsilon| \approx 0$. The color scale shows the ground state photon number and the red solid lines indicate the same phase boundaries as in Fig. 4.1. The dashed line is the critical value ε_c given Eq. (4.55) and the dotted line indicates the value of ε_c obtained from the classical transition point in Eq. (4.56). (b) The adiabatic potential $V_{\rm ad}(X) = X^2/2 + E_0(X)$ for the cavity mode is plotted together with the resulting ground state wavefunction for different values of the interaction parameter ε. (c) Dependence of the mean cavity field and the voltage and spin fluctuations as a function of ε for $\alpha = 2$. In (b) we have used $N = 4$ qubits and in (a) and (c) $N = 8$. In all plots $\omega_0 = \omega_c$ and a symmetry-breaking bias field, $H_{\rm bias} = \lambda S_x$, where $\lambda/\omega_c = 10^{-3}$, has been assumed.

4.9 Beyond the EDM: short range interactions

In this chapter we have studied the ground state properties of cavity QED always from the perspective of the extended Dicke model. Of course it is natural to ask what modifications appear when we abandon this highly idealised scenario. A complete understanding here is naturally hopeless, but it is still possible to relax some approximations and have a feeling of a more realistic system. We have at least up to three crucial approximations:

1. single mode approximation,
2. two level approximation,
3. collective dipole-dipole interaction approximation.

In the following we keep the first two approximations, but investigate what happens when more realistic, short-range dipole-dipole interactions are taken into account. Instead it is highly relevant to understand what can be achieved without having the collective dipole-dipole interaction $\sim \varepsilon S_x^2$

which characterised the EDM.

So here we consider what we called the cavity QED Hamiltonian

$$H_{\text{cQED}} = \omega_c a^\dagger a + \omega_0 S_z + g(a + a^\dagger) S_x + \frac{g^2}{\omega_c} S_x^2 + J \sum_{ij} \mathcal{D}_{ij} s_x^i s_x^j, \tag{4.59}$$

where $\mathcal{D}_{ij}$ is the full adimensional electrostatic dipole-dipole interaction, where all the dimensional parameters are condensed into the single free parameter J. Notice that, in principle, this parameter in our dipole-LC circuit toy model is fixed to be $J = (g^2 N)/(\omega_c \nu)$, but, in order to have a more general picture, valid also for generic cavities we simply keep it as a free parameter.

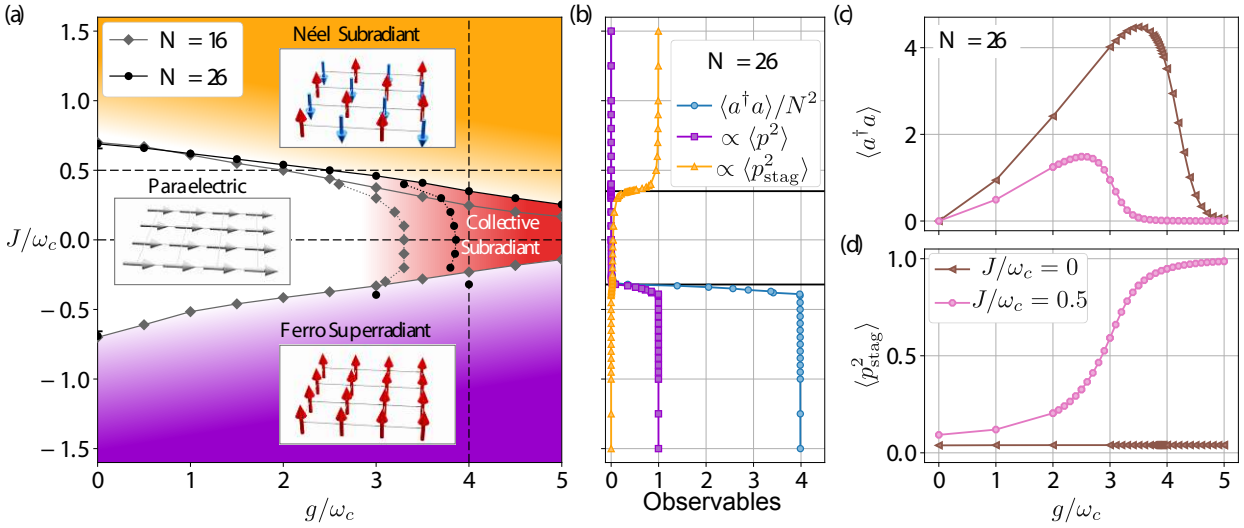

Figure 4.8: The ground state of cQED for a planar simple square lattice of dipoles. (a) Phase diagram of the ground state of H_{cQED} for finite N number of dipoles. The lines show the boundaries between the different phases, and the dotted lines show the boundary between the different crossovers. In the insets we show the sketch of each dipole's configuration. (b) Observables which characterise the different phases for a cut at $g/\omega_c = 4$. (c-d) Ground state photon number and order parameter for the paraelectric/subradiant transition. For $J/\omega_c \simeq 0$ the collective subradiant regime appears for large g/ω_c, which is fundamentally different from the antiferroelectric Néel order one encounters for finite $J/\omega_c > 0$, as it is clearly shown by the behaviour of the staggered momentum.

We can re-derive the ground state phase diagram in Fig. 4.1 and look for modifications to the various phases due to the finite range dipole-dipole interaction. In order to catch all the different ordered phases we introduce the normalised structure factor

$$\Sigma(\vec{k}) = \frac{4}{N} \sum_{i=1}^{N} e^{i\vec{k}\cdot(\vec{r}_i - \vec{r}_0)} \langle s_x^i s_x^0 \rangle \,. \tag{4.60}$$

Contrary to the EDM case, here the geometry of the dipolar lattice is of central importance. In a simple square lattice all the phases are characterised by the structure factor calculated in the points

$\Gamma = (0,0)$ and $M = (\pi, \pi)$, that we call, respectively, standard and staggered momenta

$$\begin{aligned} \Sigma(\Gamma) &= \frac{4}{N^2} \langle p^2 \rangle \,, \\ \Sigma(M) &= \frac{4}{N^2} \langle p_{\text{stag}}^2 \rangle \,. \end{aligned} \tag{4.61}$$

Here p and p_{stag} denotes the two order parameters for ferroelectric and antiferroelectric phases, defined by

$$\begin{aligned} p &= \sum_{i=1}^{N} s_x^i \\ p_{\text{stag}} &= \sum_{i \in A} s_x^i - \sum_{i \in B} s_x^i, \end{aligned} \tag{4.62}$$

where in the staggered order parameter we split the polarization between two sublattices A and B.

In Fig. 4.8(a) we can see the phase diagram for a planar two dimensional simple square lattice, where we approximated the dipole-dipole interactions just as nearest neighbour interactions

$$\mathcal{D}_{ij} \simeq \delta_{ij}, \tag{4.63}$$

(this approximation is almost exact when the image charges are included). As already described in the previous sections, we have three main phases: the normal phase, which we also call *paraelectric*, because the dipole's polarisation is very weak, a ferroelectric one (or superradiant) and an anti-ferroelectric phase (or subradiant). When the single particle coupling is in the USC regime, $g/\omega_c > 1$, we see a smooth crossover into what we call the *collective subradiant* phase. While we are not sure that this phase is a proper phase, since it is not clear that it will survive in the thermodynamics limit when $N \to \infty$, it is highly relevant for finite N when the system is in the USC regime. The collective subradiant phase is characterised by some sort of anti-ferroelectric state which is not triggered by the dipole-dipole interaction, but by the ultra-strong coupling with the cavity mode, as we can see from the fact that it exist even for $J/\omega_c = 0$. In Fig. 4.8(b) we plot the ground state's expectation value of a few observables as a function of J/ω_c, for a fixed value of $g/\omega_c > 1$. We can see that the collective subradiant phase is well separated from the superrdiant phase, but also from the Néel subradiant phase. This rather sharp separation means that the collective subradiant state is fundamentally different from the anti-ferroelectric Néel state, where the latter is stabilized by sufficiently strong positive dipole-dipole interactions. This collective subradiant phase was also present in our first phase diagram in Fig. 4.1, but, because of the particular scaling of the dipole-dipole interaction, linked to the cavity-dipole coupling as $J \sim g^2/\omega_c$, the phase boundaries looked different. Also, in the case of collective coupling, there was no transition to a competeing,

Néel -ordered subradiant phase. In Fig. 4.8(c-d) we illustrate this difference. We see that both the collective subradiant and the Néel subradiant state decouple from the cavity, as we see from the photon number operator $\langle a^\dagger a\rangle \approx 0$, when $g/\omega_c \gg 1$. But when we look at the staggered momentum, we see that, while it becomes different from zero in the anti-ferroelectric transition at finite $J > 0$, it vanishes for all values of g/ω_c when $J = 0$.

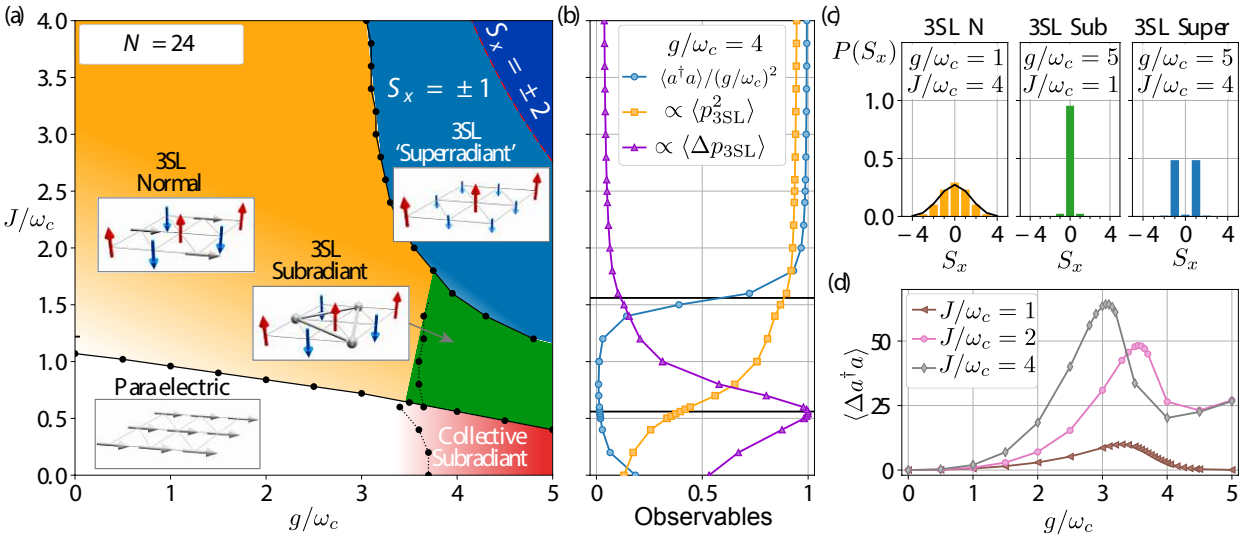

Figure 4.9: The ground state of cQED for a planar triangular lattice of dipoles. (a) Ground state phase diagram of $H_{\rm cQED}$ for a finite system with $N = 24$. The insets shows a sketch of each dipole's configuration. Solid lines mark the phase transitions, while dotted lines are the crossovers. The red dashed line mark the boundary between the 3SL superradiant phases with different value of S_x. (b) Some observables which characterise the different phases for a cut at $g/\omega_c = 4$. (c) Histograms of the dipole's polarization in the 3SL norma, subradiant and superradiant phases. (d) Photon's number fluctuations. The peaks of this quantity are used to mark the boundaries to the 3SL superradiant phase. We have used the general notation $\langle \Delta\mathcal{O}\rangle = \langle \mathcal{O}^2\rangle - \langle \mathcal{O}\rangle^2$.

As already argued in the previous section, we see that the cavity-dipole coupling can substantially modify the ground state properties of the dipolar lattice, due to the presence of the quantum fluctuations provided by the cavity field. It is then interesting to ask what happens if we couple the cavity field to a dipolar lattice which is already characterised by strong dipolar quantum fluctuations. We explore this possibility by looking at the triangular lattice of dipoles. In this case, because of the geometric frustration due to the triangular configuration, when $J > 0$, the lattice is heavily affected by fluctuations. The main quantity here is the structure factor calculated at the $K = (\pm 4/3\pi, 0)$ point, which is related to the *three sub lattices* (3SL) order parameter

$$\Sigma(K) = \frac{4}{N^2}\langle p^2_{3SL}\rangle\,, \tag{4.64}$$

where the 3SL order parameter operator is defined by

$$p_{3\mathrm{SL}} = \sum_{i\in A} s_x^i + e^{-i4/3\pi} \sum_{i\in B} s_x^i + e^{+i4/3\pi} \sum_{i\in C} s_x^i, \tag{4.65}$$

in which A, B, C represent the three different sub lattices.

The phase diagram for the planar triangular lattice in a cavity is shown in Fig. 4.9(a). We can see that new USC phases have appeared, which can be characterised by different polarizations of the three sub lattices. The paraelectric and collective subradiant phases do not change, since they exist in the region of weak dipole-dipole interactions, where the effect of the geometry is negligible. At small light-matter coupling $g/\omega_c < 1$, the antiferroelectric Neel subradiant state is replaced by the 3SL normal state, which is the proper ground state for the frustrated triangular lattice, with positive dipole-dipole interaction. The situation drastically changes at large light-matter coupling, depending on the dipole-dipole interaction strength. Indeed, for moderate $J/\omega_c \sim O(1)$ and $g/\omega_c > 1$ we encounter the *3SL subradiant* phase, where the ground state combines the features of the collective subradiant phase with the 3SL state. At large $J/\omega_c > 1$, quite surprisingly, we see that the state partially polarises and $\langle S_x \rangle \neq 0$. There is still a 3SL type of ordering, but with some left over polarization. This characterisation of the USC part of the phase diagram is shown in Fig. 4.9(b), by looking at different observables which take very different values in all the different phases. In Fig. 4.9(c) we further characterise the various phases by looking at the S_x-components of the ground state, which highlight a strong difference between the three different 3SL phases, the normal one, the subradiant one and the superradiant one. The difference between 3SL subradiant and 3SL superradiant is also remarked in Fig. 4.9(d), where we plot the photon number fluctuations as a function of g/ω_c for various J/ω_c. In the 3SL subradiant phase the photon fluctuations are strongly suppressed, similarly to the light-matter decoupling of the collective subradiant phase, while they remain well visible in the 3SL superradiant phase.

In conclusion to this chapter we have discussed the ground states (or vacua) of cavity QED when the electrostatic interaction is treated consistently with the single cavity mode. By approximating the dipole-dipole interaction as infinite range we obtained the extended Dicke model (EDM) which is particularly useful to draw a minimal ground state phase diagram. The collective USC is characterised mainly by the normal phase and the superradiant phase, which is triggered by geometries in which the mean dipole-dipole interaction is negative. When the system is pushed into the single particle USC regime the situation is much richer and a new subradiant phase appears. In the case where the short range of the dipole-dipole interaction is kept new other phases that mix subradiance and superradiance appear in this regime dependently on the geometry of the lattice cell.

Chapter 5

Thermodynamics of the extended Dicke model

After having studied the ground state of cavity QED through a detailed analysis of the approximated extended Dicke model and a couple of paradigmatic examples using the full cQED Hamiltonian, it naturally raises the question: what's about the excited states? As usual this problem becomes very quickly intractable, and a complete understanding of the dynamics is far beyond the scope of this thesis. Nevertheless, we can still have a glimpse of the excited states properties by looking at what we can consider the "continuation" of ground state physics: the equilibrium states. Indeed, by assuming that the system is in thermal equilibrium with an external bath with temperature T, the system is fully characterised by its thermal density matrix [94]

$$\hat{\rho} = \frac{e^{-\hat{H}/(k_B T)}}{Z}, \tag{5.1}$$

where

$$Z = \mathrm{Tr}[e^{-\hat{H}/(k_B T)}] \tag{5.2}$$

is the partition function and k_B is the Boltzmann constant. Therefore probing the thermodynamics properties of the system is equivalent to take a first look at its excited states. Even though exploring a system by warming it up seems to destroy all quantum features, one should keep in mind that the very discovery of quantum mechanics is based on thermodynamical observations, from the theory of the black body radiation to the first observations of atomic lines by burning different types of materials.

In this chapter we first review the basics of thermodynamics in quantum mechanics and then we will explore the thermodynamics of cavity QED from the weak coupling to the USC regime. In doing so we will always work with the extended Dicke model, which permits a sufficiently simple

treatment. A more detailed study with the full cQED Hamiltonian is left for future works.

The results contained in this chapter are published in Quantum 4, 335 (2020). This project was done by Philipp Pilar as leading author under the supervision of Peter Rabl. I contributed as second author with analytical and numerical calculations. In particular I derived most of the analytic formulas regarding the Dyson expansion and the black body radiation. All the figures have been produced by Philipp Pilar.

5.1 Thermodynamics in the quantum theory

Thermodynamics is the theory of infinitesimal transformation between equilibrium states. These transformations are expressed by changes in the Hamiltonian or the bath parameters and they give rise to various relations between the observables. Since we work just in the canonical ensemble the only parameter characterising the bath is its temperature T. On the other hand the Hamiltonian can depend on an arbitrary number of parameters, which we just summarise as λ, and so we have

$$H = H(\lambda). \tag{5.3}$$

We take for granted that every equilibrium state is described by a density matrix of the form (5.1). All the thermodynamics quantities are considered to be expectation values of a particular observable, which are calculated as

$$\langle \mathcal{O} \rangle = \mathrm{Tr}[\hat{\rho}\mathcal{O}]. \tag{5.4}$$

These expectation values are in general functions of the temperature and the internal parameters of the Hamiltonian

$$\langle \mathcal{O} \rangle = f(T, \lambda). \tag{5.5}$$

We explore now how the derivatives of various observables are linked together giving rise to the usual thermodynamics relations.

From here on we will set $k_B = 1$ for simplicity. We will also often use $\beta = 1/T$, as usual in statistical mechanics. Very intuitively we define the internal energy of the system as

$$U = \langle H \rangle , \tag{5.6}$$

which then gives

$$dU = d \langle H \rangle = \langle dH \rangle + \mathrm{Tr} \left(H d\rho \right). \tag{5.7}$$

From the usual definition of the von Neumann entropy for a quantum system

$$S = -\mathrm{Tr}\left[\rho \log[\rho]\right], \tag{5.8}$$

we find the entropy variation of the system

$$dS = -d\mathrm{Tr}\left(\rho \log[\rho]\right) = -\frac{1}{T^2}\left(\langle H dH\rangle - \langle H\rangle \langle dH\rangle\right) + \frac{1}{T^3}\left(\langle H^2\rangle - \langle H\rangle^2\right) dT = \frac{1}{T}\mathrm{Tr}\left(H d\rho\right). \tag{5.9}$$

Consistently with this definition we recover

$$dU = dW + TdS, \tag{5.10}$$

where we identify the *work* done by/on the system as

$$dW = \langle dH\rangle. \tag{5.11}$$

The free energy is defined as the Legendre transform of the internal energy,

$$F = U - TS, \tag{5.12}$$

where, combining with the definition we gave for U and S we recover the correct statistical mechanics relation

$$F = -T \log[Z]. \tag{5.13}$$

Following the usual thermodynamical relations we find

$$\begin{aligned} dF &= (dU - TdS) - SdT = dW - SdT \\ &= -(Td\log(Z) + \log(Z)dT) = \langle dH\rangle + (F - \langle H\rangle)\frac{dT}{T}, \end{aligned} \tag{5.14}$$

which gives the thermal expectation value of the derivative of the Hamiltonian from the derivative of the free energy with respect to the internal parameter λ

$$\partial_\lambda F(\lambda) = \langle \partial_\lambda H\rangle. \tag{5.15}$$

Note that this remains true even if $[\partial_\lambda H, H] \neq 0$ (see App. [G]). From this equation we find that every observables can be computed as the derivative of a perturbed free energy. Indeed let's consider the observable $\mathcal{O}$, and let's consider the perturbed Hamiltonian $\tilde{H} = H + \tilde{\lambda}\mathcal{O}$, with its

corresponding free energy $\tilde{F}(\tilde{\lambda})$. Then we have

$$\partial_{\tilde{\lambda}} \tilde{F}(\tilde{\lambda}=0) = \langle \mathcal{O} \rangle \,, \tag{5.16}$$

where the expectation value is taken over the unperturbed state. From this relation we can introduce the *susceptibility* of the system to the $\tilde{\lambda}$ perturbation as

$$\chi_{\tilde{\lambda}} = \partial_{\tilde{\lambda}} \langle \mathcal{O} \rangle \big|_{\tilde{\lambda}=0} = \partial^2_{\tilde{\lambda}} \tilde{F}(\tilde{\lambda}=0) \tag{5.17}$$

If, instead, we want to probe the response of the system to a change in the temperature (which is the only bath parameter we have in our system), the central quantity is the specific heat $\mathcal{C}$, which is defined from the variation of internal energy due to the temperature. Using the various definitions above we have the following equalities

$$\begin{aligned} \mathcal{C} = \frac{dU}{dT} &= \frac{1}{T^2}\left(\langle H^2 \rangle - \langle H \rangle^2\right) \\ &= T\frac{dS}{dT} = -T\frac{d^2F}{dT^2}, \end{aligned} \tag{5.18}$$

and we see that it is also related to the second derivative of the free energy, confirming it as the temperature-susceptibility.

5.2 The free energy of the extended Dicke model

We investigate the thermodynamics of cavity QED by using the extended Dicke model defined in Eq. (4.15). In contrast to the previous chapter, here we leave the dipole-dipole interaction as a free parameter, through the replacement

$$\eta \frac{g^2}{\omega_c} \longmapsto \frac{J}{N}, \tag{5.19}$$

where J is now free, and we introduce a rescaling over the number of dipoles just for future convenience. The high symmetry of the EDM, expressed in Eq. (4.17) makes the thermodynamics description very convenient to handle numerically. Indeed the EDM Hamiltonian results in a block diagonal form, where each blocks can be labelled by its total spin quantum number s, which is defined by

$$\vec{S}^2 |s\rangle = s(s+1)|s\rangle. \tag{5.20}$$

So the partition function can be expressed as a sum over the different spin-sectors, but every term in the sum must be weighted according to its degeneracy. The resulting form is

$$Z = \sum_{s=0}^{N/2} \zeta_{s,N} Z_s, \tag{5.21}$$

where the degeneracy factor is given by [6]

$$\zeta_{s,N} = \frac{N!(2s+1)}{(N/2-s)!(N/2+s+1)!}, \tag{5.22}$$

and $s = 0, 1, 2 \ldots N/2-2, N/2-1, N/2$.

We also consider two different ways to look at the EDM, which will be very useful in the examination of the WC (weak coupling) and USC regimes. For WC it is convenient to split the EDM in the following contributions

$$H = H_{\text{LMG}} + H_c + H_g, \tag{5.23}$$

where

$$H_{\text{LMG}} = \omega_0 S_z + \frac{J}{N} S_x^2, \qquad H_c = \omega_c a^\dagger a, \qquad H_g = g(a + a^\dagger) S_x + \frac{g^2}{\omega_c} S_x^2, \tag{5.24}$$

In this form it is quite evident that H_g is amenable of a perturbative treatment with respect to H_{LMG} and H_c. Notice that H_{LMG} represent actually a well known model, the Lipkin-Meshkov-Glick model [95], used to describe strongly interacting dipoles. To have a better idea of the impact of the interaction on the free energy, we also define the interaction part of the free energy

$$F_g = F - F_{\text{LMG}} - F_c, \tag{5.25}$$

where F_{LMG} is the free energy of the LMG Hamiltonian, and $F_c = T \log[1 - e^{-\beta\omega_c}]$ is the free energy of the bare cavity mode. In general F_g must be evaluated numerically by computing the total free energy of the EDM and then by subtracting the other two free energies (which can be calculated analytically when $J = 0$).

In the USC regime instead $g/\omega_c > 1$ and one has to rethink a bit the hierarchy. Here we indeed consider the different split

$$H = H_{\text{e.m.}} + H_z, \tag{5.26}$$

where

$$H_{\text{e.m.}} = \omega_c \left(a + \frac{g}{\omega_c} S_x\right)^\dagger \left(a + \frac{g}{\omega_c} S_x\right) + \frac{J}{N} S_x^2, \qquad H_z = \omega_0 S_z. \tag{5.27}$$

This kind of repartition put an emphasis on what it could be called "the electromagnetic energy" of the system, represented by $H_{\text{e.m.}}$ and the "quantum fluctuations of the dipoles" represented by H_z. Using the polaron transformation defined in Eq. (4.42) we can further bring this Hamiltonian into the form

$$\tilde{H}_{\text{e.m.}} = U H_{\text{e.m.}} U^\dagger = \omega_c a^\dagger a + \frac{J}{N} S_x^2, \qquad \tilde{H}_z = U H_z U^\dagger = \omega_0 \left(\cos(\hat{\theta}) S_z - \sin(\hat{\theta}) S_y\right), \tag{5.28}$$

where $\hat{\theta} = ig/\omega_c(a^\dagger - a)$. This representation is very convenient to study a USC regime in which $\omega_0 < \omega_c, J/N$, where we can profit from a perturbative treatment on $\tilde{H}_z$ for any value of g/ω_c (due to the fact that cos and sin are bounded operators).

5.3 The free energy in the collective USC regime

First of all we want to clarify the role of the "collective" USC regime, which means that the single particle coupling $g/\omega_c \ll 1$, but the collective coupling $G/\omega_c = \sqrt{N} g/\omega_c \gg 1$. This type of analysis is motivated by the growing interest on the question whether the vacuum quantum fluctuations of a single cavity mode can eventually change the properties of matter, for instance, the binding energy of molecules and their reaction rate, or the band structure of semiconductor materials [96, 97, 98, 99, 100]. Following what we have seen in the last chapter there is no doubt that in the USC there will be important modifications properly due to the vacuum fluctuations of the cavity mode, but this is true only when the single particle coupling $g/\omega_c > 1$. In the collective USC regime each single particle is weakly coupled posing some doubts whether there can be any significant quantum vacuum effects. In thermodynamics we can introduce another simple argument regarding the absence of quantum vacuum effects in the collective USC regime. We just need to count the degrees of freedom and acknowledge that the dipolar ensemble has a macroscopically large number of degrees of freedom, compared to the cavity, which has just one. How can a single degree of freedom have a so large impact on a macroscopic property or system? So, when $G/\omega_c > 1$ and $g/\omega_c < 1$, we expect that actually nothing extraordinary happens. Now we are going to prove this intuition more rigorously in the EDM framework (the generalisation to H_{cQED} with the real short range dipole-dipole interaction is actually straightforward, but numerically more demanding.

Since the single particle coupling is small, it is reasonable to apply perturbation theory in H_g following the partition of Eq. (5.23).

Using the Dyson series to implement second order perturbation theory in g/ω_c we find (see App. H for the derivation of interacting free energy through the Dyson expansion)

$$F_g^{(2)} = \frac{g^2}{\omega_c}\langle S_x^2\rangle_0 - \frac{g^2}{\beta}\int_0^\beta d\tau_1 \int_0^{\tau_1} d\tau_2\, C(\tau_1,\tau_2)\langle S_x(\tau_1)S_x(\tau_2)\rangle_0, \tag{5.29}$$

where we took as the free Hamiltonian $H_0 = H_{\rm LMG} + H_c$, and where $\langle\cdot\rangle_0$ is the expecation value over the thermal state given by H_0. Under the integral we have the two "thermal correlators"

$$C(\tau_1,\tau_2) = \langle [a(\tau_1)+a^\dagger(\tau_1)][a(\tau_2)+a^\dagger(\tau_2)]\rangle_0 = (N_{\rm th}+1)e^{-\omega_c(\tau_1-\tau_2)} + N_{\rm th}e^{\omega_c(\tau_1-\tau_2)}, \tag{5.30}$$

$$\langle S_x(\tau_1)S_x(\tau_2)\rangle_0 = \frac{1}{Z_{\rm LMG}}\sum_{n,m} e^{-\beta E_n + (\tau_1-\tau_2)(E_n-E_m)} \times |\langle E_n|S_x|E_m\rangle|^2, \tag{5.31}$$

where we introduced the energies E_n and eigenstates $|E_n\rangle$ of $H_{\rm LMG}$ and the thermal cavity occupation is $N_{\rm th} = 1/(e^{\beta\omega_c}-1)$. In general, to obtain these quantities we need to diagonalise the LMG model numerically.

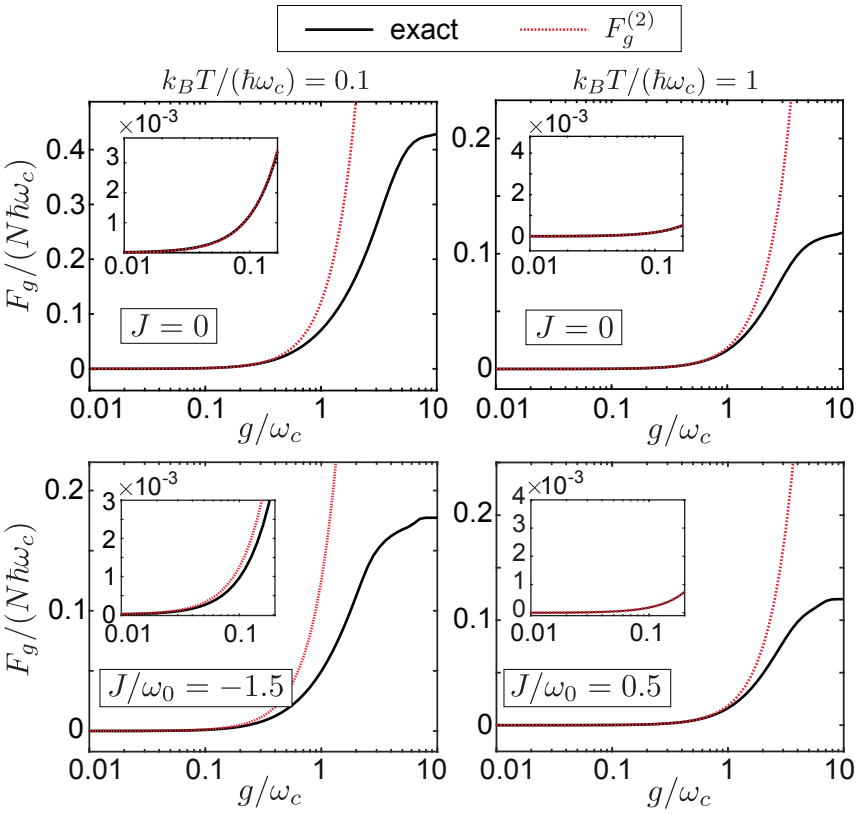

Figure 5.1: Dependence of the coupling-induced part of the free energy, F_g, on the cavity-dipole coupling strength, g. This dependence is shown in the individual plots for different temperatures and dipole-dipole coupling strengths, J, and for $\omega_c = \omega_0$. In each plot the exact numerical results for $N = 20$ dipoles are compared with approximate results obtained second-order perturbation theory ($F_g^{(2)}$) .

In Fig. 5.1 we compare this perturbative approach with the exact numerics for some important cases. We see that the matching is very good in the WC regime and even holds for the collective USC regime, $G \lesssim \omega_c$. We see that the effect of the interaction always leads to a positive contribution in the free energy. This is in stark contrast to the case of the Dicke model, where the effect of the interaction lowers the free energy [101]. Based on the Eq. (5.29) we can actually prove it in complete generality. Due to the "thermal ordering" $\tau_1 > \tau_2$, we have

$$\langle S_x(\tau_1) S_x(\tau_2)\rangle_0 \leq \langle S_x^2\rangle_0. \tag{5.32}$$

We thus find that

$$0 \leq \frac{g^2}{\beta}\int_0^\beta d\tau_1 \int_0^{\tau_1} d\tau_2\, C(\tau_1,\tau_2)\langle S_x(\tau_1)S_x(\tau_2)\rangle_0 \leq \frac{g^2}{\omega_c}\langle S_x^2\rangle_0 \frac{\omega_c}{\beta}\int_0^\beta d\tau_1 \int_0^{\tau_1} d\tau_2\, C(\tau_1,\tau_2) = \frac{g^2}{\omega_c}\langle S_x^2\rangle_0, \tag{5.33}$$

where the last equality is due to the fact that the cavity integral can be computed analytically

$$\frac{\omega_c}{\beta}\int_0^\beta d\tau_1 \int_0^{\tau_1} d\tau_2\, C(\tau_1,\tau_2) = 1. \tag{5.34}$$

We conclude that

$$0 \leq F_g^{(2)} \leq \frac{g^2}{\omega_c}\langle S_x^2\rangle_0. \tag{5.35}$$

It is then convenient to introduce the rescaling

$$F_g^{(2)} = \frac{N g^2}{4\omega_c} f_g. \tag{5.36}$$

The bound on the interacting free energy can be made even stricter, by replacing $\langle S_x^2\rangle_0 \mapsto (\Delta S_x)^2 = \langle S_x^2\rangle_0 - \langle S_x\rangle_0^2$. This can be justified by displacing the annihilation operator in the EDM with $a \mapsto a - g/\omega_c\langle S_x\rangle_0$ and then repeating the calculation. It then gives a bound on the rescaled adimensional free energy

$$0 \leq f_g < \frac{4(\Delta S_x)^2}{N}. \tag{5.37}$$

Evidently, the coupling part of the free energy is bounded by the fluctuations in the polarization rather than its mean amplitude. In any dipolar system in which the dipole-dipole correlation length is finite (basically any regular system far from a critical point), we find that $(\Delta S_x)^2 \sim N$. This means that

$$f_g \sim O(1), \tag{5.38}$$

bringing us to the main result of this section

$$\lim_{N\to\infty} \frac{F_g^{(2)}}{N} = 0. \tag{5.39}$$

This limit is very important because it says that in the collective USC regime the interacting free energy per particle vanishes, stating the impossibility that the light-matter coupling could non-perturbatively change the single particle properties of the dipolar ensemble in the usually considered thermodynamic limit.

It is worth to mention that for free dipoles, when $J = 0$, we can actually find an analytical solution for the thermal correlator in (5.31), and consequently for $F_g^{(2)}$. In this case we have

$$\langle S_x(\tau_1)S_x(\tau_2)\rangle_0 = \frac{1}{4}e^{(\tau_1-\tau_2)\omega_0}\langle S_+S_-\rangle_0 + \frac{1}{4}e^{-(\tau_1-\tau_2)\omega_0}\langle S_-S_+\rangle_0 \tag{5.40}$$

and $\langle S_\pm S_\mp\rangle_0 = N\left[1 \mp \tanh\left(\omega_0/2T\right)\right]/2$. We then obtain

$$\begin{aligned} Nf_g = N &- (N_{\rm th}+1)\langle S_+S_-\rangle_0 I(\omega_0-\omega_c) - (N_{\rm th}+1)\langle S_-S_+\rangle_0 I(-\omega_0-\omega_c) \\ &- N_{\rm th}\langle S_+S_-\rangle_0 I(\omega_0+\omega_c) - N_{\rm th}\langle S_-S_+\rangle_0 I(\omega_c-\omega_0), \end{aligned} \tag{5.41}$$

where

$$I(\Delta) = \frac{\omega_c}{\beta}\int_0^\beta d\tau_1 \int_0^{\tau_1} d\tau_2\, e^{\Delta(\tau_1-\tau_2)}. \tag{5.42}$$

Combining everything together, we find

$$f_g(J=0) = \frac{\omega_0^2 - \omega_0\omega_c \tanh\left(\frac{\omega_0}{2T}\right)\coth\left(\frac{\omega_c}{2T}\right)}{(\omega_0^2-\omega_c^2)}. \tag{5.43}$$

With this solution, which is also depicted in Fig. 5.1, we can explore the low temperature and high temperature limits. When $T \to 0$ we recover the perturbative corrections to the ground state energy [5]

$$E_0^{(2)} = F_g^{(2)}(T\to 0, J=0) = N\frac{g^2}{4\omega_c}\frac{\omega_0}{\omega_0+\omega_c}. \tag{5.44}$$

Instead, when $T \to \infty$ the cavity induced corrections to the free energy vanish quadratically

$$F_g^{(2)}(T\to\infty) \simeq N\frac{g^2\omega_0^2}{48\omega_c T^2}. \tag{5.45}$$

5.4 The free energy in the low frequency regime

Here we consider the EDM using the partition in Eq. (5.26). Specifically, we consider the system in the polaron basis, where the electromagnetic Hamiltonian and the z-Hamiltonian take the shape

given in Eq. (5.28). As we already anticipated before, this way of looking at the EDM in the polaron basis is perfectly suitable for perturbative treatment in ω_0. So, placing no constraint on the coupling constant, we consider the detuned regime where

$$\frac{\omega_0}{\omega_c} \ll 1. \tag{5.46}$$

Here we can safely apply the perturbation theory developed in App. H, where we take $H_0 = \tilde{H}_{\text{e.m.}}$ and $H_I = \tilde{H}_z$. The corrections to the electromagnetic free energy are given by

$$F^{(2)}_{\omega_0} = -\frac{\tilde{\omega}_0^2}{\beta} \sum_{r,q=0}^{\infty} \int_0^{\beta} d\tau_1 \int_0^{\tau_1} d\tau_2 \, e^{(q-r)\omega_c(\tau_1-\tau_2)} \times \left[K_{rq} \left\langle S_z(\tau_1) S_z(\tau_2) \right\rangle_0 + Q_{rq} \left\langle S_y(\tau_1) S_y(\tau_2) \right\rangle_0 \right], \tag{5.47}$$

where the full calculation is detailed in the App. H.6, and where

$$\tilde{\omega}_0 = \omega_0 e^{-\frac{g^2}{2\omega_c^2}(1+2N_{\text{th}})}. \tag{5.48}$$

The two matrices in the sums are given by

$$\begin{aligned} K_{rq} &= \frac{[1+(-1)^{r+q}]}{2} \left(\frac{g}{\omega_c}\right)^{2(r+q)} \frac{(1+N_{\text{th}})^r N_{\text{th}}^q}{r!\, q!}, \\ Q_{rq} &= \frac{[1-(-1)^{r+q}]}{2} \left(\frac{g}{\omega_c}\right)^{2(r+q)} \frac{(1+N_{\text{th}})^r N_{\text{th}}^q}{r!\, q!}. \end{aligned} \tag{5.49}$$

We can interpret this q, r-sums as the contribution of multiphotons processes, where r-photons are emitted and q-photons are absorbed. This expression can be rewritten in a more compact form as

$$F^{(2)}_{\omega_0} = -\frac{\beta\tilde{\omega}_0^2}{2} \left[\sum_{r,q=0}^{\infty} K_{rq} \Delta_{zz}(\beta, (q-r)\omega_c) + \sum_{r,q=0}^{\infty} Q_{rq} \Delta_{yy}(\beta, (q-r)\omega_c) \right]. \tag{5.50}$$

By introducing the dipole's thermal response functions

$$\Delta_{\alpha\alpha}(\beta, \omega_c) = \frac{2}{\beta^2} \int d\omega \mathcal{S}_{\alpha\alpha}(\omega) \left[\frac{e^{\beta(\omega_c-\omega)} - 1}{(\omega_c-\omega)^2} - \frac{\beta}{\omega_c - \omega} \right]. \tag{5.51}$$

Here the structure factor $\mathcal{S}$ is defined as

$$\mathcal{S}_{\alpha\alpha}(\omega) = \sum_m \frac{e^{-\beta E_m^{\text{dip}}}}{Z_{\text{dip}}} \sum_k |S_\alpha^{km}|^2 \delta(E_{km}^{\text{dip}} - \omega), \tag{5.52}$$

where $E_m^{\rm dip}$ is the energy of the electrostatic dipoles,

$$H_{\rm dip} = \frac{J}{N} S_x^2, \tag{5.53}$$

and $E_{km}^{\rm dip} = E_k^{\rm dip} - E_m^{\rm dip}$, and S_α^{km} are the matrix elements of collective spin-α operator. Note that the structure factor respects the detailed balance condition

$$\mathcal{S}_{yy}(\omega) = e^{\beta\omega}\mathcal{S}_{yy}(-\omega). \tag{5.54}$$

It is now clear that $\Delta_{\alpha\alpha}(\beta, -\omega_c)$ is associated with the probability to jump to a lower spin state by emitting a photon, while $\Delta_{\alpha\alpha}(\beta, +\omega_c)$ is the reverse process, in which a photon is absorbed and the spins can jump up to an higher state. When the resonance condition $|E_{km}^{\rm dip} - \omega_c|/T \ll 1$ is fulfilled the response function takes its maximum value

$$\Delta_{\alpha\alpha}(\beta, \omega_c) \simeq \frac{e^{-\beta E_m^{\rm dip}}}{Z_{\rm dip}} |S_\alpha^{km}|^2. \tag{5.55}$$

It is worth mentioning that this could be an interesting approach to generate multiphoton states from a strongly interacting USC system in thermal equilibrium.

5.5 USC modifications of the Curie law

The perturbative free energy developed just above is particularly useful for the investigation of the z-susceptibility

$$\chi_z = -\frac{1}{N}\frac{\partial^2 \langle S_z \rangle}{\partial \omega_0^2}\bigg|_{\omega_0=0} = -\frac{1}{N}\frac{\partial^2 F}{\partial \omega_0^2}\bigg|_{\omega_0=0}. \tag{5.56}$$

When $J = 0$, and $g = 0$ this quantity just gives the famous Curie law

$$\chi_z = \frac{\alpha_C}{T}, \tag{5.57}$$

where the Curie constant is $\alpha_C = 1/4$ (with $\hbar = k_B = 1$). In the context of magnetic dipoles it represents the susceptibility of the magnetization of a paramagnet at temperatures above the Curie temperature. In the current setting it characterizes the change in population of the two-level dipole in response to a change in the transition frequency.

Considering $F_{\omega_0}^{(2)}$ in Eq. (5.50), we obtain

$$\chi_z \simeq \frac{e^{-\frac{g^2}{\omega_c^2}(1+2N_{\rm th})}}{T}\left[\sum_{r,q=0}^{\infty} K_{rq}\frac{\Delta_{zz}(\beta,(q-r)\omega_c)}{N} + \sum_{r,q=0}^{\infty} Q_{rq}\frac{\Delta_{yy}(\beta,(q-r)\omega_c)}{N}\right]. \tag{5.58}$$

First we notice that in the low temperature limit, $T \to 0$, the only term that is non-negligible in the sum is for $r = q = 0$, for which $K_{00} = 1$, $Q_{00} = 0$. This means that everything in this regime just depends on $\Delta_{zz}(\beta, 0)$. For the special case of non interacting dipoles, $J = 0$ (where $H_{\rm dip} = 0$), we find that

$$\Delta_{zz}(\beta, 0) \simeq \langle S_z^2 \rangle = \frac{N}{4}. \tag{5.59}$$

Therefore, we obtain

$$\lim_{T\to 0} \chi_z = \frac{\alpha_c(g)}{T}, \tag{5.60}$$

where the Curie constant gets exponentially suppressed by the coupling to the cavity,

$$\alpha_c(g) = \frac{1}{4} e^{-\frac{g^2}{\omega_c^2}(1+2N_{\rm th})}. \tag{5.61}$$

This is somehow not completely surprising if we follow the intuition developed from the USC low energy theory in Ch. 4.8. Indeed, for zero temperature

$$\chi_z \sim \partial^2_{\omega_0} E_0 \sim e^{-g^2/\omega_c^2}. \tag{5.62}$$

This shows that the susceptibility can be directly used to observe USC effects. But there is more.

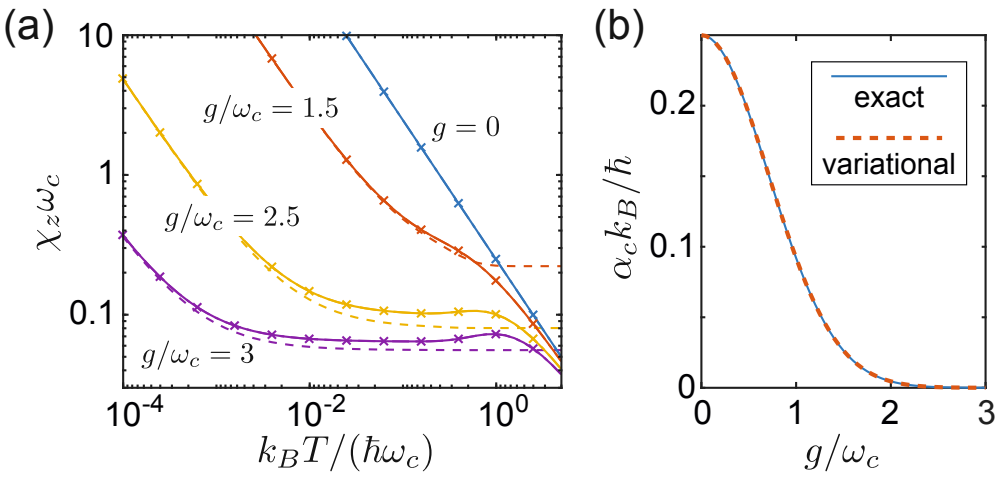

Figure 5.2: (a) Plot of the zero-field susceptibility χ_z (solid lines) for different coupling parameters g/ω_c. The dashed lines indicate the predictions from the approximate formula given in Eqs. (5.63)-(5.64). The x-markers show the results obtained from the perturbation theory given by Eq. (5.58). (b) Dependence of the Curie constant $\alpha_C(g)$ on the dipole-field coupling strength. The exact numerical results are in perfect agreement with the analytic scaling derived in Eq. (5.61). For all plots $N = 20$, $\omega_c = \omega_0$ and $J = 0$ have been assumed.

In Fig. 5.2 we show the dependence of χ_z as a function of the temperature for different values of the light-matter coupling. First we see that the perturbation theory given in Eq. (5.58) is basically exact and the modified Curie constant fits perfectly at low temperature. This is expected, since

the susceptibility is evaluated at $\omega_0 \to 0$, where the perturbation theory must hold. Secondly, we see that for larger temperatures we have an intermediate regime where the susceptibility develops a plateau when $g/\omega_c > 1$, followed by a bump and then falling again as a modified Curie law. This is a very important observation since it is directly linked to the USC and cannot be observed in the standard WC regime.

To better understand the formation of the USC-plateau at intermediate temperatures we consider a simple toy model where the z-susceptibility is made by the modified Curie law plus some corrections due to the derivatives of the first excited states

$$\chi_z \approx \frac{\alpha_C(g)}{T} - \frac{1}{N\hbar}\sum_n p_n \left.\frac{\partial^2 E_n}{\partial \omega_0^2}\right|_{\omega_0=0}, \tag{5.63}$$

where p_n and E_n are the thermal occupation probabilities and the energy of the n-th eigenstate, respectively. If we consider the low energy USC theory from Ch. 4.8 we can explicitly calculate also the second term in this equation. Assuming that all the lowest levels are equally populated (because they are almost degenerate) $p_n \approx 1/2^N$, we have

$$-\frac{1}{N\hbar}\sum_n p_n \left.\frac{\partial^2 E_n}{\partial \omega_0^2}\right|_{\omega_0=0} \approx \frac{\omega_c}{2g^2}. \tag{5.64}$$

In Fig. 5.2 we can see that this simple toy model perfectly fits both the low and intermediate temperature regime, with the correct reproduction of the USC-plateau. This is an important observation because it explicitly relates the z-susceptibility to the vacuum energy and the lowest excited states, which in the USC limit of the EDM form an almost degenerate ground-state manifold.

5.6 Black body radiation

When one thinks about thermodynamics and quantum mechanics the first thing that comes to mind is the black body radiation. It is indeed well known that the very origin of the quantum theory lies in the understanding of radiation in thermal equilibrium inside a body where it cannot escape, precisely a black body. Here we calculate the black body spectrum of our LC cavity QED system and we explicitly show how it can be used to directly observe the USC regime. We also provide a detailed operational description about how to measure it in a realistic situation. The main idea is represented in Fig. 5.3 where the cavity QED system is attached to a transmission line via a small capacitor. Warming up the system generates excitations, which eventually decay into the transmission line and leave the system. At the end of the line there is a detector which scans through the frequencies of the emitted excitations, effectively measuring the black body radiation. Keeping the capacitive coupling extremely weak leaves the system always thermalised, since the

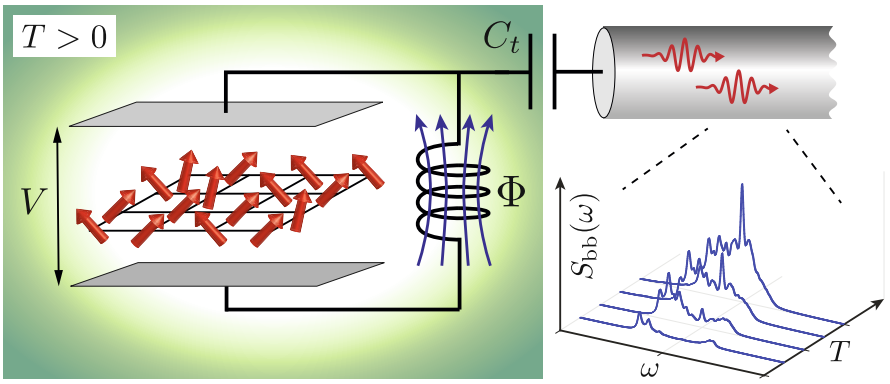

Figure 5.3: Sketch of a cavity QED setup where an ensemble of dipoles is coupled to the electric field of a lumped-element LC resonator. The system is in thermal contact with a bath of temperature T. The black-body spectrum of the cavity mode, $S_{\rm bb}(\omega)$, can be measured through a weak capacitive link to a cold transmission line. See text for more details.

emitted excitations are just a negligible fraction of the whole thermal excitations contained in the system. This is exactly the idea behind the back body radiation: the radiation is fully confined in the box, in thermal equilibrium with its walls, but we can probe it by a small hole from where just a tiny fraction of the radiation can escape. In such a regime, $C_t \ll C$, the coupling Hamiltonian between the circuit and the transmission line is

$$H_{\rm c-t} = C_t V V_t, \tag{5.65}$$

where C_t is the capacitor between the transmission line and the LC circuit and C is the capacitance of the LC circuit, V is the voltage drop across the capacitor C and V_t is the voltage drop at the end of the line. As usual in circuit QED we model the transmission line as a bosonic chain [68], where

$$V_t = \sum_k V_k (b_k^\dagger + b_k), \tag{5.66}$$

and $[b_k, b_{k'}^\dagger] = 1$. The transmission line is then fully characterised by the frequency of each mode, ω_k, and the corresponding coupling parameter $\lambda_k = C_t V_0 V_k/\hbar$. It is also convenient to introduce a rescaled voltage operator for the LC circuit $V = V_0 X$. Then the Hamiltonian of the system coupled to the transmission is

$$H_{\rm tot} = H + \sum_k \omega_k b_k^\dagger b_k + \sum_k \lambda_k (b_k^\dagger + b_k) X. \tag{5.67}$$

For a conventional transmission line we have $\lambda_k \sim \sqrt{\omega_k}$.

Using the equations of motion, we can obtain the formal solutions for the Heisenberg operators b_k

$$b_k(t) = b_k(0) e^{-i\omega_k t} - i\lambda_k \int_0^t dt'\, e^{-i\omega_k (t-t')} X(t'), \tag{5.68}$$

and assuming that the transmission line is initially in the vacuum state we have

$$\langle b_k^\dagger b_k \rangle (t) = \lambda_k^2 \int_0^t \int_0^t dt' dt'' \, e^{i\omega_k (t''-t')} \langle X(t') X(t'') \rangle \, . \tag{5.69}$$

We introduce now the positive/negative frequency coupling operators by $X(t) = X_-(t) + X_+(t)$, such that $X_+(t) = \sum_{n \geq m} X_{nm} e^{i\omega_{nm} t}$ contains only contributions that oscillate with a positive frequency, $\omega_{nm} = (E_n - E_m)/\hbar \geq 0$, and $X_-(t) = X_+^\dagger(t)$. We then introduce the thermalization rate of our system γ, and for times $t \gg \gamma^{-1}$ we have

$$\langle b_k^\dagger b_k \rangle (t) \simeq \lambda_k^2 t \times 2\mathrm{Re} \int_0^\infty d\tau \, \langle X_+(\tau) X_-(0) \rangle_0 \, e^{-i\omega_k \tau}. \tag{5.70}$$

The total power emitted into the transmission line is

$$P_{\mathrm{rad}} = \sum_k \hbar \omega_k \partial_t \langle b_k^\dagger b_k \rangle (t) \tag{5.71}$$

and by writing $P_{\mathrm{rad}} = \int_0^\infty d\omega \, S_{\mathrm{bb}}(\omega)$ we obtain the general expression for the black-body spectrum

$$S_{\mathrm{bb}}(\omega) = \hbar \omega J(\omega) C_X(\omega). \tag{5.72}$$

Here we introduced $J(\omega) = \sum_k \lambda_k^2 \delta(\omega - \omega_k)$, the spectral density of the transmission line, and

$$C_X(\omega) = 2\mathrm{Re} \int_0^\infty d\tau \, \langle X_+(\tau) X_-(0) \rangle_0 \, e^{-i\omega\tau}. \tag{5.73}$$

We assume that the spectral density is Ohmic and so we can write $J(\omega) = \kappa\omega/(2\pi\omega_c)$, where κ is the leakage rate from the cavity into the transmission line. For a completely isolated system the correlation function of the system operator X is given by

$$C_X(\omega) = 2\pi \sum_{n>m} \frac{e^{-\beta E_n}}{Z} |\langle n|X|m\rangle|^2 \delta(\omega - \omega_{nm}). \tag{5.74}$$

The effect of having a finite thermalization rate γ is that the delta functions in this correlation function get broadened and acquire a finite linewidth. This effects can be modelled by hand by replacing $\delta(\omega - \omega_{nm}) \mapsto \delta_\gamma(\omega - \omega_{nm})$, where δ_γ is a smeared delta function. In our case we chose a Lorentzian profile. Since the linewidth is still assumed to be very small with respect to the level spacing we approximate $\omega J(\omega) \simeq \omega_{nm} J(\omega_{nm})$. By re-expressing the voltage operator as $V = V_0(A + A^\dagger)$ we have the final expression for the black body spectrum seen by a detector at the end of the line

$$S_{\mathrm{bb}}(\omega) = \frac{\hbar\kappa\gamma}{2\pi\omega_c} \sum_{n>m} \frac{e^{-\beta E_n}}{Z} \frac{\omega_{nm}^2 |\langle n|A + A^\dagger|m\rangle|^2}{(\omega - \omega_{nm})^2 + \gamma^2/4}. \tag{5.75}$$

Notice that we have introduced the "gauge invariant cavity annihilation operator" A. In the polaron frame $A = a$, but in general it is a combination of dipole and cavity operators. For instance in the standard frame $A = a + g/\omega_c S_x$.

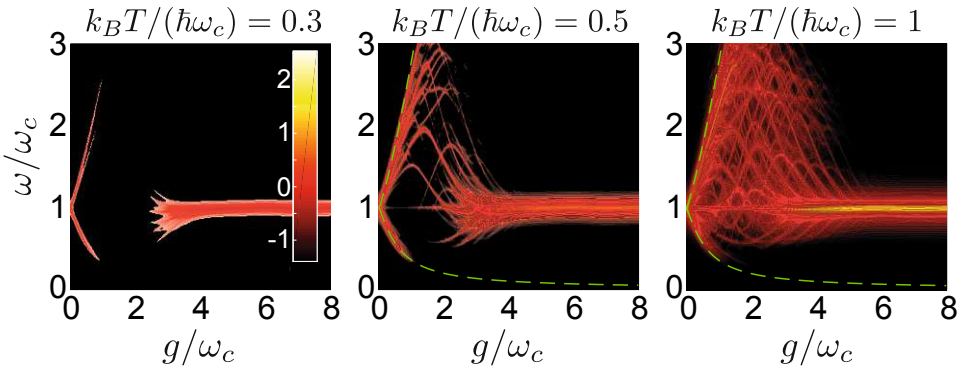

Figure 5.4: The black-body spectrum $S_{\rm bb}(\omega)/(\hbar\kappa)$ is plotted on a logarithmic scale as a function of g for three different temperatures. The green dashed lines indicate the frequencies $\omega_\pm$ of the two polariton modes obtained from a Holstein-Primakoff approximation. For all plots $N = 6$, $J = 0$ and $\gamma/\omega_c = 0.04$ have been assumed.

In Fig. 5.4 we plot the spectrum as a function of the light-matter coupling g. For very small coupling $g \ll \omega_c$ the most populated states are given by the polariton frequencies $\omega_\pm$ given in Eq. (4.22) in Ch. 4. If the temperature is large enough also other lines get populated, effectively appearing as a linewidth broadening for the two polaritons. This effect is particularly evident for large N dipoles. It is worth noticing that the two polaritons are not equal in amplitude, and, in particular, the upper polariton is brighter than the lower one. This seems to be a bit counter intuitive, but it will be clear later when we discuss in more detail the matrix elements of the voltage operator. When the system is in the USC regime, and $g \gg \omega_c$, we observe a rather sharp collapse of the two polariton branch and the spectrum is reduced to a single line at the cavity frequency $\omega = \omega_c = \omega_0$. Somehow it seems that the coupling between dipoles and photons has disappeared. This collapse is a signature of what we called light-matter decoupling, which we encountered in the discussion of the ground state properties of cavity QED in Ch. 4.8.

By integrating the spectrum over all positive frequencies we get the emitted radiation

$$P_{\rm rad} = \frac{\hbar\kappa}{\omega_c} \sum_{n>m} \frac{e^{-\beta E_n}}{Z} \omega_{nm}^2 |\langle n|A + A^\dagger|m\rangle|^2. \tag{5.76}$$

Without the dipoles we have just the free LC circuit radiation, which gives

$$P^0_{\rm rad} = \hbar\omega_c \kappa N_{\rm th}. \tag{5.77}$$

We will use this value of $P^0_{\rm rad}$ as normalisation constant, in order to highlight the coupling effects.

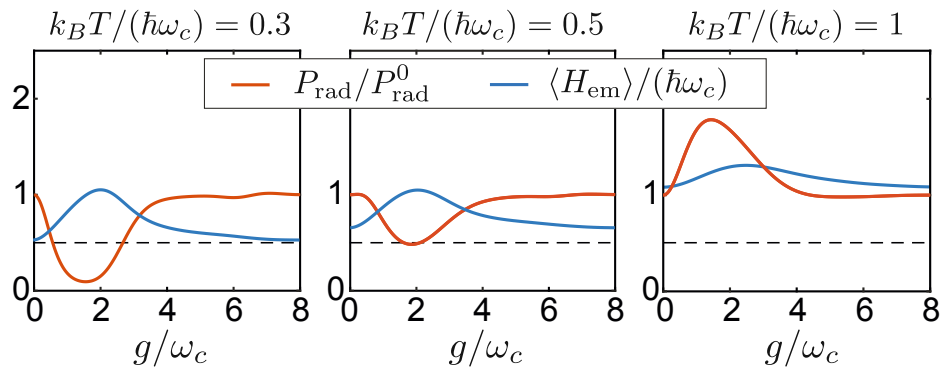

Figure 5.5: Plot of the total emitted power, $P_{\rm rad}$, and the average value of the EM energy, $\langle H_{\rm em}\rangle/(\hbar\omega_c) = \langle A^\dagger A\rangle + 1/2$, for the same parameters. Note that for better visibility we have included for this plot the offset $\hbar\omega_c/2$ (indicated by the dashed line) into the definition of $H_{\rm em}$. For all plots $N = 6$, $J = 0$ and $\gamma/\omega_c = 0.04$ have been assumed.

In Fig. 5.5 we plot the normalised radiated power as a function of the coupling strength g for a few fixed temperatures. Together with the radiated power we also plot the expectation value of the electromagnetic Hamiltonian for $J = 0$, i.e. when the electrostatic dipole-dipole interaction is zero

$$\langle H_{\rm e.m.}\big|_{J=0}\rangle = \omega_c\langle A^\dagger A\rangle. \tag{5.78}$$

This value represents the electromagnetic radiation energy stored in the LC-circuit and we would intuitively expect that it follows the behaviour of the radiated power. Quite surprisingly, for small temperatures, the electromagnetic energy seems to be anti-correlated with the radiated power, as we can see in the first two figures in Fig. 5.5.

To obtain a better understanding of this behaviour we investigate the system under the Holstein-Primakoff approximation, which is explained in App. D. The extended Dicke model is then approximated by two bosonic modes

$$H \approx \Omega_+\left(c_+^\dagger c_+ + \frac{1}{2}\right) + \Omega_-\left(c_-^\dagger c_- + \frac{1}{2}\right), \tag{5.79}$$

where the two polaritons frequencies are given by Eq. (4.22). We can then rewrite the two quadratures of the A operator in terms of this polaritons

$$A^\dagger + A = V_+\left(c_+^\dagger + c_+\right) + V_-\left(c_-^\dagger + c_-\right), \tag{5.80}$$

$$(A^\dagger - A) = \Phi_+\left(c_+^\dagger - c_+\right) + \Phi_-\left(c_-^\dagger - c_-\right), \tag{5.81}$$

where $V_\pm$ and $\Phi_\pm$ are the adimensional matrix element of the voltage/flux operators. We plot these matrix elements as a function of the collective light-matter coupling $G = \sqrt{N}g$ in Fig. 5.6(a).

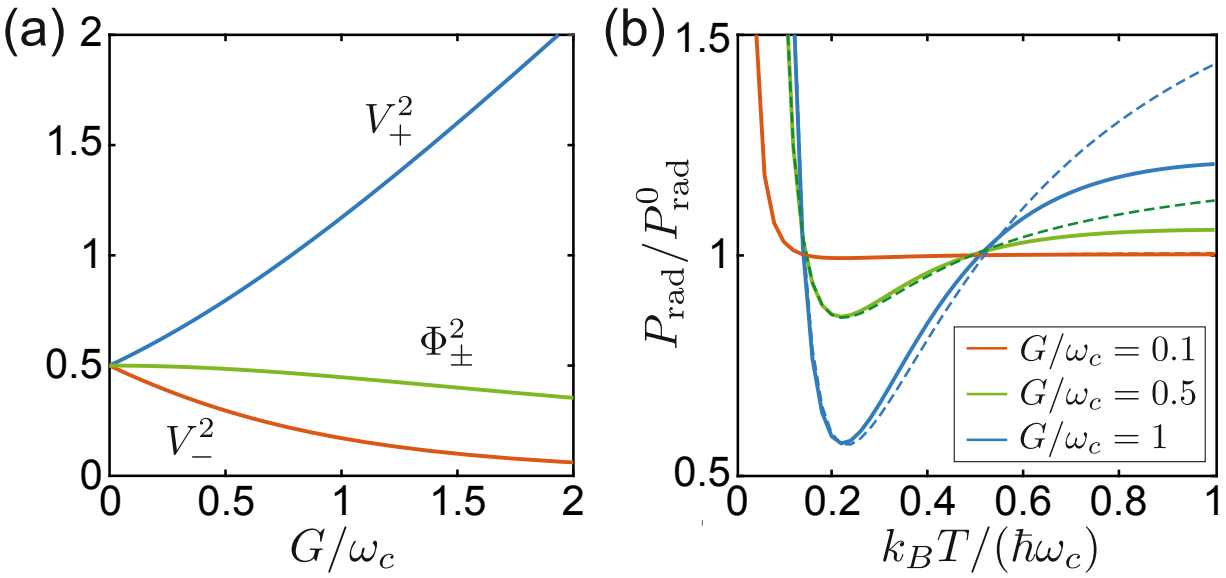

Figure 5.6: (a) The dimensionless matrix elements $V_\pm$ and $\Phi_\pm$, which determine the decomposition of the voltage and the magnetic flux operators in terms of the polariton operators $c_\pm$ [see Eqs. (5.80) and (5.81)] are plotted as a function of the collective coupling strength, G. (b) Plot of the ratio between the total power emitted from the coupled cavity QED system ($P_{\rm rad}$) and from the bare cavity ($P^0_{\rm rad}$) as a function of temperature. The solid lines are obtained from exact numerical calculations for $N = 6$ and the dashed lines show the corresponding results predicted by Eq. (5.82) based on a Holstein-Primakoff approximation.

Under the HP approximation we can also derive an approximated expression for the emitted power

$$\frac{P_{\rm rad}}{P^0_{\rm rad}} \simeq V_+^2 \left(\frac{\omega_+^2}{\omega_c^2}\right) \frac{N_{\rm th}(\omega_+)}{N_{\rm th}(\omega_c)} + V_-^2 \left(\frac{\omega_-^2}{\omega_c^2}\right) \frac{N_{\rm th}(\omega_-)}{N_{\rm th}(\omega_c)}. \tag{5.82}$$

From Fig. 5.6(a) we see that the upper polariton has a matrix element of the voltage operator which increases with G, while it is the opposite for the lower polariton. At the same time the upper polariton increases its frequency, while the lower decreases. This means that the thermal population of the upper polariton gets exponentially suppressed, while the thermal population of the lower one is non-negligibly populated even for small temperatures. Together with the fact that the Ohmic spectral density of the line filters low frequencies, we can put together these observations and explain why the power decreases when increasing coupling G (before the collapse due to USC). In Fig. 5.6(b) we see that this competition of effects gives a very non-monotonic behaviour in the emitted power.

We can also understand why the electromagnetic energy increases instead. To do so we consider the electromagnetic energy in the HP approximation

$$\frac{\langle H_{\rm em}\rangle}{\hbar\omega_c} = \frac{(V_+^2+\Phi_+^2)}{2} N_{\rm th}(\omega_+) + \frac{(V_-^2+\Phi_-^2)}{2} N_{\rm th}(\omega_-) + \left(\frac{V_+^2+\Phi_+^2+V_-^2+\Phi_-^2}{4} - \frac{1}{2}\right). \tag{5.83}$$

In the last part of this equation we see that a new vacuum energy term has appeared. This is responsible for the increasing of the electromagnetic energy, but it is not due to thermal fluctuations and so it is not really detectable in the emitted radiation.

So Eq. (5.82) correctly predicts the drop of the emitted power for intermediate coupling strengths g in Fig. 5.5 , but we see that at higher temperatures this trend may be reversed. It turns out that this effect is also present at very low temperatures, as we can see in Fig. 5.6(b). This can be intuitively understood considering that when $T \ll \omega_c$ the upper polariton's population is completely suppressed, but the population of the lower polariton instead scales like

$$N_{\rm th} \sim \frac{T}{\Omega_-}, \tag{5.84}$$

and can takes quite large values when $G/\omega_c \sim 1$, since $\Omega_- \to 0$. In this regime we also observe $P_{\rm rad}/P^0_{\rm rad} \gg 1$.

5.7 USC modifications of the ferroelectric transition

In Ch. 4 we have studied in details the ground state superradiant phase transition which is induced by the dipole-dipole interaction (which is here modelled by the generic parameter J). In particular, we have seen that strong modifications appear in the USC regime. Here we repeat this study, but including the effect of the temperature.

By using a mean-field approach, very common in the study of the LMG or Dicke model [102, 103, 104], one can derive a simple formula for the critical dipole-dipole coupling strength as a function of the critical temperature

$$\tanh\left(\frac{\hbar\omega_0}{2k_B T_c}\right) = -\frac{\omega_0}{J_c}. \tag{5.85}$$

We see that for $T \to 0$ we recover the usual ferroelectric transition in the LMG model, with $J_c = -\omega_0$. On the other side, when $\omega_0 \to 0$, the ferroelectric transition exists just below the critical temperature

$$T_c = -\frac{J}{2}. \tag{5.86}$$

In Fig. 5.7(a) we report the phase diagram of this system, where the dashed line indicates the LMG transition given by Eq. (5.85). The color scale plot instead represents

$$\bar{m} = \sqrt{\langle S_x^2 \rangle}, \tag{5.87}$$

which is the relevant order parameter in a finite system [104] . However in a system with only a few dipoles, where N is small, $\bar{m}$ is still rather smooth and it is quite difficult to identify the critical

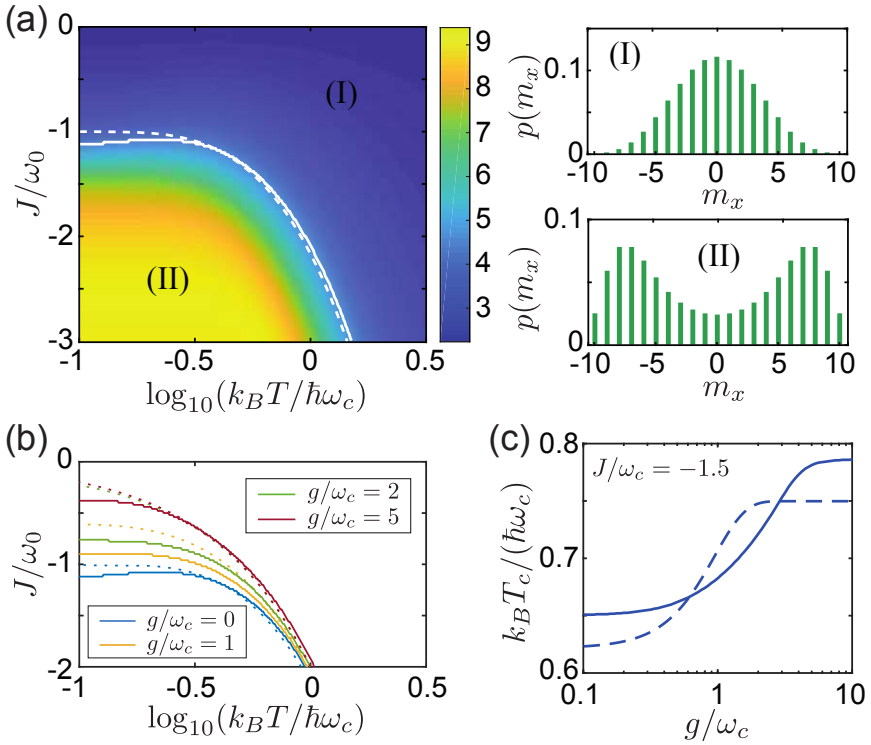

Figure 5.7: (a) Phase diagram of the LMG model without cavity, where the color scale shows the value of the parameter $\bar{m} = \sqrt{\langle S_x^2 \rangle}$ for $N = 20$ dipoles. For each point, we also evaluate the probability distribution $p(m_x)$ for the projection quantum number m_x, which exhibits a single maximum in the paraelectric phase (I) and two maxima in the ferroelectric phase (II). The transition between the single- and bi-modal distribution is indicated by the solid line, while the dotted line depicts the phase boundary obtained from mean-field theory, see Eq. (5.85), combined with the cavity-induced exponential suppression of ω_0. The same boundaries are shown in (b) for different coupling strengths g, where for the mean-field results ω_0 has been replaced by $\tilde{\omega}_0$. (c) Dependence of the critical temperature T_c on the coupling parameter g/ω_c for a fixed inter-dipole coupling strength of $J/\omega_c = -1.5$. In all plots $\omega_0 = \omega_c$ and $N = 20$.

point. An even better indicator for the phase transition in these cases is the polarization probability distribution

$$p(m_x) = \mathrm{Tr}\{\mathbb{P}_{m_x}\rho_{\mathrm{th}}\}, \tag{5.88}$$

where $\mathbb{P}_{m_x} = \sum_s \mathbb{P}_{s,m_x}$ and $\mathbb{P}_{s,m_x}$ is the projector on all states with $S_x|\psi\rangle = m_x|\psi\rangle$ and total spin s. One can define unambiguously the phase transition point when $p(m_x)$ transforms from a single peak distribution to a bi-modal distribution. An example is reported in Fig. 5.7(a), the two panels on the right. Using $p(m_x)$ we estimated numerically the phase boundary (T_c, J_c) for various values of the light-matter coupling g. This is reported in Fig. 5.7(b), where the dashed line indicates the mean-field result in Eq. (5.85), where we replaced $\omega_0 \mapsto \omega_0 \exp[-g^2/(2\omega_c^2)(1 + 2N_{\mathrm{th}})]$. This crude approximation is actually not so bad, at least qualitatively, and it follows from the intuition that we have developed in the Ch. 4, from the USC low energy theory. In Fig. 5.7(c) we plot again the transition temperature, but for a fixed J_c and continuously varying the light-matter coupling. We

thus conclude that the USC helps to stabilise the ferroelectric phase against thermal fluctuations.

In summary this chapter shows that non-perturbative modifications of the thermodynamic of a cavity QED system are possible but only in the single particle USC regime. On contrary the collective USC regime does not influence the thermodynamics at all. Despite based on a very simple toy model the conclusions drawn in this chapter are extensible also to more complicated and realistic settings. In particular we expect to have a deep impact on the debate about polaritonic chemistry and its applications.

Chapter 6

Light-matter interactions with topological photons

In this final chapter of the thesis we leave the USC regime behind and address a different aspect of light-matter interactions, namely the coupling of two-level emitters to photonic lattice systems with synthetic magnetic fields.

The system we will consider is sketched in Fig. 6.1. It consists of a two dimensional simple square lattice of coupled cavities, with a few quantum emitters coupled to it. The photon can hop from one cavity to the other and if an emitter is contained in the cavity it can be absorbed. This system can be generically described by

$$H = H_{\mathrm{ph}} + \frac{\omega_0}{2}\sum_{n=1}^{N}\sigma_z^n + g\sum_{n=1}^{N}\left[\Psi(\vec{r}_e^{\,n})\sigma_+^n + \mathrm{h.c.}\right] \tag{6.1}$$

where H_{ph} is the photon's Hamiltonian, which will be given later. In general we can say that,

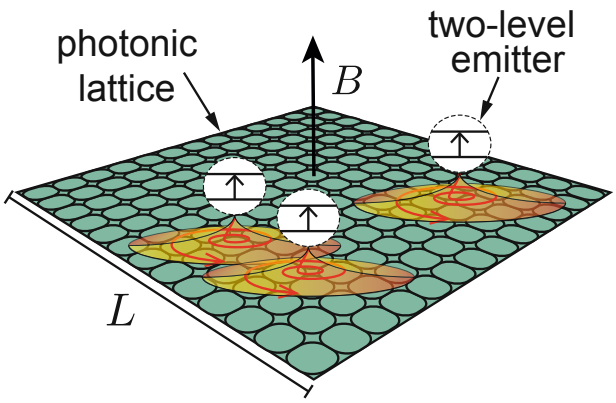

Figure 6.1: Sketch of a system of two-level emitters coupled to a photonic lattice with a synthetic magnetic field B.

defining $\Psi(\vec{r})$ as the photon's annihilation operator at the position $\vec{r}$, $H_{\rm ph}$ will be just a quadratic combination of these creation/annihilation operators. All the emitters are described as two levels atoms, with fixed resonance ω_e, the coupling to the electromagnetic field is local at the position $\vec{r}_e^{\,n}$ which is the position of the n-th two level emitter. Note that different ways to realize such systems have been discussed in the literature and later below we will give a quick outline how to realize such systems in the context of cavity QED.

In this context we want to still look at some new exotic realisation of light-matter interaction, but, instead of looking at non-trivial effects due to large coupling with just one mode, we consider small coupling but many modes. And it is properly tailoring the system in the correct way that we can explore new non-perturbative light-matter phenomena. Here we focus on a two dimensional photonic lattice where the photon feels a synthetic magnetic field perpendicular to the lattice, as represented in Fig. 6.1 and we explore the atom/photon interactions in this exotic scenario.

The results contained in this chapter are published in Physical Review Letters 126, 103603 (2021). This project was done together with Ze-Pei Chan, Iacopo Carusotto, Mohammad Hafezi and Peter Rabl, and I was the leading author. All the results in this publication have been derived by me under the supervision of Peter Rabl.

6.1 Synthetic magnetic fields for photons

We describe here the details of this two dimensional lattice for photons and the implementation of the synthetic magnetic field. Considering just a single mode per lattice site, we realise a tight binding model for confined photons, with frequency ω_p and a tunneling amplitude J_{ij} between neigbouring sites i and j. The Hamiltonian reads [25]

$$H_{\rm ph} = \omega_p \sum_{i=1}^{M} \Psi_i^\dagger \Psi_i - \sum_{ij} \left(J_{ij} \Psi_i^\dagger \Psi_j + \text{h.c.} \right), \tag{6.2}$$

where we use Ψ_i to indicate the annihilation operator of a confined photon in the i-th cavity.

If the system is engineered to break time reversal symmetry the hopping matrix is complex, so we can write it generically in terms of amplitude and phase

$$J_{ij} = |J_{ij}| e^{i\phi_{ij}}. \tag{6.3}$$

With an accurate construction of our system these phases can be chosen as

$$\phi_{ij} = \frac{e}{\hbar} \int_{\vec{r}_j}^{\vec{r}_i} \vec{A}(\vec{r}) \cdot d\vec{r}, \tag{6.4}$$

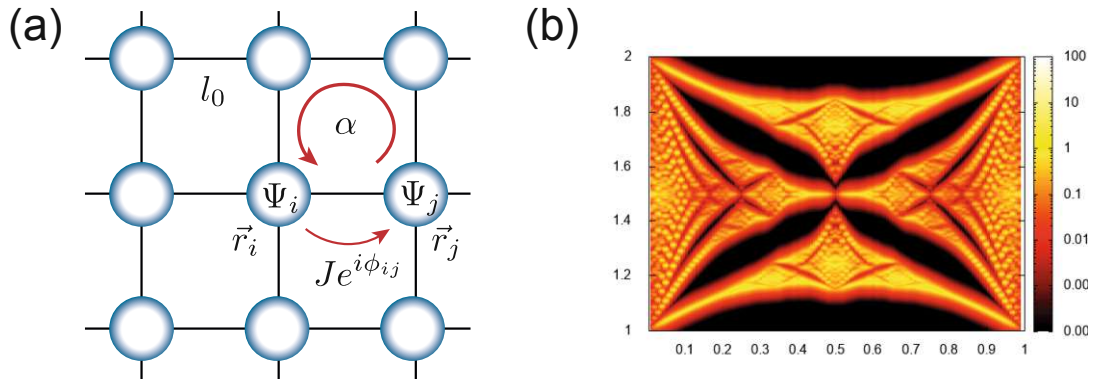

Figure 6.2: (a) Sketch of the photonic lattice with synthetic magnetic field. The magnetic field is implemented by adjusting the hopping phases ϕ_{ij} between neighbouring lattice sites such that around each plaquette $\sum_{\square} \phi_{ij} = 2\pi\alpha$. (b) Spectrum of the magnetic photonic lattice in function of its magnetic flux α. The color scale shows the projected density of states, $\rho(\vec{r}_i, \omega)$ for a lattice of $M = 20 \times 20$ sites. For this plot, $\vec{r}_i = (10, 10)$ and each resonance is represented by a broadened δ-function with a finite width of $\gamma/J \approx 10^{-3}$.

where we introduced a fictitious charge e and the two lattice positions $\vec{r}_i$, $\vec{r}_j$ are adimensional. In this way we may associate to our phase a synthetic, magnetic field

$$\vec{B}(\vec{r}) = \vec{\nabla} \times \vec{A}(\vec{r}). \tag{6.5}$$

The origin of this identification comes from the physics of electrons in lattices when the system is embedded in a magnetic field. Such systems are usually described by a tight binding Hamiltonian, in which each electron can hop between different sites. In the presence of a magnetic field, one must correct the hopping rate with the complex phase in Eq. (6.4), which is the so called "Peirls substitution" [105]. So by analogy, we say that a photon following the same hopping dynamics is coupled to a magnetic field.

In the following we specialise on the case of a simple square lattice in two dimensions with nearest neighbour hopping. The hopping matrix is

$$J_{ij} = J\delta_{\langle ij \rangle} e^{i\phi_{ij}}, \tag{6.6}$$

where $\langle \cdot \rangle$ indicates nearest neighbour sites. This system is pictorially represented in Fig. 6.2(a). The photon's Hamiltonian can in general be rewritten as

$$H_{\text{ph}} = \sum_{\lambda} \omega_\lambda \Psi_\lambda^\dagger \Psi_\lambda, \qquad [\Psi_\lambda, \Psi_{\lambda'}^\dagger] = \delta_{\lambda\lambda'}, \tag{6.7}$$

where $\Psi_\lambda = \sum_i f^*_\lambda(\vec{r}_i)\Psi_i$ and the $f_\lambda(\vec{r}_i)$ are the eigenmodes, which obey

$$(\omega_\lambda - \omega_p) f_\lambda(\vec{r}_i) = -J\left[e^{-i\phi_x} f_\lambda(\vec{r}_i + \vec{e}_x) + e^{i\phi_x} f_\lambda(\vec{r}_i - \vec{e}_x) + e^{-i\phi_y} f_\lambda(\vec{r}_i + \vec{e}_y) + e^{i\phi_y} f_\lambda(\vec{r}_i - \vec{e}_y)\right]. \tag{6.8}$$

For a short-hand notation we introduce the unit vectors $\vec{e}_{x,y}$ pointing in x or y directions and

$$\Phi_{x,y} = \frac{e}{\hbar}\int_{\vec{r}_i}^{\vec{r}_i+\vec{e}_{x,y}} \vec{A}(\vec{r})\cdot d\vec{r} \simeq \frac{e}{\hbar}\vec{A}(\vec{r}_i)\cdot\vec{e}_{x,y}. \tag{6.9}$$

The continuum limit is taken by approximating

$$f_\lambda(\vec{r}_i + \vec{e}_x) \simeq f_\lambda(\vec{r}_i) + l_0\frac{\partial}{\partial x} f_\lambda(\vec{r}_i) + \frac{l_0^2}{2}\frac{\partial^2}{\partial x^2} f_\lambda(\vec{r}_i), \tag{6.10}$$

where we introduced the lattice spacing l_0. Up to second order in l_0 we have

$$-J\left[e^{-i\phi_x} f(\vec{r}_i + \vec{e}_x) + e^{i\phi_x} f_\lambda(\vec{r}_i - \vec{e}_x)\right] \simeq -2J f_\lambda(\vec{r}_i) - Jl_0^2\left[\frac{\partial}{\partial x} - i\frac{e}{\hbar}A_x(\vec{r}_i)\right]^2 f_\lambda(\vec{r}_i) + O(l_0^3), \tag{6.11}$$

leading to the differential equation

$$\hbar(\omega_\lambda - \omega_b) f_\lambda(\vec{r}) = \frac{1}{2m}\left[-i\hbar\vec{\nabla} - e\vec{A}(\vec{r})\right]^2 f_\lambda(\vec{r}), \tag{6.12}$$

where $\omega_b = \omega_p - 4J$ and $m = \hbar/(2Jl_0^2)$ is the effective mass in the lattice. At this point the discrete field operators are approximated as a continuous quantum field

$$\Psi_i \longmapsto \Psi(\vec{r}) = \sum_\lambda f_\lambda(\vec{r})\Psi_\lambda. \tag{6.13}$$

The photon Hamiltonian in the continuum limit becomes

$$H_{\text{ph}} \simeq \int \Psi^\dagger(\vec{r})\frac{1}{2m}\left[-i\hbar\vec{\nabla} - e\vec{A}(\vec{r})\right]^2 \Psi(\vec{r}) d^2r, \tag{6.14}$$

which is exactly the second quantized form of a bosonic field in a magnetic field.

6.2 The Hofstadter butterfly and the Landau-photon

In our work we consider the simplest case of a homogeneous magnetic field perpendicular to the lattice plane

$$\vec{B}(\vec{r}) = B\vec{e}_z, \tag{6.15}$$

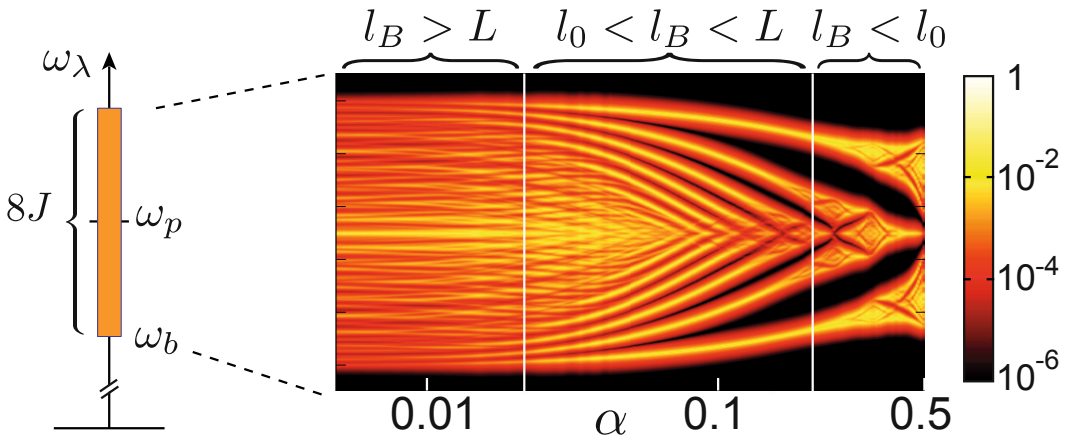

Figure 6.3: The projected density of states, $\rho(\vec{r}_e, \omega)$, is plotted on a logarithmic scale (arbitrary units) as a function of α and for a lattice of $M = 20 \times 20$ sites. For this plot, $\vec{r}_e/l_0 = (10, 10)$ and each resonance is represented by a broadened δ-function with a finite width of $\gamma/J \approx 10^{-3}$.

where B is a constant and $\vec{e}_z$ is a unit vector perpendicular to the (x, y) plane. Using the so-called *symmetric gauge*, the associated vector potential is given by

$$\vec{A}(\vec{r}) = \frac{B}{2}(-y, x, 0). \tag{6.16}$$

When we use this vector potential to generate the magnetic phase in our hopping model (6.2), we obtain the Hofstadter-Harper model [106]. The magnetic phase can be rewritten as

$$\phi_{ij} = 2\pi\alpha \left[-\frac{y_i}{2}(x_j - x_i) + \frac{x_i}{2}(y_j - y_i) \right], \tag{6.17}$$

where we remind that the lattice's positions $\vec{r}_i$ are given in units of the lattice constant l_0. The parameter $\alpha = eBl_0^2/(2\pi\hbar)$ represents the magnetic flux enclosed in a single plaquette, as illustrated in Fig. 6.2(a). Solving the eigenvalue equation, generically given by (6.8), we obtain the spectrum of the system. A good way to visualise this spectrum is to introduce the *local density of states*

$$\rho(\vec{r}_i, \omega) = \sum_\lambda |f_\lambda(\vec{r}_i)|^2 \delta(\omega - \omega_\lambda). \tag{6.18}$$

The plot of $\rho(\vec{r}_i, \omega)$ as a function of α, for a fixed lattice position far away from the borders, represents the famous *Hofstadter butterfly* [106], which is shown in Fig. 6.2(b). The Hofstadter butterfly is a spectrum enclosed in the finite bandwidth given by $\Delta_{\text{HB}} \sim 8J$, and symmetrically centred around ω_p. Increasing the magnetic field, controlled by α, the spectrum collapses into a set of narrow bands, well separated by spectral gaps. With further increasing α, new patterns with a self-replicating fractal structure appear.

In the last section we have shown that this system supports a continuous limit, which might be

quite convenient to extract some analytical properties. To see when this continuum limit can be applied we must compare the two intrinsic length scales in the system, the lattice spacing l_0 and the magnetic length l_B, as well as the size of the system, L, in case it is finite. For the expansion in Eq. (6.10) we require that the functions f_λ don't vary too much over the lengthscale given by l_0. In this way we can neglect higher order derivatives. The same must be applied to the magnetic phase, requiring that it does not vary too much in the same interval. The scale of spatial variation of the magnetic potential is exactly given by l_B, and the phase scales consistently as $e\vec{A}\cdot d\vec{r} \sim l_0^2/l_B^2$. Since it gets smoother with larger magnetic length, the correct limit in which we need to stay is $l_B \gg l_0$. When the system has finite size we realise that the vector potential is bounded by $|e\vec{A}| < \hbar L/l_B^2$. Assuming we are in the correct continuous limit, i.e. $l_B > l_0$ still holds, we need to compare it with the smallest momentum scale in the system, which is given by $|\vec{p}| \sim \hbar/L$. In order to have effects beyond the perturbative regime we require

$$\frac{|e\vec{A}|}{|\vec{p}|} \gg 1, \tag{6.19}$$

which implies $l_B \ll L$. This can be interpreted semiclassically as the condition that the system must be large enough to contain at least one quanta of cyclotron orbit. So we can finally say that the regime of applicability of the continuous limit is given by

$$l_0 < l_B < L. \tag{6.20}$$

Since $l_B = l_0/\sqrt{2\pi\alpha}$, we can translate this condition on the magnetic length into a condition on the magnetic flux α

$$\frac{1}{2\pi M} < \alpha < \frac{1}{2\pi}, \tag{6.21}$$

where M is the total number of lattice sites. The continuous limit is then valid in an *intermediate regime* of magnetic flux.

We can actually visualise these three regimes by an inspection of the Hofstadter butterfly in a logarithmic scale, as shown in Fig. 6.3. The intermediate regime extends up to values of about $\alpha \simeq 1/6$, but with some quantitative disagreements, one can show numerically that it can be stretched till $\alpha \simeq 1/4$, which is the value of the magnetic flux realized in a recent experiment [107].

Using the expression in Eq. (6.16) and plugging it into Eq. (6.12), we recognise the Schrödinger equation for a charged particle in two dimensions in an homogeneous magnetic field. This equation was first solved in [108], its eigenfrequencies are equispaced and given by $\omega_\ell = \omega_b + \omega_c(\ell + 1/2)$, with $\ell = 0, 1, 2 \ldots$. Here

$$\omega_c = \frac{eB}{m} = 4\pi\alpha J \tag{6.22}$$

is the *cyclotron frequency*. It turns out that each energy level is infinitely degenerate, and each degenerate state is labelled by another quantum number k. The eigenfunctions are given by

$$f_{\ell k}(\vec{r}) = \frac{l_0}{\sqrt{2\pi l_B^2}} \sqrt{\frac{\ell!}{k!}} \xi^{k-\ell} e^{-\frac{|\xi|^2}{2}} L_\ell^{k-\ell}(|\xi|^2), \tag{6.23}$$

where

$$l_B = \hbar/\sqrt{eB} \tag{6.24}$$

is the magnetic length, $L_n^\alpha(x)$ is the generalised Laguerre polynomial, and $\xi = (x+iy)/\sqrt{2l_B^2}$. They form an orthogonal basis in the continuum, so we obtain

$$\int d^2r f^*_{\ell' k'}(\vec{r}) f_{\ell k}(\vec{r}) = l_0^2 \delta_{\ell\ell'} \delta_{kk'}. \tag{6.25}$$

Notice that in a finite system each level cannot be consider infinitely degenerate, but we can estimate the degeneracy of the lowest level as

$$k_{max} \sim \alpha M, \tag{6.26}$$

where M is the total number of lattice sites. For later convenience we give a special name to the wave function having $k = \ell$ and we define

$$\Phi_\ell(\vec{r}) = f_{\ell\ell}(\vec{r}). \tag{6.27}$$

These states are circularly symmetric, composed out of a Gaussian envelope and a radial Laguerre polynomial, which results in concentric circles separated by a node, around a central bump at a radial distance $\sim \sqrt{2\ell+1} \times l_B$. Page [108] first used these wavefunctions to create an analogy between the classical cyclotron trajectories and the quantized problem. This is why we can also refer to l_B as the quantum cyclotron radius.

The equation (6.12) can be solved equivalently in the so-called *Landau gauge* $\vec{A}(\vec{r}) = B(0, x, 0)$, giving the same results, but having all the degenerate wave functions in each level expressed in a different basis [109] (with Hermite polynomials, instead of Laguerre). Even though Page and Landau solved this problem at the same time, the degenerate energy levels are known in the literature only as *Landau levels*, so we just stick to this convention.

Since the continuous approximation is only exact in the limit $\alpha \to 0$, it is worth to have a look at higher order corrections due to the discreteness of the lattice. Indeed in the continuous approximation the energy levels are just equispaced, with the spacing given by the cyclotron frequency ω_c, but, by looking at the Hofstadter butterfly 6.2(b), it is clear that this is not exactly the case in the lattice, even for quite small α. Since the resulting corrections are gauge independent, to proceed

with the calculation it is more convenient to work in the Landau gauge. In this case the eigenvalues equation (6.8) takes a quite compact shape and is called *the Harper equation* [110]

$$-J[\chi_\lambda(x_j+1)+\chi_\lambda(x_j-1)]-2J\cos(2\pi\alpha j-k_y)\,\chi_\lambda(x_j)=(\omega_\ell-\omega_p)\chi_\lambda(x_j). \tag{6.28}$$

Here k_y labels the momentum in the y-direction, which is a good quantum number in the Landau gauge, and $f_\lambda(\vec{r}_j)=\chi(x_j)e^{ik_y y_j}$. Without loss of generality we can set $k_y=0$. Following the derivation of the continuous limit above, we can repeat the same expansion, but this time we keep terms up to fourth order in l_0 (restoring the correct units of length, i.e. $\vec{r}_i\to\vec{r}_i/l_0$)

$$-J[\chi_\lambda(x+l_0)+\chi_\lambda(x-l_0)]\simeq-2J\chi_\lambda(x)-Jl_0^2\frac{\partial^2}{\partial x^2}\chi_\lambda(x)-\frac{Jl_0^4}{12}\frac{\partial^4}{\partial x^4}\chi_\lambda(x), \tag{6.29}$$

and

$$-2J\cos(2\pi\alpha j)\,\chi_\lambda(x)\simeq\left[-2J+J\frac{l_0^2}{l_B^4}x^2-J\frac{l_0^4}{12l_B^8}x^4\right]\chi_\lambda(x). \tag{6.30}$$

We obtain again our Schrödinger equation for a charged particle in a magnetic field in the Landau gauge, including the corrections $O(l_0^4)$ due to the discrete nature of the lattice

$$\hbar(\omega_\ell-\omega_p-4J)\chi_\lambda(x)=\left[-\frac{\hbar^2}{2m}\frac{\partial^2}{\partial x^2}+\frac{1}{2}m\omega_c^2x^2\right]\chi_\lambda(x)-\frac{1}{48\hbar J}\left[\frac{\hbar^4}{m^2}\frac{\partial^4}{\partial x^4}+m^2\omega_c^4x^4\right]\chi_\lambda(x). \tag{6.31}$$

The first term in parenthesis on the right hand side is just the Hamiltonian of an harmonic oscillator, which gives a spectrum $\omega_\ell=\omega_c(\ell+1/2)$, as expected for Landau levels. The second term can be instead included by using first order perturbation theory, which amounts to calculating the expectation values of $\langle\ell|p^4|\ell\rangle$ and $\langle\ell|x^4|\ell\rangle$, where $|\ell\rangle$ is the ℓ-th harmonic oscillator eigenstate and p and x are momentum and position operators. Since these expectation values are well known from any standard textbook of quantum mechanics, we can finally write the corrected energies as

$$\omega_\ell\simeq\omega_b+\omega_c\left(\ell+\frac{1}{2}\right)-\frac{\omega_c^2}{32J}(2\ell^2+2\ell+1). \tag{6.32}$$

For instance, the gap between the zeroth and the first Landau level is now given by

$$\omega_1-\omega_0\approx4\pi\alpha J\left(1-\frac{\pi}{2}\alpha\right). \tag{6.33}$$

For a value of $\alpha=0.08$, which we will assume in many of the following examples, we obtain

$$\frac{\omega_1-\omega_0}{J}\approx0.874. \tag{6.34}$$

This value is off from the continuous approximation by about 13%.

6.3 Photon propagator and Landau Green's function

As already anticipated in the introduction of the chapter, after having introduced the properties of a photonic lattice with an homogeneous synthetic field, our task will be to study the light-matter dynamics when the photons follows this unusual dynamics imposed by the magnetic force. We have already anticipated that the light-matter coupling in this system is generally weak, so we will just consider a linear interaction between photons and atoms, subjected to the rotating wave approximation. Under such conditions the central quantity that gives all the information about the photons is the two point correlator, also called the photon propagator [111]

$$G(t,\vec{r}_i,\vec{r}_j) = \langle \mathrm{vac}|\Psi_i(t)\Psi_j(0)^\dagger|\mathrm{vac}\rangle\,. \tag{6.35}$$

Decomposing the field operator using the mode functions of the hopping matrix, the photon's propagator is given by

$$G(t,\vec{r}_i,\vec{r}_j) = \sum_\lambda f_\lambda(\vec{r}_i) f^*_\lambda(\vec{r}_j) e^{-i\omega_\lambda t}. \tag{6.36}$$

In the continuum limit it represents the Green's function of the time dependent Schrödinger equation, since

$$i\hbar\partial_t G(t,\vec{r},\vec{r}^{\,'}) = \frac{1}{2m}\left[-i\hbar\vec{\nabla} - e\vec{A}(\vec{r})\right]^2 G(t,\vec{r},\vec{r}^{\,'}), \tag{6.37}$$

with initial condition

$$G(t=0,\vec{r},\vec{r}^{\,'}) = \delta^{(3)}(\vec{r}-\vec{r}^{\,'}). \tag{6.38}$$

In general deriving a closed expression for this Green's function is not possible, but in the specific case of the homogeneous magnetic field discussed above, and in particular employing the continuum limit, we do have an analytical result. To derive it we start by approximating the mode functions by Landau orbitals

$$G(t,\vec{r}_i,\vec{r}_j) \simeq \sum_{\ell k} f_{\ell k}(\vec{r}_i) f^*_{\ell k}(\vec{r}_j) e^{-i\omega_\ell t}, \tag{6.39}$$

and make use of the fact that, thanks to the exact degeneracy of the continuum approximation, the time dependent exponential depends only on the principal quantum number ℓ. So we can sum over the degenerate index k. To do so, we notice that each of these wave functions can be expressed as a matrix element between Fock states of the displacement operator

$$f_{\ell k}(\vec{r}_i) = \sqrt{\alpha}\,\langle k|\mathcal{D}(\xi_i)|\ell\rangle\,, \tag{6.40}$$

where $\xi = (x_i + iy_i)/\sqrt{2l_B^2}$, and $\mathcal{D}(\xi) = e^{\xi a^\dagger - \xi^* a}$ with a the annihilation operator for a fictitious

harmonic oscillator. Using the property $\mathcal{D}^\dagger(\xi)\mathcal{D}(\beta) = \mathcal{D}(\beta-\xi)e^{-\frac{1}{2}(\xi\beta^*-\xi^*\beta)}$, we have

$$\begin{aligned}\sum_k f_{\ell k}(\vec{r}_i) f^*_{\ell k}(\vec{r}_j) &= \alpha \sum_k \langle \ell|\mathcal{D}^\dagger(\xi_j)|k\rangle \langle k|\mathcal{D}(\xi_i)|\ell\rangle \\ &= \alpha \langle \ell|\mathcal{D}^\dagger(\xi_j)\mathcal{D}(\xi_i)|\ell\rangle = \alpha e^{\frac{1}{2}(\xi_i\xi_j^*-\xi_i^*\xi_j)} \langle \ell|\mathcal{D}(\xi_i-\xi_j)|\ell\rangle\,, \\ &= \sqrt{\alpha} e^{i\theta_{ij}} \Phi_\ell(\vec{r}_i - \vec{r}_j),\end{aligned} \tag{6.41}$$

where

$$\theta_{ij} = -\frac{i}{2}(\xi_i\xi_j^* - \xi_i^*\xi_j) = -\frac{1}{2l_B^2}(x_i y_j - x_j y_i). \tag{6.42}$$

From the first to the second line we have used a completeness relation $\mathbf{1} \simeq \sum_k |k\rangle\langle k|$, which in principle holds if the approximated degeneracy is large enough, i.e. $k_{max} \sim M\alpha \gg 1$, which is equivalent to the condition about finite size derived above, $L \gg l_B$.

In summary the approximated photon Green's function in the continuum limit is given by

$$G(t, \vec{r}_i, \vec{r}_j) \simeq \sqrt{\alpha} e^{i\theta_{ij}} \sum_{\ell=0} \Phi_\ell(\vec{r}_i - \vec{r}_j) e^{-i\omega_\ell t}. \tag{6.43}$$

This is a very remarkable result, since now it allows us to express everything within this system in terms of a rather simple analytic function.

Before we start to use this machinery to discuss actual physical predictions, we want to discuss two interesting aspects of this Green's function, which will be useful in the next sections.

We first notice that the Schrödinger equation for the Landau Green's function possesses what is know as a *gauge symmetry*. This is not very surprising since we know that a basics property of electromagnetism expressed in terms of potentials is that it is defined only up to a gauge transformation. Indeed by replacing $\vec{A}(\vec{r}) \longmapsto \vec{A}(\vec{r}) - \vec{\nabla}\Lambda(\vec{r})$, with $\Lambda(\vec{r})$ an arbitrary function, the resulting physical predictions do not change. In order to preserve Eq. (6.37), this means that the Green's function changes accordingly to

$$G(t, \vec{r}_i, \vec{r}_j) \longmapsto e^{ie(\Lambda(\vec{r}_i)-\Lambda(\vec{r}_j))/\hbar} G(t, \vec{r}_i, \vec{r}_j). \tag{6.44}$$

But this means that the Green's function splits into a gauge dependent phase and a gauge independent part (which may be still complex)

$$G(t, \vec{r}_i, \vec{r}_j) = e^{i\theta_{ij}^{\text{gauge}}} G^{\text{inv.}}(t, \vec{r}_i, \vec{r}_j). \tag{6.45}$$

Notice that this applies as well to the discrete case, in exactly the same way. In the continuum

approximation we find that the gauge invariant part is given by

$$G^{\text{inv.}}(t,\vec{r}_i,\vec{r}_j)=\sqrt{\alpha}\sum_{\ell=0}\Phi_\ell(|\vec{r}_i-\vec{r}_j|)e^{-i\omega_\ell t}, \tag{6.46}$$

while the phase θ_{ij} needs an explicit gauge fixing to be determined. It is interesting that Eq. (6.45) is true in general even for the discrete case.

The second important property that we want to show here is that the Green's function can be used a projector on a specific Landau level. In particular, let us consider the expression in Eq. (6.43), which is explicitly decomposed into a sum over its harmonics, and each harmonic is a Landau level. Isolating one harmonic in that sum, for a particular ℓ, we have a real-space projector into that specific ℓ-th Landau level

$$G_\ell(\vec{r}_i,\vec{r}_j)=\sqrt{\alpha}/l_0^2 e^{i\theta_{ij}^{\text{gauge}}}\Phi_\ell(|\vec{r}_i-\vec{r}_j|)=\frac{1}{l_0^2}\sum_k f_{\ell k}(\vec{r}_i)f^*_{\ell k}(\vec{r}_j)=\langle r_i|\hat{\mathcal{P}}_\ell|r_j\rangle, \tag{6.47}$$

where $\hat{\mathcal{P}}_\ell$ is the projection operator in the abstract Hilbert space and the last equality just follows from the fact that the mode functions form an orthonormal set. This observation can be quite useful to define new creation/annihilation operators that creates/destroys a photon in a given Landau level. But one has to be careful that the merely projected operator $\tilde{\Psi}_\ell(\vec{r}_i)=\sum_j G_\ell(\vec{r}_i,\vec{r}_j)\Psi(\vec{r}_j)$ does not fulfill the correct commutation relation. However we will see that, once we introduce the emitter's degrees of freedom, the Landau projector will be a quite useful tool.

6.4 Single photon emission and resonant dynamics

In this section we present the simplest observations of light-matter dynamics mediated by magnetic photons. We also highlight the striking difference to the case without magnetic field. We start by restricting our investigation to the class of states that contain only a single excitation

$$|\psi\rangle(t)=\left[\sum_{n=1}^{N}c_n(t)\sigma_+^n+\sum_\lambda\varphi_\lambda(t)\Psi_\lambda^\dagger\right]|g\rangle|\text{vac}\rangle. \tag{6.48}$$

The excitation number operator is defined by

$$N_{\text{exc}}=\sum_\lambda\Psi_\lambda^\dagger\Psi_\lambda+\frac{1}{2}\sum_{n=1}^{N}(\sigma_z+\mathbf{1}), \tag{6.49}$$

and one can immediately verify that $\langle\psi|N_{\text{exc}}|\psi\rangle(t)=1,\forall\, t$. Moreover, the light-matter Hamiltonian in Eq. (6.1) has the property

$$[N_{\text{exc}},H]=0, \tag{6.50}$$

which makes the excitation number a good quantum number.

Considering the Schrödinger equation

$$i\partial_t|\psi\rangle(t) = H|\psi\rangle(t), \tag{6.51}$$

and then projecting the two orthogonal components, we obtain the equations of motion for the emitter's and photon's amplitudes

$$\begin{aligned} i\dot{c}_n &= (\omega_e - i\gamma_e/2)\, c_n + g\sum_\lambda f_\lambda(\vec{r}_e^{\,n})\varphi_\lambda, \\ i\dot{\varphi}_\lambda &= (\omega_\lambda - i\gamma_p/2)\varphi_\lambda + g\sum_m f_\lambda^*(\vec{r}_e^{\,m})c_m, \end{aligned} \tag{6.52}$$

where we recall that $\vec{r}_e^{\,n}$ is the position of the n-th emitter, $f_\lambda(\vec{r}_e^{\,n})$ is the lattice's mode function calculated at the emitter's position. Note that here we have also included the decay of the emitter and the photon with rates γ_e and γ_p, respectively, to model a realistic open system dynamics. We can now integrate the equation for the photon's amplitude and obtain

$$\varphi_\lambda(t) = -ig\sum_m f_\lambda^*(\vec{r}_e^{\,m})\int_0^t e^{-i(\omega_\lambda - i\gamma_p/2)(t-t')}c_m(t')dt'. \tag{6.53}$$

Plugging this expression into the equation for the emitter amplitudes c_n we end up with a closed integral-differential equation

$$\dot{c}_n(t) = -i(\omega_e - i\gamma_e/2)c_n - g^2\sum_m\int_0^t G(t-t', \vec{r}_e^{\,n}, \vec{r}_e^{\,m})e^{-\gamma_p(t-t')/2}c_m(t')dt', \tag{6.54}$$

where the photon's contribution is given by the convolution in time between the emitter's amplitude and the photon's Green's function. This result is completely general and shows that the light-matter interaction dynamics is completely determined by the photonic Green's function.

In the following we briefly review the standard case of spontaneous emission in a two dimensional non-magnetic lattice using the formula derived just above. The single emitter equation is

$$\dot{c}_e(t) = -g^2\int_0^t G(t-t')e^{\bar{\gamma}(t-t')/2}c_e(t')dt', \tag{6.55}$$

where we have made the transformation $c_e(t) \mapsto c_e(t)e^{-i(\omega_e - i\gamma_e/2)t}$, $\bar{\gamma} = \gamma_e - \gamma_p$, and where $G(t-t') = G(t-t', \vec{r}_e, \vec{r}_e)$. The integral kernel, given by the Green's function, can be expressed in terms of the photonic density of states

$$G(t) = \int_{-\infty}^{+\infty}\rho(\vec{r}_e, \omega)e^{-i(\omega-\omega_e)t}d\omega, \tag{6.56}$$

with $\rho(\vec{r}_e, \omega) = \sum_\lambda |f_\lambda(\vec{r}_e)|^2\delta(\omega - \omega_\lambda)$, as defined previously. When the system is large enough, we

can consider this density of states as a continuous function in ω, and, considering a weak enough light-matter coupling, and having the emitter's resonance far away from eventual singularities, we can approximate it as constant

$$\rho(\vec{r}_e, \omega) \simeq \rho(\vec{r}_e, \omega_e) = \tau/(2\pi). \tag{6.57}$$

The integral kernel becomes $G(t-t') \simeq \tau\delta(t-t')$, reducing the single emitter's dynamics to

$$\dot{c}_e(t) = -\frac{g^2\tau}{2} c_e(t), \tag{6.58}$$

which describes an exponentially decaying emitter's population, with decay rate $\Gamma = g^2\tau$. In particular, focusing on a two dimensional lattice, with plane waves eigenmodes, $f_\lambda \sim e^{i\vec{k}\cdot\vec{r}}$, and particle-like quadratic dispersion $\omega_k \simeq \omega_b + J|\vec{k}|^2$, we have $\tau \simeq 1/(2J)$ and the decay rate takes the explicit value of

$$\Gamma \simeq \frac{g^2}{2J}. \tag{6.59}$$

Notice that the decay process itself does not depend on the details of the photon's dynamics, nor whether we consider a lattice or a continuum. The only thing that matters here is the assumption that we have a smooth density of states which does not vary too much around the energy scales of the emitter.

We now focus our attention on the case in which we do have a synthetic magnetic field in the two dimensional lattice, as described in Sec. 6.2. The main difference in treating Eq. (6.55) is that the density of states is not smooth at all. Indeed, if we consider the intermediate flux regime we have

$$\rho(\vec{r}_e, \omega) \simeq \alpha \sum_{\ell=0} \delta(\omega_\ell - \omega), \tag{6.60}$$

and the integral kernel cannot be approximated by a delta function in time $G(t) \neq \delta(t)$. But we can make another approximation. We still assume that the coupling is very small, more precisely that the light-matter coupling is much smaller than the separation between the Landau levels

$$g \ll |\omega_\ell - \omega_{\ell\pm1}|. \tag{6.61}$$

In addition we now assume that the emitter is in resonance with the ℓ-th Landau level

$$|\omega_e - \omega_\ell| \ll g. \tag{6.62}$$

Under these conditions we can isolate a single Landau level out of the discrete density of states and

obtain

$$\dot{c}_e(t) \simeq -\frac{\bar{\gamma}}{2} c_e - \alpha g^2 \int_0^t c_e(t')dt', \tag{6.63}$$

where $\bar{\gamma} = \gamma_e - \gamma_p$ is the difference between the loss rates. Taking another time derivative we arrive at the equation of a damped harmonic oscillator

$$\ddot{c}_e(t) \simeq -\frac{\bar{\gamma}}{2} \dot{c}_e - \alpha g^2 c_e, \tag{6.64}$$

with frequency

$$\Omega = \sqrt{\alpha} g. \tag{6.65}$$

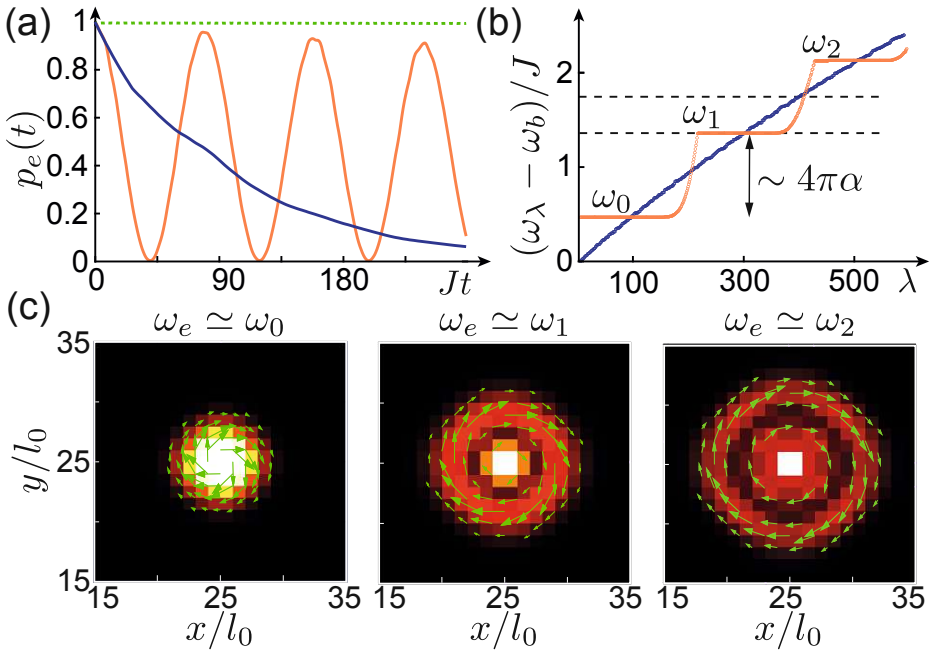

Figure 6.4: (a) Evolution of the excited-state population, $p_e(t)$, of an emitter located at $\vec{r}_e/l_0 = (25, 25)$ in a lattice of 50×50 sites. The parameters are $\alpha = 0$ and $\delta_e/J = 1.35$ (blue line), $\alpha = 0.08$ and $\delta_e/J = 1.35$ (orange line), and $\alpha = 0.08$ and $\delta_e/J = 1.76$ (green dashed line). (b) Plot of the lowest eigenfrequencies ω_λ of the two photonic lattices as used for the simulation shown in blue and orange in (a). The dashed black lines indicate the corresponding emitter's frequencies. (c) Photon density, $|\varphi(\vec{r}_i, t_\pi)|^2$, combined with the profile of the photon current, $\langle \vec{j}_p \rangle(\vec{r}_i, t_\pi)$, after half a Rabi-cycle, $t_\pi = \pi/(2\Omega)$, for $\alpha = 0.08$ and $\omega_e = \omega_{\ell=0,1,2}$. For all plots $g/J = 0.14$ and for each lattice site in the bulk (on the edge) a photon decay rate of $\gamma_p/J = 4 \times 10^{-4}$ ($\gamma_{\text{edge}}/J \sim 10^{-1}$) has been introduced.

In Fig. 6.4(a) we show a simple numerical experiment that reproduces both the results with and without magnetic field in a two dimensional square lattice

$$\begin{aligned} p_e(t) &\simeq e^{-\Gamma t}, \quad \alpha = 0, \\ p_e(t) &\simeq \cos^2(\Omega t), \quad \alpha \neq 0, \end{aligned} \tag{6.66}$$

where $p_e = |c_e|^2$. Moreover we also show the case in which the emitter is not resonant with any of the Landau levels. The spectral gap is filled only with states that are exponentially localised at the boundary of the lattice [112], and thus do not couple to the emitter. The emission is then strongly suppressed and, apart from it slow bare decay, the emitter remains just in its excited state.

Using Eq. (6.53) and the definition of the photon's wave function, $\varphi(\vec{r}_i, t) = \sum_\lambda \varphi_\lambda(t) f_\lambda(\vec{r}_i)$, we obtain

$$\varphi(\vec{r}_i, t) = -i\frac{\sin(\Omega t)}{\sqrt{\alpha}} G_\ell(\vec{r}_i, \vec{r}_e). \tag{6.67}$$

For a time $t_\pi = \pi/(2\Omega)$ the excitation is fully converted into a photon localised in a Landau orbital $\sim \Phi_\ell(\vec{r}_i - \vec{r}_e)$, centred around the emitter. This photon carries a current $\langle \vec{j}_p \rangle(\vec{r}_i, t_\pi)$, due to its circulating nature, which can be calculated from the operators

$$j_p^x(\vec{r}_i) = i\frac{J}{2}\left[\left(e^{i\phi_x}\Psi^\dagger(\vec{r}_i + \vec{e}_x) - e^{-i\phi_x}\Psi^\dagger(\vec{r}_i - \vec{e}_x)\right)\Psi(\vec{r}_i) - \text{H.c.}\right], \tag{6.68}$$

$$j_p^y(\vec{r}_i) = i\frac{J}{2}\left[\left(e^{i\phi_y}\Psi^\dagger(\vec{r}_i + \vec{e}_y) - e^{-i\phi_y}\Psi^\dagger(\vec{r}_i - \vec{e}_y)\right)\Psi(\vec{r}_i) - \text{H.c.}\right]. \tag{6.69}$$

In the continuous limit it takes the shape of the usual gauge invariant current

$$\vec{j}_c(\vec{r}) = \frac{1}{2m}\left[\Psi_c^\dagger(\vec{r})\left(-i\hbar\vec{\nabla}\right)\Psi_c(\vec{r}) - \text{H.c.}\right] - \frac{e}{m}\vec{A}(\vec{r})\Psi_c^\dagger(\vec{r})\Psi_c(\vec{r}). \tag{6.70}$$

In Fig. 6.4(c) we see three numerical examples of the photon's wave function at time t_π and the corresponding current profile. The emitter's resonance select a particular Landau level, which then defines the extension and the shape of the photon's wave packet. From this plot it is also evident that for the considered values of α the continuum description gives very accurate results.

All the above discussion can be generalised quite easily to the case of multiple emitters, giving the general single excitation equation

$$\ddot{c}_n(t) = -\frac{\bar{\gamma}}{2}\dot{c}_n(t) - g^2\sum_m G_\ell(\vec{r}_e^{\,n}, \vec{r}_e^{\,m})c_m(t), \tag{6.71}$$

where $n = 1, 2 \ldots N$. The complete solution of this system of equations can be obtained considering the Fourier transform of the $c_n(t)$ in Eq. (6.71), giving the eigenvalues equation

$$(\omega^2 + i\omega\bar{\gamma}/2 - \Omega^2)c_n(\omega) = g^2\sum_{m\neq n} G_\ell(\vec{r}_e^{\,n}, \vec{r}_e^{\,m})c_m(\omega). \tag{6.72}$$

Solving this equation we can derive the complex eigenvalues of the dissipative system, which represent the resonance frequencies and the decay rates of the coupled eigenmodes. This eigenmodes are actually the polariton modes of the system. Because they involve the Landau photons, we name them *Landau-photon polariton*. After transforming back into the original frame, these complex

eigenvalues are

$$\omega_\nu = \omega_e - i\frac{\gamma_e+\gamma_p}{4} \pm \Omega\sqrt{1+\Lambda_\nu - \bar{\gamma}^2/(16\Omega^2)}, \tag{6.73}$$

where the Λ_ν are the eigenvalues of the matrix

$$\mathcal{M} = \frac{1}{\alpha}\begin{pmatrix} 0 & G_\ell(\vec{r}_e^{\,1},\vec{r}_e^{\,2}) & G_\ell(\vec{r}_e^{\,1},\vec{r}_e^{\,3}) & \cdots & G_\ell(\vec{r}_e^{\,1},\vec{r}_e^{\,N}) \\ G_\ell(\vec{r}_e^{\,2},\vec{r}_e^{\,1}) & 0 & G_\ell(\vec{r}_e^{\,2},\vec{r}_e^{\,3}) & \cdots & G_\ell(\vec{r}_e^{\,2},\vec{r}_e^{\,N}) \\ \vdots & & \ddots & & \cdots \end{pmatrix}. \tag{6.74}$$

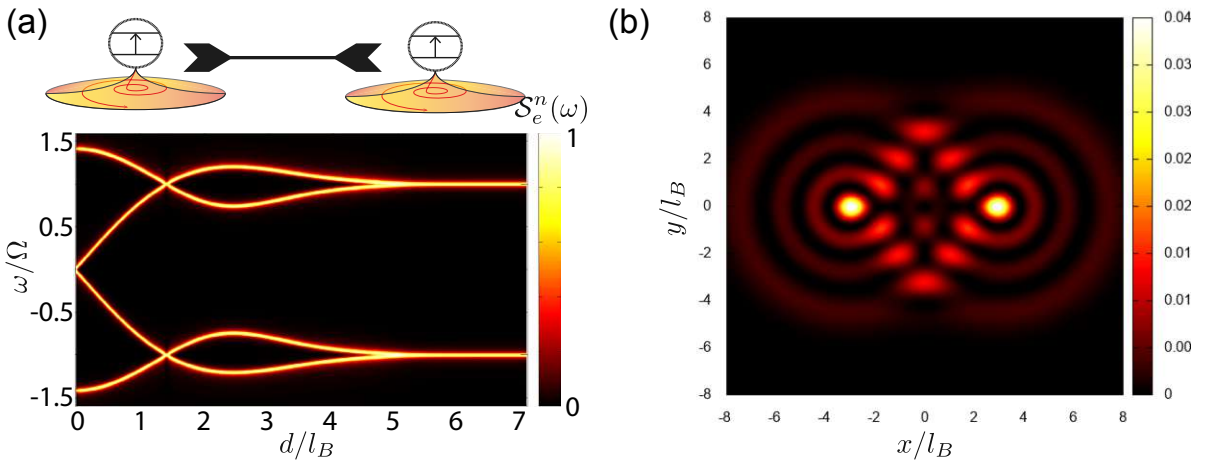

Figure 6.5: (a) Excitation spectrum $\mathcal{S}_e^n(\omega)$ of $N = 2$ emitters resonant with the $\ell = 1$ Landau level, as a function of their relative distance d. The excitation spectrum is normalised to one, and the color scale is linear.(b) Photon's density of the lowest eigenstate for $N = 2$ emitters resonant with the Landau level $\ell = 3$ and at the distance of $d/_B = 6$.

It is quite interesting to study Eq. (6.73) for a few paradigmatic case as a function of the distance between the emitters. The simplest extension is the case of two emitters. Considering the emitters at a relative distance d the spectrum is given by two symmetrical branches below and above the emitter's frequency (which is assumed the same for all emitters and to be in resonance with a specific Landau level). Each branch is composed of two sub-branches. In this case the problem can be solved analytically, giving the frequencies

$$\begin{aligned} \omega^{\pm}_{\ell,\mathrm{low}} &= \omega_e - \Omega\sqrt{1 \pm e^{-\frac{d^2}{4l_B^2}} L_\ell^0\left(\frac{d^2}{2l_B^2}\right)}, \\ \omega^{\pm}_{\ell,\mathrm{up}} &= \omega_e + \Omega\sqrt{1 \pm e^{-\frac{d^2}{4l_B^2}} L_\ell^0\left(\frac{d^2}{2l_B^2}\right)}. \end{aligned} \tag{6.75}$$

We can see the behaviour of these two polariton branches in Fig. 6.5(a), where we plot the *excitation*

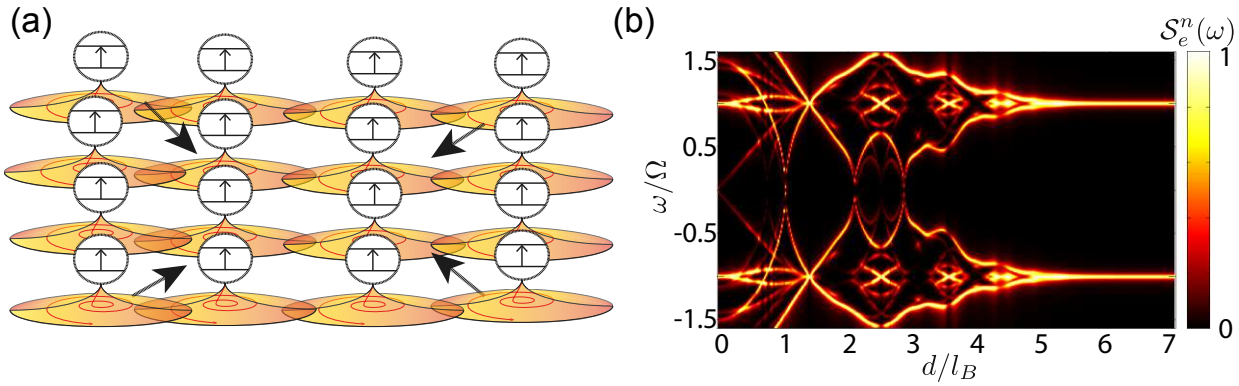

Figure 6.6: (a)Sketch a lattice of $N = 4\times4$ emitter. (b) Excitation spectrum of $N = 4\times4$ emitters resonant with the $\ell = 1$ Landau level. The emitters are arranged in a square lattice with lattice spacing d, which is then varied across the plot. We take $\vec{r}_e^n$ as the position of one of the four inner emitters. The excitation spectrum is normalised to one, and the color scale is linear.

spectrum, given by

$$\mathcal{S}_e^n(\omega) = \left|\langle G|\sigma_-^n \frac{1}{H-\omega-i\frac{\gamma_e}{2}\sum_m \sigma_+^m\sigma_-^m}\sigma_+^n|G\rangle\right|^2, \tag{6.76}$$

where $|G\rangle$ is the ground state and γ_e is the bare decay rate of the emitters. When $d \gg l_B$ the two sub-branches are almost degenerate and reproduce the spectrum of a single emitter. This is due to the fact that the emitters are so far apart that the respective Landau orbitals do not overlap. When the separation becomes on the same order of $d \sim l_B$, the two Landau orbitals start to have a significant overlap. This leads to a hybridisation of the orbitals, in analogy to a pair of atoms forming a molecule. In Fig. 6.5(b) we see an example of a hybridised orbital. When the distance is close to zero $d \sim 0$ the emitters can be considered as being all localized in the same orbital and we recover the physics of the Tavis-Cummings model [71], where multiple emitters are collectively coupled to a single harmonic mode.

When more than two emitters are present the situation is very similar, but the spectrum looks much more complicated, exhibiting curious patterns, reminiscent of the Hofstadter butterfly. In Fig. 6.6(b) we see the spectrum of a square array of emitters, with d being the separation between nearest neighbours.

The last important case, which will be further discussed also in the following sections, is an equilateral triangle of emitters with distance d. The spectrum has the same structure as before, with two symmetric branches, and three sub-branches each

$$\omega^\nu_{\ell,\text{up/low}} = \omega_e \pm \Omega\sqrt{1+e^{-\frac{d^2}{4l_B^2}}L_\ell^0\left(\frac{d^2}{2l_B^2}\right)\lambda_\nu}, \tag{6.77}$$

where $\lambda_{\nu=1,2,3} = 2\cos[(\theta_\triangle + 2\pi\nu)/3]$ and

$$\theta_\triangle = \theta_{12} + \theta_{23} + \theta_{31} = eBA_\triangle/\hbar \tag{6.78}$$

is the normalized magnetic flux through the area $A_\triangle = \sqrt{3}/2d^2$ enclosed by the three emitters.

6.5 Landau-projected Hamiltonian and multiphotons physics

The last section can be incorporated into a more generic framework. We have seen that the single excitation physics is fully described in terms of Landau orbitals surrounding each emitter, forming a local polariton, and that the multi emitters polaritonic states are just given by considering the overlapping orbitals of each local polariton. It thus seems that the actual degrees of freedom involved are much less than the total number of emitters and lattice sites, which would give a single excitation Hilbert space scaling like $\sim N + M$, where N is the number of emitters and $M \gg N$ the number of lattice sites. It seems more appropriate instead to think that the number of relevant degrees of freedom here are given by the emitters and their Landau orbitals, giving a single excitation Hilbert space scaling $\sim N + N$. This would be of course a huge simplification, especially when we consider the multi photons case, where the Hilbert space is exponentially large in M. We will see now that this simplification is possible and that it will also give very nice conceptual insights.

When we re-express the light-matter Hamiltonian in the Landau level basis (assuming the continuous limit) we have

$$H = \sum_{\ell=0} \omega_\ell \sum_k \Psi^\dagger_{\ell k}\Psi_{\ell k} + \frac{\omega_0}{2}\sum_{n=1}^{N}\sigma_z^n + g\sum_\ell \sum_{n=1}^{N}\sum_k \left[f_{\ell k}(\vec{r}_e^{\,n})\Psi_{\ell k}\sigma_+^n + \text{h.c.}\right]. \tag{6.79}$$

If we assume that just a single Landau level contributes we can neglect all the terms but that particular ℓ, assuming that $\omega_\ell \simeq \omega_0$ (the resonance condition). Switching to a rotating frame, we then obtain the interaction Hamiltonian

$$H_I \simeq g\sum_{n=1}^{N}\sum_k \left[f_{\ell k}(\vec{r}_e^{\,n})\Psi_{\ell k}\sigma_+^n + \text{h.c.}\right]. \tag{6.80}$$

Using the identity

$$\sum_k f_{\ell k}(\vec{r}_e^{\,n})\Psi_{\ell k} = \int G_\ell(\vec{r}_e^{\,n},\vec{r})\Psi(\vec{r})d^2r = \tilde{\Psi}_n, \tag{6.81}$$

which still holds in the lattice, just replacing the integrals with the sum over all lattice sites, we

have

$$H_I \simeq g \sum_{n=1}^{N} \left[\tilde{\Psi}_n \sigma_+^n + \text{h.c.} \right]. \tag{6.82}$$

From this perspective it is pretty clear that N emitters interact only with N degrees of freedom. But we need to be careful because

$$[\tilde{\Psi}_n, \tilde{\Psi}_m^\dagger] = G_\ell(\vec{r}_e^{\,n}, \vec{r}_e^{\,m}) \neq \delta_{nm}, \tag{6.83}$$

meaning that the $\tilde{\Psi}_n$ do not represent canonical degrees of freedom. To find again the correct commutation relation we need to introduce the normalised operators

$$B_{\ell n} = \sum_{m=1}^{N} (K^{-1})_{nm} \tilde{\Psi}_m, \tag{6.84}$$

and we choose the normalisation is such a way that

$$\begin{aligned} [B_{\ell n}, B_{\ell n'}^\dagger] &= \sum_{m,m'} K^{-1}_{nm} (K^{-1}_{n'm'})^* \sum_{ij} G_\ell(\vec{r}_e^{\,m}, \vec{r}_i) G_\ell^*(\vec{r}_e^{\,m'}, \vec{r}_j) \delta_{ij} \\ &= \sum_{m,m'} K^{-1}_{nm} (K^{-1}_{n'm'})^* G_\ell(\vec{r}_e^{\,m}, \vec{r}_e^{\,m'}) \\ &= \left[K^{-1} G (K^{-1})^\dagger \right]_{nn'} \stackrel{!}{=} \delta_{nn'}. \end{aligned} \tag{6.85}$$

This means that the K-matrix must be the square root of the matrix with entries $G_{nm} = \{G_\ell(\vec{r}_e^{\,n}, \vec{r}_e^{\,m})\}$. Introducing this new normalised operators we can rewrite the interaction Hamiltonian as

$$H_I = g \sum_{n,m=1}^{N} \left(\sigma_+^n K_{nm} B_{\ell m} + B_{\ell m}^\dagger K_{nm}^* \sigma_-^n \right), \tag{6.86}$$

transforming back to the static frame we have the *Landau-photon polariton* Hamiltonian

$$H \simeq H_{\text{LPP}}^{(\ell)} = \omega_\ell \sum_{n=1}^{N} B_{\ell n}^\dagger B_{\ell n} + \frac{\omega_e}{2} \sum_{n=1}^{N} \sigma_z^n + g \sum_{n,m=1}^{N} \left(\sigma_+^n K_{nm} B_{\ell m} + B_{\ell m}^\dagger K_{nm}^* \sigma_-^n \right). \tag{6.87}$$

Each emitter interacts with the photonic field localised in a Landau orbit centered on the emitter position, and with the photonic field localised around the other emitters by the overlap between their Landau orbitals. We can thus say that each emitter is surrounded by its own cavity, which is given by the Landau orbital, and when the orbitals overlap each emitter can exchange photons with its own orbital or with the overlapping orbital of another emitter. Importantly, this Hamiltonian now only describes N emitters and N photonic modes, which reduces quite a lot the complexity of

the system. So we can easily explore the multi-photons physics. Of course all the results will be given in the space of Landau orbitals, which we can call the B-space, but we can translate them to the lattice (or real space) Hilbert space with the help of the photon Green's function. From here on we will just use the continuous Green's function, which gives cleaner and analytic results. But in principle one could generate an arbitrary Green's function numerically and then use it to translate the results from one space to the other.

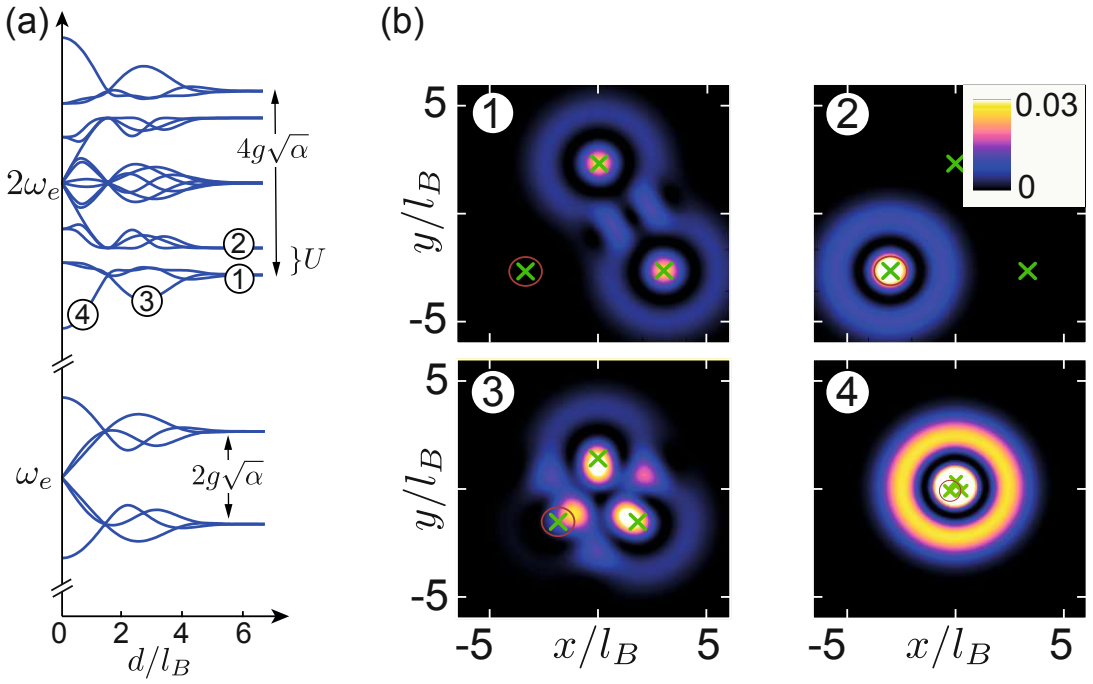

Figure 6.7: (a) The spectrum of $H^{(\ell)}_{\mathrm{LPP}}$ in the single- and two- excitation sector for $N = 3$ equidistant emitters with varying spacing d and for $\ell = 1$ and $\omega_e = \omega_1$. (b) Plot of the two-photon correlation function $C(\vec{r}_i, \vec{r}^{\,1}_e)$ for the different two-photon eigenstates indicated in (a). The green crosses represent the emitters position, and the red circle marks the reference emitter's position $\vec{r}^{\,1}_e$.

Here we use the LPP Hamiltonian to investigate a system of three emitters in the equilateral triangle configuration and in the two excitation sector. In Fig. 6.7(a) we see the polariton spectrum as a function of the distance between the emitters, for the one and the two excitation sector. Focusing on the two excitation sector, centered around the frequency $2\omega_e$, we notice that for the large distance limit, when $d \gg l_B$, the spectrum collapses into five degenerate manifolds, symmetric around $2\omega_e$. For large distances the three emitters are basically not coupled with each other, and they are just coupled with their own Landau orbital. Therefore, these different degenerate states represent all the possible combination of Jaynes-Cummings (JC) dressed states with two excitations on three uncoupled cavity QED systems. In particular, the lowest manifold, which is marked by "1" in Fig. 6.7(a), consists of states in which two over three emitters contains one excitation. Just above this manifold we have the manifold marked by "2". This manifold contains all the JC-states in which the two excitations are localised on the same emitter. The energy separation between these

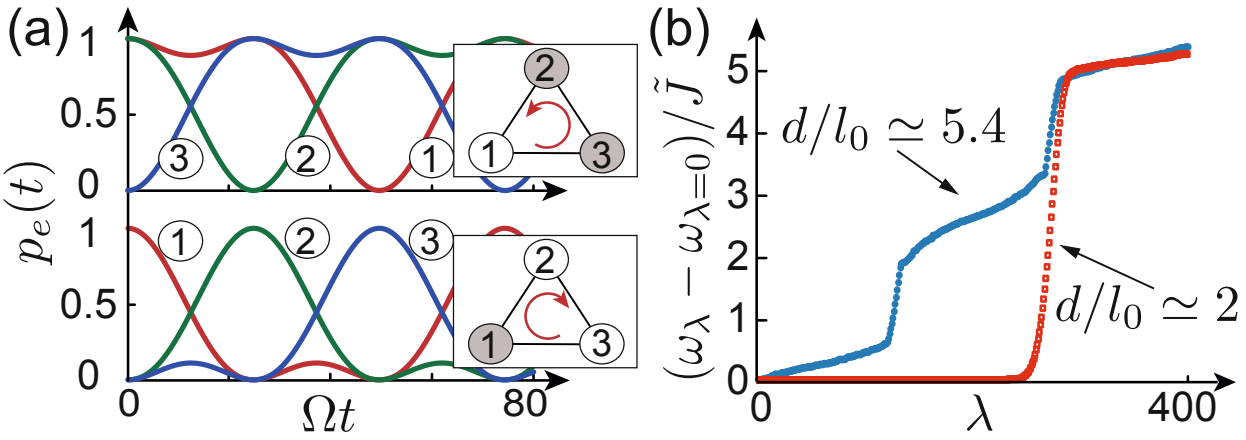

Figure 6.8: (a) Evolution of the excited state populations $p_e^n(t)$ of $N = 3$ emitters arranged in a triangle of length $d/l_0 = 4$. For this plot $\ell = 0$, and $\alpha = 1/(16\sqrt{3}) \approx 0.036$, such that the enclosed effective flux is $\theta_\triangle \simeq \pi/2$ and the dipole-dipole interactions become fully chiral. In the upper panel the initial state contains two excitations in emitter 1 and 2. In the lower panel the initial state contains just one excitation in emitter 1. (b) Single-excitation spectrum of H_{eff} for a square lattice of 20×20 emitters and normalized to the nearest-neighbor coupling strength $\tilde{J} = |\tilde{J}_{12}|$. The two spectra are obtained for the spacings $d/l_0 = 2$ ($\alpha_{\text{eff}} = 0.32$) and $d/l_0 = 5.39$ ($\alpha_{\text{eff}} = 2.32$) and in both cases $\alpha = 0.08$ and $\ell = 0$ has been assumed.

two manifolds is given by

$$U = \Omega(2 - \sqrt{2}), \tag{6.88}$$

which can be seen as an effective repulsion between single photons (it costs more energy to push two photons into the same orbital rather than spreading them between two different orbitals). We can further explore this feature by measuring the two body correlation function

$$C(\vec{r}, \vec{r}') = \frac{\langle \Psi^\dagger(\vec{r}')\Psi^\dagger(\vec{r})\Psi(\vec{r})\Psi(\vec{r}')\rangle}{\langle \Psi^\dagger(\vec{r}')\Psi(\vec{r}')\rangle}. \tag{6.89}$$

In Fig. 6.7(b) we report four examples, where the correlation function is calculated for the states indicated in the spectrum in Fig. 6.7(a). As expected the states in the lowest manifold at large distance $d \gg l_B$ exhibit strong antibunching and the two photons remain always separated and localised on different emitters. For smaller distances $d \sim l_B$ more patterns emerge and the strong antibunching smoothly disappears. For distances $d \ll l_B$ the system behaves like all the three emitters would be coupled to the same orbital, reproducing the Tavis-Cummings model. In the upper manifold instead we see that there is strong bunching and the two photons always want to stay together localised on the same emitter.

6.6 Band-gap effective emitter-emitter interaction

So far we have discussed the case in which the emitters were in resonance with a particular Landau level. Now we want to explore the case in which the emitter's frequency lies in a band gap of the magnetic photonic lattice, following the condition

$$|\omega_e - \omega_\ell| \gg g. \tag{6.90}$$

In this regime the emitters are just weakly dressed by the Landau-photon, and cannot really be described as polaritons. By using perturbation theory [25] we can eliminate the photons in favour of an effective Hamiltonian just for the undressed emitters

$$H_{\text{eff}} = \sum_{m,n} \left(\tilde{J}_{nm} \sigma_+^n \sigma_-^m + \text{h.c.} \right), \tag{6.91}$$

where

$$\tilde{J}_{nm} \simeq \frac{g^2}{\omega_e - \omega_\ell} |G_\ell(\vec{r}_e^{\,n}, \vec{r}_e^{\,m})| e^{i\theta_{nm}}. \tag{6.92}$$

The effective hopping between the emitters is still complex, with its phase given by Eq. (6.42), so it will still keep all the magnetic properties of the underlying lattice. This is quite striking when we consider again the equilateral triangle configuration. The amplitude of the effective hopping is the same for all the emitters, but the phase changes, which makes a big difference. The single excitation sector is fully described by the matrix

$$\tilde{J} = G_0 \begin{pmatrix} 0 & e^{i\theta_{12}} & e^{i\theta_{13}} \\ e^{-i\theta_{12}} & 0 & e^{i\theta_{23}} \\ e^{-i\theta_{13}} & e^{-i\theta_{23}} & 0 \end{pmatrix}, \tag{6.93}$$

where, in the continuum limit, $G_0 = g^2/(\omega_a - \omega_\ell)\Phi_\ell(|\vec{r}_a^{\,n} - \vec{r}_a^{\,m}|)$ can be regarded constant, since we consider an equilateral triangle geometry. The equation for the single-excitation eigenvalues is then given by

$$\lambda^3 - 3G_0^2\lambda - 2G_0^3 \cos(\theta_\Delta) = 0, \tag{6.94}$$

which is exactly the same polynomial that already appeared in the LPP spectrum in Eq. (6.77). When the magnetic flux through the triangle is $\theta_\Delta = n\pi/2$ two eigenstates become degenerate and one expects that something special occurs. By considering the eigenstates of the single excitation sector, we can see that this is actually the case. The population amplitude of the three emitters

can be expressed by using the eigenstates of Eq. (6.93),

$$c_n(t) = \sum_{\nu} \sum_{m} c_m(t=0) f_\nu(m) f_\nu(n) e^{-i\lambda_\nu t}, \tag{6.95}$$

where $m, n, \nu = 1, 2, 3$ and

$$\sum_{m=1}^{3} \tilde{J}_{nm} f_\nu(m) = \lambda_\nu f_\nu(n). \tag{6.96}$$

If we consider the initial condition in which the excitation is loaded just in a single emitter $c_m(t = 0) = \delta_{m1}$, we can explicitly find the solution of the equations of motion for the case in which $\theta_\Delta = n\pi/2$

$$\begin{aligned} |c_1(t)| &= \left| \frac{1}{3} + \frac{2}{3} \cos\left[\sqrt{3} G_0 t\right] \right|, \\ |c_2(t)| &= \left| \frac{1}{3} + \frac{2}{3} \cos\left[\sqrt{3} G_0 t + \frac{4\pi}{3}\right] \right|, \\ |c_3(t)| &= \left| \frac{1}{3} + \frac{2}{3} \cos\left[\sqrt{3} G_0 t + \frac{2\pi}{3}\right] \right|. \end{aligned} \tag{6.97}$$

This solution exhibits a chiral circulation of the excitation, which is fully reproduced by the numerics in Fig. 6.8(a) (upper figure). The other interesting case is when $\theta_\Delta = n\pi$ and there is no degeneracy between the three eigenstates, but one eigenvalue is zero. In this case one finds no chirality. This simple observation can be recovered again in the two excitation sector. In this case we have identical dynamics, but with opposite sign of circulation. The simplest interpretation is that with two excitation on three emitters we have a single "hole". The hole follows the equations of a single excitation, but with opposite charge. Therefore it circulates in the opposite direction. This can be seen explicitly in Fig. 6.8(a)(lower figure).

Moving forward, the effective Hamiltonian H_{eff} can be used more generally to generate setups of lattices of magnetic hardcore bosons models with tunable parameters. For example, the phase can be tuned by varying the relative position of the emitters. For a simple square lattice arrangement of the emitters we recover a phase with an effective flux

$$\alpha_{\text{eff}} = \alpha \left(\frac{d}{l_0} \right)^2. \tag{6.98}$$

Furthermore, the effective hopping is not constrained to neighboring lattice sites, opening up the possibility to explore a whole zoo of magnetic models with various band structures. In Fig. 6.8(b) we show a simple example of a square lattice of emitters with spacing $d/l_0 = 5.39$ and $d/l_0 = 2$, but equivalent effective field strengths. In the first case, only nearest-neighbor couplings are relevant and we recover the regular Hofstadter butterfly with $\alpha_{\text{eff}} \approx 2.32$ (which is equivalent to $\alpha_{\text{eff}} \approx 0.32$).

In the second example, long-range hoppings are important and the spectrum of the bulk modes becomes essentially flat. This situation falls in the class of the so-called Kapit-Muller Hamiltonians [113], which are toy models to study the fractional quantum Hall effect.

6.7 Disorder

One of the main feature characterising systems with magnetic fields or non-trivial topologies is their robustness with respect to disorder [24]. In the case of a two dimensional lattice subject to a homogeneous magnetic field, as in our case, it is well known that the edge states are robust against disorder, while the bulk states are sensitive to its presence. In particular, in the presence of disorder each ℓ-th Landau levels acquires a finite width J_ℓ [114]. However, contrary to what is often assumed, this does not mean that all the physics involving bulk states is not robust against disorder. Indeed, intuitively one expects that up to the point where the bandwidth J_ℓ of a Landau level is smaller than separation from neighboring Landau levels,

$$J_\ell \ll |\omega_{\ell+1} - \omega_\ell|, \tag{6.99}$$

the system still retains its magnetic features. Similarly, we expect that the physics of the LPP discussed above remains robust against disorder as long as the condition

$$\omega_c \gg g \gg J_\ell, \tag{6.100}$$

is fulfilled. If we consider only emitter in the bandgap, as discussed in the last section, the condition (6.99) is enough.

In this section we explore numerically the validity of these conditions by focusing on the case in which the photonic lattice is subjected to local disorder, where we replace

$$\omega_p \longmapsto \tilde{\omega}_p^i = \omega_p + \delta\omega_p^i. \tag{6.101}$$

Here the $\delta\omega_p^i$ are sampled from a Gaussian distribution with a width $\Delta\omega_p$ and centered around zero. Using Eq. (6.76), we define the average spectrum by

$$\bar{\mathcal{S}}_e^n(\omega) = \frac{1}{N_{\text{dis}}} \sum_{k=1}^{N_{\text{dis}}} \mathcal{S}_e^n(\omega), \tag{6.102}$$

where N_{dis} is the number of independent disorder realisations, where in each realisation we take a new random set of $\{\delta\omega_p^i\}$. In Fig. 6.9(e) we show the average spectrum as a function of the disorder strength $\Delta\omega_p$, for the paradigmatic case of a single emitter, resonantly coupled to the

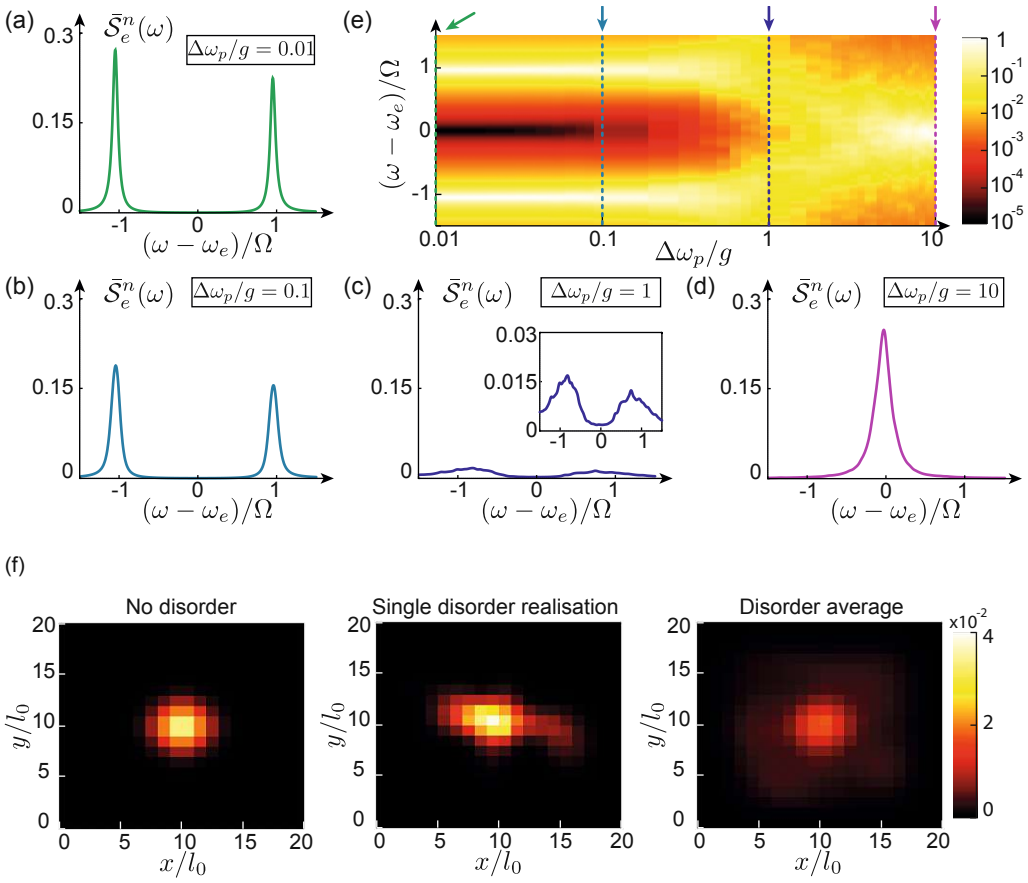

Figure 6.9: (a-d) Disorder averaged excitation spectrum $\bar{\mathcal{S}}_e^n(\omega)$ for fixed value of the disorder strength (as indicate in each plot). Each plot is averaged over $N_{\rm dis} = 1000$ realisations. (e) Disorder averaged excitation spectrum $\bar{\mathcal{S}}_e^n(\omega)$ as a function of $\Delta\omega_p$. For each value of $\Delta\omega_p$ the excitation spectrum is averaged over $N_{\rm dis} = 50$ realisations. (f) Plot of the photon wavefunction $|\varphi(\vec{r}_n)|^2$ of the lowest LPP. The disorder strength in this plot is chosen as $\Delta\omega_p/g = 0.7$. The left panel shows the case without disorder, the center panel the wavefunction for a single disorder realisation and the right panel depicts the average over $N_{\rm dis} = 200$ realisations. For all figures we have assumed a $M = 20 \times 20$ photonic lattice, $\alpha = 0.08$, $\delta_e/J = 0.47$ (corresponding to the resonance with the $\ell = 0$ Landau level) and $g/J = 0.08$.

zeroth Landau level. When the disorder is very weak, $\Delta\omega_p \ll g < \omega_c$, the Rabi splitting is clearly visible and the only effect of the disorder is to broaden the two Rabi peaks. This situation holds even up to disorder strengths of about $\Delta\omega_p/g \simeq 1$. When the disorder crosses this threshold the condition in Eq. (6.100) is no longer satisfied and the Rabi splitting disappears in favour of a single broadened resonance, peaked around ω_p. This can be seen from the cuts in Fig. 6.9(a-d) taken at fixed disorder strength. In Fig. 6.9(f) we plot an example of the photon's wave function in the lowest LPP state. Local disorder deforms the wave function profile, generally breaking its rotational symmetry. Averaging the photon's density over many realisation we can see that its original shape is approximately recovered. Notice that for this simulation we have used quite strong disorder, $\Delta\omega_p/g \simeq 0.7$.

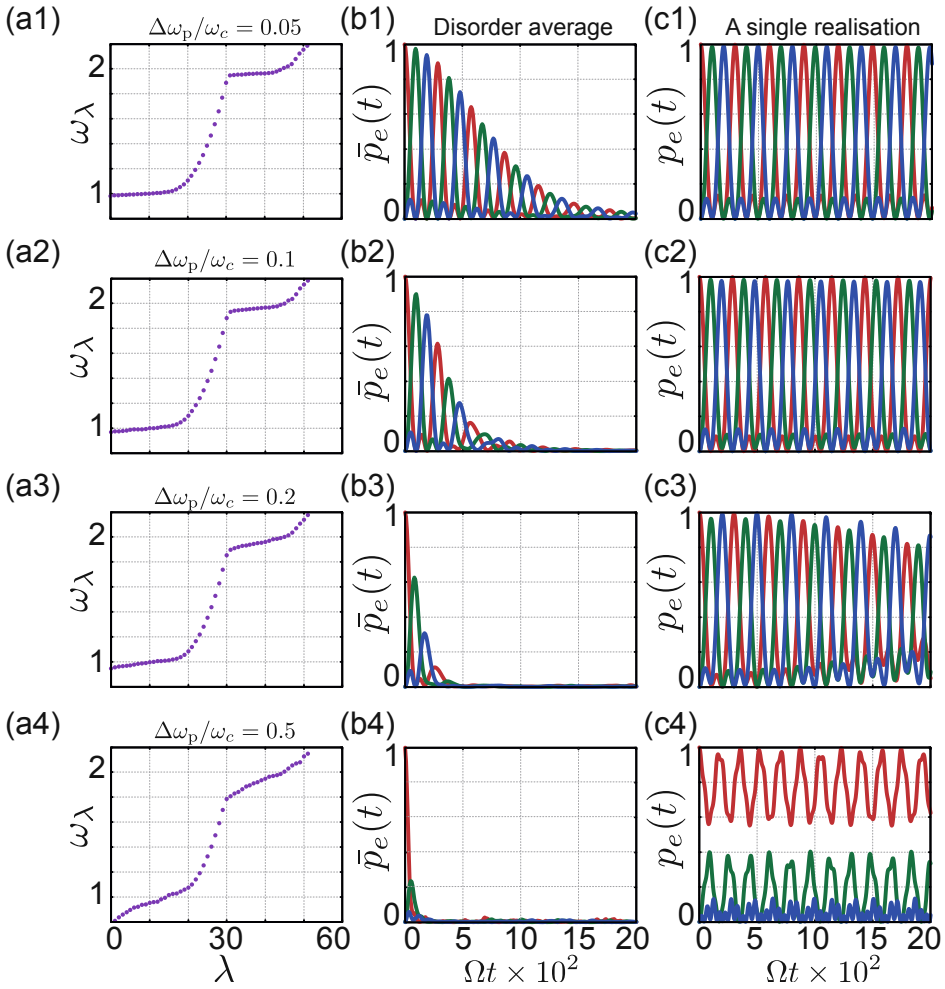

Figure 6.10: (a1-a4) Plot of the lowest eigenvalues ω_λ of $H_{\rm ph}$ in the presence of disorder and for a 31×31 triangular lattice. (b1-b4) Disorder averaged evolution of the excited state population, $\bar{p}_e$, for three equidistant emitters with $d/l_0 = 4$. Here the bar denotes the average over $N_{\rm dis} = 100$ realizations, see Eq. (6.103). The disorder strength used is the same as reported in the respective panel (a) plots. (c1-c4) Single realization of the population's time evolution under the same conditions as the panel (a-b) plots. The other parameters used in all the plots are $\omega_{\rm p} = 9.5$, $\omega_e = 0.5$, $J = 0.75$, $g = 0.1$, $\alpha = 1/(16\sqrt{3})$, $d/l_0 = 4$, $\gamma = 10^{-5}$ (all frequencies are given in arbitrary units).

We continue with the case in which the emitters are not resonant with any Landau level. In particular, we study the case of three emitters in an equilateral triangle, as discussed above. Focusing on the chiral circulation expressed in Fig. 6.10(b), we consider the average emitter's population

$$\bar{p}_e(t) = \left| \frac{1}{N_{\text{dis.}}} \sum_{\text{dis.}} c_e(t) \right|^2 . \tag{6.103}$$

In Fig. 6.10 we plot four examples. In each row we consider a different disorder strength, in increasing order. In the first column we plot a single sample of the lowest part of the photon's spectrum given by H_{ph}. In the second column there is the average population evolved in time. The third column displays a single shot of the population's time evolution. When the disorder is small compared to the cyclotron frequency $\Delta\omega_{\text{p}}/\omega_c \lesssim 0.1$ the chirality is still clearly visible and the dynamics is very regular even without averaging. The effect of disorder manifests itself on the average population through an effective damping induce by the dephasing effect. When the disorder starts to be comparable to the cyclotron frequency the chirality is still present clearly, but the damping induced by dephasing becomes dominant. Finally, when $\Delta\omega_{\text{p}}/\omega_c \geq 0.5$, even though the gap between the last two Landau level is still open, the dynamics is completely destroyed. On average the damping is too extreme to still see any oscillations, and on the single shots the chirality is completely broken.

6.8 Experimental implementations

In this very last section we briefly comment on the possibility to realize such LPP systems in experiments. As anticipated in the introduction of this chapter this kind of physics could in principle be realized in a quite broad variety of systems. For example photons subjected to synthetic magnetic fields are already available in the optical as well microwave regime [28, 107]. An recent review about different experimental approaches for implementing effective fields can be found in [24]. Here we focus on the specific case of microwave photons, which are experimentally most promising.

ω_{p}	ω_e	J	g	$\gamma_{p,e}$	$\Delta\omega_p$	
5.4×10^3	5×10^3	100	20	0.05	1	MHz

Table 6.1: A possible choice of realistic set of parameters to observe the LPP physics with microwave photons in circuit QED.

Microwave photonic systems are implemented using superconducting circuits architectures [115]. In recent experiments [107] it was demonstrated that these systems can be used to realize complex hopping amplitudes which mimic an homogeneous magnetic field with $\alpha = 1/4, 1/6$. Despite the fact that these values of the synthetic magnetic flux in the lattice are on the edge of the intermediate

regime, they are still small enough to use the continuum approximation without introducing a huge error. The onsite frequency of this system can vary from hundreds of MHz to tens of GHz, having a quality factor of $Q = 10^3 - 10^5$. The tunneling rate amplitude can be designed to be around $J \sim 100$ MHz, and the onsite disorder can be made quite small, $\Delta\omega_p \lesssim 1$ MHz [116].

In the experiment in Ref. [107] there was no quantum emitter coupled to the lattice. But is has been shown in many other experiments that it is possible to couple to these types of lattices quantum emitters, for example, in the form of non-linear elements based on Josephson junctions. In such experiments couplings of about $g \sim 1 - 100$ MHz have been demonstrated [117, 118]. These emitters, or superconducting qubits, have internal frequency typically around $\omega_e \sim 3 - 5$ GHz, and coherence times of about $\sim 0.1 - 1$ ms, which is given by a decay time $\gamma_e \sim 1$ kHz. The frequencies of these qubits can be easily tuned over a range of many 100 MHz, so it is possible to tune them into resonance with one of the first Landau levels. The current estimates are summarised in the table 6.1, which represents an example of a concrete realistic implementation.

Summary and outlook

In conclusion, in this doctoral thesis we have discussed the theory to describe light-matter interactions with non-perturbative single photon coupling, and its possible observations for a multi-qubits system in equilibrium. Moreover we have discussed the non-trivial behaviour of light-matter interactions in photonic structures where the photon is subjected to a synthetic magnetic field. In particular we have shown the strong relation with the physics of atom-photon bound states in waveguide QED and its relevance in the field of quantum simulations of quantum Hall and fractional quantum Hall physics. We briefly summarise here the content of the thesis.

In the first two chapters we mainly focus on the abstract theory, discussing all the approximations that we need to arrive to a simple basic description and eventual issues, confusions and mistakes related to the different representations given by different gauges.

First we introduced the general theory of non-relativistic light-matter interactions, with great care for the boundary conditions of the electromagnetic field. This is a very important aspect to develop a consistent theory of cavity QED, where the light modes are confined and the Dirichtlet (or metallic) boundary conditions are applied. Introducing the Green's function of the Laplace operator we generalised the definition of the transverse and longitudinal delta function. Then we were able to repeat the usual derivation of the non-relativistic light-matter Hamiltonian in the Coulomb gauge, keeping all the information related to the boundary conditions in the new transverse/longitudinal delta functions. Having assumed the dipole approximation (or long wavelength approximation) we developed the equivalent description in the dipole gauge. Here we showed that the resulting dipole Hamiltonian for a system of localised dipoles is fully local and the usual direct dipole-dipole interaction is cancelled. However this cancellation is only apparent, because the dipole-dipole interaction is recovered by taking the electrostatic limit and adiabatically eliminating the electromagnetic modes. This is one of the main points in the correct derivation of a cavity QED Hamiltonian which is valid also in the USC regime. Indeed, once we assume resonance with a single cavity mode, we cannot just throw away the other modes but we need to keep them in their electrostatic limit. This introduced two new terms with respect to the usual simplified models considered in the literature: the direct dipole-dipole interaction and the so-called P^2-term, which

compensate for the resonant mode that we did not eliminate.

After having developed a reasonable single mode theory for a cavity resonant with a dipole ensemble, we focus on the dipoles themselves. We discussed the possibility to truncate the dipole's Hilbert space to just two levels, in such a way to have a strongly simplified theory. We remark here that this is not just a convenient way to treat numerically and analytically our dipoles, but it has also a conceptual relevance. Indeed for technological applications we want to be sure that our system is composed of two level systems, that represent the qubits of our eventual machine. We then showed that in the USC regime the TLA is far from trivial and it depends crucially on the gauge which was originally chosen. In most of the relevant cases the dipole gauge is the only one that guarantees the correct TLA even for large coupling strength.

In the Ch. 3 and 4 we discussed the consequence of the USC in a realistic setting of an LC circuit where the capacitor is filled by dipoles. We first focused our discussion on the large collective coupling regime (relevant in solid state materials). We showed how the polariton branches are modified by the dipole-dipole interaction. In particular we identified three main scenarios which depend from the geometry of the dipole ensemble. We also commented on the usual definition around the coupling regimes of light-matter interactions, introducing the concept of effective fine structure constant, and highlighting the difference between collective USC and single dipole USC. After having review the properties of the celebrated Dicke superradiant phase transition, we establish the connection between our theory and the Dicke model. We explicitly showed that the superradiant phase transition must be interpreted as a standard ferroelectric transition, which just depends on the details of the electrostatic environment of the dipoles. Moving on we focused on the ground-state of an USC system with major attention to the single particle USC regime. We made a phase diagram to represent all the main different phases achievable in this system, and we explore all the three main phases that emerges under approximating the dipole-dipole interaction with an infinite range interaction. The last part of this section was devoted to study the consequence of dropping this last approximation, keeping the dipole-dipole interaction as a short range one. With few paradigmatic examples we showed that even more interesting phases appear from the competition between short range dipole-dipole interaction and single dipole USC regime.

In Ch. 5 we completed our tour in the physics of USC regime by illustrating the effect of USC on the thermodynamic of cavity QED. After developing an approximated free energy, based on the imaginary-time ordered Dyson expansion, we analysed the consequence of the light-matter coupling on the free energy. We realised that the collective USC coupling do not play any role in the thermodynamics properties, giving a negligible contribution in the free energy. However the single particle USC is highly relevant. We showed that it can be probed nicely from a susceptibility measure, giving strong deviations from the expected Curie law. Moreover it gives a substantial shift

in the ferroelectric transition point. We also computed the black body radiation expected from this system. Interestingly, even for few dipoles, the polariton branches are well visible for small coupling. In the USC limit we saw a sharp collapse of the polaritons, indicating the so-called light-matter decoupling that we already commented in the ground state properties.

The thesis ended with the chapter about light-matter interactions with synthetic magnetic fields. Here we started explaining the theory of photonic lattices with an homogeneous synthetic magnetic field. After having introduced the single photon spectrum of the lattice in function of the synthetic magnetic flux, we found three main regimes, characterised by comparing the three length scales: the system size, the lattice spacing and the magnetic length. In the intermediate flux regime we approximated the low energy modes as continuous Landau levels and we were able to explicitly find the Green's function of the magnetic photonic lattice. We then showed that coupling a two level emitter to this lattice one can generate new emitter-photon bound states, which carry a chiral current. We called these type of bound states Landau-photon polariton states, because they are hybrid light-matter polaritonic states, where the photonic part is provided by Landau levels. Going further in the exploration of the chiral emitter-photon bound states, we developed an effective theory to treat multiple emitters and multiple photons bound states. We were then able to investigate a simple system with two excitations and to show that the bound state physics in this case looks very similar to what one could expect from a fractional quantum Hall photonic system. In the end we developed the effective band-gap interaction between different emitters that emerge from the exchange of virtual photons in the case where the emitters are far detuned from any photonic Landau level. Also in this case various features proper of fractional quantum Hall systems arise.

In conclusion in this thesis we went deep into the theory of light-matter interactions applied to the ultra-strong coupling regime of cavity QED. We showed that such theoretical modelling is fundamentally important to avoid mistakes and misunderstandings due to representational issues. By considering a simple toy model we showed the main consequences of USC on the ground state and on thermal states. Doing this we hoped to bring novel clarity on the debate about superradiance phase transition and modifications of chemistry due to USC effects. We developed all the discussion in a rather abstract way, because we kept it as simple as possible, trying to avoid the complications related to a more realistic modelling of the matter part. This is motivated by our focus on the cavity, and about what the cavity can and cannot do as a function of the coupling strength. In particular we were able to make a clear distinction between fully electrostatic and dynamical effects, understanding their consequences on the ground-state of cavity QED and on its finite temperature equilibrium states. At the end we discussed a different system, where the photons can propagate in a multimode photonic structures with a synthetic magnetic field. Interacting with atoms, or, more generally, two level emitters the photon can be trapped in a chiral bound state around the

emitter. This opens up a new of physics, where atoms can interact through the overlap between these new bound states. Playing with the position of the emitters and their detuning with respect to the photonic lattice one can simulate physical situations reminiscent of fractional quantum Hall physics.

Acknowledgements

These five years of PhD were a long way in which I grew as a scientist but also as a person. It is not just the scientific research, but also all the people that I met, all around the world, which made the real difference. All the friends, from everywhere, from any race, nationality or religion with whom we shared the extraordinary experience of science and the beauty of human curiosity.

It is very hard to fit just in a few lines all the acknowledgements that I own to all the people I met in these five years. I think I want to start from my fiancée Rosa, that always stayed with me and supported me in every situation and against every difficulties. I am so lucky that life chose such a beautiful pairing!

Then I want to explicitly thank Giuseppe Calajò, which strongly encouraged me to apply for a PhD with Peter Rabl and which was always very supportive, especially in the early stage. Then, of course, Peter Rabl for being the possibly best supervisor ever. He really had a major role in my PhD realisation, and I am grateful for all the help that he provided to me, and especially for trying to wash away my sloppyness and to make me a more ordered and clean mind (hopefully!). Special thanks to the whole Rabl group, which was my home in the last years: thanks to Yuri, Julian and Tuomas for all the discussions, arguments and for supporting but also bearing me in all our scientific fights. Moreover thanks for all the special moments in which we have been all together, like all our trips around the world or all the nights spent trying to climb at the boulderbar, but then ended up discussing about some field theory related problem.

Thanks to my friends Yijian and Mr. Luke with whom I shared the organization of the 2017 CoQus-summerschool, I owe them 6 apples. And also special thanks to Jakob and Hardy, the German ambassadors of my mind. Thanks for all the Gürtel moments that we shared all together.

Thanks to all the CoQus and ATI friends, with special attention to the Entdenker and their celebrated Christmas show. Thanks for bringing the quality music to the austere halls of science (even fighting against censorship, when "gay bar" became $\hbar$).

Thanks to all the friend related or not related to science, thanks to the Spanish crew that first introduced me to the city from Burggasse "123", thanks to the little Italy club for all the gossips and all the culinary experiences, thanks to all the "music friends" with whom we shared so many

beautiful moments of creativity and fun. Special thanks to David, the living room jam sessions together and all the breakfast-brunch-lunch-dinner on the amazing Burggasse balcony.

Thanks for all the trips and journeys, from the Balkans to Greece, from Spain to Sicily, from America to China. Special mention for the Krk trip and the Vigo Meano experience.

Thanks to all my Trento-friends and the association Megaras, that, even though most of the time they weren't physically with me, I always felt them close on my side and I always carry all of them in my heart. Special thanks to Torbisi that at a certain point was even physically in Vienna. We all know now that Torrisi is a Sicilian surname.

Thanks to my parents and my whole family, that always supported and encouraged me against any doubt and any difficulty.

Thanks to Vienna, that, despite all my complains, always managed to take care of all my needs.

Finally, thanks to all the people I met for being there.

Appendix A

Transverse modes and Laplace Green's function

A.1 Transverse and longitudinal projectors

Here we construct explicitly the transverse and longitudinal delta functions (or projectors). This correspond to finding the *Helmholtz decomposition* [22] for a vector field

$$\vec{V}(x) = \vec{\nabla}\Phi(x) + \vec{\nabla} \times \vec{A}(x), \tag{A.1}$$

where we use $x = (x^1, x^2 \ldots x^D)$ to indicate generically a D-dimensional coordinate.

A key step is to consider the normalised eigenfunctions of the Laplace operator

$$-\nabla^2 \phi_k(x) = \omega_k^2 \phi_k(x), \tag{A.2}$$

from which we immediately get the Laplace Green's function

$$G(x,y) = \sum_k \frac{\phi_k^*(x)\phi_k(y)}{\omega_k^2}. \tag{A.3}$$

We point out that in order to solve for the Laplace eigenfunctions one must specify the boundary conditions. But then the whole discussion proceeds independently on this choice.

A suitable basis on which we can decompose any given smooth vector field is

$$\vec{v}_{\lambda,k}(x) = \begin{cases} (\phi_k(x), 0, 0 \ldots) \\ (0, \phi_k(x), 0 \ldots) \\ (0, 0, \phi_k(x) \ldots) \\ \quad \vdots \end{cases} \tag{A.4}$$

where we introduced the polarization index $\lambda = 1, 2, 3 \ldots D$. It is clear that

$$\sum_{\lambda,k} v^i_{\lambda,k}(x) v^j_{\lambda,k}(y) = \delta_{ij} \delta^{(D)}(x - y). \tag{A.5}$$

We introduce now the *longitudinal modes*

$$\vec{g}_k(x) = \frac{\vec{\nabla}\phi_k(x)}{\omega_k}, \tag{A.6}$$

where we notice that they have only one polarization. We define the longitudinal delta function as

$$\begin{aligned} \delta^{\parallel}_{ij}(x, y) &= \sum_k (g^i_k(x))^* g^j_k(y) = \frac{\partial^2}{\partial x^i \partial y^j} \sum_k \frac{\phi^*_k(x)\phi_k(y)}{\omega^2_k} \\ &= \frac{\partial^2}{\partial x^i \partial y^j} G(x, y). \end{aligned} \tag{A.7}$$

When the system has vanishing boundary conditions (Dirichtlet or von Neumann in a bounded domain, or simply vanishing at infinity in an unbounded space), the longitudinal delta function is a projector, with the property $P^2 = P$,

$$\begin{aligned} \sum_l \int ds \delta^{\parallel}_{il}(x, s)\delta^{\parallel}_{lj}(s, y) &= \sum_l \int ds \frac{\partial^2}{\partial x^i \partial s^l} \sum_k \frac{\phi^*_k(x)\phi_k(s)}{\omega^2_k} \frac{\partial^2}{\partial s^l \partial y^j} \sum_{k'} \frac{\phi^*_{k'}(s)\phi_{k'}(y)}{\omega^2_{k'}} \\ &= \sum_{kk'} \sum_l \frac{\partial^2}{\partial x^i \partial y^j} \frac{\phi_k(x)\phi_{k'}(y)}{\omega^2_k} \frac{1}{\omega^2_{k'}} \int ds \frac{\partial}{\partial s^l}\phi_k(s) \frac{\partial}{\partial s^l}\phi_{k'}(s) \\ &= \delta^{\parallel}_{ij}(x, y), \end{aligned} \tag{A.8}$$

where we used $\sum_l -\partial^2/\partial(s^l)^2 \phi_k(s) = -\nabla^2_s \phi_k(s) = \omega^2_k \phi_k(s)$, and $\int ds \phi_k(s)\phi_{k'}(s) = \delta_{kk'}$. It is then straightforward to see that it projects any given vector field on the longitudinal subspace of vector fields with vanishing rotor, in a symbolic way, $\delta^{\parallel} \star \vec{V} = \vec{V}^{\parallel}$, where $\vec{\nabla} \times \vec{V}^{\parallel} = 0$.

The transverse delta function is simply given by its own complement with respect to the identity

(the Dirac's delta function)

$$\begin{aligned}\delta^{\perp}_{ij}(x,y) &= \delta_{ij}\delta^{(D)}(x-y) - \delta^{\parallel}_{ij}(x,y) \\ &= \delta_{ij}\delta^{(D)}(x-y) - \frac{\partial^2}{\partial x^i \partial y^j} G(x,y).\end{aligned} \tag{A.9}$$

Also in this case, it is straightforward to check that the transverse delta function is a projector on the subspace of vector fields with vanishing divergence, in a symbolic way, $\delta^{\perp} \star \vec{V} = \vec{V}^{\perp}$, where $\vec{\nabla} \cdot \vec{V}^{\perp} = 0$.

A.2 The Laplace Green's function in bounded domains

We briefly review here the main points related to the Laplace Green's function in three dimensions:

$$-\nabla^2 G(x,y) = \delta^{(3)}(x-y). \tag{A.10}$$

In unbounded domain, i.e. $\mathbf{D} = \mathbb{R}^3$, imposing vanishing boundary conditions at infinity, it is given by the well known Coulomb potential [119]

$$G_{\text{unb.}}(x,y) = -\frac{1}{4\pi}\frac{1}{|x-y|}. \tag{A.11}$$

When we consider a bounded domain $\mathbf{D} \subset \mathbb{R}^3$, with vanishing boundary condition,

$$\begin{aligned}-\nabla^2 G(x,y) &= \delta^{(3)}(x-y) \quad x \in \mathbf{D} \\ G(x,y) &= 0 \quad x \in \partial\mathbf{D},\end{aligned} \tag{A.12}$$

the new Green's function can be written in general as

$$G(x,y) = G_{\text{unb.}}(x,y) + g(x,y), \tag{A.13}$$

where $g(x,y)$ is itself a solution of the Poisson equation

$$\begin{aligned}-\nabla^2 g(x,y) &= 0 \quad x \in \mathbf{D} \\ g(x,y) &= -G_{\text{unb.}}(x,y) \quad x \in \partial\mathbf{D}.\end{aligned} \tag{A.14}$$

It is possible to show that such a solution exists as the solution generated by an external charge distribution which mirrors the internal one [119],

$$g(x,y) = \int_{\mathbb{R}^3 \setminus \mathbf{D}} \tilde{\rho}(s,y) G_{\text{unb.}}(x,s) d^3 s. \tag{A.15}$$

A.3 The Laplace Green's function between parallel mirrors

In this section we consider the "capacitor problem", where we need to compute the electrostatic potential from the Laplace Green's function assuming its domain is bounded on the z-axis by the two capacitor plates. We assume that the capacitor plates are grounded and built out of ideal metal, which means that they act as perfect mirrors for the electromagnetic field, imposing zero field and zero potential on the boundary. In the simplest case of metallic (Dirichtlet) boundary conditions along the z-axis and periodic boundaries along the (x, y)-plane it is possible to find a general solution of this problem, involving the Green's function of the Laplacian. Notice that here we restore the standard three-dimensional notation $\vec{r} = (x, y, z)$,

$$-\nabla^2 G(\vec{r}, \vec{r}') = \delta^{(3)}(\vec{r} - \vec{r}'). \tag{A.16}$$

Applying Fourier transform with respect to (x, y) on both sides of equation (A.16) we obtain

$$\left(-\partial_z^2 + k^2\right) G_k(z, z') = \delta(z - z'), \tag{A.17}$$

with the metallic boundary conditions

$$G_k(z = 0, z') = G_k(z = d, z') = 0. \tag{A.18}$$

Here we used $k = \sqrt{k_x^2 + k_y^2}$ and d is distance between the capacitor plates.

The solution of Eq. (A.17) is well know in the literature [119] and is given by:

$$G_k(z, z') = g_k(z, z')\Theta(z - z') + g_k(z', z)\Theta(-(z - z')), \tag{A.19}$$

where

$$g_k(z, z') = \frac{e^{-k(z-z')}}{2k} - \frac{1}{2k\sinh(kd)}\left[\sinh(kz)e^{-k(d-z')} + \sinh(k(d-z))e^{-kz'}\right], \tag{A.20}$$

and $\Theta(z)$ is the usual *Heaviside* step-function. It is straightforward to verify that this is the solution of (A.17) with the correct boundary conditions, in the interval $z, z' \in [0, d]$. Thus the total Green's function is

$$G(\vec{r}, \vec{r}') = \frac{1}{L^2}\sum_{k_x, k_y} e^{\vec{k}_\parallel \cdot (\vec{r} - \vec{r}')} G_k(z, z'), \tag{A.21}$$

where L^2 is the area of the square plates and $\vec{k}_\parallel = (k_x, k_y, 0)$. To compute the Green's function in

real space we write

$$G_k(z,z') = \frac{1}{2k}\sum_{n\in\mathbb{Z}}\left(e^{-k|z-z'+2dn|} - e^{-k|z+z'+2dn|}\right), \tag{A.22}$$

where we used the expansion

$$\frac{1}{\sinh(kd)} = 2\sum_{n=0}^{\infty} e^{-kd(2n+1)}. \tag{A.23}$$

Continuing the calculation, we use the following identity

$$\frac{e^{-k|z|}}{k} = \int dxdy \frac{e^{i\vec{k}_\parallel\cdot\vec{r}}}{r}. \tag{A.24}$$

Altogether, we then obtain

$$G_k(z,z') = \sum_{n\in\mathbb{Z}}\int dxdy\left(\frac{e^{i\vec{k}_\parallel\cdot(\vec{R}+2\vec{l}n)}}{|\vec{R}+2\vec{l}n|} - \frac{e^{i\vec{k}_\parallel\cdot(\vec{R}_*+2\vec{l}n)}}{|\vec{R}_*+2\vec{l}n|}\right), \tag{A.25}$$

where $\vec{l}=(0,0,d)$, $\vec{R}=(x,y,z-z')$ and $\vec{R}_*=(x,y,z+z')$. Thus the Green's function in real space is

$$G(\vec{r},\vec{r}') = \frac{1}{L^2}\sum_{n\in\mathbb{Z}}\int dxdy\sum_{k_x,k_y}\left(\frac{e^{i\vec{k}_\parallel\cdot(\vec{r}-\vec{r}')}}{|\vec{r}+2\vec{l}n|} - \frac{e^{i\vec{k}_\parallel\cdot(\vec{r}_*-\vec{r}')}}{|\vec{r}_*+2\vec{l}n|}\right), \tag{A.26}$$

where we used the fact that $\vec{k}_\parallel\cdot(\vec{r}-\vec{r}'+2\vec{l}n) = \vec{k}_\parallel\cdot(\vec{r}-\vec{r}')$, and $\vec{r}_* = (x,y,-z)$. When we consider periodic boundary conditions along the (x,y) plane we can conclude the calculation using the *Poisson formula* from the theory of distributions, which states that

$$\frac{1}{L^2}\sum_{k_x,k_y} e^{i\vec{k}_\parallel\cdot\vec{r}} = \sum_{\vec{m}\in\mathbb{Z}^2}\delta^{(2)}(\vec{r}_\parallel - L\vec{m}). \tag{A.27}$$

The Green's function of Eq. (A.16) with metallic boundaries along z and periodic boundary conditions along (x,y) is

$$G(\vec{r},\vec{r}') = \sum_{m\in\mathbb{Z}^3}\left(\frac{1}{|\vec{r}-\vec{r}'-\vec{h}|} - \frac{1}{|\vec{r}-\vec{r}'_*-\vec{h}|}\right), \tag{A.28}$$

where $\vec{h} = (Lm_x, Lm_y, 2dm_z)$

In our particular case we give the charge distribution as a collection of point-like dipoles,

$$\rho(\vec{r}) = \sum_{i=1}^{N} q_i\vec{\xi}_i\cdot\nabla\delta^{(3)}(\vec{r}-\vec{r}_i), \tag{A.29}$$

where q_i, $\vec{\xi}_i$ and $\vec{r}_i$ are the electric charge, the dipole moment and the position of the $i-th$ dipole,

respectively. The general expression for the Coulomb potential is now

$$\phi(\vec{r}) = \frac{1}{\epsilon_0} \sum_{i=1}^{N} q_i \vec{\xi}_i \cdot \nabla_i G(\vec{r}, \vec{r}_i), \tag{A.30}$$

where ∇_i is the gradient with respect the positions of the dipoles $\vec{r}_i$. Now we can write down the full local field

$$\vec{E}_{local} = -\nabla \phi(\vec{r}), \tag{A.31}$$

which is given by

$$\vec{E}_{local}(\vec{r}) = -\frac{1}{4\pi\epsilon_0} \sum_{\vec{m}\in\mathbb{Z}^3} \sum_{i=1}^{N} \nabla \left(\nabla_i \cdot \left[\frac{q_i \vec{\xi}_i}{\left|\vec{r} - \vec{r}_i - \vec{h}\right|} + \frac{e_i \vec{\xi}_{*i}}{\left|\vec{r} - \vec{r}_{*i} - \vec{h}\right|} \right] \right), \tag{A.32}$$

where $\vec{h} = (Lm_x, Lm_y, 2dm_z)$, $\vec{\xi}_{*i} = (-\xi_i^x, -\xi_i^y, \xi_i^z)$ and $\vec{r}_{*i} = (x_i, y_i, -z_i)$. This compact expression is nothing else but the field generated by the N dipoles, plus the field generated by the infinite series of images of each dipole reflected by the metallic boundaries along z, plus the field generated by the infinite copies of the system because of the periodic boundaries along (x, y). For our aims we don't need such a general expression and we can simplify it just assuming that the dipole moment is always directed along the z-axis and that all the dipoles have the same charge q. Then, only the component along z of the local field evaluated at the position of the $i-th$ dipole becomes relevant for our discussion. It's worth noticing that when we used the Poisson formula (A.27) we artificially introduced in the system the field generated by infinite copies of the system in adjacent cells. This is clearly a consequence of the periodic boundary conditions along the plane. Relaxing this assumption to an infinite plane with vanishing field at infinity we can use an integral instead of the Fourier sum

$$\frac{1}{L^2} \sum_{k_x, k_y} \longmapsto \frac{1}{(2\pi)^2} \int dk_x dk_y, \tag{A.33}$$

and the Poisson formula simplifies to

$$\frac{1}{(2\pi)^2} \int_{\mathbb{R}^2} dk_x dk_y \; e^{i\vec{k}_\parallel \cdot \vec{r}} = \delta^{(2)}(\vec{r}_\parallel). \tag{A.34}$$

A.3.1 Dipoles along z

For the sake of simplicity, in this section we define $\xi = \xi^z$ and $q = q_i$. In the infinite plane the local field becomes the same as (A.32), but without the summation over the infinite adjacent copies. We can rewrite it in a nice expression, which is just the sum of the field generated by the dipoles in free

space plus the field generated by an infinite series of image dipoles,

$$E^z_{local}(\vec{r}_i) = \frac{q}{4\pi\epsilon_0}\left(\sum_{j\neq i} D_{i,j}\xi_j + \sum_{i,j}\sum_{n>0}(F^{n,+}_{i,j} + F^{n,-}_{i,j})\xi_j\right), \tag{A.35}$$

where

$$D_{i,j} = \frac{3(z_i - z_j)^2}{|\vec{r}_i - \vec{r}_j|^5} - \frac{1}{|\vec{r}_i - \vec{r}_j|^3}, \tag{A.36}$$

$$F^{n,+}_{i,j} = \frac{3(z_i - \zeta^u_{j,n})^2}{|\vec{r}_i - \vec{R}^u_{j,n}|^5} - \frac{1}{|\vec{r}_i - \vec{R}^u_{j,n}|^3}, \tag{A.37}$$

$$F^{n,-}_{i,j} = \frac{3(z_i + \zeta^l_{j,n})^2}{|\vec{r}_i - \vec{R}^l_{j,n}|^5} - \frac{1}{|\vec{r}_i - \vec{R}^l_{j,n}|^3}. \tag{A.38}$$

Here $\vec{R}^{u/l}_n = (x, y, \pm\zeta^{u/l}_n)$, $\zeta^{u/l}_{j,n}$ is the z-coordinate for the n-th image of the j-th dipole on the upper/lower plate, respectively, and $\vec{u}_z$ is the unit vector along z. The explicit expression for $\zeta^{u/l}_{j,n}$ is:

$$\begin{aligned} \zeta^u_{j,n} &= nl_c + (-1)^n z_i \qquad \text{upper plate,} \\ \zeta^l_{j,n} &= nl_c - (-1)^n z_i \qquad \text{lower plate.} \end{aligned} \tag{A.39}$$

Here we have assumed that the origin of the coordinate system is located in the center of the cavity.

A.3.2 Tilted dipoles

Here we consider again the electric field only along the z axis, but we allow that all the dipole moments are tilted by the same azimuthal angle θ, pointing in the positive x direction. Moreover, we use a different scheme to organize the contributions coming from the images. Instead of classifying the images as "upper/lower" images (like from the upper/lower plates), we classify them as "same/opposite" images. The dipole moment of each dipole can be written as

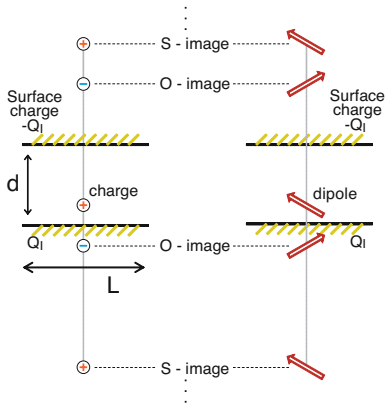

Figure A.1: Schematic representation of the charge/dipole and its images. This figure is taken from [120].

$$\vec{\xi_i} = \xi_i(\sin(\theta),\ 0,\ \cos(\theta)). \tag{A.40}$$

Now we must consider the component of the local field along the dipole (which is not any more fully oriented along the z axis). To evaluate it we just rotate the frame, in such a way that the z axis coincides with the direction of the dipole moments. Thus the local field is still written as

$$E_{local}(\vec{r}_i) = \frac{q}{4\pi\epsilon_0}\left(\sum_{j\neq i} D_{i,j}\xi_j + \sum_{i,j}\sum_{n\in\mathbb{Z}/\{0\}} (F_{i,j}^{n,S} + F_{i,j}^{n,O})\xi_j\right). \tag{A.41}$$

The bare dipole dipole interaction is given by

$$D_{i,j} = \frac{3((z_i - z_j)\cos(\theta) + (x_i - x_j)\sin(\theta))^2}{|\vec{r}_i - \vec{r}_j|^5} - \frac{1}{|\vec{r}_i - \vec{r}_j|^3}, \tag{A.42}$$

the S images contribution is given by

$$F_{i,j}^{n,S} = \frac{3((z_i - z_j + 2dn)\cos(\theta) + (x_i - x_j)\sin(\theta))^2}{|\vec{r}_i - \vec{r}_j - \vec{h}_n|^5} - \frac{1}{|\vec{r}_i - \vec{r}_j - \vec{h}_n|^3}, \tag{A.43}$$

and the O images one is

$$F_{i,j}^{n,O} = \frac{3((z_i + z_j + 2dn)\cos(\theta) + (x_i - x_j)\sin(\theta))((z_i + z_j + 2dn)\cos(\theta) - (x_i - x_j)\sin(\theta))}{|\vec{r}_i - \vec{r}_{*j} - \vec{h}_n|^5} - \frac{1}{|\vec{r}_i - \vec{r}_{*j} - \vec{h}_n|^3}, \tag{A.44}$$

where $\vec{h}_n = (0, 0, 2dn)$ and $\vec{r}_* = (x, y, -z)$.

A.3.3 Homogeneous induced charge

From the local field we can also evaluate the induced charge Q_I on the lower plate, using

$$Q_I = \int dxdy\ \sigma(x, y) = \int dxdy\ \epsilon_0 E_{local}^z(x, y, z = 0). \tag{A.45}$$

Note that the charge evaluated at d is nothing else than $-Q_I$, for symmetry (for this calculation we considered the origin of the reference frame centred on the lower plate). This calculation has been performed in the infinite capacitor case, but the same procedure holds also in the finite capacitor with periodic boundaries (one has just to be careful with the definition of delta functions and Fourier

transform). To do this we use the exact expression (A.30). Together with the fact that

$$\frac{1}{(2\pi)^2}\int dxdye^{\vec{k}\cdot\vec{r}} = \delta^{(2)}(\vec{k}), \tag{A.46}$$

and

$$\frac{1}{L^2}\sum_{k_x,k_y} \longmapsto \frac{1}{(2\pi)^2}\int dk_x dk_y \tag{A.47}$$

we get

$$Q_I = -q\sum_{i=1}^{N}\xi_i\cos(\theta)\partial_z\partial_{z_i}G_{k=0}(z,z_i)\Big|_{z=0}, \tag{A.48}$$

where we used $\vec{\xi} = (\sin(\theta)\xi, 0, \cos(\theta)\xi)$, as in the previous section. To evaluate $G_{k=0}$ we use

$$\lim_{k\longrightarrow 0} G_k(z,z_i) = \frac{(z+z_i-|z-z_i|)}{2} - \frac{zz_i}{d}, \tag{A.49}$$

from which we immediately obtain

$$Q_I = q\sum_i \frac{\xi_i\cos(\theta)}{d}. \tag{A.50}$$

Thus the induced current in the circuit, due to the dipole dynamics is

$$I_{ext} = \dot{Q}_i = q\sum_i \frac{\dot{\xi}_i\cos(\theta)}{d}. \tag{A.51}$$

We notice that this expression is independent of the choice of the boundaries along the (x,y) plane, and indeed, in the case of a finite system with periodic boundary conditions, it doesn't depend on the planar size L.

Appendix B

An alternative derivation of the dipolar Hamiltonian

Let's consider the electromagnetic Lagrangian density in the Coulomb gauge in SI units (we use here, for brevity, Einstein sum convention)

$$\mathcal{L} = \frac{\varepsilon_0}{2}\left(\partial_t A_i\right)^2 + \frac{\varepsilon_0 c^2}{2} A_i \nabla^2 A_i + \mathcal{L}_{matter} + \mathcal{L}_{coulomb} + J_i(t,\vec{x})A_i(t,\vec{x}), \tag{B.1}$$

where, for point-like particles

$$\vec{J}(t,\vec{x}) := \sum_n q_n \dot{\vec{x}}_n \delta^{(3)}(\vec{x} - \vec{x}_n), \tag{B.2}$$

and $\mathcal{L}_{coulomb}$ contains the usual direct instantaneous Coulomb interaction. When we consider the matter system represented by an ensemble of dipoles, we can introduce the *dipole approximation*, for which we assume that the negative charges of the microscopic dipoles can be displaced from the positive nuclei only for a very short length, which means that the position of the negative charge is roughly the position of its nucleus, thus

$$\delta^{(3)}(\vec{x} - \vec{x}_n) \simeq \delta^{(3)}(\vec{x} - \vec{R}_n), \tag{B.3}$$

where $\vec{R}_n$ is the fixed position of the $n-th$ nucleus. Under this assumption we have the following identity:

$$\partial_t \vec{P}(t,\vec{x}) \simeq \vec{J}(t,\vec{x}), \tag{B.4}$$

where

$$\vec{P}(t,\vec{x}) = \sum_n q_n \left(\vec{x}_n(t) - \vec{R}_n\right) \delta^{(3)}(\vec{x} - \vec{R}_n) \tag{B.5}$$

is the polarization vector related to the matter. The light-matter interaction is now described by the Lagrangian density

$$\mathcal{L}_I \simeq \partial_t P_i(t,\vec{x}) A_i(t,\vec{x}). \tag{B.6}$$

We can make a gauge transformation

$$\mathcal{L} \longmapsto \mathcal{L} - \frac{d}{dt}\left(P_i A_i\right). \tag{B.7}$$

At this point it's worth noticing that the vector potential A_i is a transverse vector field, because of the Coulomb gauge $\partial^i A_i(t,\vec{r}) = 0 \Longleftrightarrow k^i A_i(t,\vec{k})$. This means that all the longitudinal terms in the Lagrangian density drop out when we integrate over the whole volume. Therefore, we are allowed to write

$$P_i \dot{A}_i = P_i^{\perp} \dot{A}_i, \tag{B.8}$$

where $P_i^{\perp}$ is the projected transverse polarization, which is defined by taking the convolution between the polarization vector and the transverse delta function defined in Eq. (1.14). In free space it takes the form

$$P_i^{\perp}(\vec{x}) = \frac{2}{3}P_i(\vec{x}) - \frac{1}{4\pi}\int d^3r' \left[\frac{\delta_{i,j}}{|\vec{x}-\vec{x}'|^3} - \frac{3(\vec{x}-\vec{x}')_i(\vec{x}-\vec{x}')_j}{|\vec{x}-\vec{x}'|^5}\right] P_j(\vec{x}'). \tag{B.9}$$

Then we switch to the Hamiltonian formalism:

$$D_i := \varepsilon_0 \dot{A}_i + P_i^{\perp}, \tag{B.10}$$

$$\Pi_i := \frac{\partial \mathcal{L}_{matter}}{\partial \dot{P}_i}, \tag{B.11}$$

$$\mathcal{H} = \frac{(D_i - P_i^{\perp})^2}{2\varepsilon_0} - \frac{\varepsilon_0 c^2}{2} A^i \nabla^2 A_i + \mathcal{H}_{matter} + \mathcal{H}_{coulomb}. \tag{B.12}$$

Under the *dipole approximation* we can write

$$\mathcal{H}_{coulomb} \simeq \frac{1}{2\varepsilon_0}(P^2 - P_i P_i^{\perp}), \tag{B.13}$$

and

$$\mathcal{H} = \frac{D_i^2}{2\varepsilon_0} - \frac{\varepsilon_0 c^2}{2} A^i \nabla^2 A_i + \mathcal{H}_{matter} - \frac{D_i P_i^{\perp}}{\varepsilon_0} + \frac{1}{2\varepsilon_0} P_i^2, \tag{B.14}$$

which is another way to express the result in Eq. (1.37).

Appendix C

Matrix element inequality

We consider here the two quantities

$$\begin{aligned}\Delta_\xi &= \frac{\sum_{n>1} |\langle 1|\xi|n\rangle|^2 + \sum_{n>1} |\langle 0|\xi|n\rangle|^2}{2|\langle 1|\xi|0\rangle|^2},\\ \Delta_p &= \frac{\sum_{n>1} |\langle 1|p|n\rangle|^2 + \sum_{n>1} |\langle 0|p|n\rangle|^2}{2|\langle 1|p|0\rangle|^2}.\end{aligned} \tag{C.1}$$

By definition $\Delta_\xi \geq 0$, $\Delta_p \geq 0$.

Assuming the dipole's Hamiltonian can be written as $H_d = p^2/(2m) + V(\xi)$, where $V(\xi)$ is a bounded from below potential for which $\lim_{\xi\to\pm\infty} V = +\infty$, we want to prove that

$$\Delta_p \geq 1. \tag{C.2}$$

First we rewrite

$$\Delta_p = \Delta_\xi + \Delta_{\text{res}}, \tag{C.3}$$

where the "residual" quantity is

$$\Delta_{\text{res}} = \frac{\sum_{n>1}\left[\frac{(\omega_{n0}+\omega_{10})}{\omega_{10}}(\omega_{n0}-\omega_{10})|\xi_{n0}|^2 + \frac{(\omega_{n1}+\omega_{10})}{\omega_{10}}(\omega_{n1}-\omega_{10})|\xi_{n1}|^2\right]}{2\omega_{10}|\xi_{10}|^2}. \tag{C.4}$$

Using $(\omega_{n0}+\omega_{10})/\omega_{10}, (\omega_{n1}+\omega_{10})/\omega_{10} \geq 1$ we have

$$\Delta_{\text{res}} \geq -\Delta_\xi + \frac{\sum_{n>1}\left[\omega_{n0}|\xi_{n0}|^2 + \omega_{n1}|\xi_{n1}|^2\right]}{2\omega_{10}|\xi_{10}|^2}. \tag{C.5}$$

In the last term we can add and remove $\omega_{10}|\xi_{10}|^2$ in the numerator and then use the TRK sum rule to obtain

$$\Delta_{\text{res}} \geq -\Delta_\xi + \frac{1}{2m\omega_{10}|\xi_{10}|^2}. \tag{C.6}$$

Using again the TRK sum rule to say that $\omega_{10}|\xi_{10}|^2 \leq 1/(2m)$ we have

$$\Delta_{\text{res}} \geq -\Delta_\xi + 1, \tag{C.7}$$

which immediately implies

$$\Delta_p \geq 1. \tag{C.8}$$

Appendix D

Holstein-Primakoff approximation

The Holstein-Primakoff map for the dipoles reduces the collective spin operators to bosonic operators of a single harmonic oscillator. This is an exact map and indeed the bosonic representation of spin operators is strongly nonlinear. Consider the spin-S operators

$$\begin{aligned}\hat{S}^2|S,m\rangle &= S(S+1)|S,m\rangle,\\ \hat{S}_z|S,m\rangle &= m|S,m\rangle,\\ \hat{S}_\pm|S,m\rangle &= \sqrt{S(S+1)-m(m\pm 1)}|S,m\rangle.\end{aligned} \tag{D.1}$$

We can then define $S_x = (S_- + S_+)/2$, $S_y = i(S_- - S_+)/2$. The total spin operator is then given by $S^2 = S_x^2 + S_y^2 + S_z^2$. The spin operators S_x, S_y, S_z obey the $SU(2)$ algebra

$$[S_\alpha, S_\beta] = i\epsilon^{\alpha\beta\gamma}S_\gamma, \tag{D.2}$$

from which we also obtain

$$[S_+, S_-] = 2S_z. \tag{D.3}$$

One can show [121] that, introducing the bosonic operators $[b, b^\dagger] = 1$, one can represent such spin operators and their algebra with

$$\begin{aligned}\hat{S}_z &= b^\dagger b - S,\\ \hat{S}_- &= \sqrt{2S}\sqrt{1-\frac{b^\dagger b}{2S}}b,\\ \hat{S}_+ &= \sqrt{2S}b^\dagger\sqrt{1-\frac{b^\dagger b}{2S}},\end{aligned} \tag{D.4}$$

provided that $\langle b^\dagger b\rangle \leq 2S$.

If we then assume that the spin is almost polarized $\langle S_z\rangle \approx -S$, with just small fluctuations

around it, we can expand these operators in $b^\dagger b/(2S)$. To lowest order we obtain

$$\begin{aligned} S_z &\simeq b^\dagger b - S, \\ S_x &\simeq \frac{\sqrt{2N}}{2}(b + b^\dagger), \\ S_y &\simeq -i\frac{\sqrt{2N}}{2}(b - b^\dagger). \end{aligned} \tag{D.5}$$

Appendix E

Macroscopic dielectrics

Here we briefly review the electrostatic properties of a dielectric medium, treated as a polarizable object. Let's start from the most generic electrostatic problem:

$$\nabla^2\Phi(\vec{r}) = \frac{\rho(\vec{r})}{4\pi\epsilon_0}. \tag{E.1}$$

Using the Green function of the Poisson operator, we have immediately the general solution for any integrable distribution ρ :

$$\Phi(\vec{r}) = \frac{1}{4\pi\epsilon_0}\int d^3r' \ \frac{\rho(\vec{r}')}{|\vec{r}-\vec{r}'|}. \tag{E.2}$$

Using an expansion in spherical harmonics of the Green's function $\frac{1}{|\vec{r}-\vec{r}'|}$, we express the general solution of the Poisson equation as a series expansion (multipole expansion); the first two terms of the expansion represent the monopole (the Coulomb potential) and the dipole contribution:

$$\Phi(\vec{r}) \simeq \frac{1}{4\pi\epsilon_0}\left[\frac{q}{r} + \frac{\vec{\mu}\cdot\vec{r}}{r^3} + \cdots\right], \tag{E.3}$$

where $q = \int d^3r \ \rho(\vec{r})$ is the total electric charge, and $\vec{\mu} = \int d^3r \ \vec{r}\rho(\vec{r})$ is the dipole moment of the charge distribution. From now we will consider just distributions of charge in which only the first two terms of the multipole expansion are non negligible. Now let's consider a macroscopic dielectric. It consists of microscopic constituents (atoms or molecule) that we will model as dipoles. By superposition, the total electric potential in the material is given by:

$$\Phi(\vec{r}) = \sum_i \Phi_i(\vec{r},\vec{r}_i), \tag{E.4}$$

where the sum runs over all the microscopic constituents. The potential generated by every microscopic constituent is :

$$\Phi_i(\vec{r},\vec{r}_i) = \frac{1}{4\pi\epsilon_0}\left[\frac{q_i}{|\vec{r}-\vec{r}_i|} + \frac{\vec{\mu}_i\cdot(\vec{r}-\vec{r}_i)}{|\vec{r}-\vec{r}_i|^3}\right]. \tag{E.5}$$

What we want to do now is to pass from a discrete microscopic description to a continuous one, which is more appropriate to discuss the macroscopic problem. For every microscopic constituent we can define a microscopic density of charge and density of polarization, defined in the characteristic volume ΔV_i containing the i-th microscopic constituent:

$$\begin{aligned} \rho(\vec{r}_i) &= \frac{q_i}{\Delta V_i}, \\ \vec{P}(\vec{r}_i) &= \frac{\vec{\mu}_i}{\Delta V_i}. \end{aligned} \tag{E.6}$$

The potential in the dielectric becomes:

$$\Phi(\vec{r}) = \sum_i \frac{1}{4\pi\epsilon_0} \left[\frac{\rho(\vec{r}_i)}{|\vec{r} - \vec{r}_i|} + \frac{\vec{P}(\vec{r}_i) \cdot (\vec{r} - \vec{r}_i)}{|\vec{r} - \vec{r}_i|^3} \right] \Delta V_i. \tag{E.7}$$

Considering the sum goes to infinity and each microscopic volume go to zero, $\Delta V_i \to 0$, we can replace the sum as an integral:

$$\Phi(\vec{r}) = \int d^3r' \frac{1}{4\pi\epsilon_0} \left[\frac{\rho(\vec{r}')}{|\vec{r} - \vec{r}'|} + \frac{\vec{P}(\vec{r}') \cdot (\vec{r} - \vec{r}')}{|\vec{r} - \vec{r}'|^3} \right]. \tag{E.8}$$

Using

$$\frac{\vec{r} - \vec{r}'}{|\vec{r} - \vec{r}'|^3} = \vec{\nabla}' \left(\frac{1}{|\vec{r} - \vec{r}'|} \right), \tag{E.9}$$

integrating by parts and considering the usual Gauss theorem for volume integrals of divergences, we obtain

$$\Phi(\vec{r}) = \frac{1}{4\pi\epsilon_0} \int_V d^3r' \left[\frac{\rho(\vec{r}')}{|\vec{r} - \vec{r}'|} - \frac{\vec{\nabla}' \cdot \vec{P}(\vec{r}')}{|\vec{r} - \vec{r}'|} \right] + \frac{1}{4\pi\epsilon_0} \int_{\partial V} d\vec{S}' \cdot \frac{\vec{P}(\vec{r}')}{|\vec{r} - \vec{r}'|}. \tag{E.10}$$

The first two terms are, respectively, the free charge bulk contribution and the dipole density bulk contribution. The last term is a surface term, coming from the accumulated charge on the boundary ∂V enclosing the volume V in which the dielectric is defined. From this point on we will always consider the case of a charge-neutral medium, so $\rho = 0$. The total electric field inside the dielectric can be written as

$$\vec{E} = \vec{E}_{bulk} + \vec{E}_{surface}, \tag{E.11}$$

where

$$\vec{E}_{bulk} = \frac{1}{4\pi\epsilon_0} \int_V d^3r' \frac{\vec{\nabla}' \cdot \vec{P}(\vec{r}')}{|\vec{r} - \vec{r}'|^3} (\vec{r} - \vec{r}'), \tag{E.12}$$

and

$$\vec{E}_{surface} = -\frac{1}{4\pi\epsilon_0} \int_{\partial V} d\vec{S}' \cdot \frac{\vec{P}}{|\vec{r} - \vec{r}'|^3} (\vec{r} - \vec{r}'). \tag{E.13}$$

From these formula it seems that in a homogeneously polarised medium $\vec{E}_{bulk} = 0$, since the

polarization in the bulk does not depend on the position, $\vec{\nabla} \cdot \vec{P}(\vec{r}) = 0$. However we must consider the correction due to the discrete orgin of our medium, which is a collection of point like dipoles. So the vanishing contribution from the bulk is an artefact of the continuum description, and it must be corrected by introducing the famous "Lorentz sphere", [39], correcting the bulk field to

$$\vec{E}_{bulk} \approx -\frac{\vec{P}}{3\epsilon_0}, \tag{E.14}$$

where $\vec{P}$ is the homogeneous polarization, oriented on a certain fixed direction.

In the following sections we discuss the results for a dielectric sphere and a dielectric thin, large slab. These are two very paradigmatic examples that help to clarify the role of the η-parameter in the main text.

E.1 The macroscopic field inside a polarized sphere

We consider a polarized sphere of radius R. The polarization is homogeneous and directed only along z. The total electric field along the z-axis is given by

$$E_z^{sphere} = -\frac{P}{3\epsilon_0} + E_z^{surface}, \tag{E.15}$$

where

$$E_z^{surface}(\vec{r}) = -\frac{1}{4\pi\epsilon_0} \int d\theta d\phi \; R^2 \sin(\theta) \frac{P\cos(\theta)}{|\vec{r} - \vec{R}|^3}(z - Z). \tag{E.16}$$

While it is straightforward to find the solution of this integral when $\vec{r} = 0$ (the field in center of the sphere), the general solution it is not so simple to compute. But there is another way to compute it, which is much easier. The idea is to find first of all the potential and then derive the field. The potential is given by a solution of Poisson equation. Using a general expansion in terms of the Legendre polynomials (which is very suitable because of the cylindric symmetry) and using the constraints given by the boundary conditions, it is possible to find the potential, and so the field, in a very straightforward way. The solution for the field inside of the sphere is (see [122] pag. 142, ex. 3.9)

$$E_z^{surface}(\vec{r}) = +\frac{P}{3\epsilon_0}. \tag{E.17}$$

This means that the total electric field generated by the homogeneous polarised medium inside the sphere is zero

$$E_z^{sphere} = 0. \tag{E.18}$$

E.2 The macroscopic field inside a polarized slab

Here we consider a cylindrical flat slab of dielectric, with very large radius R and very small thickness h. Again, the polarization is homogeneous and directed only along z. The surface contribution is given by

$$E_z^{surface}(\vec{r}) = +2\frac{P}{4\pi\epsilon_0}\int dx'dy' \ \frac{h}{((x-x')^2+(y-y')^2+h^2)^{3/2}}. \tag{E.19}$$

The factor of 2 takes account of the fact that the surface is made by two parallel plates charged with opposite charge, while the '+' sign comes from the fact that we are inside the slab. The integral can be easily computed considering

$$I = \int_A dxdy \ \frac{h}{(x^2+y^2+h^2)^{3/2}} = 2\pi\int_0^{R/h} dr \ \frac{r}{(1+r^2)^{3/2}} = 2\pi\left(1-\frac{1}{(1+R^2/h^2)^{1/2}}\right). \tag{E.20}$$

Taking the limit $R\to\infty$, but keeping h fixed, this integral becomes $I = 2\pi$ So we end up with

$$E_z^{surface}(\vec{r}) = +\frac{P}{\epsilon_0}. \tag{E.21}$$

The total electric field, again considering the Lorentz correction, is

$$E_z^{slab} = +\frac{2}{3}\frac{P}{\epsilon_0}. \tag{E.22}$$

E.3 The macroscopic field inside a polarized elongated-cigar shape

We consider here the same conditions as before. But the dielectric is now a cylinder elongated along z. Evidently we have to repeat the same calculation above, with the only difference that now we take the limit $h \gg R$. Under this condition $I \approx \pi R^2/h^2 \approx 0$, which gives

$$E_z^{cigar} \approx -\frac{1}{3}\frac{P}{\epsilon_0}. \tag{E.23}$$

E.4 Dipole ensemble as a macroscopic dielectric

In this appendix we show how to explicitly connect the results obtained using the standard methods of macroscopic dielectrics to the discrete microscopic model that we use in the main text.

We define the local field as the electric field generated by solving the Poisson equation for the exact microscopic distribution of charge. We will make assumptions only on the shape of the microscopic distribution of charge, but no coarse graining assumption will be made here. We model the dielectric as an ensemble of dipole fixed on a lattice (which may be regular or not regular), the

charge distribution it is given by

$$\rho(\vec{r}) = \sum_i \vec{\mu}_i \cdot \vec{\nabla}\delta^{(3)}(\vec{r} - \vec{r}_i). \tag{E.24}$$

The electric field given by this charge distribution is the well known dipole field:

$$\vec{E}(\vec{r}) = \frac{1}{4\pi\epsilon_0} \sum_i \frac{1}{|\vec{r} - \vec{r}_i|^3} \left[\vec{\mu}_i - \frac{3(\vec{r} - \vec{r}_i) \cdot \vec{\mu}_i}{|\vec{r} - \vec{r}_i|^2} (\vec{r} - \vec{r}_i) \right], \tag{E.25}$$

where the sum over i is in such a way that $\vec{r} \neq \vec{r}_i$. Now we want to find a relation between the polarization density $\vec{P}$ and the field felt by each dipole. Of course for each dipole the field could be very different, so we pose the question in a slightly different way: what is the field felt by each dipole on average in the sample? So we define the spatial average local field

$$\langle \vec{E} \rangle = \frac{1}{N} \sum_{i \neq j} \frac{1}{4\pi\epsilon_0} \frac{1}{|\vec{r}_j - \vec{r}_i|^3} \left[\vec{\mu}_i - \frac{3(\vec{r}_j - \vec{r}_i) \cdot \vec{\mu}_i}{|\vec{r}_j - \vec{r}_i|^2} (\vec{r}_j - \vec{r}_i) \right]. \tag{E.26}$$

We use the assumption of homogeneous polarization and oriented along the z axis, which means

$$\vec{\mu}_i = \mu_0 \hat{u}_z, \tag{E.27}$$

and the electric field is just given by its z-component $\langle E_z \rangle$. The lattice is a simple cubic lattice, with lattice constant r_0. The relation between microscopic polarization and polarization density is then

$$P = \frac{\mu_0}{r_0^3}. \tag{E.28}$$

The average local field is thus:

$$\langle E_z \rangle = \frac{P}{4\pi\epsilon_0} \frac{1}{N} \sum_{i \neq j} \frac{1}{|\vec{j} - \vec{i}|^3} \left[1 - \frac{3(j_z - i_z)^2}{|\vec{j} - \vec{i}|^2} \right]. \tag{E.29}$$

Here $\vec{i}$, $\vec{j}$ represent the coordinate on the lattice of the i-th and j-th dipoles. Let's define

$$\eta = \frac{1}{4\pi N} \sum_{i \neq j} \frac{1}{|\vec{j} - \vec{i}|^3} \left[1 - \frac{3(j_z - i_z)^2}{|\vec{j} - \vec{i}|^2} \right]. \tag{E.30}$$

so we have the compact form

$$\langle E_z \rangle = \eta \frac{P}{\epsilon_0}. \tag{E.31}$$

Accordingly to the results derived with the continuum theory in E.1-E.2-E.3, we have numerically evaluated η for simple similar geometries. In all cases we have found good agreement with the

predictions of the continuum theory, which we summarise in the following. For a system consisting of one or multiple finite layers, and much larger in extension on the (x, y)-plane we have

$$\eta \simeq \frac{2}{3}, \tag{E.32}$$

while for a sphere

$$\eta \simeq 0, \tag{E.33}$$

and a cigar (or tower) shape

$$\eta \simeq -\frac{1}{3}. \tag{E.34}$$

In the next subsection we explicitly report the calculation for a single layer and for multiple layers. We will show that these numerical results match quite well the predictions for a thin slab from the continuum theory.

E.4.1 Single layer

For an infinite single layer we can find the analytic solution of η. Indeed we have

$$\eta = \frac{1}{4\pi N} \sum_{i_x, i_y, j_x, j_y} \frac{1}{((i_x - j_x)^2 + (i_y - j_y)^2)^{3/2}}, \tag{E.35}$$

where $N = N_x N_y$. From this we can define $m = i_x - j_x$ and $n = i_y - j_y$ from which we obtain immediately

$$\eta = \frac{1}{4\pi} \sum_{m,n \neq 0} \frac{1}{(m^2 + n^2)^{3/2}}. \tag{E.36}$$

For this sum there exist an expression in terms of special functions when we take the limit $N \longrightarrow \infty$

$$\lim_{N \longrightarrow \infty} \eta = \frac{\zeta(3/2) L(3/2, \chi_4)}{\pi} \approx 0.71, \tag{E.37}$$

where ζ is the usual Riemann-zeta function, L is the Dirichtlet L-function with primitive character χ_4. This sum is well reproduced by the numerics in Fig. E.3. It is worth noticing that it is very close to the value predicted by the continuum theory $\eta \approx 0.66$, but still a bit larger. We will see that this discrepancy is resolved by adding more layers, which effectively recreates the thin slab discussed in the continuum theory in Sec. E.2.

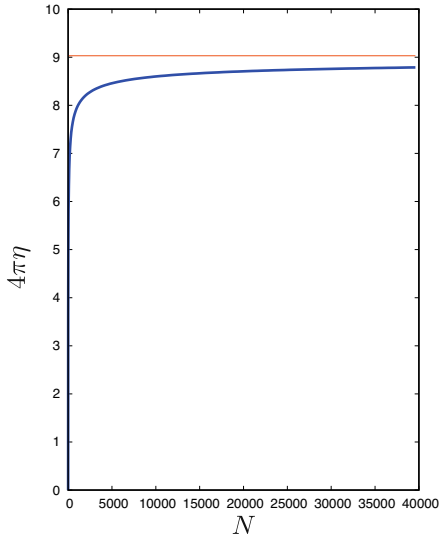

Figure E.1: η as a function of the number of dipoles N. Despite the slow convergence of the four sums in (E.35), one can see that the average local field approaches the value expected from the macroscopic description.

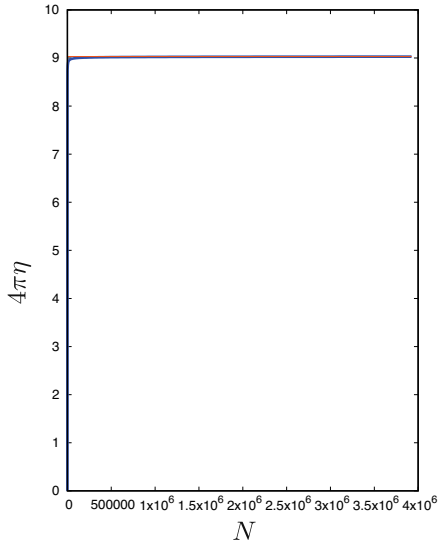

Figure E.2: η as a function of the number of dipoles N. Thanks to the simplification given by (E.36), the computational time is strongly decreased and it is possible to reach clear convergence.

Figure E.3: Numerical evaluation of η as a function of the total number of dipoles N for a square monolayer.

E.4.2 Multilayer

For a multilayer system, in which we have many layers stacked one above the others we have:

$$\eta = -\frac{1}{N} \sum_{i_x,i_y,i_z,j_x,j_y,j_z} \left[\frac{3(i_z - j_z)^2}{((i_x - j_x)^2 + (i_y - j_y)^2 + (i_z - j_z)^2)^{5/2}} - \frac{1}{((i_x - j_x)^2 + (i_y - j_y)^2 + (i_z - j_z)^2)^{3/2}} \right]. \tag{E.38}$$

Defining

$$\begin{aligned} m_x &= i_x - j_x, \\ m_y &= i_y - j_y, \\ m_z &= i_z - j_z, \end{aligned} \tag{E.39}$$

and considering $N = N_x N_y N_z$, we have

$$\eta = -\sum_{m_x,m_y,m_z} \left[\frac{3m_z^2}{(m_x^2 + m_y^2 + m_z^2)^{5/2}} - \frac{1}{(m_x^2 + m_y^2 + m_z^2)^{3/2}} \right], \tag{E.40}$$

which is worth to rewrite as

$$\eta = -\sum_{m_z}\left[3m_z^2\sum_{m_x,m_y}\frac{1}{(m_x^2+m_y^2+m_z^2)^{5/2}} - \sum_{m_x,m_y}\frac{1}{(m_x^2+m_y^2+m_z^2)^{3/2}}\right]. \tag{E.41}$$

The sum is considered on $m_\alpha \in [-N_\alpha; N_\alpha]$. We can see from Fig. E.6 that the multilayer sum

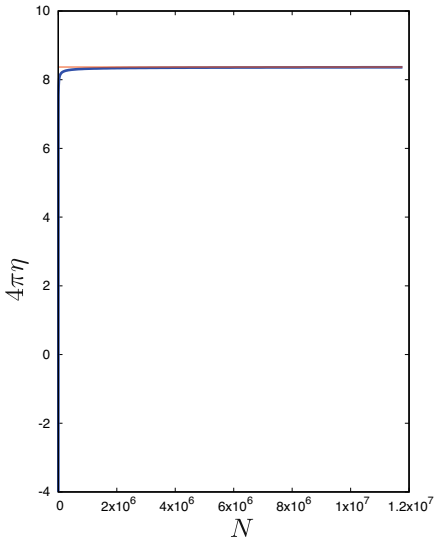

Figure E.4: η as a function of the number of dipoles N for a 3-layers system.

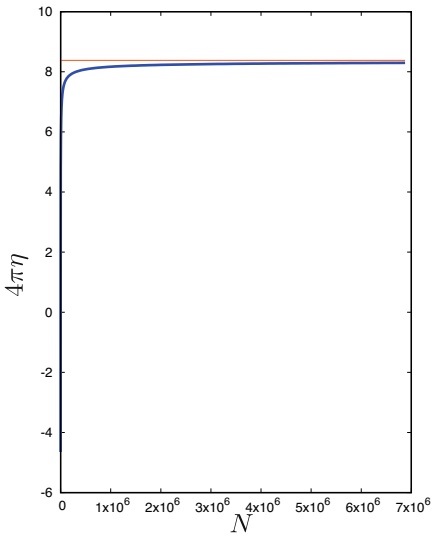

Figure E.5: η as a function of the number of dipoles N for a 7-layers system.

Figure E.6: Numerical evaluation of η as a function of the total number of dipoles N for a square multilayer system.

converges exactly to the continuum result for a thin slab.

E.5 Dipole ensemble between two grounded electrodes

When a polarised dielectric is placed in between two grounded parallel metallic plates the local electric field is modified in such a way that on the plates it is still identically zero. Under this *metallic* boundary condition, the electric field becomes equivalent to the usual dipole local field, plus the field generated by an infinite series of *image* dipoles, as we have seen in chapter 1. When we consider the case of a macroscopic homogeneously polarized system, we can say that the modifications coming from the bulk's images are negligible, and that all the contributions are due to the surface's images. The surface's image charges are the opposite of the surface charges of the dielectric, which is given by the polarization projected on the normal to the surface. So the local field inside of the dielectric will be given by

$$\langle E_z\rangle = \langle E_z\rangle_{bulk} + \langle E_z\rangle_{surface} + \langle E_z\rangle_{images}\,, \tag{E.42}$$

where, for a infinitely large thin slab we have

$$\begin{aligned}\langle E_z\rangle_{bulk} &\approx -\frac{P}{3\epsilon_0}\\ \langle E_z\rangle_{surface} &= \frac{P}{\epsilon_0}\\ \langle E_z\rangle_{images} &= -\frac{h}{d}\frac{P}{\epsilon_0},\end{aligned} \tag{E.43}$$

where h is the thickness of the dielectric slab, and d is the distance between the two plates (of course $h \leq d$). This linear dependence on h is necessary in order to keep the zero potential drop across the plates. This can be easily understood considering the relation between the induced charge (the charge needed on the capacitor plates to satisfy the metallic boundary conditions) and the surface charge on the dielectric (which is $Q_{surf.} = AP$, where A is the surface's area of the dielectric):

$$Q_{Im} = \frac{\sum_i \mu_i}{d} = \frac{\mu_0}{d} N \frac{r_0^3}{r_0^3} = \frac{\mu_0}{r_0^3}\frac{V_d}{d} = PA\frac{h}{d} = Q_{surf.}\frac{h}{d}. \tag{E.44}$$

So we have:

$$\langle E_z\rangle = -\frac{P}{3\epsilon_0} + \left(1 - \frac{h}{d}\right)\frac{P}{\epsilon_0}. \tag{E.45}$$

This means that in the case of a slab inserted in between two grounded metallic plates, with $h = d$, we expect

$$\eta \simeq -\frac{1}{3}, \tag{E.46}$$

meaning that the presence of the plates could eventually change the sign of the macroscopic field inside of the dielectric, potentially inducing a ferroelectric phase transition in the dipole's ground state.

E.5.1 Single layer

The effect of the metallic boundaries is to introduce in the system an infinite number of mirror image dipoles. The potential is thus modified in such a way that

$$\eta = \frac{1}{N}\sum_{\vec{i},\vec{j}}(D_{i,j} + \sum_{n=1}^{\infty} F_{i,j}^n + \bar{F}_{i,j}^n), \tag{E.47}$$

where $N = N_x N_y$,

$$D_{i,j} = \frac{1}{((i_x - j_x)^2 + (i_y - j_y)^2)^{3/2}}, \tag{E.48}$$

$$F_{i,j}^n = \left[\frac{3(i_z - \zeta_{j,u}^n)^2}{((i_x - j_x)^2 + (i_y - j_y)^2 + (i_z - \zeta_{j,u}^n)^2)^{5/2}} - \frac{1}{((i_x - j_x)^2 + (i_y - j_y)^2 + (i_z - \zeta_{j,u}^n)^2)^{3/2}}\right], \tag{E.49}$$

where $\zeta^n_{j,u}$ is the n-th-upper-plate image dipole z coordinate (in lattice constant units), which is defined as

$$\zeta^n_{j,u/p} = n\frac{d}{r_0} \pm (-1)^n(j_z - \frac{N_z-1}{2}) \pm \frac{N_z-1}{2}. \tag{E.50}$$

(the + holds for the upper plate images, while the − for the lower plate ones). The lower plate contribution is represented by $\bar{F}$ and is given by:

$$\bar{F}^n_{i,j} = \left[\frac{3(i_z+\zeta^n_{j,l})^2}{((i_x-j_x)^2+(i_y-j_y)^2+(i_z+\zeta^n_{j,l})^2)^{5/2}} - \frac{1}{((i_x-j_x)^2+(i_y-j_y)^2+(i_z+\zeta^n_{j,l})^2)^{3/2}}\right]. \tag{E.51}$$

The numerical result is reported in Fig. E.7. The monoloayer does not completely converge to the result expected for a thin slab between two metallic plates, but it anyway shows a very similar trend.

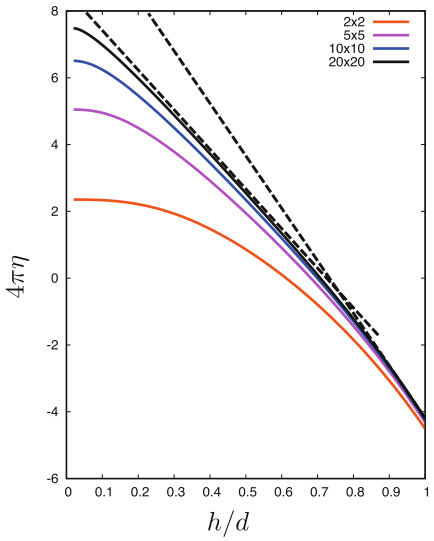

Figure E.7: η as a function of the ratio between the monolayer thickness and the plates distance h/d. The different color lines correspond to different sizes of the monolayer. We can see that by increasing the size, the dependence of the average local field on h/d approaches a linear behaviour with a knee, separating two regions with different slope. The dashed lines are just guides for the eyes.

E.5.2 Multilayer

The average local field of a dipole multilayer between two grounded plates is thus given by

$$\eta = \frac{1}{N}\sum_{\vec{i},\vec{j}}(D_{i,j} + \sum_{n=1}^{\infty} F^n_{i,j} + \bar{F}^n_{i,j}), \tag{E.52}$$

where $N = N_xN_yN_z$,

$$D_{i,j} = \frac{1}{((i_x-j_x)^2+(i_y-j_y)^2+(i_z-j_z))^{3/2}} - 3\frac{(i_z-j_z)^2}{((i_x-j_x)^2+(i_y-j_y)^2+(i_z-j_z)^2)^{5/2}}, \tag{E.53}$$

$$F^n_{i,j} = \left[\frac{3(i_z - \zeta^n_{j,u})^2}{((i_x - j_x)^2 + (i_y - j_y)^2 + (i_z - \zeta^n_{j,u})^2)^{5/2}} - \frac{1}{((i_x - j_x)^2 + (i_y - j_y)^2 + (i_z - \zeta^n_{j,u})^2)^{3/2}} \right], \tag{E.54}$$

where $\zeta^n_{j,u}$ is the n-th-upper-plate image dipole z coordinate (in lattice constant units), which is defined as

$$\zeta^n_{j,u/p} = n\frac{d}{r_0} \pm (-1)^n (j_z - \frac{N_z - 1}{2}) \pm \frac{N_z - 1}{2}. \tag{E.55}$$

(the + holds for the upper plate images, while the − for the lower plate ones). The lower plate contribution is represented by $\bar{F}$ and is given by:

$$\bar{F}^n_{i,j} = \left[\frac{3(i_z + \zeta^n_{j,l})^2}{((i_x - j_x)^2 + (i_y - j_y)^2 + (i_z + \zeta^n_{j,l})^2)^{5/2}} - \frac{1}{((i_x - j_x)^2 + (i_y - j_y)^2 + (i_z + \zeta^n_{j,l})^2)^{3/2}} \right]. \tag{E.56}$$

Using a similar argument as in Sec. E.4.1, we can reduce the sum from six variables to only three. So we have

$$\eta = \sum_{m_x,m_y,m_z} (D_{m_x,m_y,m_z} + \sum_{n=1}^{\infty} F^n_{m_x,m_y,m_z} + \bar{F}^n_{m_x,m_y,m_z}), \tag{E.57}$$

where

$$D_{m_x,m_y,m_z} = \frac{1}{(m_x^2 + m_y^2 + m_z)^{3/2}} - 3\frac{m_z^2}{(m_x^2 + m_y^2 + m_z^2)^{5/2}}, \tag{E.58}$$

the image charge contribution becomes

$$F^n_{m_x,m_y,m_z} = \left[\frac{3(m_z - \frac{d}{r_0})^2}{(m_x^2 + m_y^2 + (m_z - \frac{d}{r_0})^2)^{5/2}} - \frac{1}{(m_x^2 + m_y^2 + (m_z - \frac{d}{r_0})^2)^{3/2}} \right], \tag{E.59}$$

$$\bar{F}^n_{m_x,m_y,m_z} = \left[\frac{3(m_z + \frac{d}{r_0})^2}{(m_x^2 + m_y^2 + (m_z + \frac{d}{r_0})^2)^{5/2}} - \frac{1}{(m_x^2 + m_y^2 + (m_z + \frac{d}{r_0})^2)^{3/2}} \right], \tag{E.60}$$

and $m_\alpha \in [-N_\alpha, N_\alpha]$. We can see in Fig. E.8 the results from the numerics. The linear behaviour expected from the continuum calculation of the thin slab is recovered for increasing system sizes.

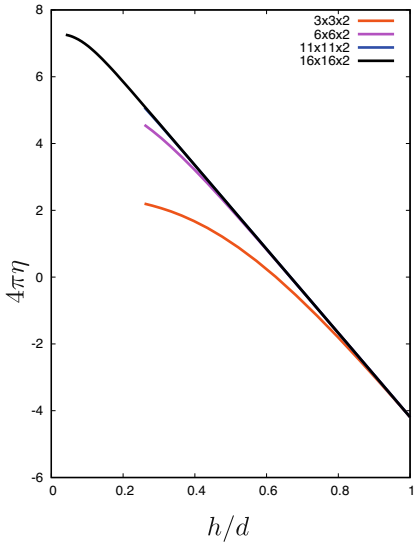

(a) η as a function of h/d, for a 2-layers system.

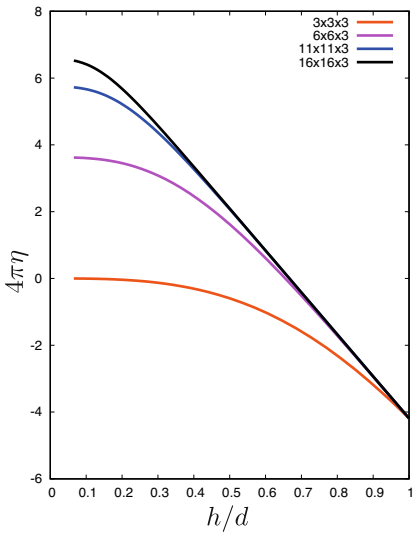

(b) η as a function of h/d, for a 3-layers system.

Figure E.8: η in function of the ratio between the k-layers thickness and the plates distance h/d, calculated with the formula (E.57). The different color lines correspond to different sizes of the k-layers system. We can see that increasing the size the dependence of the average local field from h/d approaches clearly to a linear behaviour, as expected for a macroscopic dielectric.

Appendix F

Effective Hamiltonian from perturbation theory

We develop here the effective low energy Hamiltonian given in Eq. (4.52). We start by making use of the fact that in the USC regime the spectrum of the EDM is separated into in almost degenerate manifolds, which are labelled by their photon's number. So it is convenient to consider the framework of *quasi-degenerate perturbation theory*. The concept is very simple and just relies on the standard pertrubation theory of quantum mechanics. We consider an Hamiltonian $H = H_0 + H_I$, where H_0 is degenerate or almost degenerate with respect to the energy scales of H_I. We then split the Hilber space in two subsets, labelled by "high energy" and "low energy" $\mathcal{H}_{\text{high}}$, $\mathcal{H}_{\text{low}}$, and together they give the total Hilbert space $\mathcal{H} = \mathcal{H}_{\text{low}} \oplus \mathcal{H}_{\text{high}}$. We then restrict our total Hamiltonian on the low energy space $H|_{\text{low}}$, and then diagonalise it, in this way we split the degeneracy of H_0. Its eigenvectors are labelled as $|n\rangle \in \mathcal{H}_{\text{low}}$. We then apply second order perturbation theory to correct these eigenvectors with the high energy contributions from H_I

$$|\bar{n}\rangle = |n\rangle - \sum_{\ell \in \mathcal{H}_{\text{high}}} \frac{H_I^{n\ell}}{E_\ell^0 - E_n^0} |\ell\rangle, \tag{F.1}$$

where $H_I^{n\ell} = \langle \ell | H_I | n \rangle$ and E_ℓ^0, E_n^0 are the eigenvalues of H_0. Evidently these new eigenvectors have some component in $\mathcal{H}_{\text{high}}$. Let's now project the whole H on those perturbed eigenvectors and keep the terms up to second order in the matrix elements of H_I. The result is an effective Hamiltonian which reproduce approximatively the lowest energy states of the system

$$\langle m | H_{\text{eff}} | n \rangle = E_n^0 \delta_{mn} + \langle m | H_I | n \rangle - \frac{1}{2} \sum_{\ell \in \mathcal{H}_{\text{high}}} \left(\frac{\langle m | H_I | \ell \rangle \langle \ell | H_I | n \rangle}{E_\ell^0 - E_m^0} + \frac{\langle n | H_I | \ell \rangle \langle \ell | H_I | m \rangle}{E_\ell^0 - E_n^0} \right). \tag{F.2}$$

Notice that H_{eff} just lives in $\mathcal{H}_{\text{low}}$.

In our case we consider $H_0 = \omega_c a^\dagger a + \varepsilon \frac{g^2}{\omega_c} S_x^2$ and $H_I = \omega_0 \left[\cos(\hat{\theta}) S_z - \sin(\hat{\theta}) S_y\right]$. When $|\varepsilon| \ll 1$ the states $|0_{\text{ph}}, S_x\rangle$ are almost degenerate eigenstates of H_0. So we take them to form $\mathcal{H}_{\text{low}}$. We just need to apply Eq. (F.2) and the result is in principle done. To arrive to our final form we need to apply another approximation. First we notice that the cross terms $\sim S_z S_y$ that appear taking the modulus square of H_I exactly vanish. This is due to the fact that, in the photonic part, they involve matrix elements such as $\langle 0|\cos(\hat{\theta})|\ell\rangle \langle \ell|\sin(\hat{\theta})|0\rangle$. These matrix elements must be zero because the sin and cos operators have opposite parity. At the end the only terms which survive are

$$H_{\text{eff}} = \omega_0 e^{-\frac{g^2}{2\omega_c^2}} S_z + \varepsilon \frac{g^2}{\omega_c} S_x^2 - \frac{\omega_0^2}{\omega_c} \sum_\ell \left[\frac{|\langle 0|\cos(\hat{\theta})|\ell\rangle|^2}{\ell} S_z^2 + \frac{|\langle 0|\sin(\hat{\theta})|\ell\rangle|^2}{\ell} S_y^2 \right]. \tag{F.3}$$

Using $\hat{\theta} = ix(a^\dagger - a)$, with the decomposition of the trigonometric operators via displacement operator in Eq. (4.45) and the properties of displacements [83] we have

$$\begin{aligned} \langle \ell|\cos(\hat{\theta})|0\rangle &= \sqrt{\frac{1}{\ell!}} e^{-x^2/2} L_0^\ell(x^2) \left(\frac{1+(-1)^\ell}{2}\right) |x|^\ell, \\ \langle \ell|\sin(\hat{\theta})|0\rangle &= i\sqrt{\frac{1}{\ell!}} e^{-x^2/2} L_0^\ell(x^2) \left(\frac{1-(-1)^\ell}{2}\right) |x|^\ell. \end{aligned} \tag{F.4}$$

It is possible to show that

$$\begin{aligned} \sum_{\ell\neq 0} \frac{|\langle \ell|\cos(\hat{\theta})|0\rangle|^2}{\ell} &= e^{-x^2} \sum_{\ell\neq 0} \frac{|x|^{2\ell}}{\ell!\ell} (L_0^\ell(x^2))^2 \left(\frac{1+(-1)^\ell}{2}\right)^2 \simeq \frac{1}{2x^2}, \\ \sum_{\ell\neq 0} \frac{|\langle \ell|\sin(\hat{\theta})|0\rangle|^2}{\ell} &= e^{-x^2} \sum_{\ell\neq 0} \frac{|x|^{2\ell}}{\ell!\ell} (L_0^\ell(x^2))^2 \left(\frac{1-(-1)^\ell}{2}\right)^2 \simeq \frac{1}{2x^2}, \end{aligned} \tag{F.5}$$

where $x = g/\omega_c$, and in the last equality we used $x \gg 1$. Putting everything together we have

$$H_{\text{eff}} \simeq \omega_0 e^{-\frac{g^2}{2\omega_c^2}} S_z + \varepsilon \frac{g^2}{\omega_c} S_x^2 - \frac{\omega_0^2 \omega_c}{2g^2} \left(\vec{S}^2 - S_x^2\right), \tag{F.6}$$

which is exactly Eq. (4.52).

Appendix G

Derivatives of the free energy

Let's consider

$$\partial_\lambda F \sim \mathrm{Tr}\left[\partial_\lambda e^{-\beta H(\lambda)}\right], \tag{G.1}$$

with $[\partial_\lambda H, H] \neq 0$, in general. When writing out explicitly the derivative of the exponential we obtain

$$\begin{aligned}\partial_\lambda e^{-\beta H(\lambda)} &= \sum_n \frac{1}{n!}\partial_\lambda (H(\lambda)H(\lambda)\cdots \mathrm{n-times}\cdots H(\lambda)) \\ &= \sum_n \frac{1}{n!}(\partial_\lambda H(\lambda)H(\lambda)\cdots H(\lambda) + H(\lambda)\partial_\lambda H(\lambda)\cdots H(\lambda) + \text{all possible permutation in } \partial_\lambda).\end{aligned} \tag{G.2}$$

Non-commutativity leaves us with a very complicated expression of the derivative of the exponential operator. Luckily, when the trace is taken, this doesn't matter anymore, due to its cyclic properties. Specifically

$$\mathrm{Tr}\left[\partial_\lambda H(\lambda)H(\lambda)\cdots H(\lambda)\right] = \mathrm{Tr}\left[H(\lambda)\partial_\lambda H(\lambda)\cdots H(\lambda)\right] = \cdots = \mathrm{Tr}\left[H(\lambda)H(\lambda)\cdots \partial_\lambda H(\lambda)\right], \tag{G.3}$$

meaning that

$$\mathrm{Tr}\left[\partial_\lambda e^{-\beta H}\right] = -\beta \mathrm{Tr}\left[(\partial_\lambda H)e^{-\beta H}\right]. \tag{G.4}$$

This result then implies

$$\partial_\lambda F = \langle \partial_\lambda H \rangle . \tag{G.5}$$

Appendix H

The Dyson series in thermal perturbation theory

Let's consider a generic system described by the following Hamiltonian

$$H = H_0 + H_I. \tag{H.1}$$

The canonical partition function for this system is given by

$$Z = \mathrm{Tr}\left[e^{-\beta(H_0+H_I)}\right], \tag{H.2}$$

and (setting $k_B = \hbar = 1$) its free energy is

$$\mathrm{F} = -T\log\left[Z\right]. \tag{H.3}$$

In analogy with the perturbative approach of the Dyson series in the interaction picture, we define

$$\mathcal{U} := \exp[\beta H_0]\exp[-\beta(H_0 + H_I)]. \tag{H.4}$$

The partition function is rewritten as

$$Z = \mathrm{Tr}\left[e^{-\beta H_0}\mathcal{U}\right] = Z_0\left\langle\mathcal{U}\right\rangle_0, \tag{H.5}$$

which is the expectation value of the operator $\mathcal{U}$ over a thermal state of the free system. To evaluate $\mathcal{U}$ in perturbation theory we use that it obeys the following equation

$$\frac{\partial}{\partial\beta}\mathcal{U} = -\tilde{H}_I(\beta)\mathcal{U}, \tag{H.6}$$

where

$$\tilde{H}_I(\beta) = e^{\beta H_0} H_I e^{-\beta H_0}. \tag{H.7}$$

Equation (H.6) is solved by

$$\mathcal{U} = \mathrm{T}\exp\left[-\int_0^\beta d\beta' \tilde{H}_I(\beta')\right], \tag{H.8}$$

in which T is the time ordering operator, considering β as the *imaginary time* of the problem ($\beta = -it$). This operator can now be expanded in the usual Dyson series,

$$\mathcal{U} \sim \mathbb{I} - \int_0^\beta d\beta' \tilde{H}_I(\beta') + \int_0^\beta d\beta' \int_0^{\beta'} d\beta'' \tilde{H}_I(\beta')\tilde{H}_I(\beta'') + \cdots. \tag{H.9}$$

H.1 Explicit expression of the perturbative terms

The first order can be easily rewritten as

$$\langle \mathcal{U}_1 \rangle_0 = \beta \langle H_I \rangle_0, \tag{H.10}$$

where we used the cyclic properties of the trace to get rid of the β' dependence in the integral.

Using the cyclic properties of the trace in the average and the relation

$$\int_0^t dt' \int_0^{t'} dt'' f(t'-t'') = \int_0^t dt' \int_0^{t'} d\tau f(\tau), \tag{H.11}$$

we obtain the second order contribution as

$$\langle \mathcal{U}_2 \rangle_0 = \int_0^\beta d\beta' \int_0^{\beta'} d\beta'' \langle \tilde{H}_I(\beta'')\tilde{H}_I(0)\rangle_0, \tag{H.12}$$

which is a time integral over a correlation function (notice that $\tilde{H}_I(0) = H_I$).

Inserting the identity and making explicit the trace we find this term has two components:

$$\begin{aligned}\langle \mathcal{U}_2 \rangle_0 = &\sum_n \frac{e^{-\beta E_n}}{Z_0} \sum_{m\neq n} \left[\frac{\beta}{E_{nm}} + \frac{1}{E_{nm}^2}\left(e^{-\beta E_{nm}} - 1\right)\right] |H_I^{nm}|^2 + \\ &+ \frac{\beta^2}{2} \sum_n \frac{e^{-\beta E_n}}{Z_0} (\langle n|H_I|n\rangle)^2.\end{aligned} \tag{H.13}$$

Here we used the eigenstates and eigenenergies of the free hamiltonian, $H_0|n\rangle = E_n|n\rangle$, then we defined $E_{nm} = E_m - E_n$ and $H_{nm} = \langle n|H_I|m\rangle$.

H.2 Magnus expansion

We consider now a cumulant expansion for the mean value of the interaction operator (also know as *Magnus expansion*)

$$\langle \mathcal{U} \rangle_0 = \exp[-\sum_{n=1}^{\infty} \beta^n F_n]. \tag{H.14}$$

In order to determine how to write the Magnus series in terms of our Dyson expansion, we must derive a relation between terms of the same order. One could simply expand the exponential, in the spirit of a high temperature expansion, then just equate the terms with the same power in β, and re-sum the series for low temperature. We start noticing that for high temperatures

$$\mathcal{U}_2 \sim_{\beta \to 0} \beta^2, \tag{H.15}$$

(from here on we drop the angle brakets for the sake of simplicity).

To be consistent with this observation we truncate the Magnus series at the second order, keeping just the terms of the same order and we find that

$$\begin{aligned} F_1 &= \frac{\mathcal{U}_1}{\beta}, \\ F_2 &= -\frac{\mathcal{U}_2}{\beta^2} + \frac{(\mathcal{U}_1)^2}{2\beta^2}. \end{aligned} \tag{H.16}$$

In this way the partition function becomes

$$Z \simeq Z_0 e^{-\mathcal{U}_1 - \left(\mathcal{U}_2 - \frac{(\mathcal{U}_1)^2}{2}\right)} \tag{H.17}$$

and the free energy is approximately given by

$$F \simeq F_0 + F^{(2)} = F_0 + T\mathcal{U}_1 - T\left(\mathcal{U}_2 - \frac{(\mathcal{U}_1)^2}{2}\right). \tag{H.18}$$

H.3 Low temperature limit

We consider here the limit in which $T \longrightarrow 0$, which means $\beta \longrightarrow \infty$. The free partition function goes to

$$Z_0 \xrightarrow[\beta \to \infty]{} e^{-\beta E_0}. \tag{H.19}$$

The first order Dyson expansion gives

$$\mathcal{U}_1 \xrightarrow[\beta \to \infty]{} \langle 0 | H_I | 0 \rangle. \tag{H.20}$$

The second order Dyson term gives

$$\mathcal{U}_2 \xrightarrow[\beta\to\infty]{} \beta \sum_{n\neq 0} \frac{|H_I^{0n}|^2}{E_{0n}} + \frac{\beta^2}{2} |\langle 0|H_I|0\rangle|^2. \tag{H.21}$$

Note that the term in $\mathcal{U}_1^2$ from the Magnus expansion exactly compensates the β^2 component in $\mathcal{U}_2$ in this limit. The total partition function reads

$$Z \xrightarrow[\beta\to\infty]{} e^{-\beta\left[E_0+\langle 0|H_I|0\rangle-\sum_{n\neq 0}\frac{|\langle 0|H_I|n\rangle|^2}{E_{0n}}\right]}. \tag{H.22}$$

The free energy is

$$F \xrightarrow[\beta\to\infty]{} E_0 + \langle 0|H_I|0\rangle - \sum_{n\neq 0} \frac{|\langle 0|H_I|n\rangle|^2}{E_{0n}}, \tag{H.23}$$

which is consistent with regular perturbation theory. We note that, in this limit, the free energy equals the internal energy.

H.4 High temperature limit

The high temperature limit is even simpler than the low temperature one. Indeed here we keep just the terms which are small in β and obtain

$$\mathcal{U}_2 - \frac{(\mathcal{U}_1)^2}{2} \sim \frac{\beta^2}{2}\left(\langle H_I^2\rangle_0 - \langle H_I\rangle_0^2\right). \tag{H.24}$$

The partition function is

$$Z \xrightarrow[\beta\to 0]{} Z_0 e^{-\beta\langle H_I\rangle_0 + \frac{\beta^2}{2}\left(\langle H_I^2\rangle_0 - \langle H_I\rangle_0^2\right)}. \tag{H.25}$$

The free energy becomes the bare free energy with just the first order correction,

$$F \xrightarrow[\beta\to 0]{} F_0 + \langle H_I\rangle_0 - \frac{\beta}{2}\left(\langle H_I^2\rangle_0 - \langle H_I\rangle_0^2\right). \tag{H.26}$$

It's interesting to note that it seems that the temperature washes out the interaction.

H.5 Generalised displacement

We consider here the generalized displacement operator

$$\hat{T}(f,g) = e^{fa^\dagger - ga}. \tag{H.27}$$

We want to compute its expectation value over a photon thermal state $\rho = e^{-\beta a^\dagger a}/Z$. We have

$$\begin{aligned}
\mathrm{Tr}\left(\frac{e^{-\beta a^\dagger a}}{Z}\hat{T}\right) &= e^{-fg/2}\sum_n \frac{e^{-\beta n}}{Z}\langle n|e^{fa^\dagger}e^{ga}|n\rangle \\
&= e^{-fg/2}\sum_n \frac{e^{-\beta n}}{Z}\sum_{r,q}(-1)^q\frac{f^r}{r!}\frac{g^q}{q!}\langle n|(a^\dagger)^r a^q|n\rangle \\
&= e^{-fg/2}\sum_n \frac{e^{-\beta n}}{Z}\sum_{q=0}^{n}(-1)^q\frac{(fg)^q}{q!}\binom{n}{q} \\
&= e^{-fg/2}\sum_n \frac{e^{-\beta n}}{Z}L_n(fg) \\
&= e^{-fg/2(1+N_{th}(\beta))},
\end{aligned} \tag{H.28}$$

where $N_{th}(\beta) = 1/(e^\beta - 1)$. $L_n(x)$ is the Laguerre polynomials.

H.6 General Dyson formula for the EDM

Here we show the main ingredients to explicitly calculate Eq. (5.47) and (5.50). The starting point is Eq. (H.12). Note that using $H_0 = H_{\text{e.m.}}$, as it is given by Eq. (5.27), the bare dipole eigenstates are all S_x-eigenstates. This implies that the first order of the perturbation vanishes, since it is proportional $\sim \langle S_z\rangle_0$. In the case of the EDM, the integrand in Eq. (H.12) is

$$\langle \tilde{H}_I(\tau)\tilde{H}_I(0)\rangle_0 = \omega_0^2\left(\langle\cos[\hat{\theta}](\tau)\cos[\hat{\theta}]\rangle_0\langle S_z(\tau)S_z\rangle_0 + \langle\sin[\hat{\theta}](\tau)\sin[\hat{\theta}]\rangle_0\langle S_y(\tau)S_y\rangle_0\right). \tag{H.29}$$

To shorten the notation we consider $\omega_c = 1$. To simplify the calculation we introduce a couple of definitions

$$\begin{aligned}
D &:= e^{g(a^\dagger - a)}, \\
\tilde{D} &:= e^{\tau H_0}De^{-\tau H_0}, \\
\tilde{\tilde{D}} &:= e^{\tau H_0}D^\dagger e^{-\tau H_0}.
\end{aligned} \tag{H.30}$$

Using that $e^{\tau H_0}ae^{-\tau H_0} = ae^{-\tau}$, we realise that all the above defined operators are generalised displacements, as in Eq. (H.27). We then express the sin and cos photonic operators using these generalised displacements

$$4\cos[\hat{\theta}](\tau)\cos[\hat{\theta}] = \tilde{D}D + \tilde{D}D^\dagger + \tilde{\tilde{D}}D + \tilde{\tilde{D}}D^\dagger, \tag{H.31}$$

$$4\sin[\hat{\theta}](\tau)\sin[\hat{\theta}] = -\tilde{\tilde{D}}D^\dagger + \tilde{\tilde{D}}D + \tilde{D}D^\dagger - \tilde{D}D. \tag{H.32}$$

We then obtain the following expectation values

$$\begin{aligned}
\langle \tilde{D} D \rangle &= e^{g^2[\sinh(\tau)-\cosh(\tau)(1+2N_{\rm th}(\beta)]} e^{-g^2(1+2N_{\rm th})}, \\
\langle \tilde{D} D^\dagger \rangle &= e^{-g^2[\sinh(\tau)-\cosh(\tau)(1+2N_{\rm th}(\beta)]} e^{-g^2(1+2N_{\rm th})}, \\
\langle \tilde{\tilde{D}} D \rangle &= \langle \tilde{D} D^\dagger \rangle \,, \\
\langle \tilde{\tilde{D}} D^\dagger \rangle &= \langle \tilde{D} D \rangle \,.
\end{aligned} \tag{H.33}$$

For this calculation we made use of the fact that we are only dealing with generalized displacement operators, for which we can use the formula in Eq. (H.28). It's then possible to explicitly calculate all the cavity correlators and put them in a compact form

$$\begin{aligned}
\cos[\hat{\theta}](\tau)\cos[\hat{\theta}] &= e^{-g^2(1+2N_{\rm th})} \cosh\left[g^2\left(e^{-\tau}(1+N_{\rm th}) + e^{\tau} N_{\rm th}\right)\right], \\
\sin[\hat{\theta}](\tau)\sin[\hat{\theta}] &= e^{-g^2(1+2N_{\rm th})} \sinh\left[g^2\left(e^{-\tau}(1+N_{\rm th}) + e^{\tau} N_{\rm th}\right)\right].
\end{aligned} \tag{H.34}$$

This form is actually not the best to complete the calculation of $\mathcal{U}_2$. Indeed, the dependence on τ looks really complicated, making it impossible to solve the convolution integral with the spin correlators. The integral can be actually performed if we expand the sinh and cosh in a power series. This make the expression a little bit nasty, but it allows us to complete the calculation.

$$\begin{aligned}
\cos[\hat{\theta}](\tau)\cos[\hat{\theta}] &= e^{-g^2(1+2N_{\rm th})} \sum_{r,q=0}^{\infty} \frac{[1+(-1)^{r+q}]}{2} g^{2(r+q)} \frac{(1+N_{\rm th})^r N_{\rm th}^q}{r!\; q!} e^{(q-r)\tau} \\
&= e^{-g^2(1+2N_{\rm th})} \sum_{r,q=0}^{\infty} K_{rq} e^{(q-r)\tau},
\end{aligned} \tag{H.35}$$

$$\begin{aligned}
\sin[\hat{\theta}](\tau)\sin[\hat{\theta}] &= e^{-g^2(1+2N_{\rm th})} \sum_{r,q=0}^{\infty} \frac{[1-(-1)^{r+q}]}{2} g^{2(r+q)} \frac{(1+N_{\rm th})^r N_{\rm th}^q}{r!\; q!} e^{(q-r)\tau} \\
&= e^{-g^2(1+2N_{\rm th})} \sum_{r,q=0}^{\infty} Q_{rq} e^{(q-r)\tau}.
\end{aligned} \tag{H.36}$$

Note that we recompactificate the result introductiong the two matrices K and Q. It's important to notice that

$$\begin{aligned}
K_{rq} \neq 0 &\iff r+q = 2n,\ n \in \mathbb{N}, \\
Q_{rq} \neq 0 &\iff r+q = 2n+1,\ n \in \mathbb{N}.
\end{aligned} \tag{H.37}$$

We can interpret this in the following way: r is the number of photons emitted by the spins (downgrade them to a lower state), q is the number of photons absorbed by the spins (exciting them to a higher state). K is the matrix containing all the processes which involve an even number of photons (we could interpret it as spins-photons scattering). Q is the matrix containing all the

processes in which is involved an odd number of photons (we could interpret this as pair of spins decaying to photons).

Note that all the dependence on τ in the photonic correlators comes from the factor $e^{(q-r)\tau}$. With this in mind we can put it together with the dipole's correlators and then integrate it. The result can be easily computed by introducing a couple of completeness relation and it gives (replacing $(q-r)$ with a generic ω for generality)

$$\int_0^\beta d\tau' \int_0^{\tau'} e^{\omega\tau}\langle S_\alpha(\tau)S_\alpha\rangle_0 = \frac{1}{\beta^2}\sum_m \frac{e^{-\beta E_m^{\rm dip}}}{Z_{\rm dip}}\sum_k |S_\alpha^{km}|^2\left[\frac{e^{\beta(\omega-E_{km}^{\rm dip})}-1}{(\omega-E_{km}^{\rm dip})^2}-\frac{\beta}{\omega-E_{km}^{\rm dip}}\right]. \tag{H.38}$$

By using the definition given in Eq. (5.51) in the main text we can combine everything and write the final expression as

$$\mathcal{U}_2 = \frac{\beta^2\omega_0^2}{2}e^{-\frac{g^2}{\omega_c^2}(1+2n_{\rm th}(\beta))}\left[\sum_{r,q=0}^{\infty} K_{rq}\Delta_{zz}(\beta,(q-r)\omega_c)+\sum_{r,q=0}^{\infty} Q_{rq}\Delta_{yy}(\beta,(q-r)\omega_c)\right]. \tag{H.39}$$

The perturbative correction to the free energy is then given by

$$F_{\omega_0}^{(2)} = -T\mathcal{U}_2. \tag{H.40}$$

Bibliography

[1] Serge Haroche and Jean Michel Raimond. *Exploring the Quantum: Atoms, Cavities, and Photons*. Oxford Univ. Press, Oxford, 2006.

[2] J. Ignacio Cirac and Peter Zoller. Goals and opportunities in quantum simulation. *Nature Physics*, 8(4):264–266, 2012.

[3] Yoshihisa Yamamoto. *Squeezing and Cavity QED in Semiconductors*, pages 201–281. Springer Netherlands, Dordrecht, 1996.

[4] Alexandre Blais, Steven M. Girvin, and William D. Oliver. Quantum information processing and quantum optics with circuit quantum electrodynamics. *Nature Physics*, 16(3):247–256, 2020.

[5] Cristiano Ciuti, Gérald Bastard, and Iacopo Carusotto. Quantum vacuum properties of the intersubband cavity polariton field. *Phys. Rev. B*, 72:115303, Sep 2005.

[6] Klaus Hepp and Elliott H Lieb. On the superradiant phase transition for molecules in a quantized radiation field: the dicke maser model. *Annals of Physics*, 76(2):360–404, 1973.

[7] Peter Kirton, Mor M. Roses, Jonathan Keeling, and Emanuele G. Dalla Torre. Introduction to the dicke model: From equilibrium to nonequilibrium, and vice versa. *Advanced Quantum Technologies*, 2(1-2):1800043, 2019.

[8] Pierre Nataf and Cristiano Ciuti. No-go theorem for superradiant quantum phase transitions in cavity qed and counter-example in circuit qed. *Nature Communications*, 1(1):72, 2010.

[9] Motoaki Bamba, Kunihiro Inomata, and Yasunobu Nakamura. Superradiant phase transition in a superconducting circuit in thermal equilibrium. *Phys. Rev. Lett.*, 117:173601, Oct 2016.

[10] Andreas Bayer, Marcel Pozimski, Simon Schambeck, Dieter Schuh, Rupert Huber, Dominique Bougeard, and Christoph Lange. Terahertz light–matter interaction beyond unity coupling strength. *Nano Letters*, 17(10):6340–6344, 10 2017.

[11] Benjamin Askenazi, Angela Vasanelli, Yanko Todorov, Emilie Sakat, Jean-Jacques Greffet, Grégoire Beaudoin, Isabelle Sagnes, and Carlo Sirtori. Midinfrared ultrastrong light–matter coupling for thz thermal emission. *ACS Photonics*, 4(10):2550–2555, 10 2017.

[12] T. Niemczyk, F. Deppe, H. Huebl, E. P. Menzel, F. Hocke, M. J. Schwarz, J. J. Garcia-Ripoll, D. Zueco, T. Hümmer, E. Solano, A. Marx, and R. Gross. Circuit quantum electrodynamics in the ultrastrong-coupling regime. *Nature Physics*, 6(10):772–776, 2010.

[13] Fumiki Yoshihara, Tomoko Fuse, Sahel Ashhab, Kosuke Kakuyanagi, Shiro Saito, and Kouichi Semba. Superconducting qubit–oscillator circuit beyond the ultrastrong-coupling regime. *Nature Physics*, 13(1):44–47, 2017.

[14] T. Schwartz, J. A. Hutchison, C. Genet, and T. W. Ebbesen. Reversible switching of ultrastrong light-molecule coupling. *Phys. Rev. Lett.*, 106:196405, May 2011.

[15] Anoop Thomas, Jino George, Atef Shalabney, Marian Dryzhakov, Sreejith J. Varma, Joseph Moran, Thibault Chervy, Xiaolan Zhong, Eloïse Devaux, Cyriaque Genet, James A. Hutchison, and Thomas W. Ebbesen. Ground-state chemical reactivity under vibrational coupling to the vacuum electromagnetic field. *Angewandte Chemie International Edition*, 55(38):11462–11466, 2016.

[16] Shaojun Wang, Arkadiusz Mika, James A. Hutchison, Cyriaque Genet, Abdelaziz Jouaiti, Mir Wais Hosseini, and Thomas W. Ebbesen. Phase transition of a perovskite strongly coupled to the vacuum field. *Nanoscale*, 6:7243–7248, 2014.

[17] Janine Keller, Giacomo Scalari, Felice Appugliese, Shima Rajabali, Mattias Beck, Johannes Haase, Christian A. Lehner, Werner Wegscheider, Michele Failla, Maksym Myronov, David R. Leadley, James Lloyd-Hughes, Pierre Nataf, and Jérôme Faist. Landau polaritons in highly nonparabolic two-dimensional gases in the ultrastrong coupling regime. *Phys. Rev. B*, 101:075301, Feb 2020.

[18] Claude Cohen-Tannoudji, Jacques Dupont-Roc, and Gilbert Grynberg. *Photons and atoms: introduction to quantum electrodynamics*. Wiley, New York, NY, 1989. Trans. of : Photons et atomes. Paris, InterEditions, 1987.

[19] Marlan O. Scully and M. Suhail Zubairy. *Quantum Optics*. Cambridge University Press, 1997.

[20] V.I Emeljanov and Yu.L Klimontovich. Appearance of collective polarisation as a result of phase transition in an ensemble of two-level atoms, interacting through electromagnetic field. *Physics Letters A*, 59(5):366–368, 1976.

[21] Jonathan Keeling. Coulomb interactions, gauge invariance, and phase transitions of the dicke model. *Journal of Physics: Condensed Matter*, 19(29):295213, jun 2007.

[22] András Vukics, Tobias Grießer, and Peter Domokos. Elimination of the a-square problem from cavity qed. *Phys. Rev. Lett.*, 112:073601, Feb 2014.

[23] Richard P. Feynman. Qed: The strange theory of light and matter. *Science and Society*, 51(2):211–214, 1985.

[24] Tomoki Ozawa, Hannah M. Price, Alberto Amo, Nathan Goldman, Mohammad Hafezi, Ling Lu, Mikael C. Rechtsman, David Schuster, Jonathan Simon, Oded Zilberberg, and Iacopo Carusotto. Topological photonics. *Rev. Mod. Phys.*, 91:015006, Mar 2019.

[25] D. E. Chang, J. S. Douglas, A. González-Tudela, C.-L. Hung, and H. J. Kimble. Colloquium: Quantum matter built from nanoscopic lattices of atoms and photons. *Rev. Mod. Phys.*, 90:031002, Aug 2018.

[26] D. R. Yennie. Integral quantum hall effect for nonspecialists. *Rev. Mod. Phys.*, 59:781–824, Jul 1987.

[27] Horst L. Stormer. Nobel lecture: The fractional quantum hall effect. *Rev. Mod. Phys.*, 71:875–889, Jul 1999.

[28] Sabyasachi Barik, Aziz Karasahin, Christopher Flower, Tao Cai, Hirokazu Miyake, Wade DeGottardi, Mohammad Hafezi, and Edo Waks. A topological quantum optics interface. *Science*, 359(6376):666–668, 2018.

[29] Eunjong Kim, Xueyue Zhang, Vinicius S. Ferreira, Jash Banker, Joseph K. Iverson, Alp Sipahigil, Miguel Bello, Alejandro González-Tudela, Mohammad Mirhosseini, and Oskar Painter. Quantum electrodynamics in a topological waveguide. *Phys. Rev. X*, 11:011015, Jan 2021.

[30] Peter Lodahl, Sahand Mahmoodian, Søren Stobbe, Arno Rauschenbeutel, Philipp Schneeweiss, Jürgen Volz, Hannes Pichler, and Peter Zoller. Chiral quantum optics. *Nature*, 541(7638):473–480, 2017.

[31] Daniele De Bernardis, Tuomas Jaako, and Peter Rabl. Cavity quantum electrodynamics in the nonperturbative regime. *Phys. Rev. A*, 97:043820, Apr 2018.

[32] Daniele De Bernardis, Philipp Pilar, Tuomas Jaako, Simone De Liberato, and Peter Rabl. Breakdown of gauge invariance in ultrastrong-coupling cavity qed. *Phys. Rev. A*, 98:053819, Nov 2018.

[33] Philipp Pilar, Daniele De Bernardis, and Peter Rabl. Thermodynamics of ultrastrongly coupled light-matter systems. *Quantum*, 4:335, September 2020.

[34] Michael Schuler, Daniele De Bernardis, Andreas M. Läuchli, and Peter Rabl. The Vacua of Dipolar Cavity Quantum Electrodynamics. *SciPost Phys.*, 9:66, 2020.

[35] Daniele De Bernardis, Ze-Pei Cian, Iacopo Carusotto, Mohammad Hafezi, and Peter Rabl. Light-matter interactions in synthetic magnetic fields: Landau-photon polaritons. *Phys. Rev. Lett.*, 126:103603, Mar 2021.

[36] Steven Weinberg. *The Quantum Theory of Fields, Volume 1: Foundations*. Cambridge University Press, 2005.

[37] E. A. Power and T. Thirunamachandran. Quantum electrodynamics in a cavity. *Phys. Rev. A*, 25:2473–2484, May 1982.

[38] D.P. Craig and T. Thirunamachandran. *Molecular Quantum Electrodynamics: An Introduction to Radiation-molecule Interactions*. Dover Books on Chemistry Series. Dover Publications, 1998.

[39] John David Jackson. *Classical electrodynamics*. Wiley, New York, NY, 3rd ed. edition, 1999.

[40] Tobias Grießer, András Vukics, and Peter Domokos. Depolarization shift of the superradiant phase transition. *Phys. Rev. A*, 94:033815, Sep 2016.

[41] Ivan Medina, Francisco J. García-Vidal, Antonio I. Fernández-Domínguez, and Johannes Feist. Few-mode field quantization of arbitrary electromagnetic spectral densities. *Phys. Rev. Lett.*, 126:093601, Mar 2021.

[42] Willis E. Lamb. Fine structure of the hydrogen atom. iii. *Phys. Rev.*, 85:259–276, Jan 1952.

[43] Edwin Albert Power, S. Zienau, and Harrie Stewart Wilson Massey. Coulomb gauge in non-relativistic quantum electro-dynamics and the shape of spectral lines. *Philosophical Transactions of the Royal Society of London. Series A, Mathematical and Physical Sciences*, 251(999):427–454, 1959.

[44] C Leubner and P Zoller. Gauge invariant interpretation of multiphoton transition probabilities. *Journal of Physics B: Atomic and Molecular Physics*, 13(18):3613–3617, sep 1980.

[45] Kuo-Ho Yang. Gauge transformations and quantum mechanics i. gauge invariant interpretation of quantum mechanics. *Annals of Physics*, 101(1):62–96, 1976.

[46] Donald H. Kobe and Arthur L. Smirl. Gauge invariant formulation of the interaction of electromagnetic radiation and matter. *American Journal of Physics*, 46(6):624–633, June 1978.

[47] F. Bassani, J. J. Forney, and A. Quattropani. Choice of gauge in two-photon transitions: $1s - 2s$ transition in atomic hydrogen. *Phys. Rev. Lett.*, 39:1070–1073, Oct 1977.

[48] L. D. Landau and E. M. Lifshitz. *Mechanics, Third Edition: Volume 1 (Course of Theoretical Physics)*. Butterworth-Heinemann, 3 edition, January 1976.

[49] Daniel Z. Rossatto, Celso J. Villas-Bôas, Mikel Sanz, and Enrique Solano. Spectral classification of coupling regimes in the quantum rabi model. *Phys. Rev. A*, 96:013849, Jul 2017.

[50] K. Rzażewski, K. Wódkiewicz, and W. Żakowicz. Phase transitions, two-level atoms, and the A^2 term. *Phys. Rev. Lett.*, 35:432–434, Aug 1975.

[51] Omar Di Stefano, Alessio Settineri, Vincenzo Macrì, Luigi Garziano, Roberto Stassi, Salvatore Savasta, and Franco Nori. Resolution of gauge ambiguities in ultrastrong-coupling cavity quantum electrodynamics. *Nature Physics*, 15(8):803–808, 2019.

[52] Adam Stokes and Ahsan Nazir. Gauge ambiguities imply jaynes-cummings physics remains valid in ultrastrong coupling qed. *Nature Communications*, 10(1):499, 2019.

[53] P. Forn-Díaz, J. Lisenfeld, D. Marcos, J. J. García-Ripoll, E. Solano, C. J. P. M. Harmans, and J. E. Mooij. Observation of the bloch-siegert shift in a qubit-oscillator system in the ultrastrong coupling regime. *Phys. Rev. Lett.*, 105:237001, Nov 2010.

[54] Andreas Bayer, Marcel Pozimski, Simon Schambeck, Dieter Schuh, Rupert Huber, Dominique Bougeard, and Christoph Lange. Terahertz light–matter interaction beyond unity coupling strength. *Nano Letters*, 17(10):6340–6344, 2017. PMID: 28937772.

[55] Tuomas Jaako, Ze-Liang Xiang, Juan José Garcia-Ripoll, and Peter Rabl. Ultrastrong-coupling phenomena beyond the dicke model. *Phys. Rev. A*, 94:033850, Sep 2016.

[56] Markus Geiser, Fabrizio Castellano, Giacomo Scalari, Mattias Beck, Laurent Nevou, and Jérôme Faist. Ultrastrong coupling regime and plasmon polaritons in parabolic semiconductor quantum wells. *Phys. Rev. Lett.*, 108:106402, Mar 2012.

[57] Enrico Lipparini. *Modern Many-Particle Physics*. WORLD SCIENTIFIC, 2nd edition, 2008.

[58] J. J. Hopfield. Theory of the contribution of excitons to the complex dielectric constant of crystals. *Phys. Rev.*, 112:1555–1567, Dec 1958.

[59] I. Chiorescu, Y. Nakamura, C. J. P. M. Harmans, and J. E. Mooij. Coherent quantum dynamics of a superconducting flux qubit. *Science*, 299(5614):1869–1871, 2003.

[60] G. Barton. Quantum electrodynamics of spinless particles between conducting plates. *Proc. Roy. Soc. Lond. A*, 320:251–275, 1970.

[61] L. D. Landau and E. M. Lifschits. *The Classical Theory of Fields*, volume Volume 2 of *Course of Theoretical Physics*. Pergamon Press, Oxford, 1975.

[62] B. R. A. Nijboer and F. W. De Wette. The internal field in dipole lattices. *Physica*, 24(1):422–431, January 1958.

[63] Luca Dell'Anna and Michele Merano. Clausius-mossotti lorentz-lorenz relations and retardation effects for two-dimensional crystals. *Phys. Rev. A*, 93:053808, May 2016.

[64] Devoret M. H., Girvin Steven, and Schoelkopf Robert. Circuit-QED: How strong can the coupling between a Josephson junction atom and a transmission line resonator be? *Annalen der Physik*, 16(10):767, 2007.

[65] P. Forn-Díaz, L. Lamata, E. Rico, J. Kono, and E. Solano. Ultrastrong coupling regimes of light-matter interaction. *Rev. Mod. Phys.*, 91:025005, Jun 2019.

[66] Anton Frisk Kockum, Adam Miranowicz, Simone De Liberato, Salvatore Savasta, and Franco Nori. Ultrastrong coupling between light and matter. *Nature Reviews Physics*, 1(1):19–40, 2019.

[67] Iacopo Carusotto and Cristiano Ciuti. Quantum fluids of light. *Rev. Mod. Phys.*, 85:299–366, Feb 2013.

[68] Alexandre Blais, Arne L. Grimsmo, S. M. Girvin, and Andreas Wallraff. Circuit quantum electrodynamics, 2020.

[69] P. W. Milonni. *The Quantum vacuum: An Introduction to quantum electrodynamics*. 1994.

[70] R. H. Dicke. Coherence in spontaneous radiation processes. *Phys. Rev.*, 93:99–110, Jan 1954.

[71] Michael Tavis and Frederick W. Cummings. Exact solution for an n-molecule—radiation-field hamiltonian. *Phys. Rev.*, 170:379–384, Jun 1968.

[72] E. T. Jaynes and F. W. Cummings. Comparison of quantum and semiclassical radiation theories with application to the beam maser. *Proceedings of the IEEE*, 51(1):89–109, 1963.

[73] Renju Rajan, P. Ramesh Babu, and K. Senthilnathan. Photon condensation: A new paradigm for bose–einstein condensation. *Frontiers of Physics*, 11(5):110502, 2016.

[74] Pierre Nataf and Cristiano Ciuti. Vacuum degeneracy of a circuit qed system in the ultrastrong coupling regime. *Phys. Rev. Lett.*, 104:023601, Jan 2010.

[75] Oliver Viehmann, Jan von Delft, and Florian Marquardt. Superradiant phase transitions and the standard description of circuit qed. *Phys. Rev. Lett.*, 107:113602, Sep 2011.

[76] András Vukics and Peter Domokos. Adequacy of the dicke model in cavity qed: A counter-no-go statement. *Phys. Rev. A*, 86:053807, Nov 2012.

[77] Motoaki Bamba and Tetsuo Ogawa. Stability of polarizable materials against superradiant phase transition. *Phys. Rev. A*, 90:063825, Dec 2014.

[78] Y. K. Wang and F. T. Hioe. Phase transition in the dicke model of superradiance. *Phys. Rev. A*, 7:831–836, Mar 1973.

[79] F. T. Hioe. Phase transitions in some generalized dicke models of superradiance. *Phys. Rev. A*, 8:1440–1445, Sep 1973.

[80] J. M. Knight, Y. Aharonov, and G. T. C. Hsieh. Are super-radiant phase transitions possible? *Phys. Rev. A*, 17:1454–1462, Apr 1978.

[81] Iwo Bialynicki-Birula and Kazimierz Rzążewski. No-go theorem concerning the superradiant phase transition in atomic systems. *Phys. Rev. A*, 19:301–303, Jan 1979.

[82] M. Gross and S. Haroche. Superradiance: An essay on the theory of collective spontaneous emission. *Physics Reports*, 93(5):301–396, 1982.

[83] K. E. Cahill and R. J. Glauber. Ordered expansions in boson amplitude operators. *Phys. Rev.*, 177:1857–1881, Jan 1969.

[84] Lev Pitaevskii and Sandro Stringari. *Bose-Einstein condensation and superfluidity*. International series of monographs on physics. Oxford University Press, Oxford, 2016.

[85] G. M. Andolina, F. M. D. Pellegrino, V. Giovannetti, A. H. MacDonald, and M. Polini. Cavity quantum electrodynamics of strongly correlated electron systems: A no-go theorem for photon condensation. *Phys. Rev. B*, 100:121109, Sep 2019.

[86] G. M. Andolina, F. M. D. Pellegrino, V. Giovannetti, A. H. MacDonald, and M. Polini. Theory of photon condensation in a spatially varying electromagnetic field. *Phys. Rev. B*, 102:125137, Sep 2020.

[87] Juan Román-Roche, Fernando Luis, and David Zueco. Photon condensation in magnetic cavity qed, 2021.

[88] Yanko Todorov and Carlo Sirtori. Few-electron ultrastrong light-matter coupling in a quantum lc circuit. *Phys. Rev. X*, 4:041031, Nov 2014.

[89] Cristiano Ciuti and Iacopo Carusotto. Input-output theory of cavities in the ultrastrong coupling regime: The case of time-independent cavity parameters. *Phys. Rev. A*, 74:033811, Sep 2006.

[90] S. Fedortchenko, S. Huppert, A. Vasanelli, Y. Todorov, C. Sirtori, C. Ciuti, A. Keller, T. Coudreau, and P. Milman. Output squeezed radiation from dispersive ultrastrong light-matter coupling. *Phys. Rev. A*, 94:013821, Jul 2016.

[91] F. Dimer, B. Estienne, A. S. Parkins, and H. J. Carmichael. Proposed realization of the dicke-model quantum phase transition in an optical cavity qed system. *Phys. Rev. A*, 75:013804, Jan 2007.

[92] Kenji Suzuki and Shyh Yuan Lee. Convergent Theory for Effective Interaction in Nuclei*). *Progress of Theoretical Physics*, 64(6):2091–2106, 12 1980.

[93] Guillermo Díaz-Camacho, Alejandro Bermudez, and Juan José García-Ripoll. Dynamical polaron ansatz: A theoretical tool for the ultrastrong-coupling regime of circuit qed. *Phys. Rev. A*, 93:043843, Apr 2016.

[94] Richard C Tolman. *The principles of statistical mechanics*. Dover books on physics. Dover Publ., New York, NY, 1979.

[95] H.J. Lipkin, N. Meshkov, and A.J. Glick. Validity of many-body approximation methods for a solvable model: (i). exact solutions and perturbation theory. *Nuclear Physics*, 62(2):188–198, 1965.

[96] James A. Hutchison, Tal Schwartz, Cyriaque Genet, Eloïse Devaux, and Thomas W. Ebbesen. Modifying chemical landscapes by coupling to vacuum fields. *Angewandte Chemie International Edition*, 51(7):1592–1596, 2012.

[97] Javier Galego, Francisco J. Garcia-Vidal, and Johannes Feist. Cavity-induced modifications of molecular structure in the strong-coupling regime. *Phys. Rev. X*, 5:041022, Nov 2015.

[98] Yuto Ashida, Ata ç İmamoğlu, Jérôme Faist, Dieter Jaksch, Andrea Cavalleri, and Eugene Demler. Quantum electrodynamic control of matter: Cavity-enhanced ferroelectric phase transition. *Phys. Rev. X*, 10:041027, Nov 2020.

[99] Luis A. Martínez-Martínez, Raphael F. Ribeiro, Jorge Campos-González-Angulo, and Joel Yuen-Zhou. Can ultrastrong coupling change ground-state chemical reactions? *ACS Photonics*, 5(1):167–176, 2018.

[100] Yuto Ashida, Atac Imamoglu, and Eugene Demler. Cavity quantum electrodynamics at arbitrary light-matter coupling strengths, 2021.

[101] Antoine Canaguier-Durand, Eloïse Devaux, Jino George, Yantao Pang, James A. Hutchison, Tal Schwartz, Cyriaque Genet, Nadine Wilhelms, Jean-Marie Lehn, and Thomas W. Ebbesen. Thermodynamics of molecules strongly coupled to the vacuum field. *Angewandte Chemie International Edition*, 52(40):10533–10536, 2013.

[102] Arnab Das, K. Sengupta, Diptiman Sen, and Bikas K. Chakrabarti. Infinite-range ising ferromagnet in a time-dependent transverse magnetic field: Quench and ac dynamics near the quantum critical point. *Phys. Rev. B*, 74:144423, Oct 2006.

[103] H. T. Quan and F. M. Cucchietti. Quantum fidelity and thermal phase transitions. *Phys. Rev. E*, 79:031101, Mar 2009.

[104] Johannes Wilms, Julien Vidal, Frank Verstraete, and Sébastien Dusuel. Finite-temperature mutual information in a simple phase transition. *Journal of Statistical Mechanics: Theory and Experiment*, 2012(01):P01023, jan 2012.

[105] R. Peierls. Zur theorie des diamagnetismus von leitungselektronen. *Zeitschrift für Physik*, 80(11):763–791, 1933.

[106] Douglas R. Hofstadter. Energy levels and wave functions of bloch electrons in rational and irrational magnetic fields. *Phys. Rev. B*, 14:2239–2249, Sep 1976.

[107] Clai Owens, Aman LaChapelle, Brendan Saxberg, Brandon M. Anderson, Ruichao Ma, Jonathan Simon, and David I. Schuster. Quarter-flux hofstadter lattice in a qubit-compatible microwave cavity array. *Phys. Rev. A*, 97:013818, Jan 2018.

[108] Leigh Page. Deflection of electrons by a magnetic field on the wave mechanics. *Phys. Rev.*, 36:444–456, Aug 1930.

[109] L. Landau. Diamagnetismus der metalle. *Zeitschrift für Physik*, 64(9):629–637, 1930.

[110] P G Harper. Single band motion of conduction electrons in a uniform magnetic field. *Proceedings of the Physical Society. Section A*, 68(10):874–878, oct 1955.

[111] A Zee. *Quantum Field Theory in a Nutshell; 1st ed.* Nutshell handbook. Princeton Univ. Press, Princeton, NJ, 2003.

[112] Asadullah Bhuiyan and Frank Marsiglio. Landau levels, edge states, and gauge choice in 2d quantum dots. *American Journal of Physics*, 88(11):986–1005, 2020.

[113] Eliot Kapit and Erich Mueller. Exact parent hamiltonian for the quantum hall states in a lattice. *Phys. Rev. Lett.*, 105:215303, Nov 2010.

[114] B. I. Halperin. Quantized hall conductance, current-carrying edge states, and the existence of extended states in a two-dimensional disordered potential. *Phys. Rev. B*, 25:2185–2190, Feb 1982.

[115] Iacopo Carusotto, Andrew A. Houck, Alicia J. Kollár, Pedram Roushan, David I. Schuster, and Jonathan Simon. Photonic materials in circuit quantum electrodynamics. *Nature Physics*, 16(3):268–279, 2020.

[116] Brandon M. Anderson, Ruichao Ma, Clai Owens, David I. Schuster, and Jonathan Simon. Engineering topological many-body materials in microwave cavity arrays. *Phys. Rev. X*, 6:041043, Dec 2016.

[117] Mohammad Mirhosseini, Eunjong Kim, Vinicius S. Ferreira, Mahmoud Kalaee, Alp Sipahigil, Andrew J. Keller, and Oskar Painter. Superconducting metamaterials for waveguide quantum electrodynamics. *Nature Communications*, 9(1):3706, 2018.

[118] Ruichao Ma, Brendan Saxberg, Clai Owens, Nelson Leung, Yao Lu, Jonathan Simon, and David I. Schuster. A dissipatively stabilized mott insulator of photons. *Nature*, 566(7742):51–57, 2019.

[119] V.S. Vladimirov. *Equations of Mathematical Physics*. Monographs and textbooks in pure and applied mathematics. M. Dekker, 1971.

[120] Kyohei Takae and Akira Onuki. Applying electric field to charged and polar particles between metallic plates: Extension of the ewald method. *The Journal of Chemical Physics*, 139(12):124108, 2013.

[121] T. Holstein and H. Primakoff. Field dependence of the intrinsic domain magnetization of a ferromagnet. *Phys. Rev.*, 58:1098–1113, Dec 1940.

[122] 1942 Griffiths, David J. (David Jeffery). *Introduction to electrodynamics*. Fourth edition. Boston : Pearson, [2013] ©2013, [2013].